STRATEGIC MODIFICATIONS TO OPTIMIZE A CELL PENETRATING ANTIMICROBIAL PEPTIDE

by

Reena Blade

A Dissertation

Submitted to the Faculty of Purdue University

In Partial Fulfillment of the Requirements for the degree of

Doctor of Philosophy

Department of Chemistry

West Lafayette, Indiana

December 2019

THE PURDUE UNIVERSITY GRADUATE SCHOOL

STATEMENT OF COMMITTEE APPROVAL

Dr. Jean Chmielewski, Chair

Department of Chemistry

Dr. David Thompson

Department of Chemistry

Dr. Betsy Parkinson

Department of Chemistry

Dr. Herman Sintim

Department of Chemistry

Approved by:

Dr. Christine Hrycyna

Head of the Graduate Program

To my family and those who have helped light my path.

ACKNOWLEDGMENTS

First off, I want to thank Dr. Jean Chmielewski, who I owe an enormous part of the fruits that I bare from my PhD journey. During my time at Purdue Jean has served as more than a PI to me; she has been a mentor, a motivational force, and a supporter of my growth as a scientist and in other aspects of my professional development outside of the lab. I thank her for her patience over the years, her willingness to share her breadth of knowledge, and the academic expectations she held me to, which has equipped me to succeed in my future career. I must also acknowledge Jean's dedication towards the chemistry diversity initiative (CDI) we created and that she voluntarily spearheaded. This has been something I have been passionate about and that was an added bonus to my time at Purdue. I cannot fully express in words my gratitude for this opportunity and the support, time, and efforts Jean and our team put towards implementing this initiative. I can't wait to see the CDI's growth in future years. I would also like to thank my committee, without whom I would not hold my PhD today.

I guess I also must thank my lab mates. I know you all have suspensions that I secretly can't stand you all (which is partially true), but you have truly been a light for me each day in lab. As I've said before, I am so thankful that I was in lab with such kind people who support each other through every grad school milestone. Each of you have held positions that have made this PhD journey a little (a lot) easier, from coffee/ milkshake breaks to our lab outings. I have cherished my moments with you all and I thank God daily for putting me in such a conducive environment for me to grow as a scientist. To begin I thank Monessha Nambiar and Jennifer Rowe. We started this thing together and I'm so glad we have gotten to the end of this marathon together as well (we all made it!). Monessha, thank you for you immense wisdom, for being a friend to confide in and to share accomplishments with, for being a shoulder to cry on when experiments failed (literally), and being my escape route when I needed a break from work. Jenny, I'm so glad you have opened up these last couple of years because your personality has brought me so much laughter, great conversations, and all around good-times. I will miss our table talks in the lunch room regarding anything you can possibly think of. Moises Morales-Padilla and Vallabh Suresh, thank you for coming into lab and not being afraid to show your true personalities. It has been fun. Moises, thank you for being

a friend, sharing salsa dancing with me, and for being a good neighbor in 441. Late nights were cake with you and Sam. Vallabh, thank you for being the person I could go to with many of my synthesis roadblocks and for allowing me to bounce ideas around with you. Also, thank you for your corny puns (though they were mostly annoying, a joke was desperately needed sometimes). Ryan Curtis and Samantha Zeiders, thank you for joining the lab and bringing nothing, but positivity. Ryan, with you in 475 we didn't talk often, but I quickly realized you're one of the nicest and most genuine people I know and I'll miss your infectious laugh. Sam, you have become my girl. I have enjoyed all of our chats, gossip, laughter, and late night trips for food/snacks. You have been one of my favorite parts of coming to lab each day. Thomas Allen Dietsche and Corey Johnson…you two are probably the strangest part of lab, but I love(ed) it and it has been so fun working around/ with you guys over the last 2 years. Thank you for being great additions to the lab and keeping the vibe light-hearted. Michael Jorgenson and Vinay Menon, our time together has been short, but it has been so great having you both in lab. Michael, you were so quiet when you started your 0 year with us, but with time you began to show more personality and I've enjoyed getting to know you. Vinay, thank you for "having my back" sitting behind me this year and letting me disrupt your train of thought with my random biochem questions. I will miss having such a friendly lab neighbor. To Colin Cane, my undergraduate researcher, thank you for showing and teaching me patience, for being so attentive and easy to work with, and for being genuinely curious. I wouldn't have chosen any other undergrad to work with. It has truly been my pleasure and I look forward to seeing your growth as a scientist. I also must acknowledge past lab mates that have contributed to my experience at Purdue. Manish Nepal, thank you for mentoring me and your help in getting me started on my projects. Neha Agrawal, you have been such a support and encourager. You have given me so much advice, brought me peace (frustration walks around campus), and played a great role in my PhD journey. Thank you. Lastly, I would like to thank Dr. Mohamed Seleem and Hassan Eldesuokey for their dedication to collaborations on my projects.

Finally, I need to thank my family, beginning with my parents, Robert and Nancy Blade. Thank you for instilling in me perseverance, good work ethic, and dedication, all of which I needed throughout my PhD journey. Most importantly, thank you for all the love you poured into every phone call, consistently encouraging me and for believing in me when I didn't believe in myself.

Thank you for reminding me of how proud you are of me, which motivated me to keep going. To my siblings, Robert Blade and Rashida Blade, thank you for supporting me and for being the best older siblings. You both have been positive influences/ role models to me and have nurtured me, so I can get to this point. To Michael Osunlalu, thank you my love for being my most cherished cheerleader. You have willingly stuck by me through this journey and have been the person I have confided in the most. Thank you for keeping me grounded, reminding me of joy, God's promises and, for being the sunshine I needed in cloudy days. Last and most importantly, I thank God who has given me nothing that I could not handle (despite the times I felt inadequate). The completion of this chapter in my life proves that I can do all things through Him. He has come through for me with the extra strength I needed when I felt I had absolutely nothing left to give.

TABLE OF CONTENTS

LIST OF TABLES

LIST OF FIGURES

LIST OF SCHEMES

LIST OF ABBREVIATIONS

AcOH	acetic acid
ACN	acetonitrile
AF	arbitrary fluorescence
AMP	antimicrobial peptides
Boc	t-butyl carbonate
CAPH	cationic amphiphilic polyproline helices
Cbz	carboxybenzyl
CPP	cell-penetrating peptide
Cyto D	cytochlasin D
DCM	dichloromethane
DIEA	N, N'-diisopropylethylamine
DMEM	Dulbecco's modified eagle medium
DMF	N,N-dimethylformamide
DMSO	Dimethylsulfoxide
DIW	deionized water
ESI	electrospray ionization
EtOAc	ethyl acetate
FACS	fluorescence activated cell sorting
FBS	fetal bovine serum
FDA	Food Drug Administration
Fl	fluorescein
Fmoc	fluorenylmethyloxycarbonyl
Fmoc-Osu	N-(fluorenylmethyloxycarbonyloxy) succinamide
HATU	Hexafluorophosphate Azabenzotriazole Tetramethyl Uronium
HFIP	hexafluoroisopropanol
hRBC	human red blood cells
HPLC	high performance liquid chromatography
IPTG	isopropyl β-D-1-thiogalactopyranoside

KHMDS	potassium hexamethyldisilazide
MALDI-TOF	matrix laser desorption ionization-time of flight
$MgSO_4$	magnesium sulfate
MBC	minimum bactericidal concentration
MEOH	methanol
MIC	minimum inhibitory concentration
Mtt	4-methyltrityl
MTT	3-(4,5-dimethylthiazol-2-yl)-2,5-diphenyltetrazolium bromide
MRSA	methicillin-resistant Staphylococcus aureus
N_2	Nitrogen
NaH	Sodium Hydride
NHS-Fl	N-hydroxy-succinimidyl-ester-fluorescein
ONPG	ortho-Nitrophenyl-β-galactoside
PAO	phenylarsine oxide
prAMP	proline-rich antimicrobial peptides
PBS	phosphate buffered saline
PPII	type II polyproline helix
RP-HPLC	reverse phase high performance chromatography
RT	room temperature
SCV	salmonella containing vacuoles
Tat	transactivator of transcription
TB	tuberculosis
TB	trypan blue
TFA	trifluoroacetic acid
THF	tetrahydrofuran
TIPS	triisopropylsilane
Z-Hyp-OH	N-carboxybenzyl-hydroxy-L-proline
5B	5-carbon branched motif
5C	5-carbon cyclic motif
5L	5-Carbon linear motif

ABSTRACT

Pathogenic bacteria are evolving to drug resistant strains at alarming rates. The threat posed by drug resistant bacterial infections emphasize the need to establish new antimicrobial agents. Of immediate concern regarding the dangers of antibiotic resistance is the existence of intracellular bacteria, which find refuge from bactericidal devices by hiding within mammalian cells. Unfortunately, many therapeutics, such as vancomycin, do not possess membrane penetrating abilities to achieve efficacious eradication of bacteria at the subcellular level, allowing infections to persist. In an effort to target pathogens that thrive within mammalian cells, features of cell penetrating peptides (CPPs) and antimicrobial peptides (AMPs) were combined to develop a dual action antimicrobial CPP, cationic amphiphilic polyproline helices (CAPHs). CAPHs have proven to be an effective antimicrobial agent to combat an array of both Gram negative and Gram positive bacteria.

Herein, to improve CAPHs activity, we have demonstrated how the incorporation of strategic modifications has resulted in increased cell uptake, alternative subcellular locations for CAPHs, and advanced antimicrobial potency. By simultaneously extending the helical length of CAPHs while incorporating different hydrophobic groups in place of the original isobutyl moiety that compose CAPHs we have created a **FL-P17-5R** series of peptides with five carbon aliphatic motifs: **Fl-P17-5B**, **Fl-P17-5C** and **Fl-P17-5L.** Through these modifications the peptides proved to be 2 to 5-fold more efficient in accumulating in macrophage cells than parent peptide Fl-P14LRR and where able to clear intracellular pathogenic bacteria, such as *Listeria*, from infected macrophages by 26 to 54%.

In addition to making the **Fl-P17-5R** series of CAPHs to potentiate CAPHs activity, modifications to the cationic moiety of CAPHs were explored. By incorporating a new cationic monomer into the CAPHs sequence, a guanylated amino proline (GAP) residue, we produced **Fl-P14GAP**, a CAPHs peptide with an organized cationic charge display. This modification resulted in a 5-fold increase in cell uptake and a 2 to 16-fold decrease in minimum inhibitory concentration (MIC) values against strains of enteric and ESKAPE pathogens in comparison to Fl-P14LRR. **Fl-P14GAP** also executed superior clearance of intracellular pathogenic bacteria that resulted in the

complete eradication of a drug resistant strain of *A. baumannii* from infected macrophage cells. Overall, our efforts with the **Fl-P17-5R** series of CAPHs and **Fl-P14GAP** have strengthened the therapeutic potential of CAPHs in the hopes of addressing the need for novel antibiotics with the propensity to eradicate intracellular pathogens.

CHAPTER 1. PEPTIDE THERAPEUTICS TO COMBAT THE BACTERIA CRISIS

1.1 Threat of Pathogenic Bacterial Infections

At the start of the twentieth century, infectious diseases were the leading cause of mortality in the U.S., accounting for nearly a third of all deaths.[1] Fortunately, the discovery of the first antibiotic, penicillin, in 1928 by Alexander Fleming, defined the start of the fight against bacterial infections. Once penicillin was successfully isolated it was introduced as an antibiotic and became widely available in the early 1940s, which marked the beginning of an antibiotic era.[2] Prior to antibiotics, common infections, such as strep throat caused by *Streptococcus pyogenes*, marked that onset of fatal diseases like scarlet fever.[3] At present, strep throat is more of a nuisance infection; however, there is a daunting possibility that diseases, like strep throat, may become a true threat once gain as we head towards an era where antibiotics will be ineffective in treating bacterial infections.

Despite the advances of modern medicine, we are at the brink of a post-antibiotic era where common infections may once again kill.[4] The disease threat from pathogenic bacteria has been left unaddressed for far too long, which, in turn, has led to bacterial infections reemerging as serious threats to human health. In fact, the Centers for Disease Control and Prevention (CDC) estimates that, of the two million new cases of bacterial infection that occur each year in the United States, approximately 23,000 result in death.[5] Compounding the problem is the overuse of antibiotics, which has catalyzed the development of drug resistant bacteria. Moreover, the slow development of novel antibiotics has failed to match the rapid rate at which drug resistant bacteria are evolving (Figure 1.1). Thus, the development of effective, novel therapeutics is imperative in order to combat the current bacteria crisis.

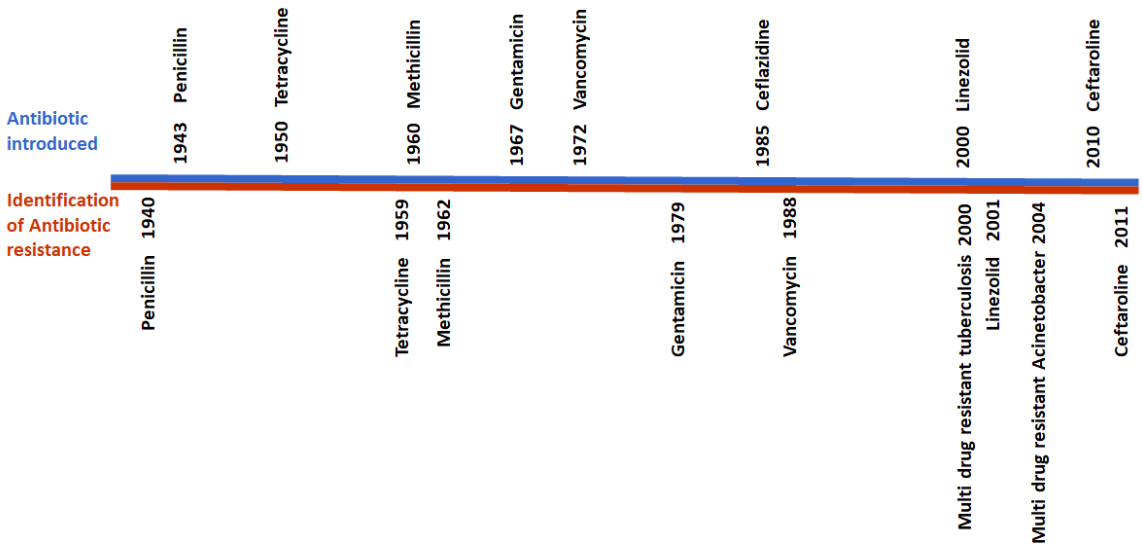

Figure 1.1 Timeline showing the introduction of antibiotics alongside the rise in antibiotic resistance.

1.1.1 Prominent pathogenic bacteria: Enteric and ESKAPE pathogens

Enteric and ESKAPE pathogens are two of the major culprits behind the current bacterial threat. Enteric pathogens are bacteria that are widely known to cause gastrointestinal infections, with the primary source of these infections being the consumption of contaminated food. Though enteric infections are typically mild, they are all capable of leading to severe health problems. Moreover, treatment options for enteric infections are quickly becoming compromised by antibiotic resistance. Despite the general perception that foodborne illnesses are not a vital threat, each year, millions of people contract enteric infections, which, in turn, can lead to hospitalization and death.[6] Among the most common genera of enteric infections are *Salmonella*, *Shigella*, *E. coli*, and *Listeria.* As of 2019, *Salmonella***,** the genus of bacteria responsible for typhoid fever, has been the cause of 1.2 million illnesses, 23,000 hospitalizations, and 450 deaths in the U.S. annually.[7] Additionally, drug resistant *Salmonella* was categorized as a serious threat on the most up-to-date CDC list of biggest bacterial threats, along with drug resistant *Shigella.*[8] *Listeria* also is a prevalent enteric pathogen as there is a 20% mortality rate for those who contract *Listeriosis*.[9] Thus, enteric pathogens are a prevalent threat that require attention.

In comparison to enteric pathogens, ESKAPE pathogens pose an equally, if not more, daunting health concern.[10] The word ESKAPE is an acronym that encompasses different classes of bacteria

that fall under the category of nosocomial (hospital-associated) bacterial infections. These bacteria include, *Enterococcus*, *Staphylococcus*, *Klebsiella*, *Acinetobacter*, *Pseudomonas*, and *Enterobacter*, which prey on immunocompromised patients and wreak havoc in hospital environments.[10] The CDC has highlighted many drug resistant ESKAPE pathogens in their list of serious threats.[11] For example, a 2017 report stated methicillin-resistant *Staphylococcus aureus* (MRSA) was the cause of 80,000 severe infections and 11,000 deaths in the U.S. annually.[11] More recently, *Acinetobacter* has emerged as one of the most difficult to treat nosocomial bacteria and in 2013 it was reported to cause more than 7000 multi-drug resistant infections each year in the U.S.[11, 12] *A. buamannii* is a particularly devastating strain of *Acinetobacter* as it was selected as priority one (critical) on the World Health Organization's 2017 list of priority pathogens for new antibiotics.[13] It has evolved resistance even towards last resort antibiotics, such as colistin.[12] Additionally, *A. baumannii*, is associated with nosocomial pneumonia, especially in intensive care units (ICU), along with *Pseudomonas aeruginosa* and *Klebsiella pneumoniae*, which lead to a heightened mortality rate, especially if the bacteria are multi-drug resistant.[14] Thus, the mortal threat posed by ESKAPE pathogens necessitates the development of novel, potent antibiotics.

Of the above mentioned pertinent bacteria threats, enteric pathogens *Shigella, E. coli*, and *Salmonella* are Gram negative and *Listeria* is Gram positive.[15-18] *Enterococcus* and *Staphylococcus* are the only two ESKAPE pathogens that are Gram positive. All other ESKAPE pathogens are Gram negative, including *Klebsiella*, *Acinetobacter*, *Pseudomonas*, and *Enterobacter*. Gram positive bacteria have a thick layer of peptidoglycan in their cell wall, whereas Gram negative bacteria have an outer and an inner membrane layer surrounding a thin peptidoglycan cell wall (Figure 1.2).[19] Thus, the complex cell wall presents Gram negative bacteria as an even greater challenge for antibiotics treatment.[20] This property perpetuates the difficulty in treating bacteria, such as Gram negative *A. baumannii*, with antibiotics, like vancomycin, whose mechanism of action involves targeting cell wall peptidoglycans to destroy the structural integrity of the bacteria.[21] Thus, ideal antibiotics should have the capacity to treat both Gram negative and Gram positive bacteria.

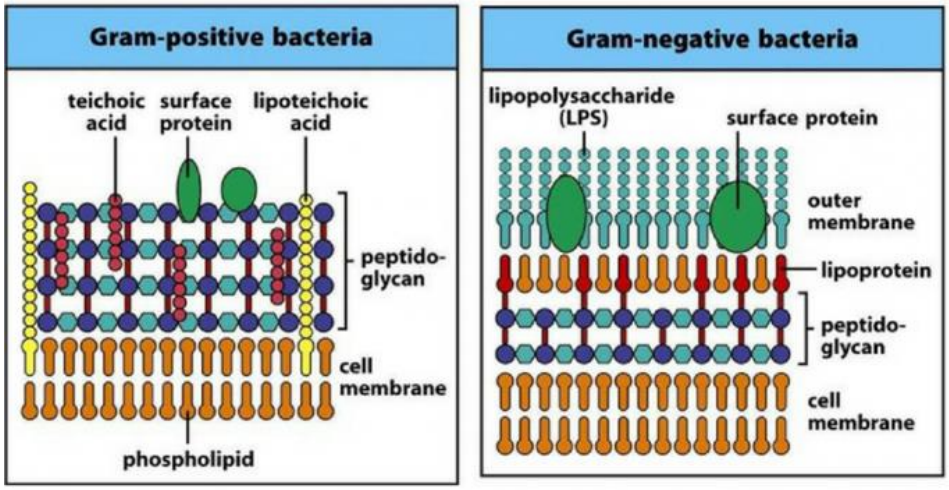

Figure 1.2 Membrane structure of Gram positive and Gram negative bacteria[22].

1.1.2 Classifications of current antibiotics

Of the many antibiotics that have emerged during the antibiotic era, many are classified according to chemical structure. Macrolides, fluoroquinolones, β-lactams, and aminoglycosides make up the major structural categories of antibiotics.[23] However, there are also other antibiotics on the market that fall outside the scope of these common classes. One example is linezolid, which has a heterocylic structure containing 2-oxazolidinone and is used to treat multi-drug resistant (MDR) bacteria.[24] Linezolid inhibits protein synthesis by interrupting protein translation, which is pertinent to bacterial survival. Additionally, there are macromolecule antibiotics, like vancomycin, which acts by inhibiting bacterial cell wall synthesis.[25] More specifically, vancomycin acts upon Gram positive bacteria by disrupting the peptioglycan cross-linkage during the bacterial cell wall. Other glycosylated, cyclic, or polycyclic peptide-based antibiotics include polymyxin B and gramicidin S, which are naturally-derived antimicrobial peptides with clinical applications.[26] Although these major classes of antibiotics provide essential treatment for bacterial infections, there have been efforts to repurpose and further improve current antibiotics.

One way in which antibiotic activity has been potentiated is through improved drug delivery. To unlock greater antibacterial potency of antibiotics for enhanced treatment of pathogenic bacteria, drug delivery systems, like liposomes and nanoparticles, and conjugate antibacterial therapies have been employed.[27, 28] For example, the antibiotic/ antibody drug conjugate, THIOMAB, is currently in phase I clinical trials for its ability to target and eradicate multidrug resistant *Staphylococcus aureus* at the subcellular level.[29] Still, regardless of the promise of such efforts, some limitations

of these systems include instability of liposome vesicles and inefficient drug loading capacities, aggregation of nanoparticles, and the complexity/cost of antibody production.[27, 30, 31] Still, attention should be given to achieve targeted antibacterial delivery in order to attain optimal bactericidal activity while taking these shortcomings into consideration. In order to strategically combat the immediate bacterial threat, it will be ideal to engineer novel antibiotics that are cost effective and exhibit both efficient deliverability and potent bactericidal activity.

1.2 Antimicrobial Peptides (AMPs)

Antimicrobial peptides (AMPs) play a fundamental role in the innate immunity of many organisms, including microbes, plants, insects, and animals.[32] Lysozyme, the first reported human antimicrobial protein, was identified in 1922 by Alexander Fleming, which was the onset to the discovery of thousands of AMPs to date.[33, 34] AMPs, such as defensins and cathelicidins, serve as part of the immune response against microbes, such as parasites, viruses, and bacteria, either by directly targeting bacterial pathogens or through stimulation of inflammatory responses. [35] Though it has been decades since the first discovered AMP, the therapeutic potential of AMPs has not been cultivated, hence, typically AMPs are limited to topical treatment or do not make it past clinical trials (Table 1.1).[36-38] Thus, in recent years, more efforts have gone towards elucidating AMPs to access their therapeutic potential.

Table 1.1 Select naturally derived antibacterial AMPs that have progressed to clinical trials. (*) indicates terminated trials.

Peptide Name	Trial Phase	Sequence	Application
OP-145	II	IGKEFKRIVERIKRFLRELVRPLR	Ear drops
Pexiganan	III*	GIGKFLKKAKKFGKAFVKILKK-NH_2	Topical
Omiganan	III	ILRWPWWPWRRK-NH_2	Topical
LL-37	II*	LLGDFFRKSKEKIGKEFKRIVQRIKDFLRNLVPRTES	Topical
PAC113	II	AKRHHGYKRKFH	Oral rinse
hLF1-11	I/II	GRRRRSVQWCA	IV

1.2.1 AMP mechanisms of action

Many AMPs have a broad range of antimicrobial activity to include both Gram-positive and Gram-negative bacteria as well as fungi, viruses, and unicellular protozoa. For the purposes of this document the focus will be bactericidal activity. AMPs antibacterial activity is enacted through two major modes of action: bacterial cell lysis or by targeting integral bacterial components important for their survival (Figure 1.3). Regardless of the mechanism of action it is widely accepted that membrane interaction is the primary and key step for AMP's antimicrobial activity.[37] Herein, the different mechanisms of antibacterial activity will be discussed.

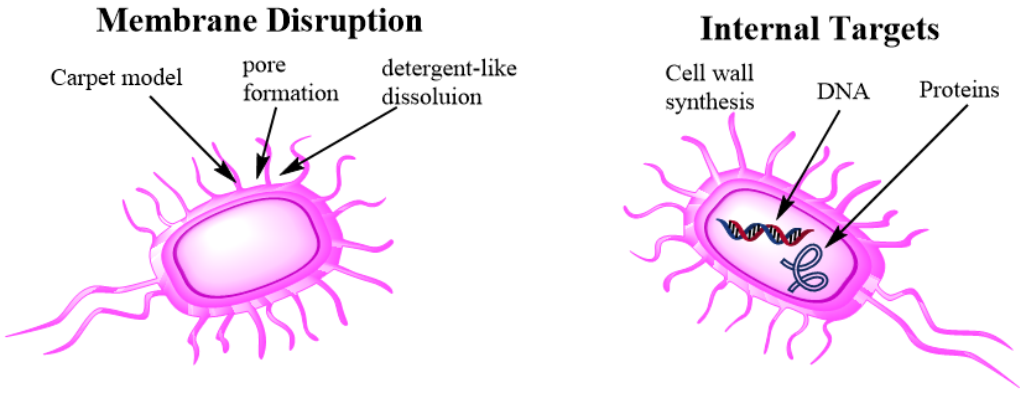

Figure 1.3 Possible mechanisms of action of AMPs.

1.2.1.1 Lytic mode of action

The most well-known mode of action of AMPs is through bacterial membrane lysis. It has been generally accepted that the majority of AMPs target bacteria cell membranes resulting in membrane depolarization, lysis, and cell death.[37] Human cathelicidin, LL-37, is an example of a

well-studied lytic AMP, which acts by destabilizing the bacterial membrane. LL-37 has shown a broad spectrum of activity against Gram negative and Gram positive bacteria and displayed both outer and inner membrane permeabilization in Gram negative *E. coli*.[39] Furthermore, several membrane destabilization actions can be executed by AMPs. These involve the formation of pores, phase separation, and promotion of a non-lamellar lipid structure to cause disruption of the membrane bilayer.[40] Additional mechanisms that cause disruption of the membrane integrity include detergent-like dissolution of areas of the membrane, the formation of peptide-lipid aggregates within the bilayer, and the execution of the carpet-like method of cell entry, which can permanently alter the integrity of the membrane (Figure 1.4C).[35]

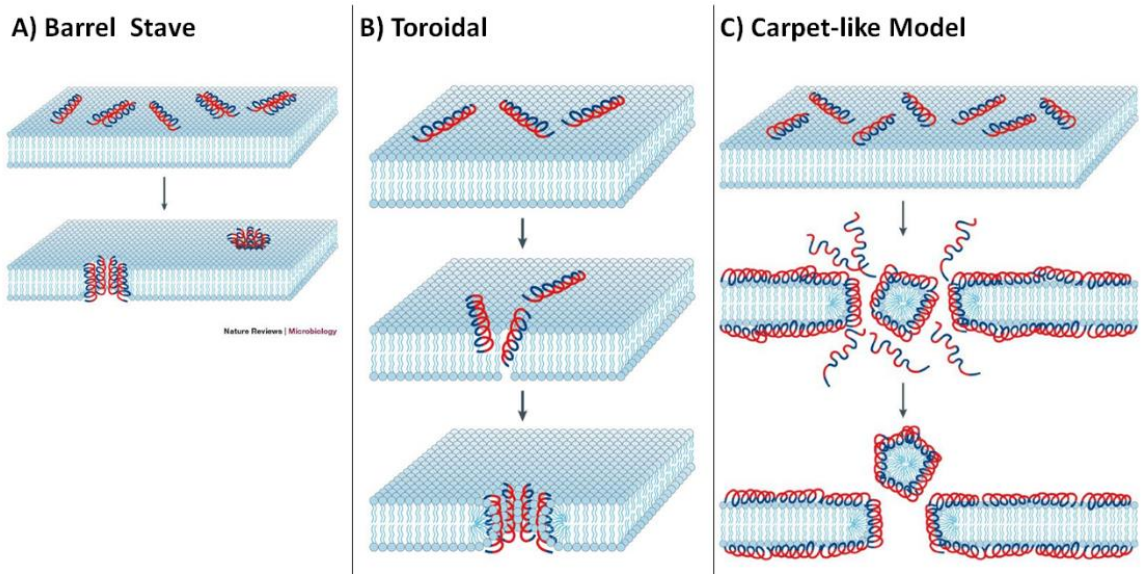

Figure 1.4 Modes of cell permeation by AMPs including the (A) Barrel Stave Model, (B) Toroidal Model, and (C) the membrane damaging carpet-like model.

1.2.1.2 Bacterial versus mammalian cell membrane

A major drawback that can be characteristic of membrane lytic AMPs is a lack of specificity towards bacteria cells, which can result in mammalian cell lysis.[41] Fortunately, the difference in membrane composition between prokaryotes and eukaryotes ideally allows AMPs to have a higher affinity towards bacterial cells. Some components of the mammalian plasma membrane, like phospholipids and glycosaminoglycans, provide it an overall net negative charge. However, eukaryotic cell membranes are also composed of zwitterionic lipids, like phosphatidylcholine,

phosphatidylethanolamine, and sphingomyelins, which pushes the membrane surface towards a more neutral state.[42] For example, the membrane of erythrocyte is exclusively composed of zwitterionic phospholipids, like phosphatidylcholine and sphingomyelin.[43] In contrast, the bacterial cell membrane is highly anionic with an abundance of negatively-charged components, like phosphatidylglycol and cardiolipin, which makes the transmembrane potential of bacteria more negative than mammalian cells. Thus, the amount of negatively-charged structures in bacterial membranes allows cationic AMPs to have a greater affinity towards bacterial cells over mammalian cells to dissipate non-specific membrane lysis.[32]

1.2.1.3 Non-lytic modes of action

AMPs exhibit antibacterial properties via non-lytic mechanisms of action as well, in which bacterial membrane association is required for AMPs to gain access to intracellular targets. Non-lytic bactericidal mechanisms involve the ability of AMPs to transiently form pores to penetrate bacterial outer (if applicable) and inner membranes by using a toroidal or barrel-stave mechanism of cell entry. Once inside the cell, the AMPs are able to make contact with targeted bacterial components that lead to cell death (Figure 1.4A and B).[44] Buforin 2, a 21 amino acid, linear peptide, is an example of an AMP that is able to cross the bacterial cell membrane in order to cause bacterial cell death from the interior of the cell. Once in the bacteria cell cytoplasm, Buforin 2 has been determined to tightly bind DNA and RNA resulting in rapid cell death, as shown with *E. coli*.[32, 45] Other non-lytic AMPs similarly enact bactericidal activity, such as Puroindoline B and Indolicidin, which act by binding DNA resulting in the inhibition of nucleic acid synthesis.[32] Another class of AMPs that have been found to utilize non-lytic modes of action are bacteriocins, like colicins and microcidins. These ribosomally synthesized AMPs are produced from bacteria and use many different modes of bactericidal action, including pore formation, nuclease type functionality, and inhibition of protein synthesis or DNA replication to inhibit bacterial cell growth.[46] Moreover, many bacteriocins utilize a "Trojan-horse" mechanism to transverse bacterial cell membranes by interacting with cell surface components, which facilitate their transport into the cell in order to reach internal targets.[32, 46] Once inside the cell bacteriocins, like the microcidin B17, for example, can target DNA gyrase, which subsequently inhibits DNA replication.[47]

To further introduce the dynamic antibacterial activity exhibited by AMPS, AMPs that simultaneously utilize multiple mechanisms of action must be acknowledged. The human defensin, HPN-1, is one example of an AMP that has been found to utilize multiple mechanisms of action that concomitantly contribute to bacterial death. Its mechanisms include the ability to target cell wall synthesis and to inhibit nucleic acid and protein synthesis in *E. coli*.[48] Such examples demonstrate the versatility of AMPs to enact bactericidal activity, which extends beyond the reputation of lytic behavior. The broad range of bactericidal activity of AMPs makes them promising candidates as therapeutic antimicrobials.

1.2.2 Structural characteristics of AMPs

In addition to diversity in modes of action, AMPs are a structurally diverse class of peptides as well. Still, certain features have been identified to be prevalent in the AMP community. Though other classes of AMPs exists (hydrophobic and anionic), amphiphatic AMPs are the predominate type. They are typically short (10-50 amino acids), have an overall positive charge (+2 to +9) due to a high content of cationic residues (arginine and lysine), are also composed of hydrophobic residues (≥ 30%) for amphiphilicity, and have organized secondary structures.[35] These physiochemical properties play an essential role in AMPs ability to associate with bacterial membranes and their aptitude to enact bactericidal activity through charge and hydrophobic interactions. Additionally, AMPs are classically categorized based on physiochemical properties: secondary structures and amino acid composition; origin: natural versus synthetic AMPs; or mode of action: lytic versus non-lytic. Despite the diversity that exists amongst amphiphatic AMPs, two rules persist: *i*) A positive charge is required for initial association with the negatively-charged bacterial membranes and *ii*) hydrophobicity is a requirement for insertion into and/or disruption of the bacterial membrane. Hence, the following section will focus on these aforementioned features and their influence on AMPs antibacterial activity.

1.2.2.1 Amino acid composition of AMPs

Negatively charged lipids on the bacterial membrane facilitate electrostatic interactions with cationic AMPs to initiate their antimicrobial activity. The significance of the net charge has been demonstrated through various studies where the overall charge of AMPs have been altered. One example using the helical AMP, C18G, (ALYKKLLKKLLKSAKKLG) showed that altering its

cationic residues (Lys) by substitution with other positively-charged residues (arginine, ornithine, di-amino propionic acid, and histidine) resulted in slight alterations in antimicrobial activity. Most significantly, substitution with histidine resulted in a peptide with a lower net charge and the highest MIC values, on average, against a number of tested bacterial isolates, which can be attributed to it exhibiting weaker electrostatic interactions with anionic bacterial membranes (Table 1.2).[49] The importance of the cationic residue has also been demonstrated in a study by Elmore *et. al.* in which they compared the activity of three AMPs, buforin II (TRSSRAGLQWPVGRVHRLLRK), DesHDAP1 (ARDNKKTRIWPRHLQLAVRN), and parasin (KGRGKQGGKVRAKWKTRSS), with analogues that contained only lysine or arginine cationic residues. Results of this study showed that the antibacterial activity against *E. coli* was enhanced in the peptides that displayed increased arginine content. The arginine peptides also showed a slight increase in membrane translocation of membrane mimicking vesicles.[50] Studies, such as this, demonstrate that the overall net charge can be adjusted within limits that allow for the attainment of more potent antimicrobial activity. In another study, when the net charge of V13K (Ac-KWKSFLKTFKSAKKKVLHTALKAISS-NH2) was increased from +8 to +9, the hemolytic activity against erythrocytes significantly increased, from 250 μg/ml to more than 7.8 μg/mL.[51] These results suggest that AMPs have a threshold limit for the net positive charge for favorable activity. Overall, these studies support the importance of the cationic residues in AMP activity.

Table 1.2 Minimum Inhibitory Concentrations (MIC) (μM) of C18G and analogues

Name	Net charge	E. coli	E coli	P. aeruginosa	S. aureus	B. subtilis
C18G	+8	1.875	7.5	15	1.875	1.875
C18G-Arg	+8	1.875	7.5	>15	3.75	1.875
C18G-His	+1	3.75	>15	>15	15	1.875
C18G-Orn	+8	1.875	3.75	3.75	1.875	3.75
C18G-Dap	+8	3.75	7.5	7.5	7.5	1.875

Studies have also emphasized the significance of hydrophobicity, especially since hydrophobic amino acids comprise a significant portion of AMP sequences. Additionally, each residue has hydrophobic moment that contributes to the hydrophobicity of the peptide. Some studies have found that when hydrophilic amino acids are replaced with hydrophobic residues, antimicrobial activity can diminish and the enhanced hydrophobicity can cause lytic behavior towards mammalian cells.[52-54] Alternatively, reports have also shown decreasing the hydrophobicity leads to increased antibacterial activity. For example, a study by Chen *et. al.*, in which the hydrophobicity of an amphiphatic AMP, V_{681} (KWKSFLKTFKSAVKTVLHTALKAISS), was varied through amino acid substitutions revealed that reduced hydrophobicity on the non-polar face of the peptide helix enhanced antimicrobial activity (Table 1.3).[53] Such studies support that there is an optimal hydrophobicity threshold unique to each AMP. Overall, combined information regarding cationic and hydrophobic residues impart that a balance of hydrophobicity and hydrophilicity is imperative for conducive AMP behavior.

Table 1.3 MICs of V_{681} post amino acid substitutions. (*) denotes the MIC of the original V_{681}.

MICs (μg/mL) of Substitutions of V_{681} (Ac-KWKSFLKTFK**S**$_{11}$A**V**$_{13}$KTVLHTALKAISS-amide)			
Substitution V13X_L (non-polar face)	*E. coli*	*S. typhimurium*	*P. aeruginosa*
Leu	6.4	32.0	12.7
Val	7.1*	20.2*	6.4*
Ala	2.5	6.4	5.0
Gly	2.5	5.0	6.4
Ser	2.5	6.4	6.4
Lys	2.5	4.0	8.0

In addition to the strategic implementation of hydrophobic and hydrophilic amino acids into AMP sequences, a particularly special subclass of AMPs are proline rich AMPs (prAMPs). The advantages of proline residues have gained recognition as positive contributors to AMP activity. Generally, proline rich AMPs are short peptides characterized by having a large quantity of proline residues (minimum 50%) and are typically rich in arginine residues as well (Table 1.4).[55, 56] These features of prAMPs, like mammalian cathelicidins Bac-5 and Bac-7, support an overall cationic charge and the execution of non-lytic bactericidal activity. Other desirable traits of prAMPs include good solubility, negligible toxicity, and good cell permeability to reach intracellular targets.[57]

Table 1.4 Select prAMPs and their modes of action.

prAMP (Source)	Peptide Amino Acid Sequence	Mode(s) of Actions
$Bac5_{1-23}$ (Bovine)	RFRPPIRRPPIRPPFYPPFRPPI	Inhibits protein biosynthesis by targeting 70S ribosomes inhibits DnaK
$Bac7_{1-35}$ (Bovine)	RRIRPRPPRLPRPRPRPLPFPRPGPRPIPRPLPFP	Inhibits protein biosynthesis by targeting 70S ribosomes inhibits DnaK
PR-39 (Wild swine)	RRRPRPPYLPRPRPPPFFPPRLPPRIPPGFPPRFPPRFP	Inhibits protein biosynthesis by targeting 70S ribosomes inhibits DnaK
A3-APO (synthetic)	$(ChexRPDKPRPYLPRPRPPRPVR)_2Dab$ Chex =1-amino-cyclohexane carboxylic acid Dab = 2,4-diamino-butyric acid	membrane disruption Inhibits DnaK
PR-39 (swine)	RRRPRPPYLPRPRPPPFFPPRLPPRIPPGFPPRFPPRFP	Inhibits DNA and protein synthesis

Primarily, prAMPs use non-lytic mechanisms of action and have been shown to enact antibacterial activity while maintaining membrane integrity.[55] PR-39, Bac-5, and Bac-7 are examples of notable prAMPs that support the non-lytic behavior of prAMPs.[56, 58] This is ideal to minimize toxicity affects that are more prevalent in AMPs with lytic modes of action. Though non-lytic behavior is more common of prAMPs, concentration dependent lytic behavior by prAMPs has been observed, in which the higher the concentration the more membrane disruptive behavior is observed.[56] Non-lytic antibacterial mechanisms that prAMPs have been found to execute include disruption of liposaccharide biosynthesis, inhibition of cell wall synthesis, prevention of the biosynthesis of phospholipids, and binding to liposaccharides. Additionally, some prAMPs can cause protein misfolding by targeting certain components involved in protein synthesis, such as DnaK.[55] Some prAMPs have also been found to use multiple bactericidal mechanisms of action simultaneously.

For example, A3-APO, has been shown to exhibit dual modes of action involving both membrane disruption and targeting DnaK to cause protein misfolding.[59]

Proline can also have a significant impact on AMP activity even when it is not abundantly present. The incorporation of proline into central regions of proline-lacking α-helical antimicrobial peptides has been reported as a useful method to design cell-selective AMPs.[60-62] Studies on the previously mentioned buforin 2 demonstrate how proline is a key component in its non-lytic permeability through comparisons with buforin analogues lacking proline, and with proline-free, magainin 2, which is similarly a linear, basic, and amphiphatic AMP (Table 1.5).[43, 45 63] In one study buforin 2 accumulated in the cell membrane of *E. coli* and exhibited non-lytic antimicrobial activity at concentrations five times its MIC, whereas magainin 2 lysed the bacteria and remained outside the cell wall under the same conditions.[45] Additionally, buforin 2 was shown to penetrate model membrane bilayers with minimal leakage of fluorescent dye observed. In contrast, magainin 2 had 100- fold greater leakage than buforin 2.[43] In a separate study, when the proline residue of buforin 2 was replaced with leucine or alanine its antimicrobial activity decreased.[63] Additionally, removal of proline caused buforin 2 to revert to membrane disruption in *E. coli*, an outcome analogous to the lytic behavior of magainin 2.[43, 63] Thus, buforin 2 is just one example of how proline incorporation may equip AMPs with specialized modes of action for antibacterial application.

Table 1.5 Peptide sequences of buforin 2, magainin 2, and analogues of buforin.

Peptide	Sequence	Charge
Magainin 2	GIGKWLHSAKKFGKAFVGEIMNS	+3
Buforin 2	TRSSRAGLQW**P**VGRVHRLLRK	+6
Leu substituted Buforin 2	TRSSRAGLQWLVGRVHRLLRK	+6
Alanine substituted Buforin 2	TRSSRAGLQWAVGRVHRLLRK	+6

1.2.2.2 Secondary structure of AMPs

Over the last few decades, the pool of AMPs has expanded significantly and is currently composed of three major conformational groups: β-sheet, α-helix, and linear/random coil.[64] Among these different groups, AMPs that adopt an amphiphilic α-helical or β-sheet structure are the most common.[53] A significant amount of AMPs exist as cationic, amphiphilic peptides that adopt an α-helical secondary structure upon membrane interaction. By folding into a stable α-helix the positive and hydrophobic amino acids are separated, resulting in an organized amphiphilic structure. Examples of such peptides include melittin, magainins, and cecropins.[54] Alternatively, peptides that adopt a β-sheet structure wherein the confirmation is stabilized by disulfide or covalent bonds, include defensins, protegrins, and gramicidin S.[54] Defensins are among the well-studied AMPs that exhibit a β-sheet structure.[32, 65] Typically, organized secondary structures promote favorable antimicrobial activity, however, ordered secondary structures have also been implicated in enhanced eukaryotic cell cytotoxicity by mediating non-specific lytic behavior of AMPs. Moreover, rather or not favorable activity is observed is dependent on the AMP's threshold for hydrophobicity and/or hydrophilicity, which is attributed to the amino acid content and is unique for each peptide.[52, 53] Regardless of the peptide configuration, it has been widely accepted that sequence organization has a major influence on AMP activity.

1.2.3 Progress towards synthetically improved AMPs

In order to hone the potential of AMPs as an alternative antibacterial therapy, the shortcomings of peptide therapeutics must be recognized. Major drawbacks of AMPs include poor bioavailability, low metabolic stability, toxicity, low bacteriological efficacy in animal models, and manufacturing difficulties, which have limited their antibiotic applicability.[35, 41, 66] Thus, through structure-activity relationship studies, progress has been made to optimize AMPs for enhanced activity and reduced challenges associated with AMPs. Implementation of D-amino acids into peptides sequences and the use of peptoid sequences are a couple of the proven methods that have made AMPs less susceptible to proteolysis and have reduced toxicity while maintaining antimicrobial potency (Figure 1.5).[41 67]

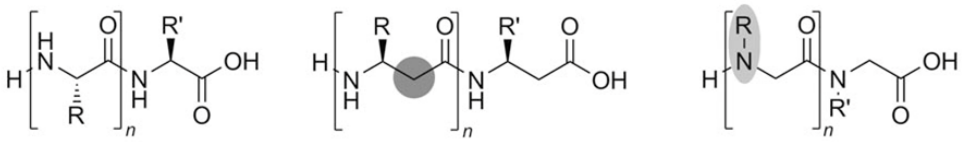

Figure 1.5 β-peptide (2), peptoid (3) structures to improve AMP activity in comparison to original peptide structures (1).[68]

1.2.3.1 Peptoid and β-peptide modified AMPs

D-amino acid substitution have been incorporated into a number of natural AMPs to achieve activity that addresses some of the aforementioned shortcomings of peptide therapeutics (Table 1.6). Although there are cases where AMP diastereomers may cause no or modestly enhanced antibacterial activity, majority of the reported studies have shown they have the propensity to decrease hemolysis and/or provide peptides with enzymatic stability.[69-75] One example of the use of D-amino acids was shown through the production of diastereomeric cytolysin, pardaxin. Pardaxin is a cationic peptide with an α-helical structure, which has been shown to exhibit antibacterial activity. By incorporating D-amino acids into its sequence at positions Pro7, Leu18, and simultaneously at both positions (Pro7 and Leu18), pardaxin's helicity was interrupted, which resulted in reduced hemolytic activity with maintained antimicrobial activity against Gram negative and Gram positive bacteria. In fact, the diastereomer analogue that was subjected to the greatest helicity disruption and displayed the lowest amount of hemolysis is the only analogue that showed specificity towards unilamellar vesicles composed of negatively charged phospholipids over zwitterionic vesicles, hence, demonstrating that it may have greater specificity for bacterial membranes.[73]

Table 1.6 Natural AMPs with D-amino acid substitutions (red) and the effects on their activity.

AMP Name	Source	Amino Acid Sequence	Result
IsCT-P[69]	IsCT (*Scorpion*)	(ILKKIWKPIKKLF-NH_2)	Random coil structure, increased antibacterial activity, less lytic membrane interaction
Esc-1a(1-21)-1cNH_2[71, 72]	Esculentin-1a (*Frog*)	GIFSKLAGKKIKNLLISGLKG-NH2	Decreased toxicity towards mammalian cells, greater serum stability, improved antibiofilm activity
D-Pin2[70]	Pandinin 2 (*Scorpion*)	FWGALAKGALKLIPSLFSSFSKKD	Improved protease stability, reduced hemolytic activity, maintained antibacterial activity
All-D-magainin[75]	Magainin-2 (*Frog*)	GIGKFLHSAKKFGKAFVGEIMNS-NH_2	Resistant to enzymatic degradation (trypsin, InA), maintained antibacterial activity
PS-PT2b[74]	PS-PT2: derivative of phylloseptin-PT (*Frog*)	FLSLIPKAIKAVGVKAKKF-NH2	Decreased hemolysis, maintained antimicrobial activity and stability in serum.
[D]P^{7} L^{18} L_{19}[73]	Pardaxin (*Fish*)	(GFFALIPKIISSPLFKTLLSAVGSA LSSSGGQE-NH2)	Decreased hemolysis, maintained antibacterial activity, lipid specificity

The functionality of D-amino acid modified AMPs was also demonstrated in the study by Chen *et. al.* with amphiphatic AMP, V_{681}, incorporating various polar and non-polar residues as well as D-/L-amino acid substitutions at the center of the hydrophobic face (position 13) and at the center of the hydrophilic face (position 11) (Table 1.7). This study revealed that D-amino acid substitutions disrupted the helicity of V_{681} to decrease hemolysis against eurthrocytes while enhancing antimicrobial activity. Namely, the series of D-amino acid substitutions identified the least hemolytic peptide with improved antibacterial activity in comparison to V_{681} to be $V13A_D$.[53] These results also support that weakened helicity thorugh D-amino acid incorporation can decrease unfavorable lytic behavior while maintain antibacterial potency. Their approach relied on point mutations to discover viable variants of V_{681}, which is a method that can and has been employed for the rational design of AMPs. These results show one example of how D-amino acids can be used to counteract undesirable lytic AMP activity. Overall, these examples represent successful strategies to combat the shortcomings of AMPs while maintaining antimicrobial competency.

Table 1.7 MICs against bacteria of peptides developed by single amino acid substitutions incorporated into $V_{681.}$ (*) denotes the MIC of the original V_{681}.

MICs (μg/mL) of Substitutions of V_{681} (Ac-KWKSFLKTFK**S$_{11}$**A**V$_{13}$**KTVLHTALKAISS-amide)			
Substitution $S11X_{L/D}$ (polar face)	*E. coli*	*S. typhimurium*	*P. aeruginosa*
Leu	16.0/ 5.0	32.0/10.1	20.2/4.0
Val	6.4/5.0	32.0/10.1	10.1/6.4
Ala	6.4/4.0	20.2/8.0	10.1/5.0
Gly	5.0	12.7	4.0
Ser	7.1*/2.5	20.2*/6.0	6.4*/2.0
Lys	10.1/3.2	25.4/3.2	25.4/2.0
Substitution $V13X_{L/D}$ (non-polar face)	*E. coli*	*S. typhimurium*	*P. aeruginosa*
Leu	6.4/3.2	32.0/16.0	12.7/6.4
Val	7.1*/2.5	20.2*/5.0	6.4*/4.0
Ala	2.5/1.6	6.4/5.0	5.0/4.0
Gly	2.5	5.0	6.4
Ser	2.5/3.2	6.4/12.7	6.4/18.3
Lys	2.5/3.2	4.0/32	8.0/32

In addition to applicability of D- amino acid substitutions, several groups have designed peptoids and β-peptides to maintain facial amphiphilicity and bactericidal potency.[76-78] Patch and Baron demonstrated that helical peptoid oligomers of lytic AMP, magainin 2, exhibited selective non-hemolytic and potent antibacterial activity against both Gram-positive and Gram-negative bacteria. In this study they synthesized several 12-17mer peptoid analogues and found that the more hydrophilic compounds show negligible hemolysis at concentrations as high as 200 μg/mL, whereas the increasingly hydrophobic peptoids have increased hemolytic activity with lysis becoming detectable a concentrations less than 10 μg/mL.[78] Furthermore, of the tested peptoids, the oligomers displaying non-aromatic bulky hydrophobic residues (Figure 1.6 A, B) had the least desirable activity in comparison to their counterparts, which contained aromatic (S)-N-(1-phenylethyl)glycine (Nspe) residues to display moderate hydrophobicity (Figure 1.6 C, D).[78] These results demonstrate the applicability of peptoids as AMPs mimics with peptoids displaying desirable amphiphilicity showing good antimicrobial potency with non-hemolytic behavior.

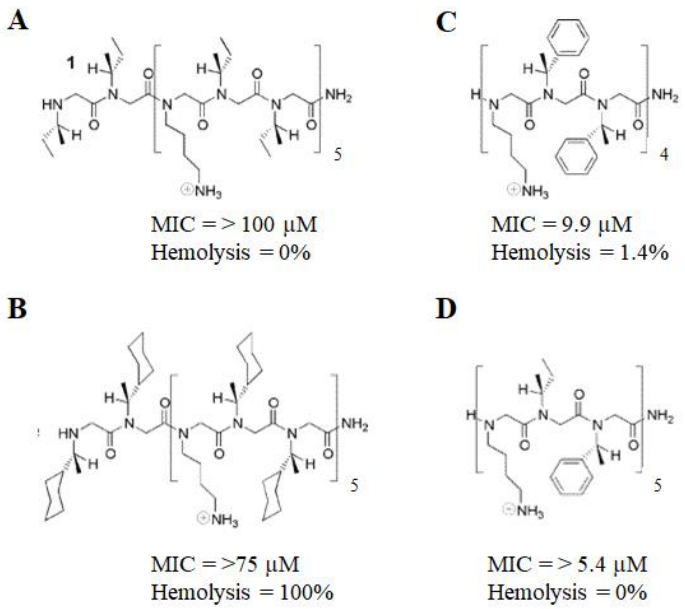

Figure 1.6 Structure of magainin mimicking peptoids and their MIC values against *E. coli* and hemolytic activity against erythrocytes.

1.2.3.2 Synthetic AMPs

Though naturally occurring AMPs have respectable inherent antimicrobial activity, in addition to the aforementioned limitations, their ability to efficiently eradicate bacteria is limited. These inadequacies have driven additional efforts to enhance AMP potential by strategically engineer pseudo-natural or synthetic AMPs or to incorporate unnatural amino acids into peptide sequences in order to hone the antibacterial activity of AMPs. Herein, some of the great strides made towards the development of synthetic AMPs with enhanced antimicrobial activity, biological stability, and minimized damage to mammalian cells will be discussed.

Oliva *et al* demonstrated the usefulness on the incorporation of unnatural amino acids into synthetic AMPs. In this study cationic AMPs composed of unnatural amino acids resulted in improved resistance to proteolysis and broad spectrum antimicrobial activity.[79] Three peptides were studied in this venture (peptide 1, 2 and 3), which consisted of nine amino acid sequences, containing three lysine residues, two aromatic residues (tryptophan or 2-naphthyl-L-alanine), two cysteine derivatives (a thioether or a disulfide) and the termini of the sequences were capped with 6-aminohexanoic acid residues to protect the peptides from enzymatic cleavage by exopeptidases

(Figure 1.7). All of the peptides exhibited modest MIC values, 1.25-10 µM against Gram negative bacteria and 10 -40 µM against Gram negative bacteria. However, in the presence of serum the MIC values of the peptides containing the disulfide and/or naphthyl residues (peptide 1 and peptide 2) decreased by 4 and 8-fold, respectively, after a 16 h preincubation with serum, which was significantly less than naturally occuring AMPs. Moreover, in contrast, peptide 3, which lacked the disulfide residue completely lost its activity. These results showed that the improved proteolytic stability was attributed to incorporation of the cysteine derivative with the disulfide moiety.[79] Furthermore, this study exemplifies the promise of the use of unnatural amino acid in AMP sequences.

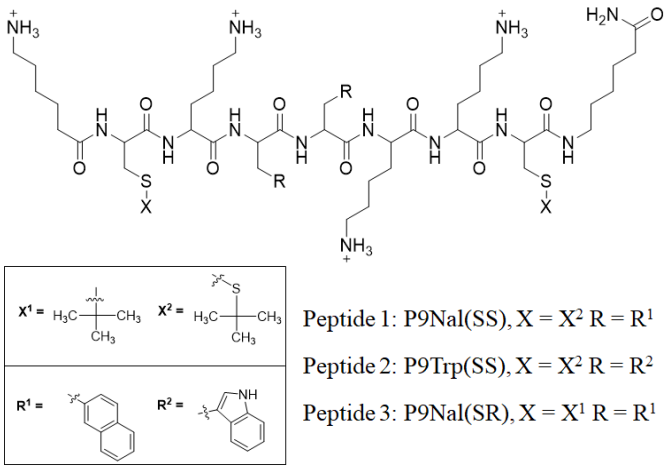

Figure 1.7 Structure of cationic AMPs composed of unnatural amino acids.

Work by the Gellman group has shown that synthetic amphiphilic β-amide copolymers are active mimics of AMPs with the ability to selectively lyse Gram positive and Gram negative bacteria (Figure 1.8A, 3).[80] These polymers were synthesized by ring-opening polymerization of the β-lactam monomers (Figure 1.8A, 1 and 2) that compose the polymer structure. The design of these AMPs focused on the monomers providing the framework for the polymers to conform into an organized amphiphatic structure. In this study it was proposed that the flexible polymers containing cationic (amine side chains) and lipophilic subunits can be induced into amphiphatic structures, unique from the helical structures assumed by amphiphilic AMPs, upon bacterial membrane association (Figure 1.8B). Varying the monomer composition of the copolymers led to polymer 3_{60} (40:60 composition of monomer 1 and 2, respectively) being identified to have

favorable antibacterial activity with minimal hemolytic activity.[80] Thus, in addition to the copolymer being an active AMP mimetic, this study also shows that a balance of hydrophobic and hydrophilic subunits is also critical for favorable antimicrobial activity, as described previously with natural AMPs. Furthermore, studies involving large unilamellar vesicles (LUVs) showed that 3_{60} effectively disrupted LUVs that mimic bacterial membranes, but not LUVs that mimic red blood cells (RBCs). It was also found that polymer 3_{60} had comparable MICs to widely studied host-defense peptides, magainin 2, cecropin A, and cecropin B. Overall, the work of Gellman and co-workers validate the potential of synthetic AMP mimics with potent antibacterial activity and selectivity for the disruption of prokaryotic cell membranes.

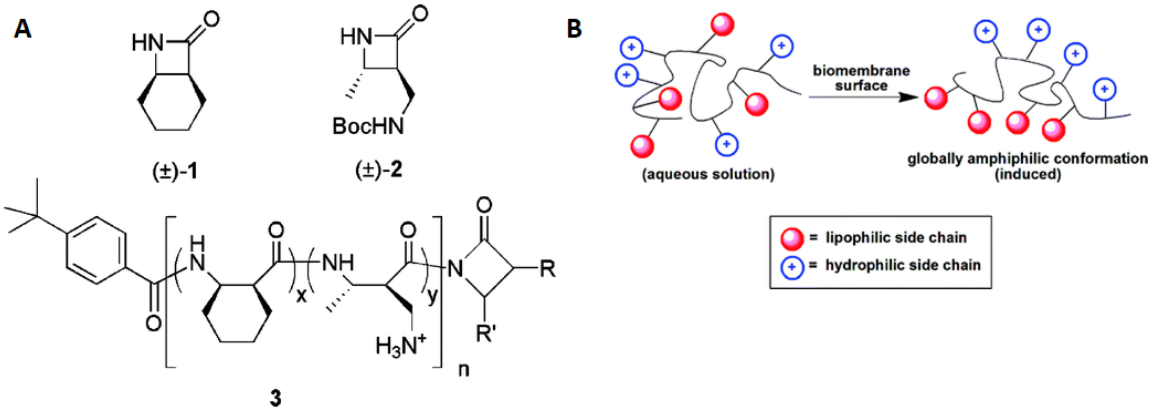

Figure 1.8 A) Monomers, 1 and 2, that compose the antimicrobial copolymer, 3, and B) proposed amphiphilic confirmation of oligomers containing cationic and lipophilic subunits upon bacterial membrane interaction.

In another study, a library of linear peptidomimetic oligomer sequences, called oligo-AKs (OAKs), consisting of alternating acyl chains and cationic amino acids (lysine) were designed and tested. The linear peptidomimetics prevented the formation of stable secondary structures and were shown to be active against Gram-negative bacteria. Of this library the oligomer that displayed the most potent MIC of all the compared OAKs against *E. coli* (3.1 µM), *P. aeruginosa* (6.2 µM), methicillin-resistant *S. aureus* (50 µM), *B. cereus* (12.5 µM) was pursued further, called $C_{12}K\text{-}7_{\alpha 8}$ (Figure 1.9A). $C_{12}K\text{-}7_{\alpha 8}$ showed stability in mouse and human plasma and maintained its MIC against *E. coli* after 3 h pre-incubation with plasma and only showed a 2-fold increase after 6 h, unlike the control AMP (S4), which exhibited a significantly increased MIC in the presence of plasma (Figure 1.9B).[81] These results suggest that $C_{12}K\text{-}7_{\alpha 8}$ was able to resist proteolytic

components that exist in plasma that reduce the bioavailability of conventional AMPs. These data demonstrate that OAKs, like other peptidomimetics, overcome limitations that hinder the therapeutic utility of conventional AMPs, such as, proteolysis and subsequent bioavailability.

A

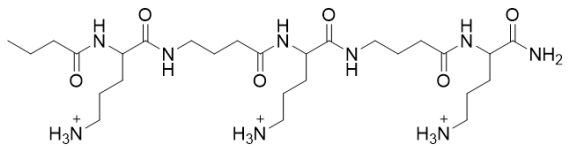

B

MIC (μM) against *E. coli*			
AMP	No Plasma	3 h incubation with plasma	6 h incubation with plasma
$C_{12}K\text{-}7\alpha_8$	3.1	3.1	6.2
S4(1-16)	3.1	> 50	>50

Figure 1.9 A) structure of OAK, $C_{12}K\text{-}7_{\alpha 8}$ and B) MICs of $C_{12}K\text{-}7_{\alpha 8}$ and control AMP, S4(1-16), before and after pre-incubation in 50% murine plasma.

DeGrado and co-workers were also able to demonstrate the benefits of incorporating characteristics of AMPs (cationic nature, amphiphilicity, stable secondary conformation) in the engineering of a generation of AMP mimetic, synthetic aryl amide oligomers with negligible cytotoxicity.[82-84] In their work on acrylamide oligomers, they found that by varying the appending residues to adjust the overall charge, hydrophobicity, and hydrophobic moment, the molecules showed good antibacterial activity and selectivity for lysis of vesicles that mimic bacterial membranes. Of the compounds tested in this series, 4 displayed the most hydrophobic substituents and showed good activity against *E. coli* and *S. aureus* with an MIC of 6.25 μg/mL (Figure 1.10). However, 4 also was most toxic towards human erythrocytes. By contrast, the introduction of more polar substituents led to compound 8, which had the most favorable activity of this series with an MIC of 6.25 and 12.5 against *Escherichia coli* and *Staphylococcus aureus*, respectively, and the disposition of no hemolytic activity (Figure 1.10).[83] Since these initial studies, Degrado's work on peptidomimetic oligomers has expanded to alter the structural and physicochemical properties of aryl amide foldamers, such as implementing conformational restrictions, to achieve enhanced activity and minimal toxicity at the *in vivo* level.[82, 84, 85]

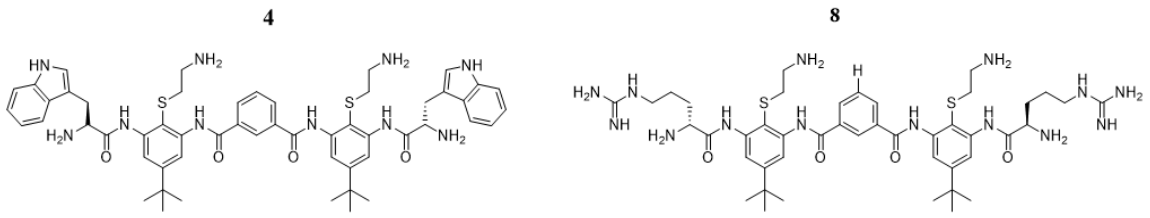

Figure 1.10 Structures of peptidomimetic acrylamide oligomers.

Overall, natural AMPs have set the foundation for peptide antibiotics and have enabled the pursuit of synthetic AMPs, which can be engineered to encompass the best characteristics for the utilization of peptides as potent, alternative antibiotics. To promote a future where AMPs have potential as antibacterial therapies, further investigation must be conducted in order to strategically engineer peptides with potent antimicrobial activity. This will aid in the rational implementation of AMP characteristics required for optimal treatment of bacterial infections. By implementing preferential features into AMP designs we can catalyze the future success of AMPs as therapeutic agents to circumvent the current bacteria crisis.

1.3 Cationic Amphiphilic Polyproline Helices (CAPHs)

A novel class of cell penetrating, antimicrobial peptides have been developed in the Chmielewski lab that mirror the best properties of AMPs and cell penetrating peptides. Cationic amphiphilic polyproline helices (CAPHs) were engineered to serve as a dual agent that is able to penetrate mammalian cells to be intracellularly delivered as a potent antibiotic. This has allowed the targeting of intracellular bacteria. A critical property implemented into the CAPHs design was its cationic, amphiphilic nature, which is a fundamental property in the most potent CPPs and AMPs. Additionally, PrAMPs, which are also found to be rich in proline residues, served as inspiration in CAPHs design as well. These combined features have resulted in a polyproline scaffold comprising the backbone of CAPHs, which contains functionalized proline derivatives that display hydrophobic and cationic characteristics for ordered amphiphilicity.[86]

1.3.1 Parent peptide CAPHs, **P14LRR**

The most well studied CAPH is the parent peptide, **P14LRR** (Figure 1.11B). The CAPHs sequence was developed to have one unit of the hydrophobic residue (PL, Figure 10A) followed by two of

the hydrophilic residues (P_R, Figure 1.11A), to create a triad repeat along the peptide scaffold. This strategic placement of the proline derived amino acids provides CAPHs with one hydrophobic face and two hydrophilic faces (Figure 1.11C).

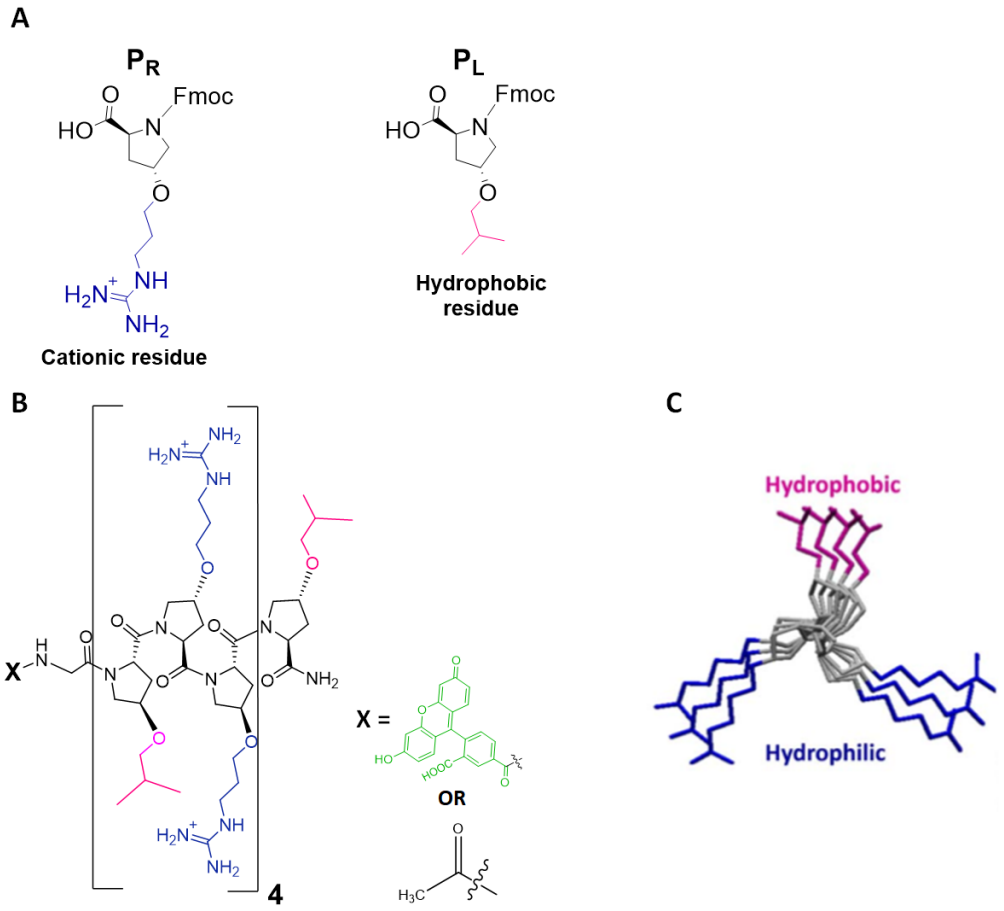

Figure 1.11 (A) Structure of the unnatural, hydroxyl proline derived amino acids used for CAPHs, B the structure of initial CAPHs, P14LRR and (C) top down view of polyproline II helix with the hydrophobic and hydrophilic faces of CAPHs.

Furthermore, in addition to contributing the necessary cationic and hydrophobic residues, the proline derivatives provide CAPHs with a polyproline backbone, which is imperative to achieve a polyproline type II (PPII) left-handed, helical structure (Figure 1.11C). The polyproline scaffold has a 10 Å pitch with three residue per turn with every 4th residue on the same face. A proline scaffold imbues CAPHs with a stable secondary structure and control over the placement of the residues to display a pre-organized secondary structure prior to membrane interaction. Moreover,

by strategically incorporating the desired hydrophobic or hydrophilic residues, P_L and P_R, CAPHs were equipped with a hydrophobic and hydrophilic face for optimal potency. Thus, we were also able to conserve the desired traits of a proline rich peptides (rigidity, stability, solubility, and control of amino acid placement) while achieving a short, ordered peptide sequence to be a potent CPP and AMP.

1.3.1.1 Activity of parent peptide, **P14LRR**

Peptides composed of variations of natural proline and arginine amino acids or lacking the P_L monomer, were used to examine the efficacy of the P14LRR sequence. These studies showed that higher cell internalization is achieved by P14LRR in comparison to the peptides lacking one or both of the functionalized proline residues (Figure 1.12A). Additionally, when P14LRR was tested against pathogenic bacteria it displayed minimum inhibitory concentrations (MIC) against bacteria with values at low micromolar levels (Figure 1.12B). The peptide analogues were much less potent than P14LRR.[86] Thus, without the PPII helix formation provided by the proline backbone (Fl-PRR)$_4$ or the hydrophobicity provided by P_L (Fl-PP$_R$P$_R$)$_4$, the activity shown by P14LRR is unattainable through use of natural arginine and proline residues.

A

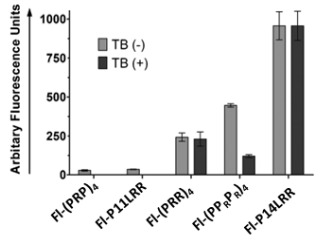

B

Peptide	E. Coli MIC (μM)	S. aureus MIC (μM)
Fl-$(PRP)_4$	>100	>100
Fl-$(PRR)_4$	40	20
Fl-$(PP_RP_R)_4$	60	>100
Fl-P11LRR	60	60
Fl-P14LRR	4	12
Melittin	4.6	2.1

C

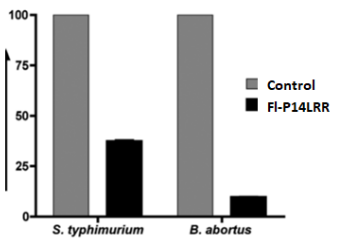

Figure 1.12 (A) Cell uptake of P14LRR compared analogous peptides, (B) MIC's of P14LRR (highlighted) and the peptide analogues against *E. coli* and *S. aureus*, (C) Activity of P14LRR against *Salmonella* and *Brucella*

With confirmation that P14LRR demonstrated successful cell penetration and antimicrobial activity, its ability to eradicate intracellular bacteria was evaluated (Figure 1.12C). He results of these studies showed that P14LRR cleared up to 60% of intracellular *Salmonella* about 90% of intracellular *Brucella* from macrophage cells.[86]

1.3.2 Efforts to optimize CAPHs

Investigations to hone CAPHs cell penetrating and antibacterial action have resulted in a series of strategically modified CAPH with the following modifications: varying peptide length[86, 87], CAPHs dimerization[88], utilizing CAPHs as a dual drug delivery vector[28, 89], and incorporating different hydrophobic motifs into CAPHs structure.[90] Herein the role of extending CAPH length and the use of hydrophobic modifications will be discussed.

1.3.2.1 Activity of extended and truncated CAPHs

As aforementioned, the parent peptide P14LRR has a total of four repeating triad units. By increasing the helical length of CAPHs to five repeating triads (P17LRR) insights were obtained on how peptide length effects CAPHs activity (Figure 1.13A).[86, 87] Increasing the number of triad repeats in CAPHs to form P17LRR, substantially increased mammalian cell accumulation and antibacterial activity was observed. P17LRR had a 2.5- to 3.5-fold greater cell accumulation than P14LRR at concentrations ranging from 5 to 25 μM.[87] In addition to enhanced mammalian cell uptake, by extending CAPHs, P17LRR also demonstrated improved antimicrobial activity relative to P14LRR. P17LRR showed a 4 to 8-fold increase in antimicrobial activity against pathogenic isolates. Against *S. enteritidis*, *L. monocytogenes*, and *A. baumannii* P17LRR had MIC values of

4, 4, and 8 micromolar, respectively. Additionally it was twice as potent as P14LRR in clearing bacteria *in cyto* from infected macrophage cells (Figure 1.13B).

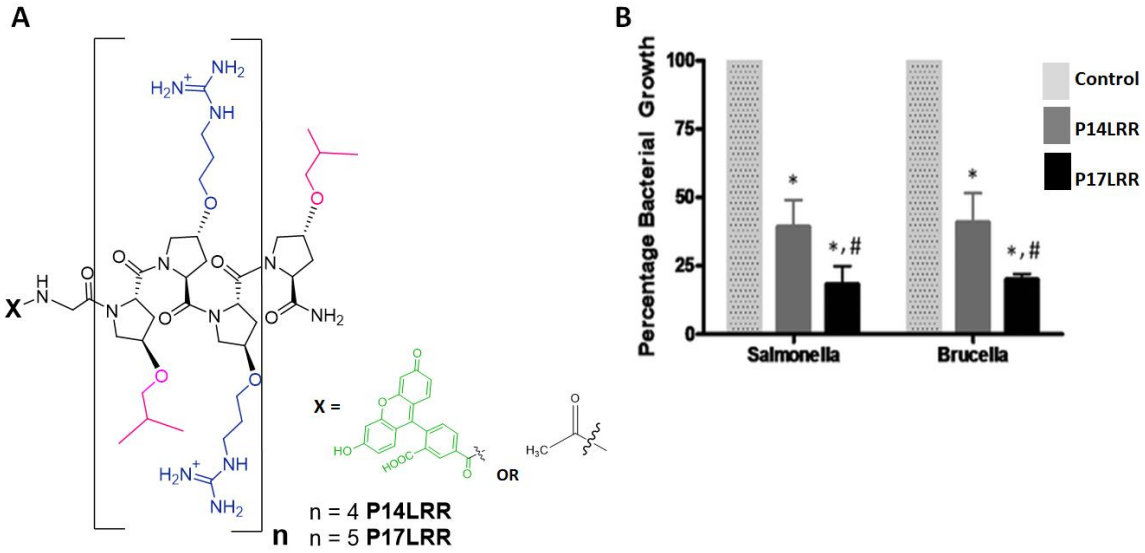

Figure 1.13 (A) Structure of CAPHs with 4 and 5 triad repeats, (B) *In cyto* activity of P17LRR as compared to P14LRR in clearing infected J774A.1 macrophage cells.

1.3.2.2 Exploring hydrophobic group modifications within CAPHs

Further investigations explored the effect of different hydrophobic motifs on CAPHs activity. Previously, a benzyl modified hydroxyproline was used in place of P_L in CAPHs, which resulted in a differences in cell uptake efficiency depending on cell type. CAPHs expressing the benzyl moiety were more readily taken up by HeLa cells as compared to P_L expressing CAPHs, however, the opposite result was observed in MCF-7 cells where P_L expressing CAPHs had higher cell uptake than benzyl expressing CAPHs.[91] More recently, a library of CAPHs was developed, in which nine different hydrophobic moieties replaced the isobutyl group of CAPHs (Figure 1.14). By using a modular synthetic approach on resin, a CAPHs library was created that incorporated different hydrophobic groups into short (3-triad repeats, P11) and standard (4-triad repeats, P14) peptide lengths.

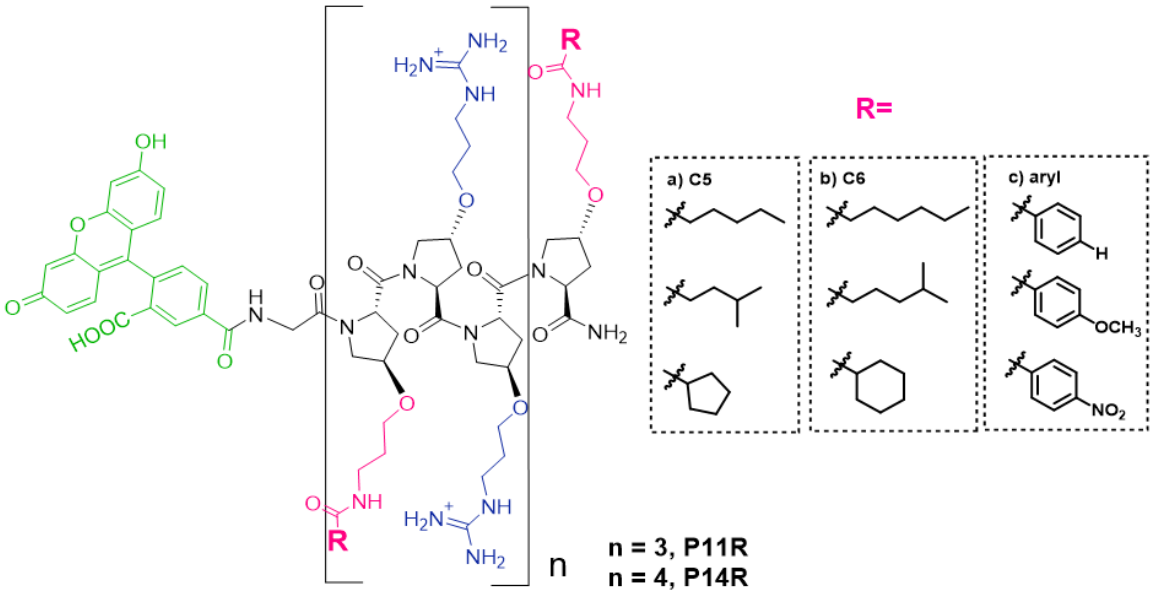

Figure 1.14 CAPHs with hydrophobic group modification where R represents the hydrophobic group incorporated into CAPHs.

After screenings for cell toxicity and cell uptake, three peptides were identified that showed great promise to improve CAPHs activity: P14-5B (branched), P14-5L (linear), and P14-5C (cyclic) five-carbon aliphatic systems (Figure 1.15). The performance of the selected hydrophobic group modified CAPHs (P14-5R) showed improved cell uptake in following order: P14-5L > P14-5B > P14LRR ≥ P14-5C.[90] To summarize, P14-5R CAPHs had comparable or 2 to 3-fold greater cell accumulation than P14LRR and had 5 to 7-fold higher uptake than their equivalent P11-5R CAPHS. Additionally, P14-5C had the least amount of cell accumulation.[90] Hence, the structural configuration of the hydrophobic groups also has an effect on cell uptake activity as well.

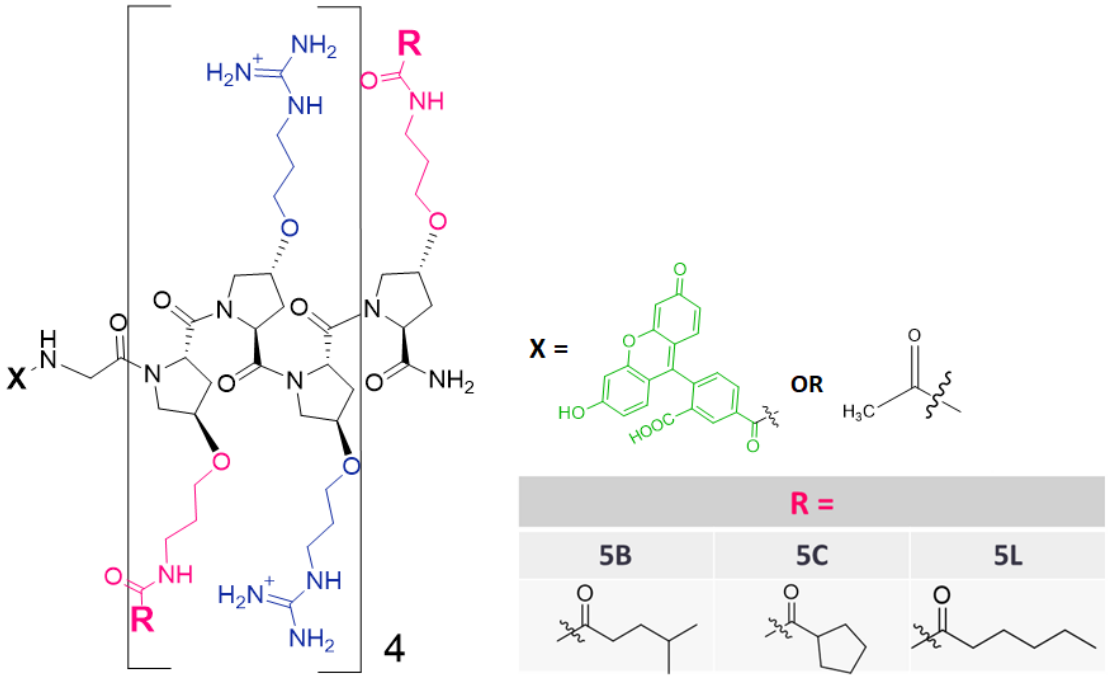

Figure 1.15 Structure of selected P14-5R CAPHs.

Further investigation found that the P14-5R CAPHs did not show consistently improved antibacterial potency against bacterial isolates in comparison to P14LRR. In the tested isolates *Salmonella*, *Listeria*, and *Shigella*, the P14-5R CAPHs were within 2 to 4-fold of the MIC value of P14LRR (Table 1.8).

Table 1.8 MIC values of P14-5R CAPHs against pathogenic bacteria isolates

MIC (μM)			
Compound	Bacteria Isolate		
	Salmonella (Gram negative)	Listeria (Gram-positive)	Shigella (Gram-negative)
P14LRR	32	8	8
P14 -5L	16	16	8
P14-5B	16	32	16
P14-5C	16	32	8

For *in cyto* experiments the P14-5R CAPHs showed significantly better clearance of bacteria from the infected J774A.1 macrophage cells than P14LRR (Figure 1.16). Even though P14-5C had comparable cell uptake ability as P14LRR it is more potent *in cyto*, which can be attributed to its

greater potency against the *Salmonella* isolate.[90] The activity of the different CAPHs analogues demonstrate that enhanced cell uptake subsequently leads to improve *in cyto* antibacterial activity, although, the potency against bacterial isolates can be improved.

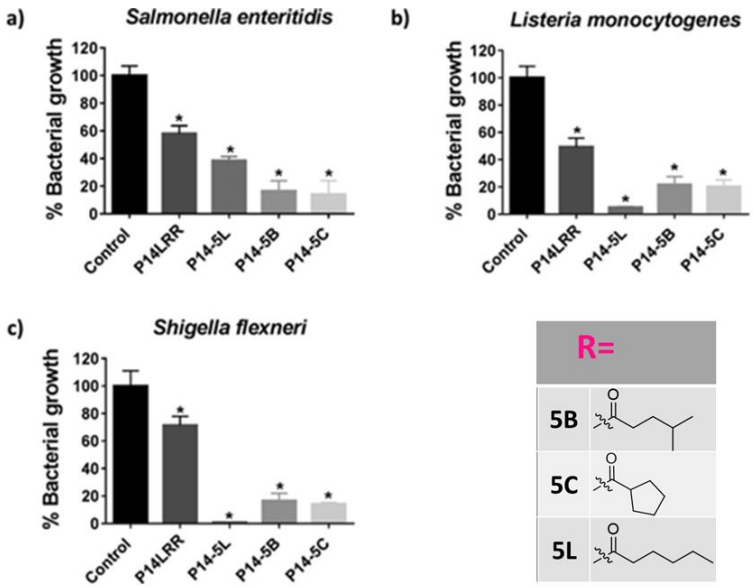

Figure 1.16 *In cyto* activity of P145R peptides compared to P14LRR in clearing infected macrophage cells.

1.3.3 Subcellular niche of CAPHs

Localization within J774A.1 macrophage cells is essential for the ability of CAPHs to interact with intracellular pathogens. Thus, the subcellular fate of the different CAPHs analogues has been determined through confocal microscopy. At a concentration of 15 µM, P14LRR localized with endosomes, but also demonstrated localization with mitochondria, showing that CAPHs are not limited by endosomal entrapment. Furthermore, the subcellular location of CAPHs was found to be concentration dependent, in which lower concentrations (below 10 µM) led CAPHs to take on a greater endosomal localization, and higher concentrations (above 10 µM) resulted in more mitochondrial localization. Altering the helical lengths of CAPHs from P11LRR to P17LRR impacts the subcellular niche of CAPHs at 15 µM, with the shorter peptide showing more endosomal entrapment and extended lengths led to greater mitochondrial localization.[86, 87, 92] Finally, changing the hydrophobic group of P14LRR from the isobutyl group of P_L to 5B, 5C or 5L in the P14-5R series changed the subcellular niche of CAPHs. P14-5B and P14-5L were found

within the cytoplasm and had some endosomal localization, whereas P14-5C resulted in solely endosomal localization.[90] Thus, the hydrophobic motif plays a critical role in the subcellular niche of CAPHs. Overall, these efforts have identified characteristics that are beneficial to enhancing CAPHs activity.

1.3.4 CAPHs mode of action

Recognizing that AMPs are capable of using an array of mechanisms of action, studies were performed to determine if CAPHs display a lytic mode of action against bacteria. The β-galactosidase release assay was used with *E. coli* to examine if the antibacterial activity of CAPHs was a result of cell lysis. Through these studies, none of the CAPH peptides we developed thus far showed any lytic behavior at their MIC concentrations. However, in the case of the P14-5B and P14-5L, at concentrations four times their MIC values bacterial lysis is observed. This suggests that lysis is not their primary mode of action, but may act at high peptide concentrations.

The lack of lytic behavior observed at CAPHs MIC values has prompted investigations to identify the bactericidal target of CAPHs. After exposure of biotinylated P14LRR to lysates of *E. coli* and *S. aureus* a protein-biotin pull-down assay was used and identified glycerol dehydrogenase and enolase, respectively, as two target of CAPHs. Enolase is responsible for converting 2 phosphoglycerate into phosphoenolpyruvate in the glycolysis cycle and glycerol dehydrogenase is responsible for the oxidation of glycerol into dihydroxyacetone. More importantly, both proteins are essential components of physiological metabolic processes to produce energy that is required for organism function. With this discovery, enolase was further confirmed as the target of P14LRR against *S. aureus* by demonstrating that the addition of a substrate of enolase, sodium pyruvate, in the presence of P14LRR resulted in a 2-fold higher concentration of P14LRR required to kill the bacteria. Additionally, when enolase deficient *S. aureus* was treated with P14LRR the MIC was 2-fold lower due to the enolase lacking bacteria being easier to kill. Combined, these studies support that enolase is inhibited by P14LRR and is a target of P14LRR.[93]

1.4 Conclusions relating to CAPHs development

CAPHs are a novel class of antibiotics that are dual antibacterial agents with cell penetration and antibiotic activity for efficient eradication of intracellular bacterial infections. Key features of

AMPs and CPPs were incorporated into the CAPHs design, which are continuously being explored in order generate CAPHs with further enhanced activity. Thus far, an optimal helical length and ideal hydrophobic parameters that provide the best activity have been identified. Along with minimal mammalian cell toxicity, the strides made thus far for the enhancement of CAPHs have brought these agents closer to reaching their potential as a novel cell penetrating AMPs.

CHAPTER 2. EXTENDED AND HYDROPHOBIC MODIFIED CAPHS FOR ENHANCED ACTIVITY

2.1 Introduction

The plasma membrane serves as a barrier, making the interior of the cell inaccessible to many therapeutics, which results in reduced or no drug accumulation at the subcellular level. This is problematic in the case of therapeutics that lack the ability to penetrate cell membranes, thereby limiting their therapeutic potential.[94] Fortunately, drug delivery vectors, such as cell penetrating peptides (CPPs), have provided a means to overcome this obstacle. CPPs have been of great interest due to their ability to cross cellular membranes and have been utilized to carry cargo into cells with minimal toxicity.[94-96] Since the discovery of the first CPP, Tat, over 30 years ago, a variety of CPPs, natural and synthetic, have been discovered and utilized for drug transport and to enhance the bio-distribution of deliverable cargoes.[28, 95, 97, 98]

Generally, CPPs are characterized as short, cell permeating peptides, with a maximum of 30 amino acids.[96, 99] However, in addition to this general description there is considerable variability among CPPs. The diversity of CPPs is attributed to differences in physical properties, such as amino acid composition, cationic, hydrophobic or amphiphilic nature, and secondary structure.[94] Cationic CPPs, like Tat and Arg-rich peptides, are some of the most well-studied CPPs,[100-102] although, the majority of CPPs are classified as amphiphilic, like transportan and penetratin, in which the peptides have a high content of both polar (typically cationic) and non-polar residues.[103-105] Cationic, amphiphatic CPPs are typically composed of positively charged residues, like lysine and arginine, with arginine deemed to be the superior choice for cell uptake.[106, 107] This is because the guanidine head group of arginine is a critical component of membrane interaction due to its ability to form bidentate hydrogen bonds with H-bond acceptors (anionic lipids) on the cell surface and its capacity to maintain its charge within the membrane.[108, 109]. Furthermore, in addition to the contribution of the cationic amino acids, the impact of hydrophobic residues, such as tryptophan and leucine, have also been studied and have demonstrated that there is a hydrophobicity threshold to achieve desirable CPP activity.[110-112] Lastly, amphiphatic CPPs are classically found to obtain ordered secondary structures; helices or β-sheets, which plays a significant role in CPP activity.[113, 114] An intrinsic characteristic of the more popular, helical amphiphatic CPPs is that the amino acids

can align to reveal a hydrophobic and hydrophilic face along the helix scaffold.[103 105, 115] Overall, this summarizes key structural components that promote CPP's membrane interaction for efficient cell uptake.

The structural diversity of CPPs leads to differences in cell uptake mechanisms through two major pathways: energy dependent endocytosis or energy independent direct transport.[96, 116] Subclasses of endosomal cell entry include receptor-mediated endocytosis and macropinocytosis.[117, 118] Alternatively, direct transport cell uptake subcategories include inverted micelle formation, the carpet-like model, barrel stave model, and toroidal pore formation.[118]. To further highlight the dynamics of CPP cell uptake, CPPs, such as Tat, may utilize simultaneous or competing modes of cell entry in which, the more favored mechanisms of cell uptake depend on peptide sequence, peptide concentration, cell type, and experimental conditions.[94, 119-122] Furthermore, multiple studies have demonstrated that CPPs can accumulate in a variety of subcellular compartments, including the mitochondria, nuclei, and endosomes, based on their mode of cell entry.[92, 96, 102, 116, 123-125] Work by Kelly and co-workers have demonstrated potentiated antimicrobial activity of methotrexate (Mtx), a bacteriostatic agent, by synthesizing a Mtx-peptide conjugate for targeted mitochondria delivery to clear intracellular *L. monocytogenes*.[125] Thus, it is beneficial to consider the possible outcomes of cell penetration with CPPs in order to achieve efficient intracellular delivery of therapeutics.

Due to many antibiotics lacking cell penetrating abilities, intracellular bacteria, bacteria that reside within mammalian cells, present a major challenge pertaining to intracellular drug delivery. Some bacteria that have the tendency to take intracellular refuge include *Mycobacterium tuberculosis*, *Listeria monocytogenes*, and *Salmonella enteritidis*. ESKAPE pathogens, such as *Staphylococcus aureus* and *Klebsiella pneumoniae*, have also been found to take intracellular residence.[126] These bacteria infect both phagocytic cells, such as macrophages, and non-phagocytic cells, such as epithelial cells, evade eradication by disrupting the host's innate immune response, and find refuge in different subcellular compartments, which vary among the classes of bacteria.[127-130] This provides intracellular bacteria an environment where they can thrive and survive, which can result in chronic and/or recurring infections.[20, 131]

Of the intracellular pathogens, *Mycobacterium tuberculosis* (TB) is one of the most devastating and persistent pathogenic bacteria. In the year 2017, TB was the cause of 10 million infections and more than 1 million deaths worldwide.[132] TB is able to evade the host immune response post-phagocytosis by shutting down the phagocytic pathway to form TB containing vacuoles.[133] TB is then able to persist by proliferating inside the cell or by becoming latent (non-replicative and below detectable limits), which allows the opportunistic infection to resurface after termination of antibacterial therapy.[134] Enteric pathogen, *Salmonella*, and ESKAPE pathogens *Staphylococcus aureus* and *Klebsiella pneumoniae* also reside in phagosomes by arresting the phagosomal process before or after the lysosome fusion stage.[27, 135] In all cases, the bacteria either remain dormant or replicate in these vacuoles for continued pathogenesis. Examples of bacteria with different subcellular niches are *Listeria* and *Shigella*. Upon phagocytosis, they lyse the phagosome to escape into the cell cytoplasm and sequester actin filaments for cell motility to spread infection.[136-138] These examples identify mammalian cells as havens for active and latent bacteria with protection from antibacterial agents. Thus, it is essential for antibiotics to be able to enter mammalian cells to target bacteria beyond the cell surface for efficient clearance of bacterial infections.

To address the dire need for novel antibiotics with effective cell penetration and antimicrobial activity, we have developed cationic amphiphilic polyproline helices (CAPHs).[139] These combined characteristics make CAPHs dual agents that are able to act as both potent antibiotics and drug delivery vehicles for the treatment of intracellular bacterial infections.[28, 92, 139, 140] We have sought to push these boundaries so that CAPHs may have a broader collection of cellular compartments that they are able to reach in order to target the widest possible range of bacteria dwelling within cells.[87, 90, 141] Despite the great strides made thus far by CAPHs toward the treatment of intracellular bacteria, there remains room for improvement. In an effort to maximize the potency of our CAPHs, we have now opted to combine the best features of extended length CAPHs with promising hydrophobic groups.

2.2 **Fl-P17-5R** CAPHs: Design

CAPHs are a class of peptides developed in the Chmielewski lab that have been shown to have both cell penetration and antimicrobial activity to target intracellular bacteria (Figure 2.1A).[87, 90, 139] This activity is attributed to their rigid polyproline backbone, which allows the controlled

placement of the amino along the polyproline type II helix, due to the conformational requirement of three residues per turn (Figure 2.1B). This allows for a repeating triad of a hydrophobic face and two hydrophilic, cationic faces on the CAPH peptides (Figure 2.1C).

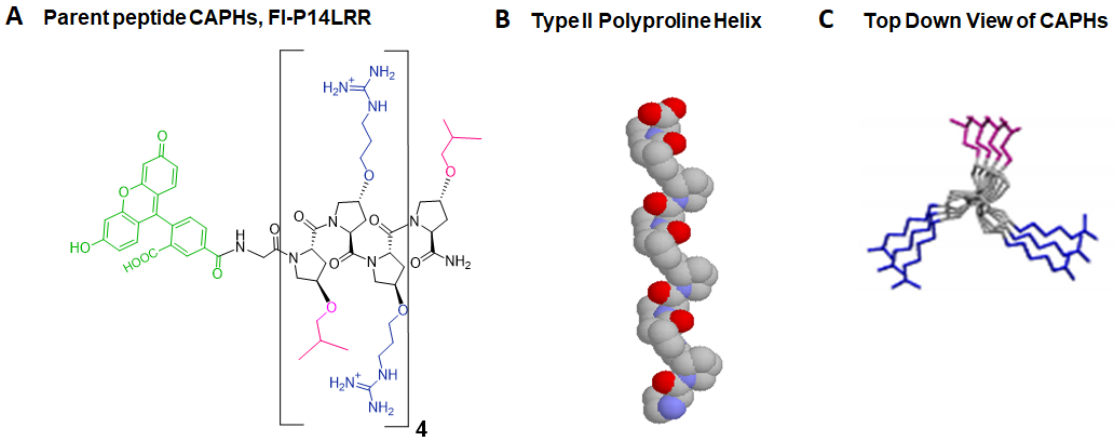

Figure 2.1 (A) Structure of typical CAPHs with fluorescein coupled to its N-terminus. (B) The secondary structure of CAPHs, a type II polyproline helix, provides specific amino acid placement resulting in (C) a distinct, repeating arrangement of hydrophobic (pink) and hydrophilic, cationic (blue) faces.

As an extension of our previous studies, we sought to further improve the potency of CAPHs by simultaneously increasing the length of the polyproline backbone while incorporating different hydrophobic groups. It has been established that CAPHs with five triad repeats (P17LRR) instead of four triad repeats (P14LRR) has enhanced cell penetration as well as antimicrobial activity.[86, 87] Additionally, a library approach was utilized to identify three hydrophobic modifications that provided the parent CAPHs, P14LRR, with promising activity: aliphatic 5-carbon cyclic (5C), branched (5B), and linear motifs (5L).[87, 90] Based on these features, we developed a P17 series of CAPH peptides with the identified hydrophobic groups, **Fl-P17-5R** (Figure 2.2).

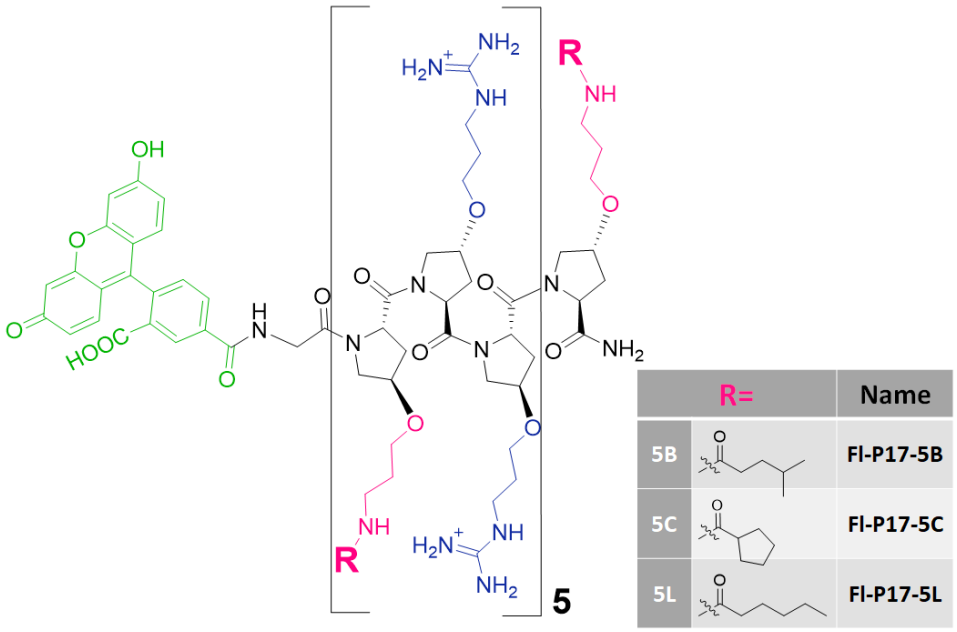

Figure 2.2 Structure of **Fl-P17-5R** CAPHs with fluorescein at the N terminus. R represents the different hydrophobic groups incorporated into the structure.

2.3 Synthesis of **Fl-P17-5R** peptides

The **Fl-P17-5R** CAPHs peptides are composed of two monomers, Fmoc-$P_R(Boc)_2$ and Fmoc-P_K(Mtt) (Figure 2.3). P_R provides the cationic characteristic of CAPHs and P_K provides the primary amine to selectively incorporate the hydrophobic group modification. Formerly, the hydrophobic and cationic group of the amino acid monomers of CAPHs were incorporated through formation of an ether linkage on the hydroxyproline residue.[139] Taking this same route to incorporate different hydrophobic groups, however, would require the synthesis of three different hydrophobic amino acids, which would have been an unnecessarily tedious task. Therefore, for maximum efficiency, we took a modular approach for the synthesis of this series of CAPH peptides. The synthesis of the **Fl-P17-5R** monomers, Fmoc-$P_R(Boc)_2$ and Fmoc-P_K(Mtt), involved an identical synthetic pathway for the two amino acids, until deviating at the final step. Additionally, we were able to selectively remove the Mtt protecting group of Fmoc-P_K(Mtt) while the peptide remained on the solid support during peptide synthesis. This allowed the resulting free amines to be modified through amide bond formation with the carboxylic acid version of the desired hydrophobic motif.

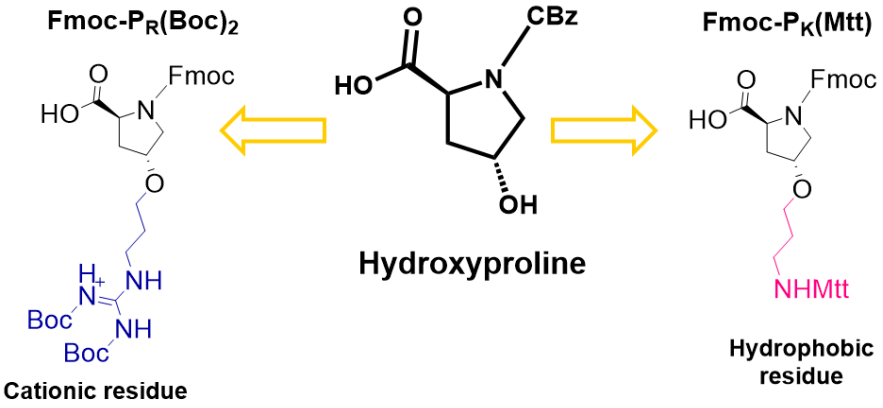

Figure 2.3 **Fl-P17-5R** CAPH monomers with protecting groups, Fmoc-P_{KMtt} and Fmoc-$P_R(Boc)_2$, derived from hydroxyproline.

2.3.1 **Fl-P17-5R** Monomer Synthesis

In detail, the synthesis of the peptide monomers began with the same amino acid precursor, benzyloxycarbonyl (Cbz) protected hydroxyproline. The hydroxyl group of the hydroxyproline was functionalized to form an ether linkage through a Michael Addition with acrylonitrile to produce product 1. The carboxylic acid of 1 was benzyl protected using benzyl bromide to yield product 2. Next, the nitrile group of 2 was reduced to a primary amine with *in situ* protection with tert-Butyloxycarbonyl (Boc) providing product 3. Palladium catalyzed hydrogenation removed the Cbz and benzyl protecting groups from 3, followed by amine protection with fluorenylmethyloxycarbonyl (Fmoc) to yield 4. Lastly, the Boc protecting group was removed under acidic conditions using trifluoroacetic acid (TFA) to yield a free primary amine, which was either protected with 4-methyltrityl (Mtt) to form Fmoc-P_K(Mtt) or functionalized with N,N′-di-boc-1H-pyrazole-1-carboxamidine to form Fmoc-$P_R(Boc)_2$ (scheme 2.1).

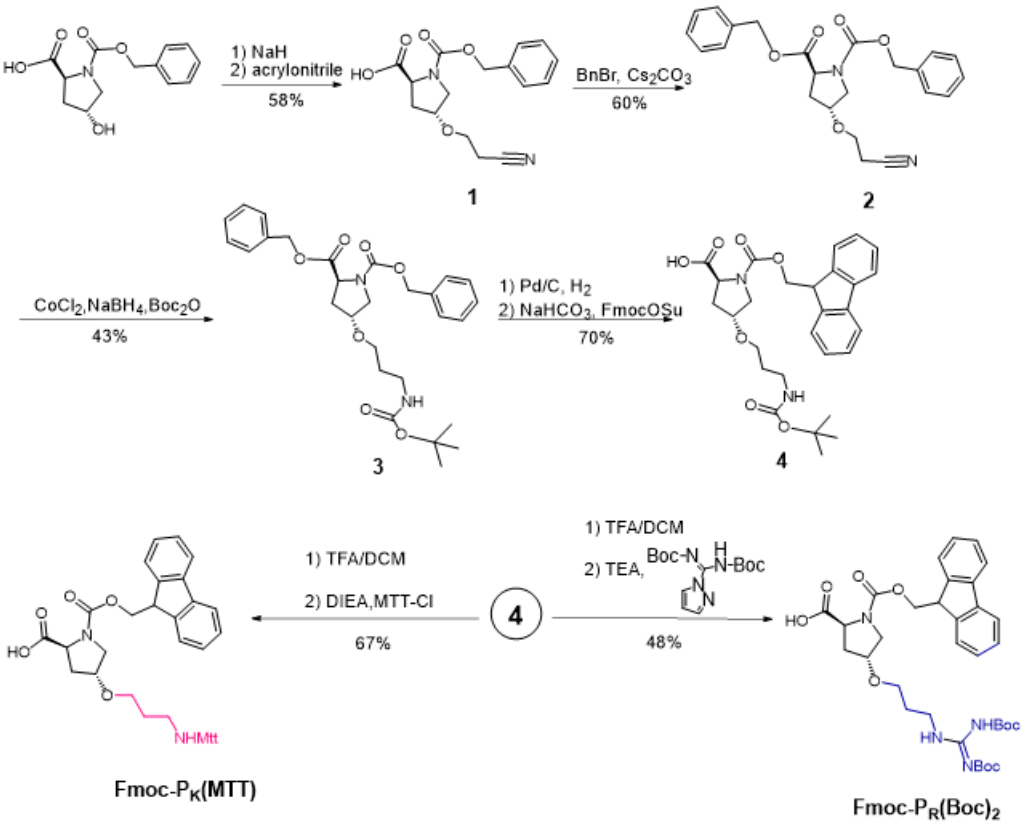

Scheme 2.1 The modular synthesis of Fmoc-P_K(Mtt) and Fmoc-P_R(Boc)$_2$.

2.3.2 **Fl-P17-5R** Peptide Synthesis

To obtain the desired resin-bound P17 peptide sequence, we used Fmoc-based solid-phase peptide synthesis with the previously prepared Fmoc-P_R(Boc)$_2$ and Fmoc-P_K(Mtt) amino acids. Upon completion, a fluorescein tag was coupled to the N-terminus of the peptide, after a glycine spacer. The peptide on resin was split into three equal batches, and the Mtt protecting group was selectively removed using 30% hexafluoroisopropanol, followed by treatment with the three activated carboxylic acids on resin (Scheme 2.2). In this way, the synthesis of three different **Fl-P17-5R** peptides was achieved: **Fl-P17-5B**, **Fl-P17-5C**, and **Fl-P17-5L**. The peptides were cleaved from resin using a TFA cocktail and purified to homogeneity using reverse phase HPLC. The desired product mass was confirmed using matrix-assisted laser desorption ionization – time of flight (MALDI ToF) mass spectrometry.

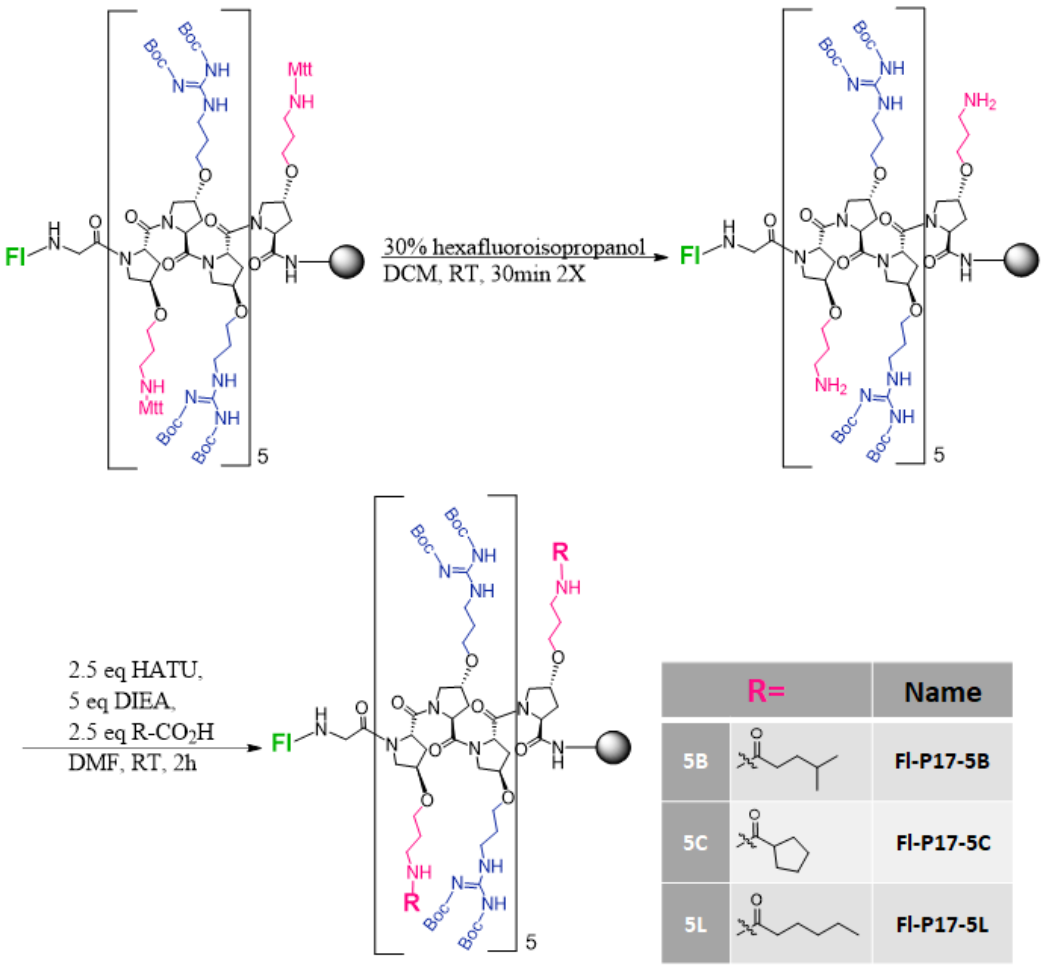

Scheme 2.2 Addition of hydrophobic groups (R) to peptide while on resin to produce desired **Fl-P17-5R** CAPHs.

2.4 Results and Discussion

2.4.1 Quantification of cell uptake

An important factor for the successful eradication of intracellular bacteria is the accumulation of the antibiotic inside the cell. As previously mentioned, some antibiotics may be effective in killing bacteria *in vitro*, but this may not be the case when the bacteria are intracellular due to the antibiotic's inability to successfully transverse the plasma membrane. Hence, cells can act as a refuge for bacteria to escape elimination by antibiotics. As macrophages are among the most common cell types for bacteria to reside, we used J774A1 cells for these studies. Macrophage cells serve as the first line of defense in the innate immune response and can clear bacteria through phagocytic mechanisms. Bacterial infections persist, however, when bacteria are able to evade

phagocytic processes and thrive with host cells.[142] Thus, J774A.1 mammalian (mouse) macrophage cells served as a good models for testing CAPHs activity.

In order to determine if the modifications made to the CAPHs resulted in enhanced intracellular accumulation, we performed cell uptake experiments using flow cytometry. J774A.1 cells were exposed to **Fl-P17-5B, Fl-P17-5C**, or **Fl-P17-5L** at concentrations ranging from 1.25 to 5 µM with a 1 h incubation period, (Figure 2.4A). This revealed that all three peptides were successful in entering the J774A.1 cells with **Fl-P17-5L** having the best intracellular accumulation. **Fl-P17-5L** cellular uptake was about 70% and 40% greater than **Fl-P17-5C** and **Fl-P17-5B**, respectively. The P17-5R peptides had better cell accumulation than their shorter-length P14 counter parts, P14-5B, P14-5C, and P14-5L, (Figure 2.4B). Cell uptake of **Fl-P17-5L** was 5.6-fold greater than Fl-P14-5L, **Fl-P17-5B** was 3.5-fold higher than Fl-P14-5B, and **Fl-P17-5C** was 2.3-fold greater than Fl-P145C at 5 µM concentrations. These data demonstrate that the increased length of CAPHs significantly increases the cell uptake of CAPHs. These results were generally expected since extended CAPHs have previously shown enhanced cell uptake.[87] The fact that the **Fl-P17-5R** CAPHs exhibited greater cell uptake than their shorter analogues, further supports the significance of increasing the cationic charge and number of hydrophobic moieties with CAPHs.

It is also important to mention that the cell uptake of **Fl-P17-5R** CAPHs was compared to Fl-P14LRR and Fl-P17LRR in J774A.1 cells after 1 h incubation at 5 µM (Figure 2.4C). Fl-P17LRR was found to have analogous cell accumulation as **Fl-P17-5B,** and, though **Fl-P17-5C** has the lowest cell uptake of the **Fl-P17-5R** peptides, it had close to 3-fold better cell uptake than Fl-P14LRR, which had the lowest cellular accumulation of all the tested CAPHs. **Fl-P17-5L** continued to show the greatest cell uptake in J774A.1 cells of all the tested CAPHs. These results demonstrate that though the length of CAPHs does play a role in cell uptake, the hydrophobic group present also has an impact on peptide activity.

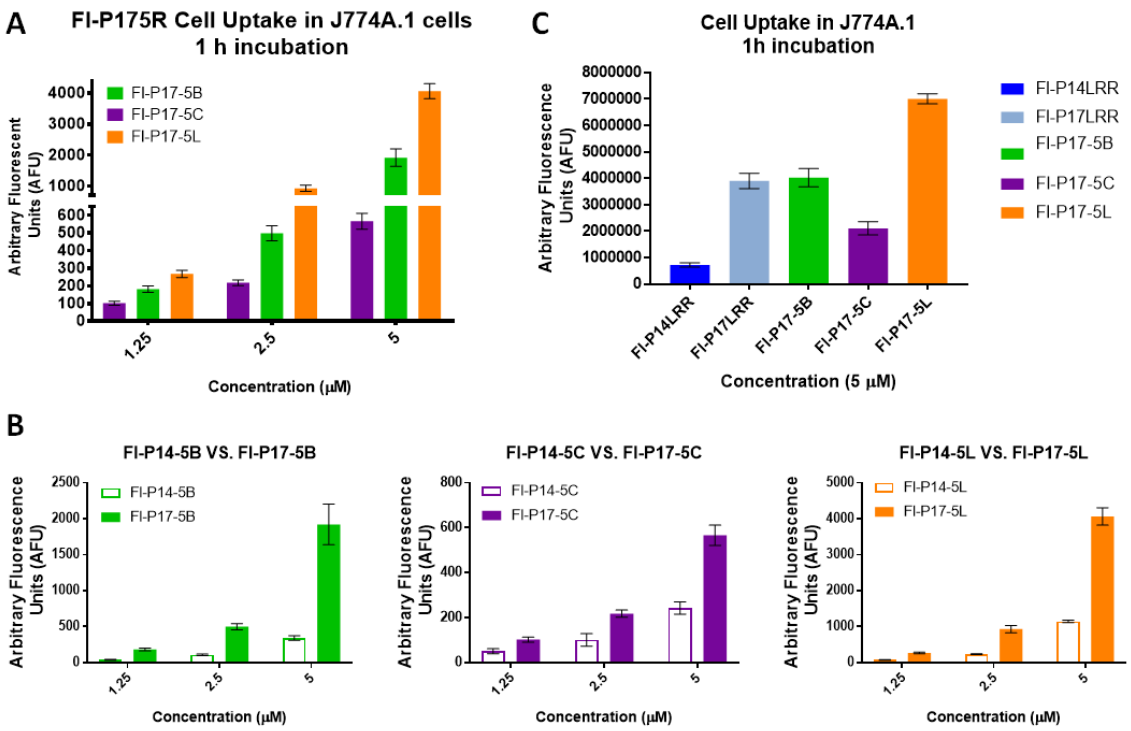

Figure 2.4 (A) Arbitrary cellular fluorescence of **FL-P17-5R** after 1 h incubation in J774A.1 cells. (B) Arbitrary cellular fluorescence comparing Fl-P14-5R cell uptake to **Fl-P17-5R** cell uptake after 1 h incubation in J774A.1 cells. (C) Arbitrary cellular fluorescence comparing Fl-P14LRR, **Fl-P17-5B**, **Fl-P17-5C**, and **FL-P17-5L** at 5 μM after 1 h incubation in J774A.1 cells.

Intracellular infection is also common in other cell types, including skin cells. The skin acts as a barrier for the body from the extracellular environment, but it also plays a role in immunity against bacterial skin infections.[143] When bacteria, such as *S. aureus*, gain intracellular access, they cause persistent percutaneous infection.[144] Taking this into consideration, we wanted to further investigate if the **Fl-P17-5R** peptides could similarly enter keratinocytes (skin cells), the cell type that makes up the majority of the epidermis. HaCat cells are immortalized keratinocytes that have been used in a number of studies regarding *S. aureus* skin infections since they closely resemble normal human keratinocytes.[144-146] In this study HaCat cells were exposed to **Fl-P17-5B**, **Fl-P17-5C**, or **Fl-P17-5L**, at concentrations ranging from 1.25 to 20 μM over a 1h incubation period (Figure 2.5). These data revealed that all three peptides were successful in entering HaCat cells, following the same trend of **Fl-P17-5L** having the best cell uptake. **Fl-P17-5B** and **Fl-P17-5L** at 10 μM had similar cell uptake to Fl-P14LRR at a 2-fold higher concentration. These data further

support that, regardless of cell type, the **Fl-P17-5R** peptides demonstrate substantial cell penetration.

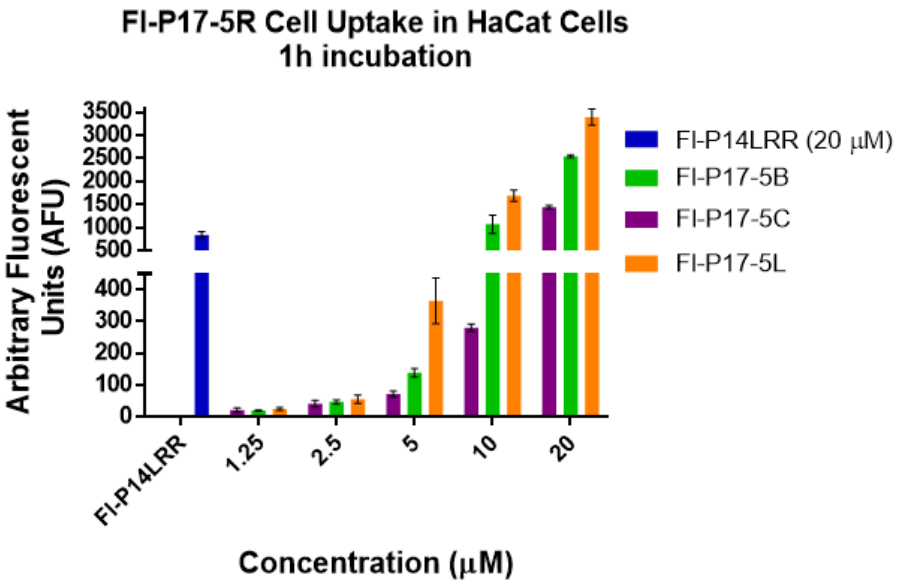

Figure 2.5 Cell accumulation studies of **Fl-P17-5R** in HaCat cells at concentrations ranging from 1.25 µM to 20 µM after 1 h incubation using flow cytometry.

2.4.2 Toxicity evaluation

2.4.2.1 *In cyto* toxicity

We next evaluated the viability of both J774A.1 and HaCat cells in the presence of **Fl-P17-5R** peptides to determine if they displayed cell toxicity using the MTT Assay. The cells were incubated for 9 h in the presence of the peptides at concentrations ranging from 1.25 to 10 µM and 1.25 to 20 µM in J744A.1 and HaCat cells, respectively (Figure 2.6A, 2.6B). The results show that **Fl-P17-5L** was the most toxic of the **Fl-P17-5R** peptides with J774A.1 cell viability decreasing to 59% at 5 µM. **Fl-P17-5C** was the least toxic in J774A.1 cells with equal to or greater than 80% cell viability at all concentrations. This trend was also observed with HaCat cells; **Fl-P17-5L** showed a decrease in cell viability to about 60% at 20 µM, and **Fl-P17-5C** showed the least toxicity with 90% cell viability or better at all concentrations.

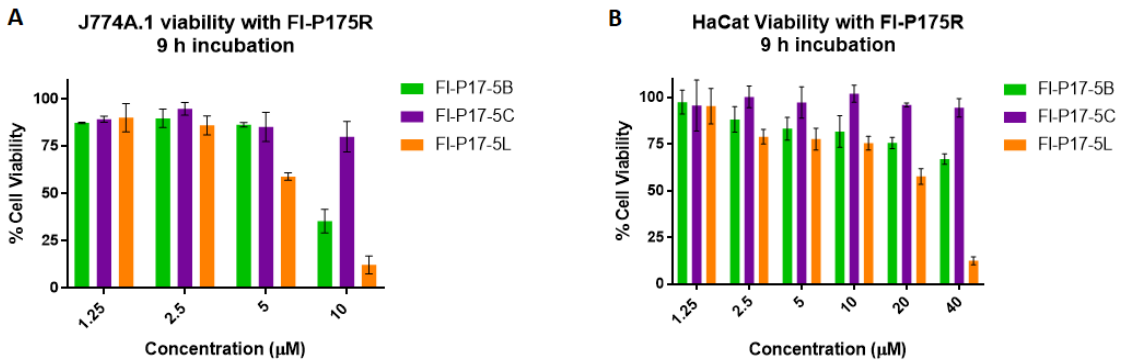

Figure 2.6 Percent cell viability of J774A.1 cells (A) and HaCat cells (B) in the presence of **Fl-P17-5R** CAPHs after 9 h incubation using the MTT assay. Formazan formation was measured by absorbance at 590 nm.

2.4.2.2 Toxicity against human red blood cells (hRBCs)

In addition to determining the cell toxicity of the **Fl-P17-5R** peptides, we were also interested to if they would lyse human red blood cells (hRBCs). One of the drawbacks of AMPs is their potential for toxicity to hRBCs. Many AMPs express bactericidal activity through a lytic pathway, and some AMPs do not show exclusivity towards bacteria and can cause lysis of human cells.[32] Thus, to further elucidate the therapeutic potential of CAPHs it was important to determine if they could be harmful to hRBCs. hRBCs we exposed to the **Fl-P17-5R** peptides for 1 h at concentrations ranging from 1.25 to 40 µM to observe the release of hemoglobin, an indication of hRBC lysis (Figure 2.7). Melittin and Triton X at 0.1% were used a positive controls. The parent peptide, Fl-P14LRR, which has been established to not cause RBC lysis was used as a negative control.[87] It was observed that at all concentrations there was no hemoglobin release from the hRBCs in the presence of the CAPHs peptides. In contrast, melittin began to show lysis at the lowest concentration of 1.25 µM. Hence, **Fl-P17-5B**, **Fl-P17-5C**, and **Fl-P17-5C** have been demonstrated to be non-hemolytic cell penetrating peptides with reasonable cell viability.

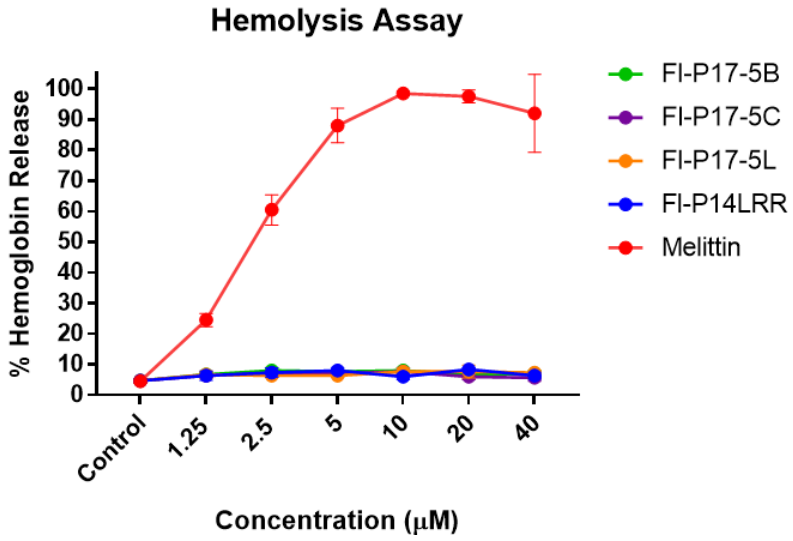

Figure 2.7 Hemolysis assay measuring the hemolytic activity of Fl-P14LRR (blue), **Fl-P17-5B** (green), **Fl-P17-5C** (purple), **FL-P17-5L** (orange) and control melittin (red) after 1h incubation. Percent of hemoglobin release from human RBCs was measured at OD_{405}.

2.4.3 Subcellular localization of internalized CAPHs

One of the difficulties in treating intracellular bacteria is that they differ in cellular locations. For example, *Salmonella* is able to reside in endosomes that become *Salmonella* containing vacuoles (SCV), *Listeria* and *Shigella* are found in the cell cytoplasm by escaping endosomes.[137, 138, 147, 148] With a multitude of possible subcellular locales, it would be ideal to have antibiotics that are able to reach these areas within the cell to effectively eradicate intracellular infections. CPPs uptake can be highly dependent on a number of properties including concentration and routes of internalization.

One route of CPP cell entry is endocytosis, which can be major limiting factor in the bioavailability of CPPs if the peptides are unable to escape the vacuole.[149, 150] Having established that the **Fl-P17-5R** peptides were able to successfully penetrate two cell types with minimal toxicity to the cells at certain concentrations, we then sought to determine their subcellular localization after cell uptake. Using fluorescent confocal microscopy, we visualized the subcellular fate of the **Fl-P17-5R** peptides (Figure 2.8). At 5 μM and after 1 h of incubation with J774A.1 macrophage cells, **Fl-P17-5L** and **Fl-P17-5B** both showed localization throughout the cytoplasm of the cell, nuclear localization, and also some endosomal localization. In contrast, **Fl-P17-5C** was predominantly in

the endosomes of the cell. All three of the **Fl-P17-5R** peptides showed no mitochondrial association. This differed from the subcellular location of both Fl-P14LRR and Fl-P17LRR in that, under these same conditions, Fl-P14LRR and Fl-P17LRR associated mostly with the mitochondria of J774A.1 cells. Mitochondrial localization is common amongst lipophilic cations, so these result show that changing the hydrophobic groups likely has an effect on CAPHs lipophilicity.[151] This difference in subcellular location between Fl-P14LRR, Fl-P17LRR, and the **Fl-P17-5R** series may also be due to a difference in the mechanism of cell accumulation. By increasing the length of CAPHs, in conjunction with replacing the isobutyl hydrophobic group from P_L to either of the three 5-carbon moieties (cyclic, branched, or linear), we found that we were able to reach areas of cells that were unattainable with Fl-P14LRR and Fl-P17LRR. These data show that the subcellular niche is highly dependent on the hydrophobic group present.

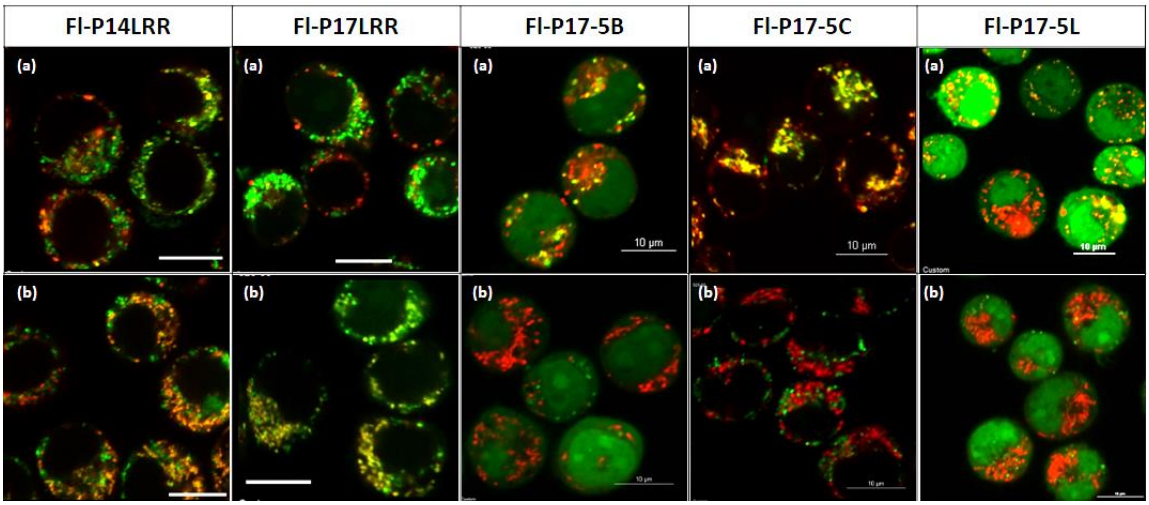

Figure 2.8 Confocal images of J774A.1 cells incubated with Fl-P14LRR, Fl-P17LRR, **Fl-P17-5B**, **Fl-P17-5C**, and **FL-P17-5L** (green) at 5 µM for 1 h. A yellow/orange color, indicative of co-localization, was studied with (a) the endosome tracking dye, Lysotracker (red) and (b) the mitochondria tracking dye, Mitotracker (red).To insert the table, follow these instructions:

With **Fl-P17-5B** and **Fl-P17-5L** showing preference for the cytoplasm and the nucleus, we examined if the subcellular location of **Fl-P17-5C** may become more cytoplasmic with increased incubation time through endosomal escape. Thus, we imaged J774A.1 cells after 3 h incubation with the peptides at the 5 µM concentration (Figure 2.9). Overall, the longer incubation time did little to effect the subcellular preference of CAPHs. Fl-P14LRR and Fl-P17LRR remain mostly

localized with the mitochondria and show little endosomal localization. Also, while **Fl-P17-5C** remained predominately localized with endosome there seems to be a slight appearance of **Fl-P17-5C** in the cell cytoplasm. Still, none of the **Fl-P17-5R** peptides showed significant co-localization with mitochondria.

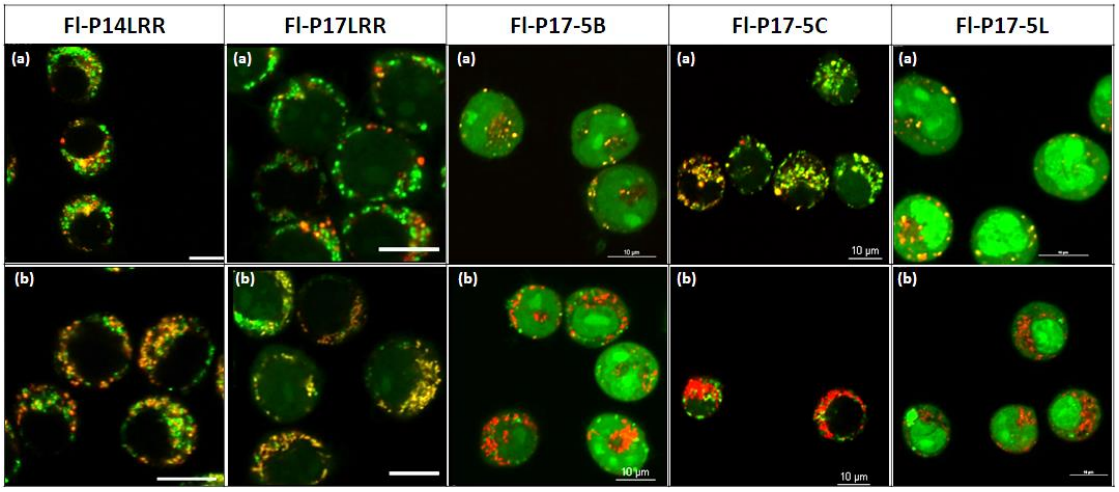

Figure 2.9 Confocal images of J774A.1 cells incubated with Fl-P14LRR, Fl-P17LRR, **Fl-P17-5B**, **Fl-P17-5C**, and **FL-P17-5L** (green) at 5 µM for 3 h. A yellow/orange color, indicative of co-localization, was studied with (a) the endosome tracking dye, Lysotracker (red) and (b) the mitochondria tracking dye, Mitotracker (red).

The faint appearance of **Fl-P17-5C** in the cell cytoplasm encouraged us to study **Fl-P17-5C** at a higher concentration, 10 µM, at 1 h incubation and at an extended incubation time of 3 h (Figure 2.10). In this study, at both time points, more significant cytoplasmic localization was observed with endosomal localization also remaining a prominent subcellular niche for **Fl-P17-5C**. It can also be seen that there is a significant amount of nuclear localization, yet the peptide remained mostly devoid of mitochondrial localization. The observed difference between the 5 µM and 10 µM treatments suggests there is a concentration dependence that affects the subcellular location of **Fl-P17-5C**. This can be the result of a couple possibilities; it can be due to a change in the route the peptide takes to enters cells or time dependent endosomal escape. With **Fl-P17-5B** and **Fl-P17-5L** accessing much of the cell, it can be suggested that they would be more effective in clearing intracellular pathogens from the cell at a range of bacteria subcellular niches. Fl-P14LRR and Fl-P17LRR are mostly located at the mitochondria, which may explained their limited capacity to eliminate intracellular pathogens.[87] Though **Fl-P17-5C** is mostly endosomal, it is effective in

accumulating in the cell at higher concentrations and longer incubation times, and, thus, has potential to demonstrate effective clearance of intracellular bacteria as well.

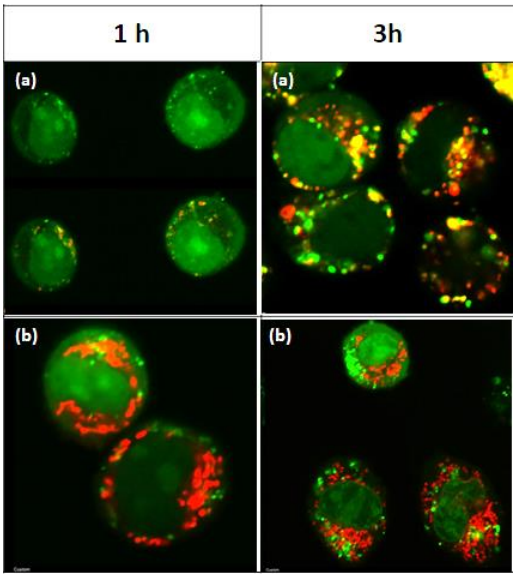

Figure 2.10 Confocal images of J774A.1 cells incubated with **Fl-P17-5C** (green) at 10 µM after 1 and 3 h. A yellow/orange color, indicative of co-localization, was studied with (a) the endosome tracking dye, Lysotracker (red) or (b) the mitochondria tracking dye, Mitotracker.

2.4.4 *In vitro* antibacterial activity

Enteric pathogens, such as *Salmonella* and *E. coli*, typically cause food borne illnesses and account for millions of illnesses in the U.S. annually.[152] ESKAPE pathogens are hospital associated infections, including bacterium *Enterococcus, Staphylococcus, Klebsiella, Acinetobacter, Pseudomonas*, and *Enterobacte*r. The rising number of multi drug resistant (MDR) strains amongst ESKAPE pathogens, such as *A. baumannii* and *Pseudomonas aeruginosa*, pose a serious health threat that puts them on the World health Organizations list of priority pathogens.[153] Thus, we aimed to determine whether the **Fl-P17-5R** series of peptides demonstrated antimicrobial activity when presented with a number of enteric and ESKAPE pathogens.

Overall, the majority of the **Fl-P17-5R** peptides had at least a 2-fold increase in antibacterial potency in comparison to their Fl-P14-5R counterparts against enteric pathogens (Table 2.1). For example the MIC values of the Fl-P14-5R peptides were all 4 µM against *Shigella*, but **Fl-P17-5B**, **Fl-P17-5C**, and **Fl-P17-5L** had MIC values of 1, 2, and 2 µM, respectively, against the same

bacterial strain. More substantial is the fact that the majority of the MIC values for **FL-P17-5R** peptides are at or below 4 µM against both Gram negative and Gram positive enteric pathogens. Notable antibacterial activity was demonstrated against ESKAPE pathogens as well. **Fl-P17-5B**, **Fl-P17-5C**, and **Fl-P17-5L** had MIC values of 0.5 to 1 µM against a multidrug resistant strain of *Acinetobacter baumannii*. They also had significant potency against *Enterococcus facieum* with MICs of 2-4 µM.

Table 2.1 Antibacterial activity (MICs in µM) of CAPH peptides against pathogenic isolates after 20 h using the broth microdilution method. Includes control antibiotics vancomycin and gentamicin (µg/ mL).

Strain ID	Fl-P14				Fl-P17				Control Antibiotics	
	LRR	-5B	-5C	-5L	LRR	-5B	-5C	-5L	Vancomycin	Gentamicin
Activity against ESKAPE pathogens										
+ E. faecium 700221	2	4	8	4	1	4	4	2	> 32	> 32
+ S. aureus NRS 384	16	32	32	32	8	32	32	32	0.5	0.5
- K. pneumoniae 1706	> 32	> 32	> 32	> 32	> 32	> 32	> 32	> 32	> 32	2
- A. baumannii 1605	1	2	2	1	1	0.5	1	1	8	> 32
- P. aeruginosa 50573	16	32	32	32	16	32	32	32	> 32	0.25
- E. cloacae 1134	32	> 32	> 32	> 32	16	> 32	> 32	> 32	> 32	0.5
Activity against more *Staphylococcus* spp.										
S. aureus ATCC 6538	16	32	> 32	32	8	16	32	16	0.5	0.125
S. epidermidis NRS 101	2	8	16	8	1	4	2	2	2	32
VRSA 10	8	32	> 32	32	8	16	32	16	> 32	0.5
Activity against more *Acinetobacter baumannii* strains										
A. baumannii 1747	1	4	4	8	0.5	2	2	4	> 32	0.25
A. baumannii 19606	2	4	4	2	2	2	1	2	32	16
A. baumannii NR 19299	ND	ND	ND	ND	8	8	16	8	ND	16
Activity against enteric pathogens										
+ L. monocytogenes 191112	8	8	8	4	2	4	8	4	1	0.5
- S. flexneri 1a	4	4	4	4	1	1	2	2	> 32	0.5
- S. enteritidis	4	8	16	8	2	4	4	4	> 32	0.25
- E.coli 21922	4	8	4	8	2	4	1	4	> 32	2
- S. typhimurium LT2	16	32	32	32	8	16	8	16	> 32	0.5

ND = Not Determined

In a couple instances the **Fl-P17-5R** peptides were not more potent than their Fl-P14-5R counterparts, including *P. aeruginosa* 50573, *K. pneumoniae* 1706, and *S. aureus* NRS 384. Additionally, in a few cases Fl-P14LRR and Fl-P17LRR had lower MICs against bacterial strains than their Fl-P14/P17 hydrophobic group modified constituents, such as *S. epidermidis* NRS 101 and *L. monocytogenes*. Nonetheless, in a number of cases the hydrophobic group modified peptides have potent antimicrobial activity. From these data and previous cell experiments we can

conclude that the **Fl-P17-5R** peptides exhibit improved cell accumulation while maintaining potent antimicrobial behavior *in vitro*.

2.4.5 *In cyto* antibacterial activity

Having confirmed the cell penetrating ability as well as *in vitro* antibacterial of our designed CAPHs against an array of pathogenic bacteria, we next sought to investigate if the **Fl-P17-5R** peptides could rescue J774A.1 cells from intracellular bacteria. J774a.1 cells were infected with different bacteria and subsequently treated with the **Fl-P17-5R** peptides (Figure 2.11). The ability of the peptides to clear the intracellular pathogens was evaluated based on the level of bacteria that remained after 9 h of incubation with the **Fl-P17-5R** treatment at 5 µM. These experiments demonstrated that, in the majority of the strains tested, **Fl-P17-5L** had the greatest ability to clear the intracellular pathogens. Treating the peptides with 5 µM of **Fl-P17-5L** resulted in a reduction of intracellular bacteria ranging from 76%, against *A. baumannii*, to 23%, against *S. aureus*. **Fl-P17-5L** was equipotent to Fl-P17LRR against *A. baumannii*, and was significantly more potent than **Fl-P17-5B** and **Fl-P17-5C**, by 34% and 54%, respectively. In regard to *S. aureus*, **Fl-P17-5B** was the most potent of the tested CAPHs reducing the bacteria by 34%. **Fl-P17-5L** followed closely behind in its activity against *S. aureus* at 23% reduction. In contrast, neither Fl-P1LRR nor Fl-P14LRR had any activity against *S. aureus* at this concentration. However, at 10 µM Fl-P17LRR was the most potent. It is interesting to note that despite Fl-P17LRR having a lower MIC value than **Fl-P17-5R** CAPHs, it was only the most potent peptide in the case of *S. aureus* at 10 µM and in two of the other cases it had little to no activity; Salmonella (4% reduction) and Listeria (0% reduction). Thus, MIC, subcellular niche and cell penetration capacity, combined, effect the capacity of CAPHs to eradicate intracellular bacteria.

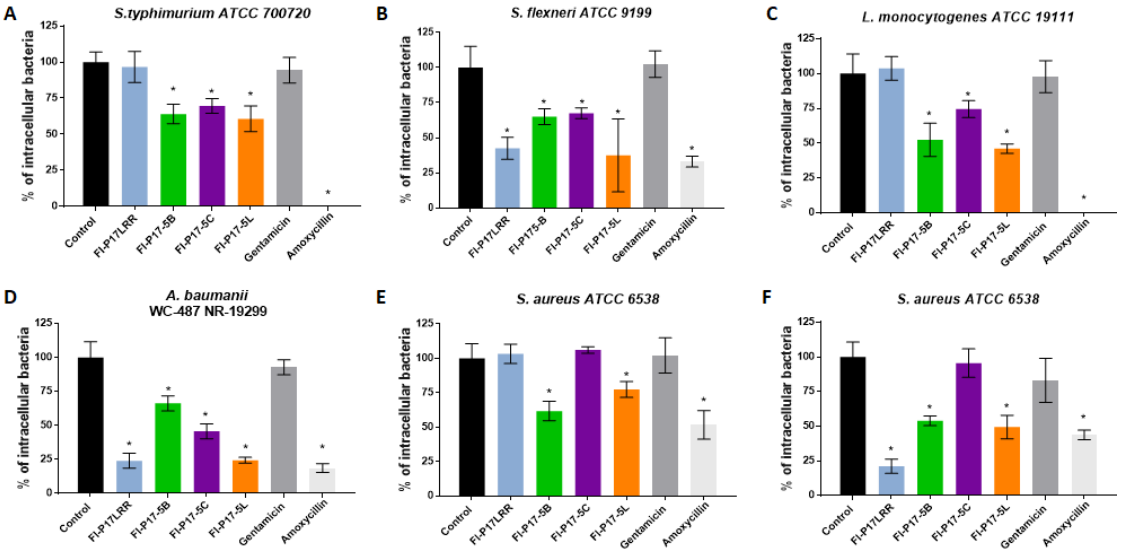

Figure 2.11 *In cyto* experiment showing the percentage of intracellular bacteria remaining after infected J774A.1 cells were treated with Fl-P17LRR, **Fl-P17-5R** peptides, and control antibiotics Gentamicin and Amoxicillin at 5 µM (A-E) and 10 µM (F) for 12 h. Statistical significance (*) was assessed with the P-test ($P < 0.05$).

Four factors must be considered when it comes to the ability of the CAPHs to clear intracellular pathogens: 1) MICs against that specified bacterial strain, 2) that bacterium's subcellular niche, 3) the CAPH peptide's subcellular location, and 4) the CAPH cell penetration efficiency (Table 2.2). Based on these factors, it can be concluded that **Fl-P17-5L** is the most potent of the tested CAPH peptides. This can be attributed to **Fl-P17-5L** having the highest cell accumulation and its cytoplasmic localization under the employed conditions. These properties give **Fl-P17-5L** a greater advantage over the other CAPHs to efficiently target bacteria at different subcellular locations. Only in the case of *S. aureus* did Fl-P17LRR not have higher potency than **Fl-P17-5L**, and this was most likely due to the tested concentrations being well below the MIC of **Fl-P17-5L** (16 µM). In the case of *Listeria*, which moves quickly throughout the cell cytoplasm by sequestering actin filaments, **Fl-P17-5B**, **Fl-P17-5C** and **Fl-P17-5L** all showed significant potency whereas Fl-P17LRR had none. Similarly, it also proved difficult for Fl-P17LRR to target *Salmonella* at its endosomal site in comparison to the **Fl-P17-5R** peptides. Conversely, Fl-P17LRR (mitochondria-localized) proved effective in clearing intracellular *A. baumannii*, which is believed to have a mitochondrial target.[12, 154] These data support that by expanding the

distribution of CAPHs within the cell we can better target a broader range of strains of pathogenic bacteria.

Table 2.2 Percent reduction of bacterial load in the intracellular clearance of bacteria from J774A.1 cells at 5 µM after 12 h.

Pathogen (5 µM)	**Fl-P17-5L (MIC)** Cytoplasm/ endosomes	**Fl-P17-5B‡ (MIC)** Cytoplasm/ endosomes	**Fl-P17LRR‡ (MIC)** Mitochondria/ endosomes	**Fl-P17-5C (MIC)** Endosomes
Salmonella	40% (4)	35% (4)	4% (2)	30% (8)
Shigella	62% (2)	35% (1)	58% (1)	32% (2)
Listeria	54% (4)	48% (4)	0% (2)	26% (8)
S. Aureus	23% (16)	38% (16)	0% (8)	0% (32)
***S. Aureus* (10 µM)**	51% (16)	46% (16)	79% (8)	5%(32)
A. baumannii	76%(8)	34% (8)	76% (8)	54%(16)

The MIC in µM of Fl-P17 peptides against those bacterial isolates is given in parenthesis. The peptide with the highest *in cyto* activity for each pathogen is highlighted in yellow. Peptides are ordered by efficiency of cell penetration in J774A.1 cells (left highest, right lowest, ǂ similar cell uptake).

2.4.6 Antibiofilm activity

Bacteria can adhere to and form a film of bacteria over inert or living surface to form a biofilm. Biofilm-forming bacteria preferentially colonize on the surface of tissues, as well as surgical devices and instruments, which promote the persistence of pathogens in the host, leading to chronic bacterial infections.[155] Specific surfaces on which biofilm are known to form include implants, prosthetics and open wounds.[156, 157] This makes biofilm formation a prominent threat in hospitals and clinics. Biofilm formation is not limited to a few specialized strains, but rather is a form of resistance that can occur through a number of bacterial strains. *Pseudomonas aeruginosa* is an avid biofilm former, which is the leading cause of fatalities in patients with cystic fibrosis, due to biofilm formation on the lungs.[158, 159] Mature biofilms are especially difficult to treat due to the complex extracellular matrix on the periphery of the biofilm that is extremely difficult to penetrate, making it very challenging to target bacteria within the biofilm. This, combined with the presence of persister cells, makes biofilm bacteria up to 1000-fold more tolerant of antibiotics than planktonic cells.[160]

Having established the potent antimicrobial activity of the **Fl-P17-5R** peptides *in vitro* and *in cyto*, we were interested in assessing activity against biofilms as well. This was determined by testing

preformed biofilm viability after 24 h treatment with the **Fl-P17-5R** peptides using the XTT assay (Figure 2.12).[161] In this way, we found that **Fl-P17-5R** CAPHs have antibiofilm activity against *K. pneumoniae, S. entrica,* and *E. facieum* biofilms. There was approximately a 70% reduction in *K. pneumoniae* preformed biofilms in the presence of **Fl-P17-5B** and **Fl-P17-5L**, in addition to **Fl-P17-5C** causing a 31% decrease. Additionally, **Fl-P17-5B**, **Fl-P17-5C**, and **Fl-P17-5L** were able to reduce *E. facieum* preformed biofilms by 43%, 27%, and 58%, respectively, and *S. entrica* preformed biofilms by 67%, 47%, and 65%, respectively, showing greater activity than established antibiotics gentamicin, linezolid, and vancomycin. Overall, **Fl-P17-5R** CAPHs are more effective than the established antibiotics vancomycin and linezolid. The only exception is with **Fl-P17-5C** against the *E. facieum* biofilm where it shows similar potency to linezolid and its Fl-P14-5C counterpart. It is also important to note that extended CAPHs have improved potency against biofilms in comparison to their shorter analogues, especially in the case of Fl-P17LRR which had up to a 3-fold increase relative to Fl-P14LRR in reducing the viability of *K. pneumoniae* biofilms. These results support the idea that increasing the chain length of CAPHs is the most beneficial factor in enhancing antibiofilm activity, most likely due to the increased cationic nature of CAPHs. It has been theorized that greater the cationic nature promotes the disruption of biofilm matrices to reach bacteria beyond the periphery of the matrix.[155, 162]

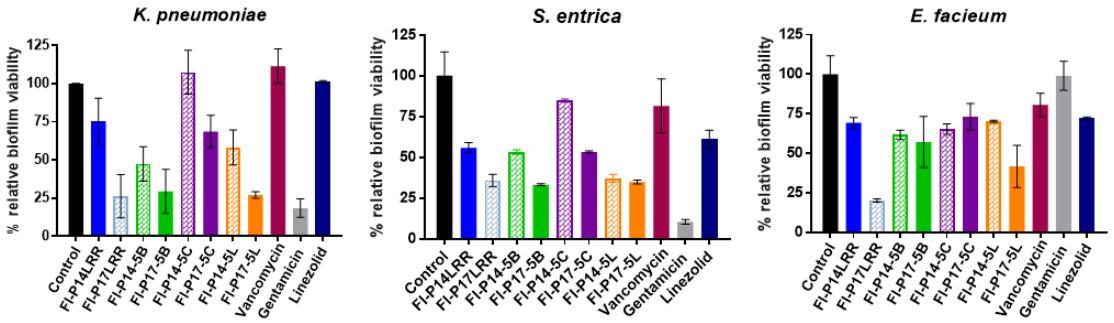

Figure 2.12 Antibiofilm activity was measured based on relative biofilm viability using the XTT assay after pre-formed biofilms were treated with Fl-P14-5R (bricked bars), **Fl-P17-5R** (solid bars), Fl-P14LRR, Fl-P17LRR, and control antibiotics gentamicin, vancomycin, and linezolid at 64 µm for 24 h.

2.4.7 Investigation of mechanisms of cell uptake

Physical characteristics result in variations in the modes of cell entry and the subcellular fate of CPPs. There are two major pathways CPPs can take to transverse the cell membrane: endocytosis or direct transport.[96, 116] Endosomal cell entry of CPPs can occur through one or multiple endocytosis pathways, including caveolae of clathrin-mediated endocytosis, fluid-phase endocytosis, and macropinocytosis.[117, 118] The differences in the subcellular fate of the **Fl-P17-5R** peptides in comparison to that of Fl-P14LRR and Fl-P17LRR made us interested in understanding how these peptides might differ in their mechanism(s) to enter mammalian cells. The most common endocytosis pathways CPPs use to enter cells is through macropinocytosis, clathrin-dependent and caveolin- dependent endocytosis, and lipid rafts.[150] Thus, to investigate CAPHs cell uptake mechanisms, J774A.1 cells were subjected to cell uptake inhibition assays to begin to understand how CAPHs interact with the cell membrane and to probe their possible internalization pathways.

2.4.7.1 Disruption of membrane potential with gramicidin

In order to analyze possible mechanisms of cell uptake of CAPHs it is also important to consider properties that contribute to CPP cell accumulation. Membrane potential is the driving force in peptide-cell interactions. Studies have demonstrated a substantial dependence on membrane potential for the translocation of highly cationic CPP, such as Tat, penetratin, and a number of additional arginine rich CPPs.[108, 163, 164] Furthermore, CPPs have been shown to localize with the mitochondria upon cell entry in response to the mitochondria membrane potential.[92, 165] To probe

if the cell uptake of CAPHs relied on membrane potential we depolarized the plasma membrane using gramicidin. Gramicidin is an ionophore that interrupts membrane potential by creating a monovalent cation channel.[166, 167] In this study, gramicidin was introduced to J774A.1 cells for 30 min prior to a 1 h incubation of the cells with the CAPH peptides at 5 µM concentration. The inhibition of cell uptake of the peptides in cells exposed to gramicidin and cells not exposed to gramicidin was then quantified using flow cytometry (Figure 2.13). By disrupting the cell membrane potential, cell accumulation of **Fl-P17-5B**, **Fl-P17-5C**, **Fl-P17-5L** by more than 90%. Fl-P14LRR cell uptake also significantly decreased by 75%.

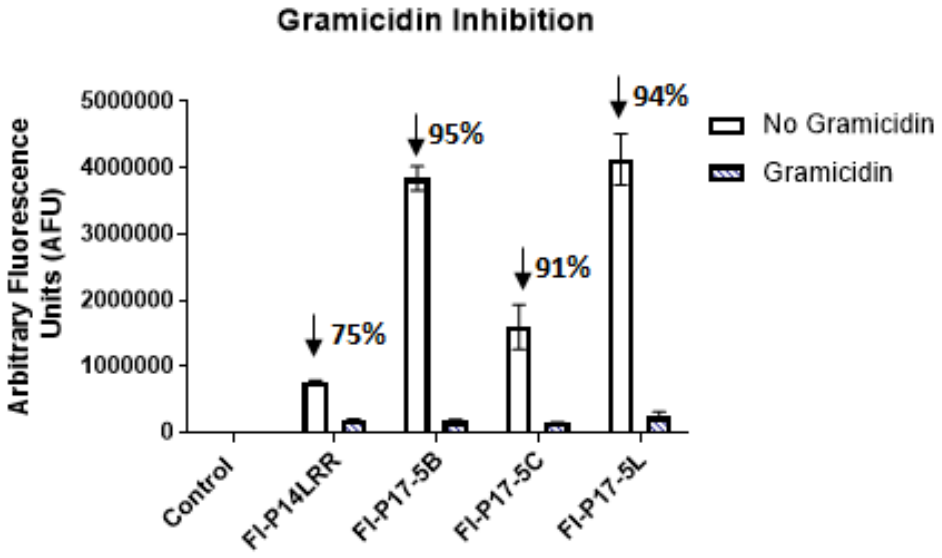

Figure 2.13 Arbitrary cellular fluorescence of J774A.1 cells exposed to Fl-P14LRR, **Fl-P17-5B**, **Fl-P17-5C**, and **FL-P17-5L** at 5 µM for 1 h with or without pre-treatment with gramicidin (1 µM) with arrows indicating the decrease in cell uptake.

The effects of disrupting the cell membrane potential was further explored using confocal microscopy (Figure 2.14). There was no longer cytoplasmic accumulation of **Fl-P17-5B** or **Fl-P17-5L**, and all of the peptide fluorescence was punctate and mostly endosomal. These results are similar to what was observed in a study where CPP, R9, was incubated with HeLa cells post Gramicidin A treatment. Membrane depolarization resulted in the peptide changing from a cytoplasmic location to punctate distribution through the cell. The authors suggest the change in subcellular location was result of depolarization forcing an alternative route of entry that did not involve accumulation of the peptide on the membrane.[94, 164] This finding indicates functional

membrane potential is required for non-endosomal cell uptake. With CAPHs taking on a predominately endosomal location in the presence of gramicidin, this suggest they took an alternative endocytic route. Some punctate fluorescence was observed outside of endosomal localization, which may be due to mitochondrial targeting as mitochondrial co-localization is slightly visible with **Fl-P17-5C** and **Fl-P17-5B**. Adding gramicidin, may have affected the mitochondria membrane potential, making it more susceptible to association with **Fl-P17-5R**. CAPHs.[168] Interestingly, Fl-P14LRR retained localization with endosomes and mitochondria.

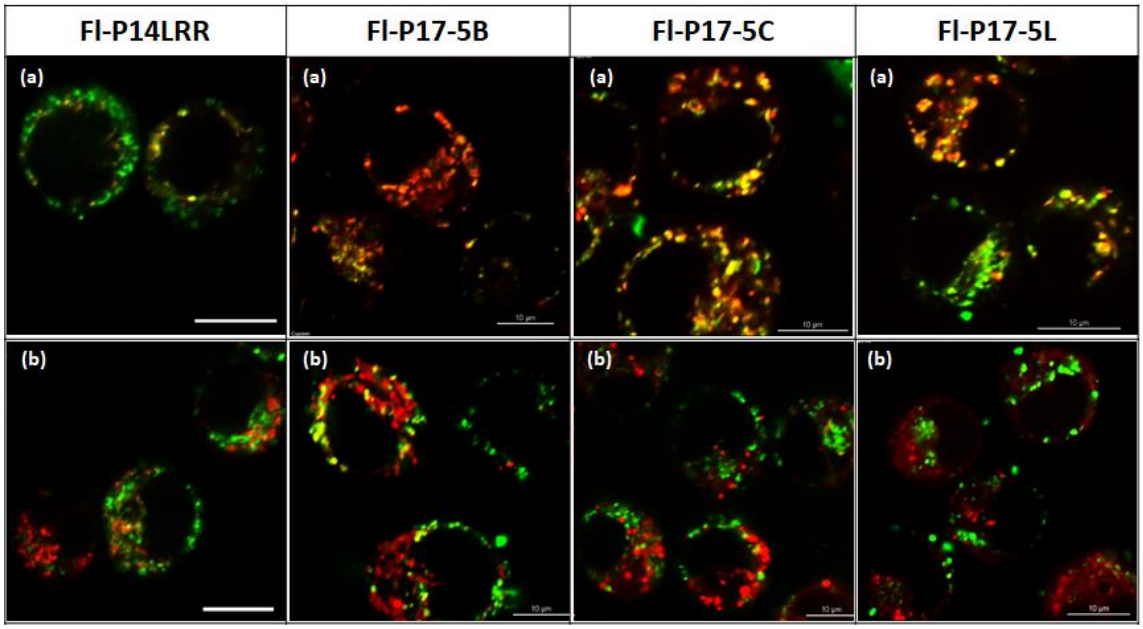

Figure 2.14 Confocal images of J774A.1 cells incubated with CAPHs (green), Fl-P14LRR, **Fl-P17-5B**, **Fl-P17-5C**, and **FL-P17-5L** at 5 µM for 1 h after pre-treatment with gramicidin (1 µM). Cell location was studied with stains (red) (a) Lysotracker and (b) Mitotracker (Scale bars = 10 µM), a yellow-orange color, indicates co-localization.

These results confirm that the membrane potential plays a critical role in the translocation of CAPHs across the lipid bilayer. Fl-P14LRR demonstrated the least dependence on membrane potential since it exhibited a smaller, but still significant, decrease in cell uptake in the presence of gramicidin. However, since Fl-P14LRR has two less guanidinium moieties, it is less cationic in charge, which could explain the smaller dependence on membrane potential for cell uptake in comparison to the **Fl-P17-5R** CAPHs. Despite **Fl-P17-5C** being endosomal in the absence of gramicidin it was interesting to find that depleting membrane potential affected its cell uptake as

well. This means its mode of cell entry is a route that requires membrane potential, but results in endosome internalization. In the case of the R9 study, membrane depolarization disrupted the ability of the peptide to nucleate at the cell surface, subsequently disrupting cell accumulation.[164] Thus, depleted membrane binding may also be a factor that affected CAPHs cell uptake. To summarize, depolarizing the cell membrane affected the mode of cell uptake of CAPHs causing a major decrease in cell uptake, which consequently affected their subcellular fate.

2.4.7.2 Inhibition of endocytosis with cytochlasin D

Cytochlasin D (Cyto D) was used as a method of endocytosis inhibition to further understand the mode of cell uptake for the **Fl-P17-5R** peptides. Cyto D inhibits endocytosis by disrupting actin filament formation, which is necessary in the formation of macropinosomes during macropinocytosis uptake.[169] J774A.1 cells were exposed to cyto D for 30 min followed by a 1 h incubation with the CAPHs peptides at 5 µM concentration. Cell uptake of the peptides with cells exposed to cyto D and cells not exposed to cyto D was then quantified using flow cytometry (Figure 2.15). Introducing cells to cyto D caused an increase in cell uptake by 15% with **Fl-P17-5C** and 20% with **Fl-P17-5B**. Fl-P14LRR had the greatest increase in cell uptake at 32%. On the contrary, cells incubated with **Fl-P17-5L** after treatment with cyto D showed no significant difference in cell uptake.

The fact that introducing cyto D enhanced the cell uptake of Fl-P14LRR, **Fl-P17-5B** and **Fl-P17-5C** does not dismiss macropinocytosis as a possible mechanism of cell uptake for these CAPHs. It does, however, dismiss the possibility that **Fl-P17-5L** enter cells through macropinocytosis since it was unaffected. In the case of the other CAPHs, these results are similar to what was observed with CPP TP10 in the presence of cyto D in HeLa cells. The authors speculated that TP10 was involved in competing cell uptake pathways with clathrin mediated endocytosis showing dominance over macropinocytosis since they were able to observe a decrease in TP10 uptake in the presence clathrin inhibitors.[149, 170]

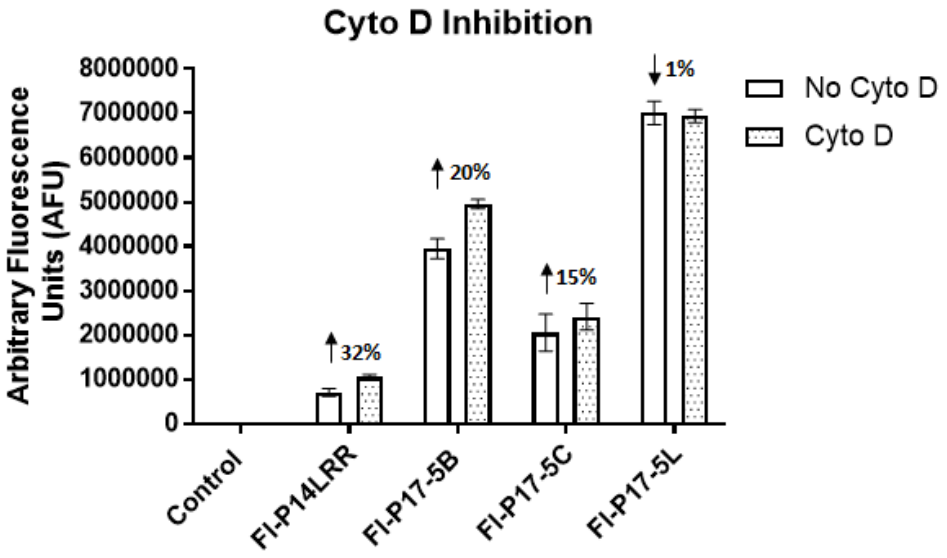

Figure 2.15 Arbitrary cellular fluorescence of J774A.1 cells exposed to Fl-P14LRR, **Fl-P17-5B**, **Fl-P17-5C**, and **FL-P17-5L** at 5 µM for 1 h with or without pre-treatment with Cyto D (10 µM)

2.4.7.3 Inhibition of clathrin-mediated endocytosis by sucrose

With the proposal that macropinocytosis may play a competing role in the uptake of CAPHs, we further expanded our investigation to understand if an additional pathway may be involved in the uptake of CAPHs. Sucrose is an inhibitor of endocytosis by disrupting the successful formation of endosomal vacuoles, specifically those developed through clathrin mediated endocytosis. This is achieved by blocking clathrin from getting to the site of endocytosis. Instead abnormal clathrin polymerization occurs to form empty clathrin micro cages, thereby disrupting clathrin-mediated endocytosis.[171] Sucrose was incubated with J774A.1 cells for 30 min followed by the incubation of the sucrose treated cell with 5 µM of the CAPH peptides for 1 h (Figure 2.16). Results were similar to, but more dramatic than what was seen in the presence of cyto D. Cell uptake increased by about 41% with **Fl-P17-5B** and 40% with **Fl-P17-5C**. Fl-P14LRR had an even greater rise in cell uptake at 67% increase. **Fl-P17-5L**, however, again had no significant change in cell uptake in the presence of sucrose.

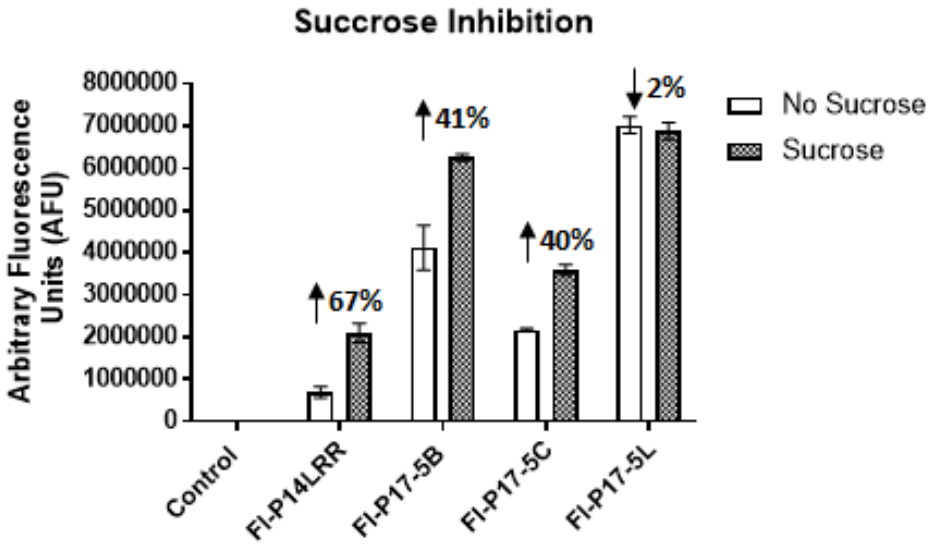

Figure 2.16 (top) Arbitrary cellular fluorescence of J774A.1 cells exposed to Fl-P14LRR, **Fl-P17-5B**, **Fl-P17-5C**, and **FL-P17-5L** at 5 µM for 1 h with or without pre-treatment with sucrose (0.4 M).

Confocal microscopy visually supported the flow cytometry data with CAPHs cell association increasing in the presence of sucrose. **Fl-P17-5C** was no longer limited to endosomal localization at 5 µM after 1 h incubation and could be seen throughout the cell cytoplasm with some co-localization with lysotracker, but no mitochondria association (Figure 2.17). **Fl-P17-5B** and **Fl-P17-5L** also showed pronounced localization in the cytoplasm, in addition to endosomal and mitochondria co-localization. Fl-P14LRR also showed a change in subcellular location from having both endosomal and mitochondria localization to only displaying mitochondria co-localization in the presence of sucrose treatment. This may suggests that clathrin mediated endocytosis plays a large role in the endosomal localization that is evident with Fl-P14LRR in non-treated cells.

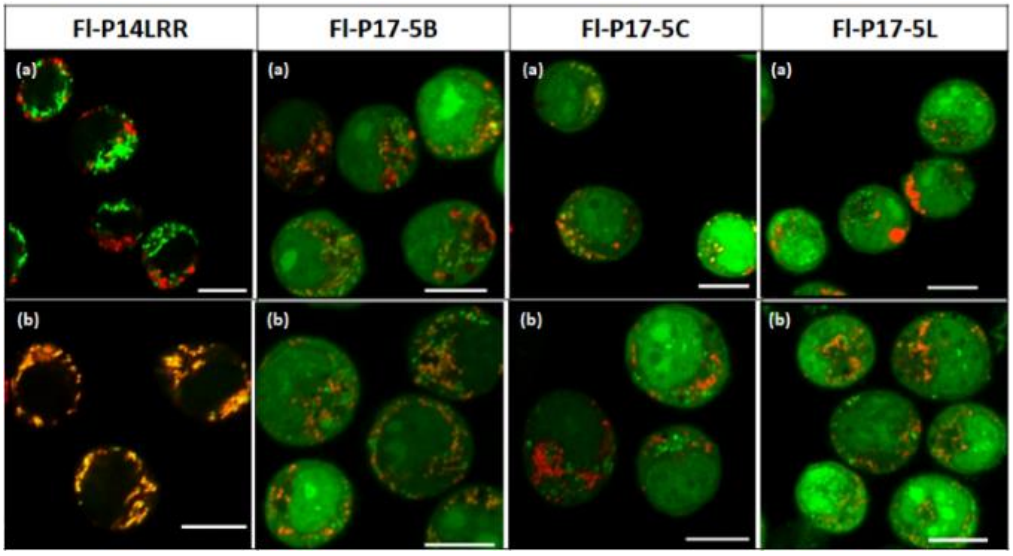

Figure 2.17 Confocal images of J774A.1 cells incubated with CAPHs (green) Fl-P14LRR, **Fl-P17-5B**, **Fl-P17-5C**, and **FL-P17-5L** at 5 µM for 1 h after pre-treatment with sucrose (0.4M). Cell location was studied with stains (red) (a) Lysotracker and (b) Mitotracker (Scale bars = 10 µM), a yellow-orange color, indicates co-localization

In one study where the mechanism of cell uptake of *retro-inverso* form of a Tat peptide was elucidated in HeLa cells, the presence of sucrose decreased its cell uptake as well as reduced the presence of punctate cytosolic peptide.[172] Another study using R9 showed that its cell uptake was clathrin dependent based on its decrease in cell uptake in the presence of hypertonic sucrose.[173] In contrast, with CAPHs either no changes were seen (**Fl-P17-5L**), peptide diffused throughout the cytoplasm (**Fl-P17-5B** and **Fl-P17-5C**) or became dominantly localized at the mitochondria (Fl-P14LRR). These results suggest CAPHs do not solely rely on clathrin mediated endocytosis for cell penetration and sucrose promoted an alternative route for enhanced cell entry. Additionally, the fact that there was more peptide outside of endosome in this experiment may be a side effect of the use of sucrose for endocytosis inhibition. Sucrose has also been reported as a lysomotrophic agent, which would explain the largely cytoplasmic and mitochondria locale of CAPHs if it facilitated their endosomal escape.[119, 174, 175] A study with a Tat-fusion protein showed enhanced nuclear delivery reportedly due to the presence of sucrose enabling endosome escape.[123] However, this would not explain the enhanced cell accumulation. Therefore, CAPHs must be capable of implementing a different pathway for cell uptake, especially in scenarios where one pathway becomes disrupted, thus, demonstrating CAPHs as persistent CPPs.

2.4.7.4 Inhibition of endocytosis with phenyl arsine oxide

To further elucidate the mechanism that the **Fl-P17-5R** series use to enter cells, we also explored the effect of phenyl arsine oxide (PAO) on cell uptake. PAO is a general endocytosis inhibitor that works by sequestering energy sources from the cell, specifically oxygen and ATP, which are necessary for energy dependent endocytosis to occur.[176] In this study PAO was introduced to J774A.1 cells for 30 min prior to a 1 h incubation of the cells in the presence of the CAPHs peptides at 5 µM concentration. The inhibition of cell uptake of the peptides in cells exposed to PAO and cells not exposed to PAO was then quantified using flow cytometry (Figure 2.18). Flow cytometry revealed that PAO caused more than a 30% decrease in cell uptake of **Fl-P17-5B** and **Fl-P17-5C** and a 50% decrease in the cell uptake of **Fl-P17-5L**. Fl-P14LRR showed an even more significant decrease in cell uptake post treatment with PAO at 64%.

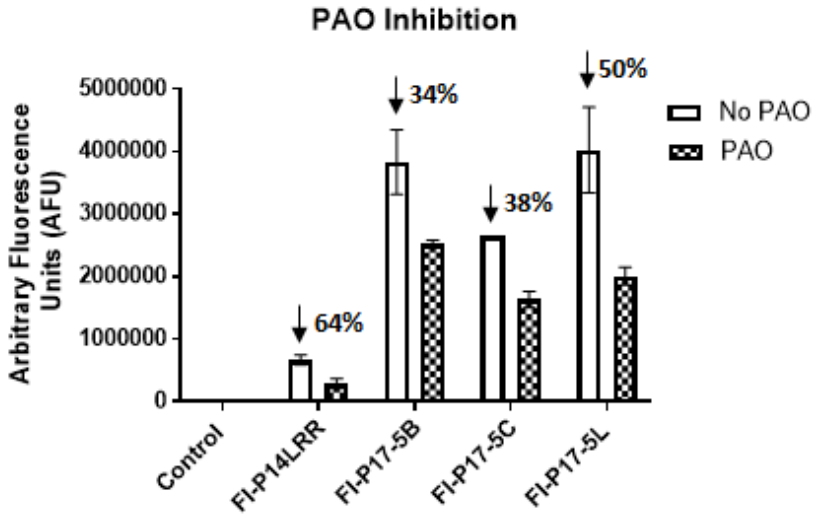

Figure 2.18 Arbitrary cellular fluorescence of J774A.1 cells exposed to Fl-P14LRR, **Fl-P17-5B**, **Fl-P17-5C**, and **FL-P17-5L** at 5 µM for 1 h with or without pre-treatment with PAO (3 µM).

Confocal microscopy was also employed to show the effects of PAO (Figure 2.19). Confocal images showed that with PAO all of the peptides no longer showed endosomal co-localization. **Fl-P17-5L** and **Fl-P17-5B** remained mostly in the cytoplasm and they both now had some co-localization with mitochondria. In spite of **Fl-P17-5L** and **Fl-P17-5B** remaining cytoplasmic, there was noticeably less peptide in the cell, which coincides with the decrease in fluorescence detected by flow cytometry. Both **Fl-P17-5C** and Fl-P14LRR remained punctate and co-localization with

mitochondria was visible, marginally for **Fl-P17-5C**. It is also interesting to note punctate areas of green fluorescence due to peptide that are not co-localized with mitochondria nor endosomes. This represents an alternate intracellular location or different peptide distribution that CAPHs have acquired in the presence of PAO.

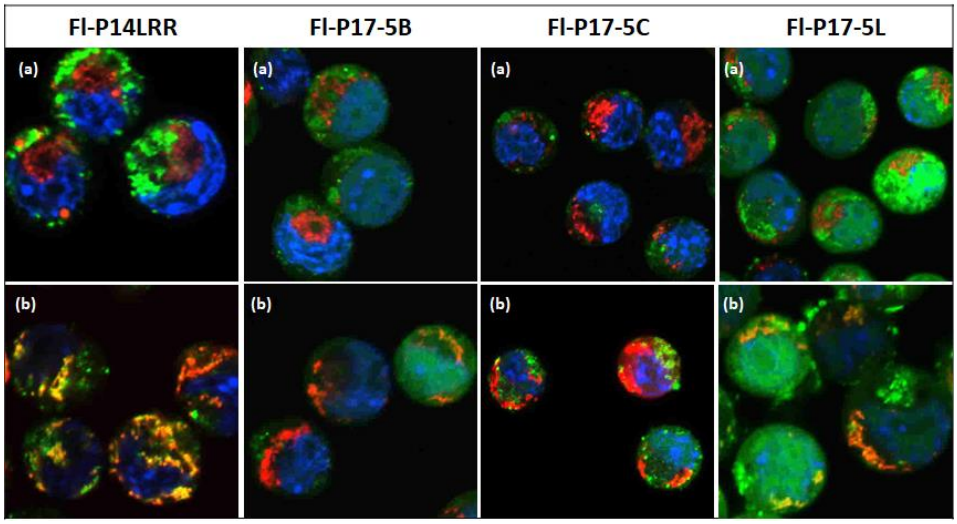

Figure 2.19 Confocal microscopy images of J774A.1 cells incubated with CAPHs (green), Fl-P14LRR, **Fl-P17-5B**, **Fl-P17-5C**, and **FL-P17-5L** at 5 µM for 1 h after pre-treatment with PAO (3 µM) Cell location was studied with stains (red) (a) Lysotracker and (b) Mitotracker (Scale bars = 10 µM), a yellow-orange color, indicates co-localization

The reduction in cellular uptake of all the peptides suggests that the mechanisms of cell entry of the tested CAPHs are all energy dependent to some extent. A few groups have limited the inhibition activity of PAO to clathrin mediated endocytosis,[177-179] but as **Fl-P17-5L** was unbothered by sucrose, an established clathrin inhibitor, it is unsupported that PAO affects only this pathway. Frost and collegues studied the effects of PAO in fluid-phase endocytosis and concluded vesicle-mediated endocytosis can occur by coated or noncoated pathway, but will still be blocked by PAO.[180] Thus, although PAO inhibition does not give exact information on the endocytic mechanism of CAPHs, the affect it had does imply that all CAPHs utilize an endocytic pathway for cell uptake to some extent. **Fl-P17-5L** falls outside the realm of macropinocytosis and clathrin mediated endocytosis, so more studies must be conducted to discover its alternative mode(s) of entry. Additionally, none of the CAPHs had complete cell uptake blockage by PAO

endocytosis inhibition, which broadens the scope of possible mechanisms CAPHs utilize to enter cells outside of endocytosis.

2.5 Conclusion

As we have shown, incorporating different hydrophobic residues into CAPHs with an extended polyproline backbone is an effective way to enhance the potency of CAPHs against intracellular pathogenic bacteria. This improved activity can be attributed to cell penetration, antibiotic activity, and the subcellular fate of CAPHs. We have successfully shown that **Fl-P17-5L** is the most potent of the CAPH analogues in eradicating an array of intracellular bacteria. Notably, it is able to clear *S. typhimurium* and *L.monocytogens* 30% and 54% better than Fl-P17LRR, with the simple replacement of the ether linked isobutyl hydrophobic group with an amide linked n-pentyl group. This exciting discovery is due to the ability of **Fl-P17-5L** to attain superior cell penetration as well as localization throughout the cytoplasm, which includes some association with endosomes and nuclei.

It's interesting to note the only difference between the Fl-P17LRR and **Fl-P17-5R** peptides are their hydrophobic groups, yet they have very different intracellular fates. Moreover, changing the hydrophobic motif of extended CAPHs to cylopentane (**Fl-P17-5C**) resulted in the lowest cell uptake ability of the **Fl-P17-5R** CAPHs and a mostly endosomal subcellular localization, whereas the isopentane (**Fl-P17-5B**) modification resulted in cell uptake levels that are comparable to Fl-P17LRR, and subcellular accumulation comparable to **Fl-P17-5L**. In fact, studies by Kelly and colleagues found there is critical lipophilicity criteria for a CPP to achieve mitochondria localization.[116] In these studies greater hydrophobicity resulted in decreased compatibility with the mitochondrial membrane and increased localization with the cytoplasm and nuclei.[116] This would explain the unfavorable association of **Fl-P17-5R** CAPHs with the mitochondria, and the cytoplasmic and nuclear localization of **Fl-P17-5B** and **Fl-P17-5L**. Herein, our findings prove that different hydrophobic groups alter CAPHs hydrophobicity, which effects their intracellular accumulation. Hence, the difference in subcellular location between CAPHs may be due to differences in their physiological properties as well as different modes of cell uptake.

In addition to the difference in subcellular niches, the mechanistic studies probing membrane potential and endocytosis inhibition support the idea that CAPHs take on different mechanisms of cell entry depending on the hydrophobic group that is present. It has been accepted that CPPs can be internalized through direct transport or multiple endocytic pathways, such as macropinocytosis, which is a common endocytosis route for arginine rich peptides.[181 182] Internalization mechanisms of arginine-rich peptides differ according to the administration conditions, including peptide sequence, peptide concentration, cell type, and culture medium, and endocytosis is no longer accepted as the sole mechanism of internalization of cationic CPPs.[122] By conducting different cell uptake inhibition studies, we were able to find that the modes of cell uptake of **Fl-P17-5C** and **Fl-P17-5B** were affected similarly to that of Fl-P14LRR. All showed increased cell uptake in the presence of vesicle dependent endocytosis inhibitors cyto D and sucrose. Though both cyto D and sucrose are expected to inhibit cell internalization through endocytic pathways, these studies showed the opposite effect. These results mirror a study done with CPP R8, which showed enhanced cell uptake in the presence of cyto D with a particular cell line.[182, 183] Based on our findings, both macropinocytosis and clathrin mediated endocytosis play a role in the uptake of **Fl-P17-5C**, **Fl-P17-5B**, and Fl-P14LRR. Thus, it is also proposed that the inhibition promoted the endosomal escape of CAPHs or enabled the peptides to take alternative modes of cellular entry, which is not an uncommon occurence.[92, 172, 183-185] This further suggests that different competing pathways may simultaneously be involved in CAPHs uptake processes, but with different efficacies. When one pathway is inhibited, other pathways may be exploited to a greater extent.

In contrast, **Fl-P17-5L** maintained the same degree of cell uptake in the presence of both cyto D and sucrose inhibitors. This shows that **Fl-P17-5R** has properties that favor a mechanism of cell uptake unlike the other CAPH peptides. It was not affected by sucrose or cyto D inhibitors, but was affected by PAO and gramicidin. Thus, the intracellular characteristics of **Fl-P17-5L**, though unidentified through these studies, may rely on its ability to quickly escape endosomes or involves an untested uptake mechanism, such as passive internalization upon binding to surface molecules. Regardless of the complexity of elucidating exact mechanisms of cell uptake of CAPHs, it does seem that a few mechanisms of cell entry play a role in the cell internalization of CAPHs, since none of the inhibition studies completely prevented the peptides from getting into cells. These

studies show that cell uptake is not mutually exclusive and multiple mechanism can be applied for CAPHs to enter cells.

2.6 Future Directions

Now that we have established that incorporating different hydrophobic groups into an extended CAPHs expands CAPHs ability to reach intracellular targets it is important to elucidate the mode of action that contributes to **Fl-P17-5R** CAPHs' cell penetration and antimicrobial activity. Herein we have demonstrated that differences in the hydrophobic motif directly impacts the subcellular fate of CAPHs as well as the mode of cell uptake. Further studies will try to understand exactly how this happens and what mechanisms of action are in place. Indisputably, **Fl-P17-5R** CAPH peptides represent a promising cell deliverable, antimicrobial agents that can be applied to the eradication of an array of intracellular pathogens.

2.7 Materials and Methods

2.7.1 Materials

H-Rink Amide ChemMatrix resin for peptide synthesis was purchased from Pcas Biomatrix Inc. (Quebec, Canada). Sterile complete media (DMEM, L-glutamine, Penicillin-Streptomycin, supplemented with 10% fetal bovine serum (FBS) and buffers (PBS) used in cell culture were purchased from VWR (VWR Direct, IL). All cell lines for cell culture were purchased form ATCC (Manassas, VA). Starting material for Fmoc-P_R and Fmoc-P_K(MTT), Z-hydroxyproline, was purchased from Chem Impex (Wood Dale, IL). All other chemicals and reagents were purchased commercially and were used without further purification unless mentioned from Sigma Aldrich (St. Louis, MO), Alfa Aesar (Haverhill, MA) or Thermo Fischer (Waltham, MA).

Each of the CAPH peptides was purified using Waters Delta Prep 4000 HPLC equipped with a Phenomenexr C18 semi-preparative column. CAPHs characterization was performed using Matrix Associated Laser Desorption Ionization time of flight (MALDI-TOF) mass spectrometry using an Applied Biosystem Voyager-DE TM BioSpectrometry workstation and analytical RP-HPLC using Waters Delta Prep 4000 HPLC equipped with a C18 reverse phase analytical column (5 µm, 4.6 mm x 250 mm; Phenomenex Luna), CAPHs cellular uptake was measured using Becton Dickton

Bioscines FACS Calibur Flow Cytometry, data was analyzed using Cell Quest (v.3.5) software. Cell uptake was also measured using BD sciences Acurri and analyzed using BD software. Absorbance readings were obtained using microplate reader TECAN SpectraFluor Plus. or TECAN Infinite F PLEX. Confocal images were obtained using Nikon A1R inverted confocal fluorescence microscope equipped with 60x oil objective. NIS Elements software was used to process images.

2.7.2 Compound 1: Z-Hyp($(CH_2)_2$CN)-OH

Two round bottom flasks equipped with stir bars were flamed dried and purged with nitrogen (N_2) until the flasks cooled to room temperature (RT). Approximately 20 mL of dry THF was added to the round bottom flasks and the flasks were cooled to 0°C. Z-Hyp-OH (0.0376 mol, 10 g) was added to one of the flasks and sodium hydride (NaH) (0.1316 mol, 3.17 g) was added to the other. The flasks were purged with N_2 after the addition of both reagents. Once the Z-Hyp-OH dissolved completely, the mixture was cannulated dropwise into the solution of NaH. After cannulation was complete, the reaction was allowed to stir for 1 h at 0°C, then acrylonitrile (0.1504 mol, 9.88 mL) was added neat using a syringe. The resulting mixture was allowed to cool to room temperature (RT) and was stirred for 24 hours at room temperature. After 12-18 h, 20 mL of water was added to quench the reaction and the THF was removed *in vacuo*. The pH of the solution was adjusted to 1 with 10% HCl and the mixture was filtered using a sintered glass funnel through vacuum filtration. The filtrate was extracted with about 100 mL EtOAc three times, and the combined organic extracts were dried using anhydrous $MgSO_4$. The EtOAc was removed *in vacuo* and product was purified by silica gel flash chromatography (95% DCM, 4% MeOH, 1% AcOH), to yield a colorless oil with a yield of 58%.

MW: 318 ESI+MS: 319 m/z (M + H+)

^{1}H NMR (300 MHz, $CDCl_3$): δ 7.36 (m, 4H), 7.18 (s, 1H), 5.18 (d, J = 18.5 Hz, 2H), 4.52 (m,1H), 4.17 (q, J = 4.0 Hz, 1H), 3.62 (m, 4H), 2.58 (t, J = 6.3 Hz, 2H), 2.35 (m, 2H), 2.17 (m, 1H).

2.7.3 Compound 2: Z-Hyp($(CH_2)_2$CN)-Bn

A stir bar was added to purified compound 1 (0.033 M, 10.5 g) in a round bottom flask. The flask was purged with N_2 prior to the addition of about 20 mL of DMF. The flask was cooled to 0°C followed by the addition of cesium carbonate (Cs_2CO_3) (0.0825 mol, 26.9 g) and benzyl bromide

(BzBr) (0.033 mol, 3.8 mL) and stirred for 2 hr. Then, the reaction mixture was filtered through celite and the filter was washed 3X with 5 mL of DCM and collected in a clean round bottom flask. The DCM was removed *in vacuo* and 15 mL of saturated aqueous LiCl was added to the mixture in the flask. This mixture was extracted 3X with about 20 mL of diethyl ether using a separatory funnel. The organic extracts were combined and dried using anhydrous $MgSO_4$, and the diethyl ether was removed *in vacuo*. The crude product was purified by silica gel flash column chromatography (60% EtOAc, 40% HX) to yield colorless oil with a yield of 60%.

MW: 408 ESI+MS: 409 m/z (M + H+)

^{1}H NMR 300 MHz, $CDCl_3$): δ 7.40 (m, 10H), 5.10 (m, 4H), 4.60 (m, 2H), 3.75 (m, 3H), 3.00 (m, 2H), 2.60 (m, 2H), 2.34 (m, 1H), 2.15 (m, 1H).

2.7.4 Compound 3: Z-Hyp(P_K(Boc))-Bn

A stir bar was added to purified compound 2 (0.0197 mol, 8.03 g) in a round bottom flask. The flask was purged with N_2 prior to the addition of about 20 mL of MeOH. Then, cobalt chloride ($CoCl_2$) (0.02955 mol, 7.03g) was added and the solution was allowed to stir for about 5 minutes until it became homogenous and cooled to 0°C. The reaction continued with the addition of di-tert-butyl dicarbonate (Boc anhydride) (0.02955 mol, 6.45 g), followed by adding sodium borohydride (Na_2BH_4) (0.197 mol, 7.45 g) very slowly. The reaction time was 12 h at room temperature. Next, the reaction mixture was filtered through celite. About 15 mL of deionized water (DIW) was added to the filtrate, and the methanol was removed *in vacuo*. The resulting solution was extracted 3X with mL of EtOAc. The organic layer was dried over anhydrous $MgSO_4$, and the EtOAc was removed *in vacuo*. The crude product was purified by silica gel flash column chromatography (60% EtOAc, 40% HX) to yield a colorless oil with a yield of 43%.

MW: 512 ESI+MS: 513 m/z (M + H+)

^{1}H NMR (300 MHz, $CDCl_3$): δ 7.30 (m, 10H), 5.12 (m, 2H), 5.02 (d, J = 18.7 Hz, 2H), 4.50 (dt, J = 16.0, 7.6 Hz, 1H), 4.09 (m, 1H), 3.64 (m, 2H), 3.45 (m, 1H), 3.16 (m, 2H), 2.36 (m, 1H), 2.07 (m, 1H), 1.72 (m, 2H), 1.45 (s, 9H).

2.7.5 Compound 4: Fmoc-P_K(Boc)

A stir bar was added to the round bottom flask containing P_K(Boc)-OH (0.0085 mol, 4.34 g) and the flask was purged with N_2. About 20 mL of 50:50 ethyl acetate/ethanol solvent mixture used to

dissolve the compound followed by the addition of palladium on carbon (Pd/C) at a 10 wt%. Two H_2 balloons were used to provide H_2 to the flask and the reaction was allowed to stir for 24 h. The resulting reaction mixture was filtered through filter paper, and the filtered paper was washed three with a total of 15mL of EtOAc. EtOAc was removed *in vacuo* and dried further under vacuum. The resulting crude material was dissolved in 10 mL of DIW/acetone 50:50 mixture followed by the addition of sodium bicarbonate (0.051 mol, 4.27 g). The sodium bicarbonate was allowed to dissolve, then the flask was cooled to 0°C. In a 50mL Falcon tube 20mL of acetone was used to dissolve Fmoc-OSu (0.00935 mol, 3.15 g) and the mixture was added dropwise to the flask. This reaction was stirred for 8 h at 0°C. The flask was allowed to warm to RT and the pH was brought to 4 with 10% HCl. The resulting solution was extracted with 3X with 30 mL of EtOAc. The organic extracts were combined and dried over anhydrous $MgSO_4$. The solvent was removed *in vacuo*. The desired product was purified by silica gel column flash chromatography (97% DCM, 3% MeOH) to yield a white foam with a yield of 70%.

MW: 510 ESI+MS: 511 m/z (M + H+)

^{1}H NMR (300 MHz, $CDCl_3$): δ 7.75 (t, J = 7.4 Hz, 2H), 7.58 (d, J = 7.9 Hz, 2H), 7.26 (m, 5H), 4.71 (s, 1H), 4.48 (m, 2H), 4.18 (m, 1H), 3.64 (m, 2H) 3.47 (m, 2H), 3.20 (s, 2H), 2.34 (m, 3H), 2.16 (s, 1H), 1.73 (s, 2H), 1.44 (s, 9H).

2.7.6 Compound Fmoc-P_R(Boc)$_2$

Fmoc-P_K(Boc) (2.93 µM, 1.5 g) was dissolved in about 10 mL of a 1:1 mixture of DCM/TFA was added to one of the flasks and the reaction went for 3 h. The solvent was removed in vacuo and the crude material was further dried under vacuum. About 10 mL of DCM was added to the flask followed by N,N′-di-boc-1H-pyrazole-1-carboxamidine (6.545 µmol, 2.03 g). Once dissolved, triethyl amine (TEA) (11.72 µmol, 1.64 mL) diluted in 2 mL of DCM was added to the reaction dropwise and the reaction was allowed to stir for 8 hr. The solution was extracted 3X with 15 mL of saturated solution of $NaHCO_3$. If an emulsion formed, the extractions were done by adding 10 mL of brine. The organic layers were combined and dried over sodium sulfate (Na_2SO_4). The solvent was removed *in vacuo*. The crude product was purified by silica gel flash column chromatography (96% DCM, 3% MeOH, 1% AcOH) to yield a white solid foam with a yield of 48%.

MW: 652 ESI+MS: 653 m/z (M + H+)

^{1}H NMR (300 MHz, $CDCl_3$)δ 11.51 (s, 1H), 8.57 (s, 1H), 7.75 (dd, J = 15.3, 7.5 Hz, 2H), 7.57 (d, J = 7.5 Hz, 2H), 7.29 (m, 5H), 7.19 (m, 2H), 4.44 (m, 3H), 4.11 (m, 2H), 3.67 (m, 2H), 3.50 (m, 2H), 2.39 (m, 4H), 1.82 (m, 2H), 1.48 (s, 16H).

2.7.7 Compound Fmoc-P_K(Mtt)

To Fmoc-P_K(Boc) (2.93 µmol, 1.5 g), 10 mL 50:50 solution of DCM/TFA was added to the flask. This reaction was allowed to stir at RT for 3 h. The solvent was removed from the flask *in vacuo* and dried further under vacuum. About 10 mL of DCM was added to the round bottom flask, which was cooled to 0°C. Diisopropylethylamine (DIEA) (29.3 µM, 5.07 mL) was added to the reaction mixture dropwise using a syringe. The mixture was allowed to stir for about 20 min. A Mtt-chloride (Mtt-cl) solution was made by adding Mtt-Cl (0.0073 mol, 2.1 g) to 10 mL of DCM. The Mtt-cl solution was added dropwise to the reaction using a syringe. The reaction was allowed to warm to RT and stirred overnight. The following day about 20 mL of methanol was added to the reaction and the solution was heated to 50°C using an oil bath and stirred for 2 h. The reaction was removed from the oil bath and allowed to cool to RT. Once at RT the reaction flask was cooled to 0°C. DIW was added equal to the total volume of the solution in the flask to quench the reaction. The solution was extracted 3X with 25 mL of DCM and the organic layer were combined and dried over Na_2SO_4. The solvent was removed *in vacuo*. The crude product was purified by silica gel flash chromatography (93% DCM,:7% MeOH) to yield a yellow solid foam with a yield of 67%.
MW: 666 ESI+MS: 667 m/z (M + H+)
^{1}H NMR (300 MHz, $CDCl_3$) δ 7.72 (m, 22 H), 5.3 (s, 1H), 4.37 (m, 1H), 4.22 (d, J=7.7 Hz, 1H), 4.03 (m, 2H), 3.56 (m, 3H), 3.44 (m, 2H), 2.26 (s, 4H), 1.73 (t, J = 6.2 Hz, 1H).

2.7.8 Peptide synthesis

The Fmoc-P17-5R peptides were synthesized using solid phase Fmoc-based peptide synthesis on 0.45 mmol/g H-Rink amide ChemMatrix Resin. The coupling reagent used was hexafluorophosphate azabenzotriazole tetramethyl uronium (HATU) along with DIEA to activate the carboxylic acid of the amino acid to be coupled. To a 25 mL synthesis flask, 200 mg Rink amide resin was added and de-clumped using a spatula. The resin was washed using 10 mL DCM (2X) and 10 mL DMF (2X). In a 10 mm culture tube Fmoc-P_K(Mtt)-OH (0.225 mmol, 140.6 mg), HATU (0.225 mmol, 85.5 mg) and DIEA (0.45 mmol, 78.2 µL) was added and dissolved in 10

mL of DMF. The solution was allowed to completely dissolve through sonication for 10 min. The solution in the culture tube was transferred to the resin in the synthesis flask and agitated for 4h at room temperature. After the 4 h the solution in the flask was drained and the resin was washed 2X with DMF (10 mL), 2X DCM (10 mL), 2X MeOH (10 mL), 2X DCM (10 mL) and 2X DMF (10 mL). Amino acid coupling completion was monitored using the Kaiser test prior to the last DMF wash.[186] Upon confirmation of coupling, 10 mL of 20% piperidine in DMF was added to the synthesis flask and agitated for 30 min at room temperature. The resin was washed 2X DMF (10 mL), 2X DCM (10 mL), 2X MeOH (10 mL), 2X DCM (10 mL) and 2X DMF (10 mL). Fmoc deprotection was confirmed using the Chloranil test prior to the last DMF wash.[187] The next amino acid, Fmoc-$P_R(Boc_2)$-OH (.225 mmol, 147 mg), was added to a 10 mm culture with DIEA and HATU as previously described. This process was repeated for each amino acid until the desired peptide sequence was achieved. The last amino acid added was Fmoc-glycine (Gly). This was done through the same coupling process, using Gly (0.27 mmol, 80.2 mg), HATU (0.27 mmol, 102.7 mg) and DIEA (0.54 mmol, 94 µL).

2.7.9 Coupling fluorescein

10 mL of 20% piperidine in DMF was added to the synthesis flask above and agitated for 30 min at room temperature. The resin was washed 2X DMF (10 mL), 2X DCM (10 mL), 2X MeOH (10 mL), 2X DCM (10 mL) and 2X DMF (10 mL). The reaction flask containing the desired peptide sequence on resin (Fmoc-P17-5R) was protected from light using foil. In a 10 mm culture tube, 10 mL of DMF was added to NHS-fluorescein (0.099 mmol, 46.9 mg) and DIEA (0.18 mmol, 31.2 µL). This solution was added to synthesis flask containing the peptide and agitated 24 hrs. The solution was drained and the resin was washed with 2X DMF (10 mL), 2X DCM (10 mL), 2X MeOH (10 mL), 2X DCM (10 mL) and 2X DMF (10 mL).

2.7.10 Mtt deprotection from P_K(Mtt)

At this step the peptide on resin was washed 2X with DCM, dried under vacuum, and split evenly into three separate 10 mL synthesis flasks, with approximately 0.03 mmol of resin per flask. The fluorescently labeled peptide on resin was washed 2X with 10 mL DCM. Then 10 mL of a 30% hexafluoroisopropanol (HFIP) solution in DCM was added to the synthesis flask and agitated for 30 min. The resin was washed 2X DCM (10 mL), 2X MeOH (10 mL), 2X DCM (10 mL). This

step was repeated once more with an additional 10 mL of 30% HFIP solution, followed by the same washing cycle. Mtt deprotection was confirmed using the Kaiser test.

2.7.11 Hydrophobic group addition

To a 10 mm culture tube the desired hydrophobic carboxylic acid (0.27 mmol, 102 mg), HATU (0.23 mmol, 89 mg) and DIEA (0.27 mmol, 47 µL) were added followed by 10 mL of DMF. This solution was added to the peptide synthesis flask and agitated for 2 h at room temperature. The solution was drained and the resin was washed 2X DMF (10 mL), 2X DCM (10 mL), 2X MeOH (10 mL), 2X DCM (10 mL) and 2X DMF (10 mL).Coupling was confirmed using the Kaiser test prior to the last DMF wash.

2.7.12 Peptide cleavage from resin

The peptide on resin was washed with 10 mL of DCM and dried *in vacuo* for 1h. A TFA cocktail was prepared from 95% TFA (9.5 mL), 2.5% TIPS (triisopropylsilane) (250 µL) and 2.5% DIW (250 µL) for a total volume of 10 mL. 5 mL of the cocktail was added to the reaction flask and agitated for 2 hr. The peptide was drained into a pre-weighed 50 mL centrifuge tube using N_2. The resin was washed 2X with 5 mL of TFA and 2X with 5 mL DCM. The washes were collected in the same 50 mL centrifuge tube. TFA solution in the centrifuge tube was removed *in vacuo* and the crude peptide was precipitated through addition of 20 mL of cold diethyl ether and kept at -80 °C overnight. The crude peptide was centrifuged at 4000 rpm for 7 min and the diethyl ether was decanted and set aside. The crude peptide was dried under nitrogen for 30 min and solubilized in DIW at 10 mg/ mL

2.7.13 Peptide purification

The crude solution was purified via reverse phase high performance liquid chromatography (RP-HPLC) on a C18 semi prep column (Phenomenex) at a flow of 12 mL per min and detection at 214 nm. A linear solvent gradient of 15% - 65% acetonitrile (ACN) to water with 0.1% TFA in both solvent systems over a 60 minute gradient was used to collect the pure peptide. The pure peptide was characterized using matrix associated laser desorption MALDI-ToF mass spectrometry

Expected Mass Fl-P17-5B: 4162, obtained: 4159. Analytical pure retention time: 17.8 min

Expected Mass Fl-P17-5C: 4150, obtained: 4148. Analytical pure retention time:15 min

Expected Mass Fl-P17-5L: 4162, obtained: 4153. Analytical pure retention time: 19.8 min
View Appendix A.1 (**Fl-P17-5B**), A.2 (**Fl-P17-5C**), and A.3 (**Fl-P17-5L**): HPLC analytical trace and MALDI-ToF spectrum of pure **Fl-P17-5R** CAPHs.

2.7.14 Determination of peptide concentration using UV-Vis spectroscopy

In order to determine the concentration of **Fl-P17-5R** peptides UV-Vis was utilized. 5 µL of the peptide solution was added to 1 mL of tris(hydroxymethyl)aminomethane (TRIS) buffer, pH 8. The absorbance value was obtained at 494 nm, the absorbance maximum of fluorescein, and the concentration was calculated using the extinction coefficient 70,000 M^{-1} cm^{-1}.

2.7.15 Cell uptake studies using flow cytometry

For all in vitro cell experiments HaCat cells and J774A.1 cells were cultured in Dulbecco Modified Eagle Medium (DMEM) media supplemented with 10% fetal bovine serum (FBS) at 37°C under 5% CO_2.

2.7.15.1 J774A.1 cells

J774A.1 cells were plated in 300 µL of complete DMEM media at 125,000 cells/well in round bottom tubes (BD Biosciences) and incubated for 18-24 h at 37°C under 5% CO_2. The cells were centrifuged at 1200 rpm and the spent media was aspirated using a Pasteur pipet and vacuum filtration system. The cells were then treated with 300 µL of peptide at concentrations ranging from 1.25 – 5 µM prepared in 10% FBS supplemented DMEM media (complete DMEM media) and were allowed to incubate for the desired incubation time period at 37°C. Cells with no treatment (complete DMEM media only) served as the negative control for the experiment. Upon completion of the incubation period, the cells were centrifuged and the spent media was aspirated. The cells were then suspended in 300 µL of cold PBS in the round bottom tubes and the fluorescence of the cells was measured using a FACS Calibur flow cytometer (BD Biosciences). All samples were run in duplicate, and each experiment was repeated at least twice. The mean arbitrary florescence values of gated cells were measured and recorded upon excitation of the fluorophore, fluorescein, using the Fl-1 laser at 488 nm. For each experiment, a negative control of cells that were not incubated with fluorescent compound was also analyzed. Results were processed using the BD software.

2.7.15.2 HaCat cells

HaCat cells were plated in a 24 well plate at a volume of 400 µL with 100,000 cells per well in complete DMEM .The seeded cells were put in the incubator for 18-24 h at 5% CO_2 atmosphere at 37°C. The spent media was aspirated from the cells and the cells were washed with 300 µL of PBS. The cells were treated with 300 µL of peptide at 1.25 – 20 µM concentrations prepared in complete DMEM media and were allowed to incubate for the desired incubation time at 37°C. Cells with no peptide (complete DMEM media only) served as the negative control for the experiment. Upon completion of the incubation period, the cells were washed with 300 µL of PBS and treated with 150 µL of trypsin for 6 min at 37°C. The trypsin was quenched with 400 µL of cold PBS and the cells were transferred to round bottom tubes. The fluorescence of the cells was measured using a FACS calibur flow Cytometer (BD Biosciences). Data were obtained in duplicates from at least two independent experiments and were processed using the BD software. The mean arbitrary florescence values of gated cells were measured and recorded upon excitation of the fluorophore, fluorescein, using the Fl-1 laser at 488 nm.

2.7.16 Cell viability assay

Cytotoxicity of the **Fl-P17-5R** CAPHs was tested using the 3-(4,5-dimethylthiazol-2-yl)-2,5-diphenyltetrazolium bromide (MTT) cell viability assay.[188] J774A.1 cells and HaCat cells were tested for cytotoxicity after 9 h incubation with peptide treatment. J774A.1 cells and HaCat cells were seeded into a 96 well plates at 100 µL at a density of 20,000 cells/well and 10,000 cells/well, respectively, in complete DMEM media. After plating the cells, they were put in the incubator under 5% CO_2 atmosphere at 37°C for 18 to 24 h. The spent media was aspirated and the cells were washed with 100 µL PBS (phosphate buffered saline). Then, 50 µL of peptide treatment made in complete DMEM media was added to the cells at a concentrations ranging from 1.25 – 40 µM. The cells were put in the incubator under 5% CO_2 atmosphere at 37°C for 9 hr. Following incubation period the treatment media was aspirated and the cells were washed with 100 µL of PBS. Then, 100 µL of fresh complete DMEM media was added followed by the addition of 10 µL of MTT solution (5 mg /mL MTT in PBS) to each well. The cells were incubated for an additional 2.5 hr. The MTT solution was aspirated and 100 µL of DMSO was added to each well to dissolve the formazan crystals that formed. For each experiment, a negative control of cells not incubated with peptide were analyzed. The samples were run in duplicates and each experiment was repeated

at least twice. The mean absorbance for each sample was measured and recorded at 590 nm. Percent viability was determined by taking ratio of treated cells to untreated cells and multiplying by 100%.

2.7.17 Hemolysis assay

5mL of human red blood cells (hRBCs) (Innovative Research, cat # IWB3CPDA).were collected by centrifugation at 2000 rpm for 5 min followed by washing three times with 5mL of PBS, pH 7.4. The supernatant of the final wash was aspirated and 100 µL of the cell pellet was added to 4.9 mL of PBS to make a 2% suspension (v/v), with a total volume of 5 mL. To a 96 well plate, 50 µL of the hRBC solution was added followed by 50 µL of peptide treatment prepared in PBS to achieve a 2-fold dilution of peptide and a final suspension of 1% (v/v) of hRBCs. The plate was incubated at 37 °C under 5% CO_2 for 1 h. The plate was subsequently centrifuged at 1000 rpm for 5 min at 4 °C. Next 75 µL aliquots of the supernatants in each well were carefully transferred to a new 96-well plate. The release of hemoglobin was monitored by measuring the absorbance at OD_{405} with a micro-plate reader. As controls, hRBCs were treated with PBS as a negative control, 0.1% Triton X-100 as a positive control, and melittin (Sigma M2272) as a positive control. The percent hemolysis was calculated based on the 100% release with 0.1% Triton X-100. Data were obtained in duplicates from two independent experiments.

2.7.18 Confocal microscopy in live cells

High resolution imaging of subcellular localization of **Fl-P17-5R** CAPHs was performed in J774A.1 cells using inverted confocal florescent microscope (Nikon A1R) with a 60x oil objective. J774A.1 cells were seeded into 4-well LabTek culture chamber in 500 mL of complete DMEM media at a density of 125,000 cells/well. The cells were grown 12-24 hr in a humidified 5% CO2 atmosphere at 37°C. After pre-incubation, the cells were washed with 500 µL PBS. Then, 400 µL of peptide treatment was added to the wells at 5 µM concentrations prepared in growth media. The cells were incubated for 1 h or 3 h in the presence of the peptide treatment. Following incubation the cells were washed with 500 µL of PBS. Then, 400 µL of 100 nM Mitotracker with Hoescht 33258 solution prepared in growth media or 300 nM Lysotracker with Hoescht 33342 prepared in growth media were added to the wells and the cells were incubated for 30 minutes. Post incubation the cells were washed with 500 µL of PBS. Next, 500 µL of complete DMEM media was added

to each well prior to imaging. Live cells were then imaged using sequential laser scanning at 415 nm (Hoescht –not included in images), 488 nm (green channel) and 572 nm (red channel).

2.7.19 Antimicrobial activity against pathogenic bacterial isolates

The minimum inhibitory concentration (MIC) of peptides (in µM/ml) and control antibiotics (vancomycin and gentamicin) in µg/ml, were determined using the broth microdilution method against different bacterial strains. The antimicrobial activity of the tested peptides and control antibiotics against the tested isolates was performed following the Clinical and Laboratory Standards Institute guidelines[189]. Briefly, bacterial cells were cultured overnight on tryptic soya agar plates (Becton Dickinson). Colonies were picked and suspended in NaCl 0.9% to a density of 0.5 McFarland. The bacterial suspensions were further diluted 1:60 in cation adjusted Mueller-Hinton Broth (CA-MHB) (Becton Dickinson), and 100 µl portions of the bacterial suspension were added to 96-well plates (Corning Incorporated) containing the tested peptides and control antibiotics prepared in filtered deionized water at a concentrations ranging from 0.125 to 32 µM. The 96-well plates were incubated for 16–20 h at 37 °C before recording the MIC values. The MICs reported represent the lowest concentration of each peptide or standard antibiotic necessary to inhibit bacterial growth from at least two separate experiments done in duplicate.

2.7.20 *In cyto* experiments

The activity of **Fl-P17-5R** against intracellular *Acinetobacter baumannii, Salmonella typhimurium, Shigella flexneri, Listeria monocytogenes, and Staphylococcus aureus* were tested according to the following protocol. Briefly, J774A.1murine macrophage-like cells were seeded at a density of 1×10^5 cells per well in 96-well plates (Corning Incorporated) for 24 hours before being infected with bacteria. The cells were routinely grown in Dulbecco's Modified Eagle Medium (DMEM) supplemented with 10% heat-inactivated fetal bovine serum. Following incubation, the cells were washed once with DMEM. Then cells were co-incubated with bacteria for 60 min (multiplicity of infection MOI were 1: 10 for *Acinetobacter, Salmonella* and *Staphylococcus* strains, while MOI for the tested *Shigella* and *Listeria* strains were 1:100 and 1: 1 respectively. Following infection, cells were washed three times with DMEM medium containing 100 µg/ mL gentamicin (Sigma) and was further incubated for 3 hours with gentamicin (100 µg/ mL) to get rid of non-phagocytized bacteria. Then DMEM medium supplemented with 10% fetal bovine serum containing the tested

compounds at the respective concentrations were added to the cells. Control untreated cells were kept exposed to gentamicin 10 µg/ml to remove any potential extracellular bacteria. The plate was then returned to the incubator and the intracellular clearance activity of **Fl-P17-5R** were assessed after 12 hours. At the end of the incubation time, the infected cells were washed three times with PBS and lysed with 100 µL of 0.01% triton-x to collect the intracellular bacteria. The colony forming units (CFUs) of the bacteria in the lysates were determined by plating a series of 10-fold serial dilutions onto tryptic soy agar (TSA) and incubating the plates at 37 °C for 24 hours. Statistical significance was assessed with one-way ANOVA, with post hoc Dunnet's multiple comparisons test ($P < 0.05$), using GraphPad Prism 6.0 (GraphPad Software, La Jolla, CA).

2.7.21 Antibiofilm activity

The anti-biofilm activity of Fl-P14 and Fl-P17 peptides was assessed using XTT assay as previously reported. [161, 190, 191] Briefly, overnight bacterial cultures of *K. pneumoniae, S. entrica,* and *E. facieum* were diluted (1:100) in TSB medium and the plates were incubated at 37°C for 24 h to allow the formation of bacterial biofilms. The plates were washed twice with PBS. CAPHs and the control antibiotics (gentamicin and vancomycin) were tested at three different concentrations (16, 32 and 64 uM). The tested compounds were serially diluted in TSB medium. 100 µl volumes of each treatment were added to the corresponding wells containing the tested biofilm and were then incubated for another 24 h at 37ºC. Wells containing the formed biofilm, but no drugs, served as negative control for each of the tested strains. Following incubation, biofilms were washed three times with sterile PBS and metabolic activity were determined using the XTT reduction assay. 100 µl volumes of XTT/ menadione solution were added to each well and the plates were incubated at 37°C in the dark for 1 h. Before reading, 80 µL of reaction mixture was transferred to a clean flat-bottomed microtiter plate and read in a microplate reader at 490 nm. Data were presented as the percentage of biofilm viability relative to the control.

2.7.22 Cell uptake inhibitory assays

J774A.1 cells were cultured in Dulbecco Modified Eagle Medium (DMEM) media supplemented with 10% fetal bovine serum (FBS) at 37°C under 5% CO2. J774A.1 cells were plated at 125,000 cells in round bottom tubes (BD Biosciences) for 18-24 h. These cells were then centrifuged and the spent media was aspirated. Next 300 µL of the inhibitor solution, 1 µM gramicidin D/ 3 µM

Phenyl Arsine Oxide/ 10 µM Cytochlasin D/ 0.4M sucrose prepared in serum free media, was added followed by a 30 min incubation period. Next CAPHs were added to the cells still suspended in the inhibitor media to achieve a 5 µM concentration of peptide prepared in a total of 300 µL of complete DMEM media, which was then gently vortexed. The cells were allowed to incubate with the peptide in the presence of inhibitor for 1h at 37°C. Cells with no treatment (complete DMEM media only) served as the negative control for the experiment. Upon completion of the incubation period, the cells were centrifuged and the spent media was aspirated. The cells were then suspended in 300 µL of cold PBS and the fluorescence of the cells was measured using a FACS Calibur Flow Cytometer (BD Biosciences). Data were obtained in duplicates from three independent experiments using filter Fl-1 (488 nm).

CHAPTER 3. INCORPORATION OF A MORE RIGID CATIONIC RESIDUE INTO CAPHS

3.1 Introduction

The continuous emergence of antibiotic-resistant pathogens worldwide has become a major threat to public health. Many therapeutics lack certain properties that would enable them to have good bio-distribution, easy administration and the ability to reach impermeable areas of the body, such as cells. We have taken advantage of some of the shared features between CPPs and AMPs to develop a new class of cell penetrating peptide antibiotics: cationic amphiphilic polyproline helices (CAPHs). The cell penetration proficiency of CAPHs combined with their antimicrobial potency allow them to be highly effective in killing intracellular bacteria,

To evaluate the characteristics required for the optimal activity of CAPHs, we have assessed varying backbone lengths, the incorporation of different hydrophobic groups, and oligomer formation with CAPHs.[87, 88, 90, 139, 165, 192] Studies have shown that the length of the side chains can be altered to promote cell uptake.[193, 194] Thus, we have sought to determine if shortening the distance between the guanidinium group and the proline backbone of CAPHs would impact antimicrobial activity and cell penetration for improved clearance of intracellular bacteria.

3.2 Design

CAPHs are composed of a polyproline helical backbone with side-chain functionality expressing hydrophobic isobutyl groups (P_L) and hydrophilic and cationic guanidinium residues (P_R) (Figure 3.1A). In this study, we sought to explore if we could modify the antimicrobial activity and cell penetration ability of CAPHs by replacing the cationic residue, P_R, of the parent peptide Fl-P14LRR with a proline monomer displaying a shorter guanidinium containing side chain. In order to achieve this, we eliminated ether moiety and the methylene chain between the proline backbone and the guanidinium group. In this way, by having the guanidinium group directly attached to the proline residue, we created a guanylated amino proline (GAP) monomer to produce a new analogue of CAPHs, **Fl-P14GAP** (Figure 3.1B).

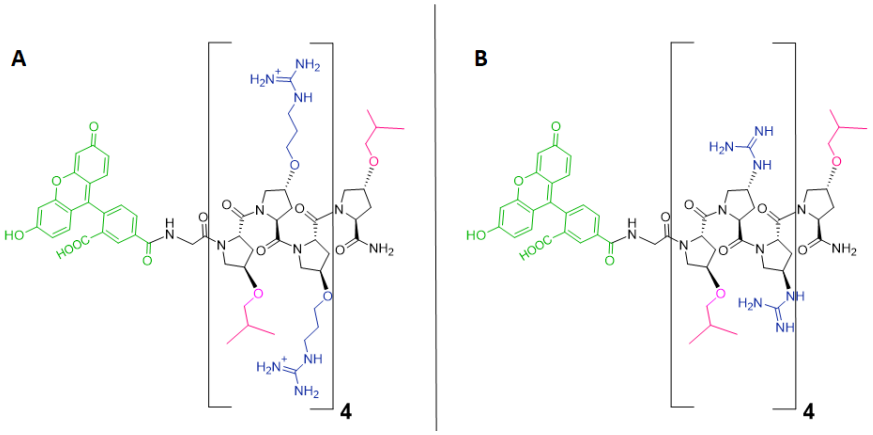

Figure 3.1 Structure of (A) P14LRR composed of P_L and P_R and (B) **Fl-P14GAP** composed of P_L and GAP. The hydrophilic monomers are shown in blue and hydrophobic monomer in pink.

3.3 Synthesis of GAP Amino Acids and **Fl-P14GAP** Peptide

The synthesis of GAP was achieved using commercially available (2S,4R)-Boc-4-amino-1-Fmoc-pyrrolidine-2-carboxylic acid (Scheme 3.1). The tert-butyloxycarbonyl (Boc) group was removed under acidic conditions to produce a free amine, which was treated with N,N′-di-boc-1H-pyrazole-1-carboxamidine to provide the desired GAP amino acid. To complete the hydrophobic, hydrophilic, hydrophilic triad that composes CAPHs the hydrophobic amino acid, P_L, was also synthesized, beginning with carboxybenzyl (Cbz) protected hydroxyproline (Scheme 1B). The hydroxyl group of hydroxyproline was functionalized with methyl propene through an SN_2 prime reaction to produce compound 5. This was followed by the simultaneous removal of the Cbz protecting group and the reduction of the alkene through a palladium catalyzed hydrogenation step. The deprotected free amine was Fmoc-protected to yield Fmoc-P_L.

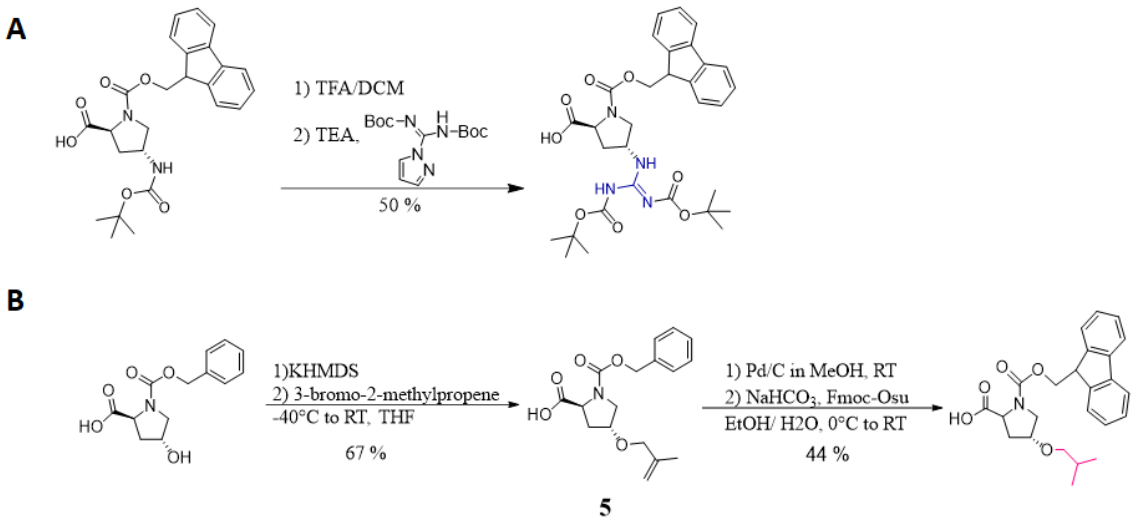

Scheme 3.1 Synthesis of monomers (A) Fmoc protected guanylated amino proline (GAP) and (B) Fmoc-P_L.

With both monomers in hand, we proceeded to Fmoc-based solid phase peptide synthesis using the Rink amide resin (Figure 3.2). Once the desired peptide sequence was complete, a fluorescein was coupled to the N-terminus of the peptide, preceded by one glycine spacer to yield **Fl-P14GAP**. The peptide was globally deprotected and detached from the resin using a TFA cocktail and subjected to reverse-phase high-performance liquid chromatography (RP-HPLC). The desired product was confirmed using matrix assisted laser desorption ionization time of flight (MALDI-ToF) mass spectrometry.

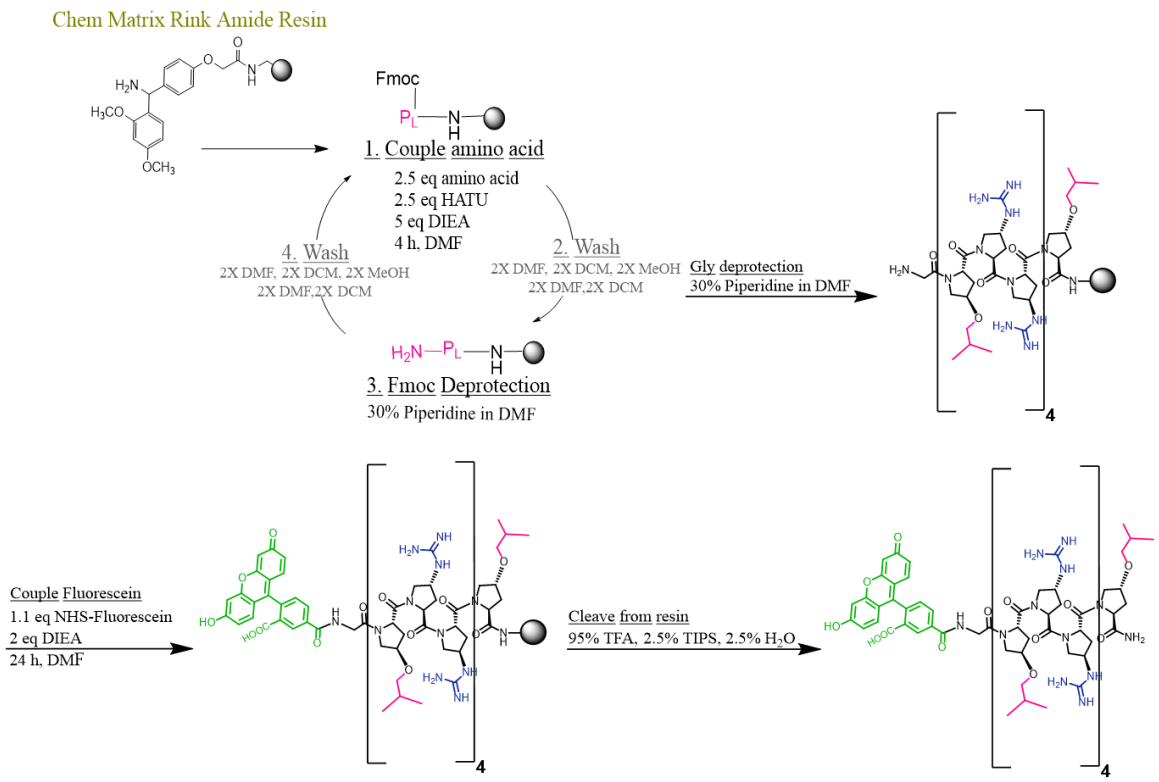

Figure 3.2 Synthesis of **Fl-P14GAP** on solid support using Fmoc based chemistry.

3.4 Results and Discussion

3.4.1 Cell uptake studies in J774A.1 and HaCat cells

Although CPPs and AMPs have been studied extensively in recent years, there remains great ambiguity regarding the properties that contribute most to their activity. The results of these studies, like many similar studies, are controversial. In one study, the methylene length between the peptoid backbone and the guanidinium group was varied from 2-6 carbons, and it was found the longer the length of the alkyl chain the greater the cell uptake.[194] Furthermore, they determined that the conformational flexibility and the sterically unencumbered nature of the alkyl chains was important for high cellular uptake.[194] On the other hand, Wenemmers and colleagues determined that an organized charge display provided by guanidinium groups in a D-oligoarginine CPP resulted in enhanced cell uptake in comparison to a D-oligoarginine CPP with guanidinium groups expressing greater flexibility.[193] In order to evaluate the effect the GAP monomer would have on CAPHs, cell accumulation studies were conducted using flow cytometry.

We were particularly interested in determining if the GAP modification enhanced cell uptake in J774A.1 macrophage cells, which are havens for intracellular bacteria.[142] The cell uptake ability of **Fl-P14GAP** was tested at concentrations of 2.5, 5, and 10 µM in J774A.1 cells (Figure 3.3A). Encouragingly, **Fl-P14GAP** exhibited a 7-fold, 10-fold, and 5-fold increase in cell accumulation at 2.5, 5, and 10 µM, respectively, in comparison to Fl-P14LRR. These results demonstrate that decreasing the conformational freedom of the side chains through the elimination of the methylene units results in enhanced cellular uptake with CAPHs.

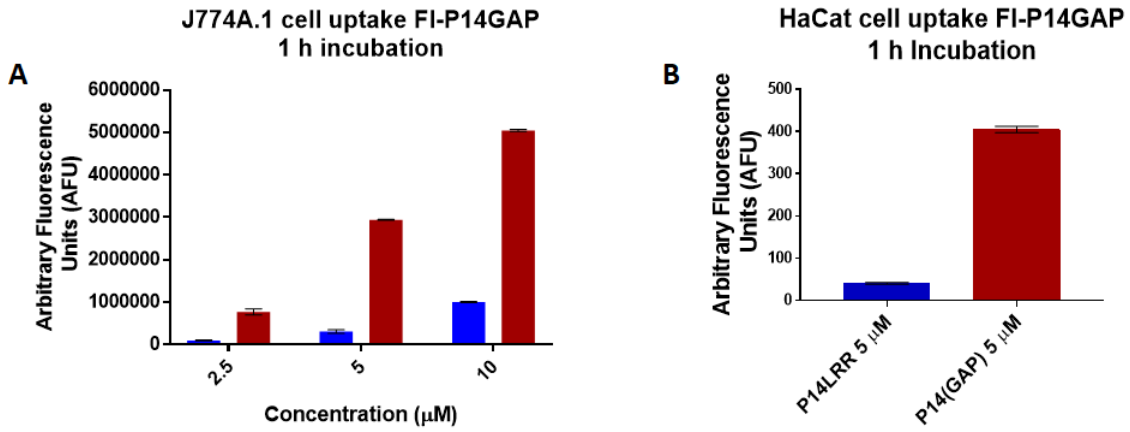

Figure 3.3 Flow cytometry results comparing arbitrary fluorescence of (A) J774A.1 cells and (B) HaCat cells after 1 h treatment with **Fl-P14GAP** (red) or Fl-P14LRR (blue).

We were also interested in using CAPHs to target intracellular bacteria that transverse skin cells, so we conducted cell uptake studies of **Fl-P14GAP** in keratinocytes. For this pursuit, HaCat cells were used. Similarly, HaCat cells were incubated with **Fl-P14GAP** for 1 h at 5 µM concentration and cell uptake was quantified using flow cytometry (Figure 3.3B). In comparison with Fl-P14LRR, **Fl-P14GAP** exhibited a 10 fold increase in cell uptake in HaCat cells, similarly to the difference observed in J774A.1 cells at this concentration.

3.4.2 Confocal microscopy to determine the subcellular location of **Fl-P14GAP**

With the drastic enhancement in cell uptake, our next step was to determine the subcellular location of **Fl-P14GAP**. Confocal microscopy was utilized to visualize the subcellular niche of **Fl-P14GAP** at concentrations of 1.25, 2.5, and 5 µM in J774A.1 cells after 1 h incubation (Figure 3.4). Endosomes and mitochondria were stained with LysoTracker and MitoTracker dyes,

respectively, to determine if **Fl-P14GAP** localized to either of these intracellular compartments. Confocal experiments revealed that at all concentrations **Fl-P14GAP** has a dominant presence in endosomes with no association with mitochondria. We also found that, starting at 2.5 μM concentration, **Fl-P14GAP** showed distinct membrane binding, which is apparent based on the distinguishable fluorescent outline around the cell (Figure 3.4, 2.5 and 5 μM). The subcellular location of **Fl-P14GAP** did not change by extending the incubation period to 3 h (Figure 3.5). At 3 h, there is more **Fl-P14GAP** present and the cell membrane binding also becomes more intense at 2.5 and 5 μM. Notably, at 5 μM, some of the cells show **Fl-P14GAP** occupying the cytoplasm. At 1.25 μM, where membrane binding was not noticeable at 1 h, after 3 h incubation, the peptide association with the cell membrane became somewhat visible. Still, there was no association of **Fl-P14GAP** with the mitochondria at any of the tested concentrations. Thus, the incorporation of GAP amino acid changes the subcellular fate of CAPHs, as Fl-P14LRR shows significant localization to the mitochondria with some endosomal localization under these conditions. Based on these findings one can conclude that **Fl-P14GAP** has an affinity to bind to the cell membrane, which may lead it to enter cells through in endocytic route based on its high association with endosomes at all concentrations. At 5 μM and after a 3 h incubation period, endosomal accumulation increases and **Fl-P14GAP** begins to appear in the cytoplasm.

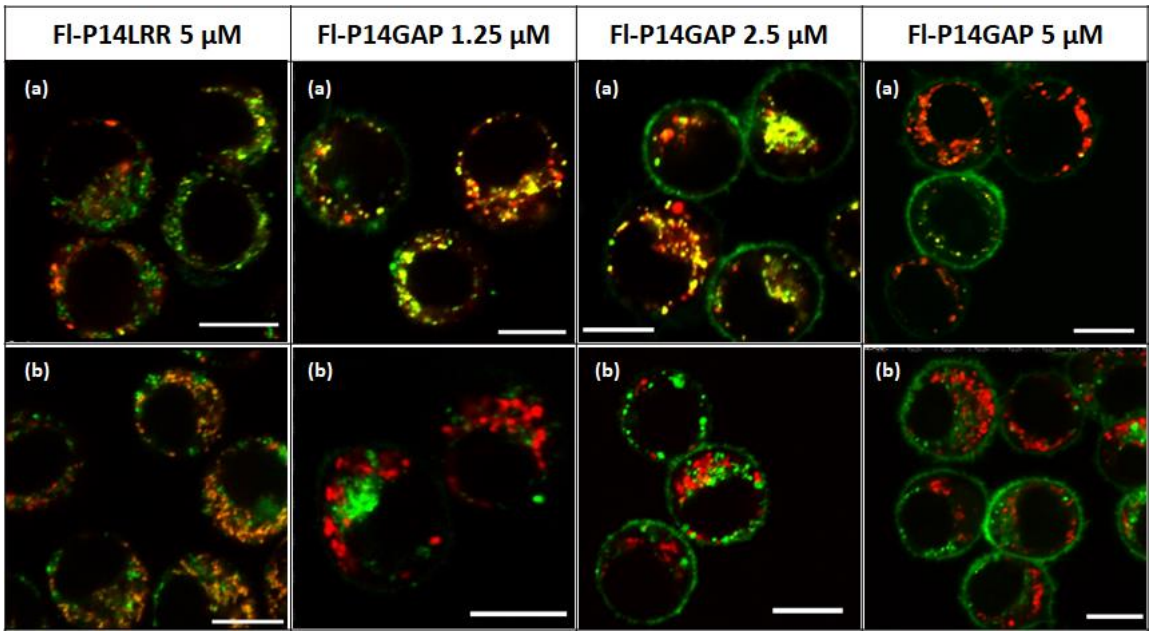

Figure 3.4 Confocal microscopy overlay images of **Fl-P14GAP** fluorescence (green) at 1.25, 2.5, and 5 µM and Fl-P14LRR fluorescence with organelle stain fluorescence (red) at 5 µM in J774A.1 cells after 1 h incubation. Cell location was studied with (a) Lysotracker and (b) Mitotracker (Scale bars = 10 µM), a yellow-orange color, indicates co-localization.

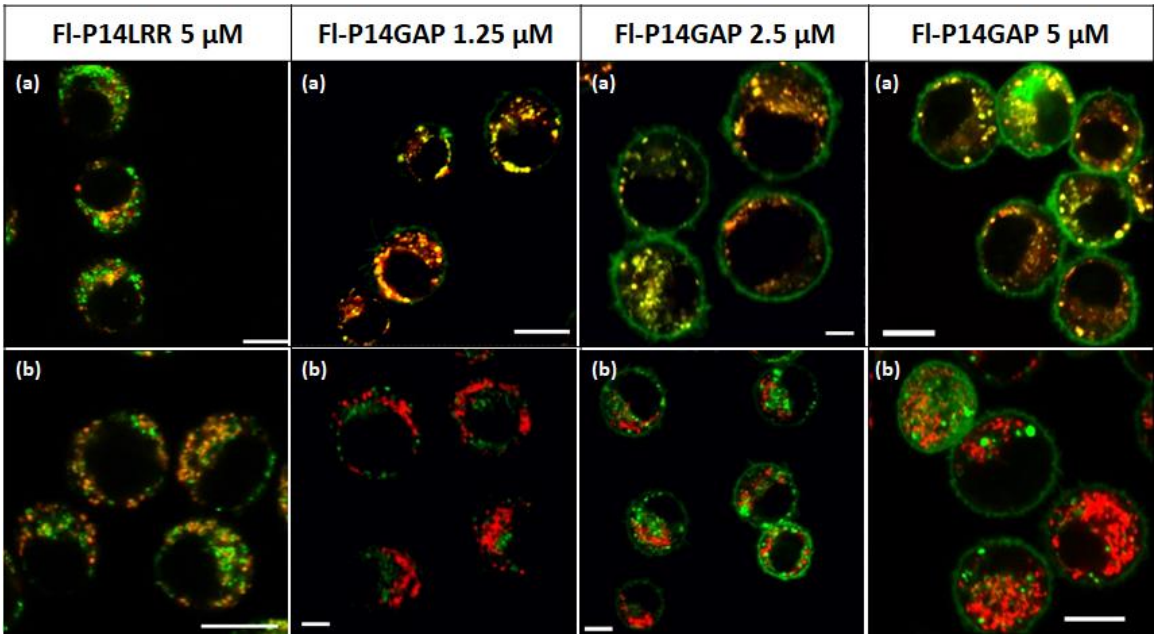

Figure 3.5 Confocal microscopy overlay images of **Fl-P14GAP** fluorescence (green) at 1.25, 2.5, and 5 µM and Fl-P14LRR fluorescence with organelle stain fluorescence (red) at 5 µM in J774A.1 cells after 3 h incubation. Cell location was studied with (a) Lysotracker and (b) Mitotracker (Scale bars = 10 µM), a yellow-orange color, indicates co-localization.

It was also of interest to obtain information regarding the subcellular fate of **Fl-P14GAP** in HaCat cells at 5 μM after 1 h and 3 h incubation (Figure 3.6). Intense green fluorescence was observed for **Fl-P14GAP** around the periphery of the cells at both time points. There was also some endosomal localization, but, once again, no interaction with the mitochondria. It was also seen that the endosomes of HaCat cells mostly group together in+ the center of the cell and there is some dispersity of endosomes throughout the cytoplasm as well. Nevertheless, zoomed images confirm that there is co-localization of **Fl-P14GAP** with endosomes in both scenarios (Figure 3.7) Despite the endosomal occupancy, the high presence of peptide around the cell indicates that **Fl-P14GAP** is significantly membrane-bound with HaCat cells under these conditions.

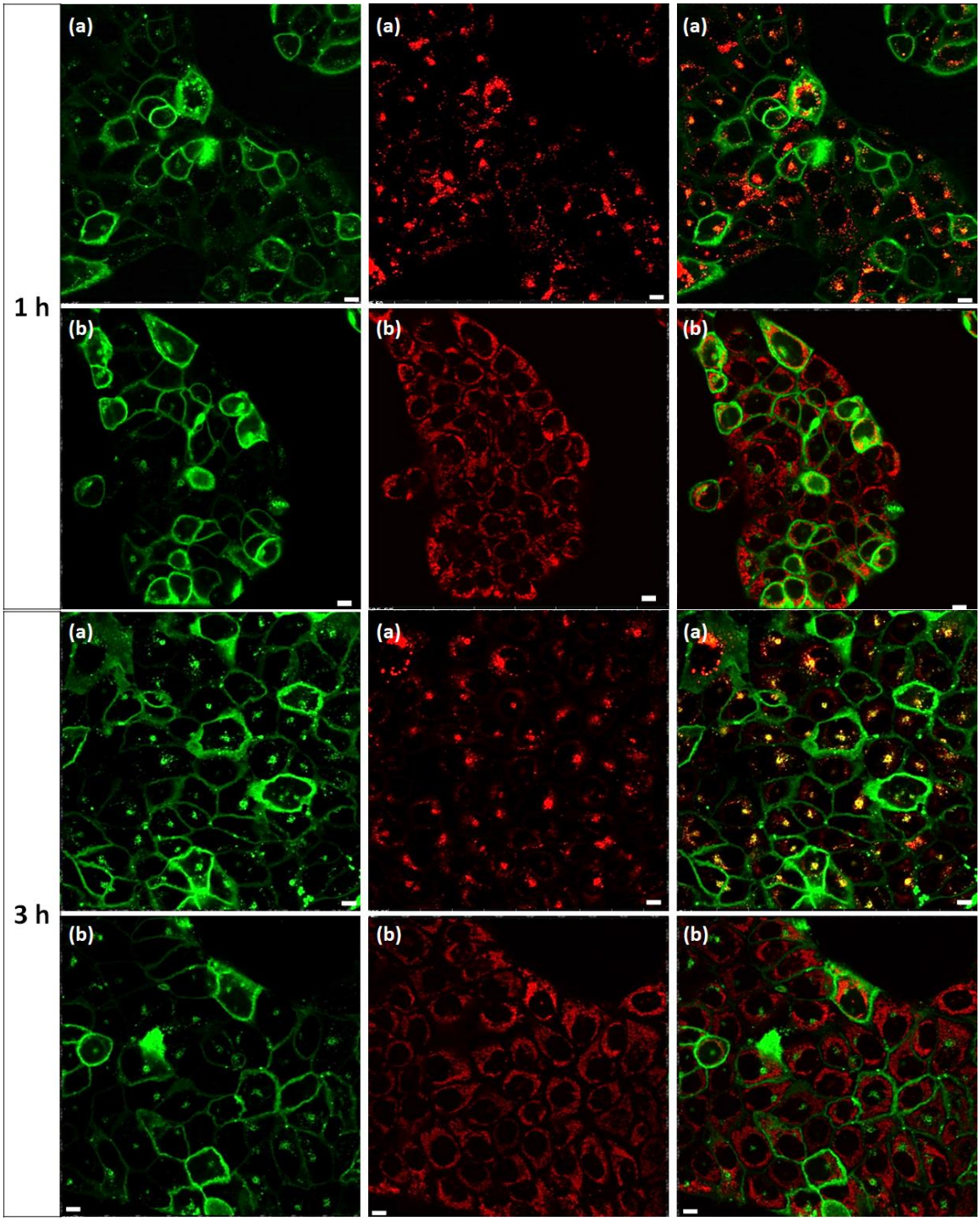

Figure 3.6 Confocal microscopy images showing the subcellular location of **Fl-P14GAP** at 5 µM in HaCat cells after 1 h and 3 h incubation.. Cell location was studied with (a) Lysotracker (red) and (b) Mitotracker. Scale bars = 10 µM, a yellow/orange color indicates co-localization. Three channels of each image are depicted: first column = peptide only (green), second column = tracking dye only (red) and third column = overlay of both channels.

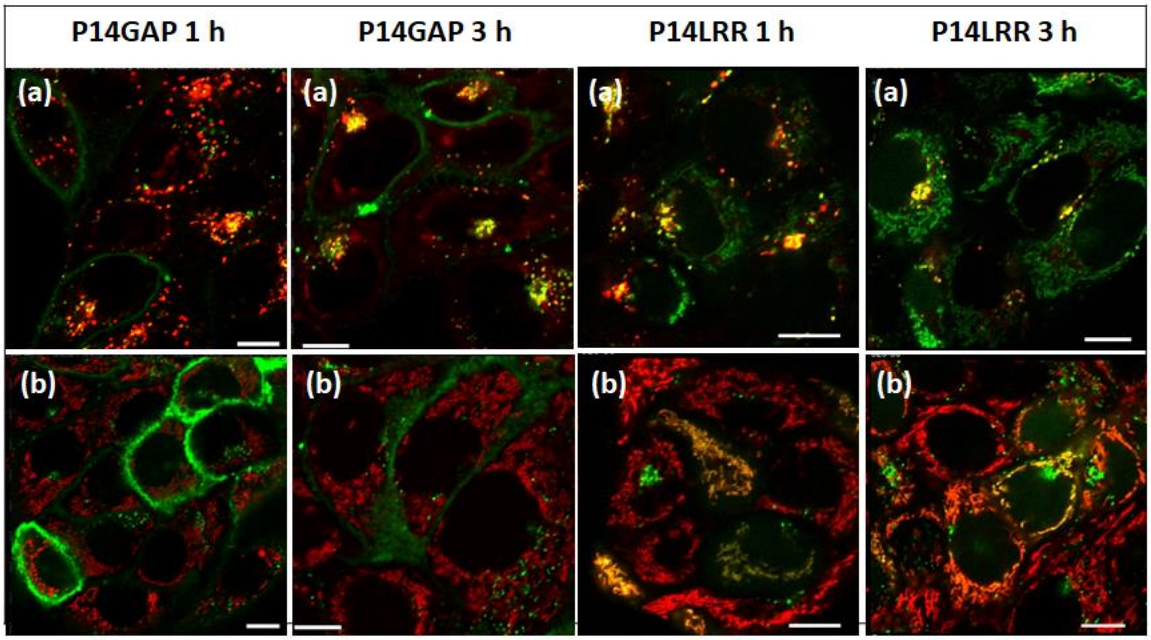

Figure 3.7 Zoomed-in overlay confocal microscopy images showing the subcellular location of CAPHs (green) **Fl-P14GAP** and Fl-P14LRR at 5 µM in HaCat cells after 1 h and 3 h incubation. Cell location was studied with (a) Lysotracker (red) and (b) Mitotracker (red). Scale bars = 10 µM, a yellow/orange color indicates co-localization.

In contrast to **Fl-P14GAP**, Fl-P14LRR localizes with both endosomes and mitochondria in HaCat cells at 5µM (Figure 3.8). Moreover, areas in which Fl-P14LRR co-localizes with endosomes are punctate and shown sporadically throughout the cell. There is significant mitochondrial co-location, as supported by the images with Mitotracker dye (Figure 3.7). In these images, especially at 3 h incubation, there is a clear outline of peptide that directly aligns with the structure of the mitochondria. It is important to note that Fl-P14LRR shows limited binding around the cell periphery. This indicates that Fl-P14LRR does not bind to the cell membrane in the manner that **Fl-P14GAP** does.

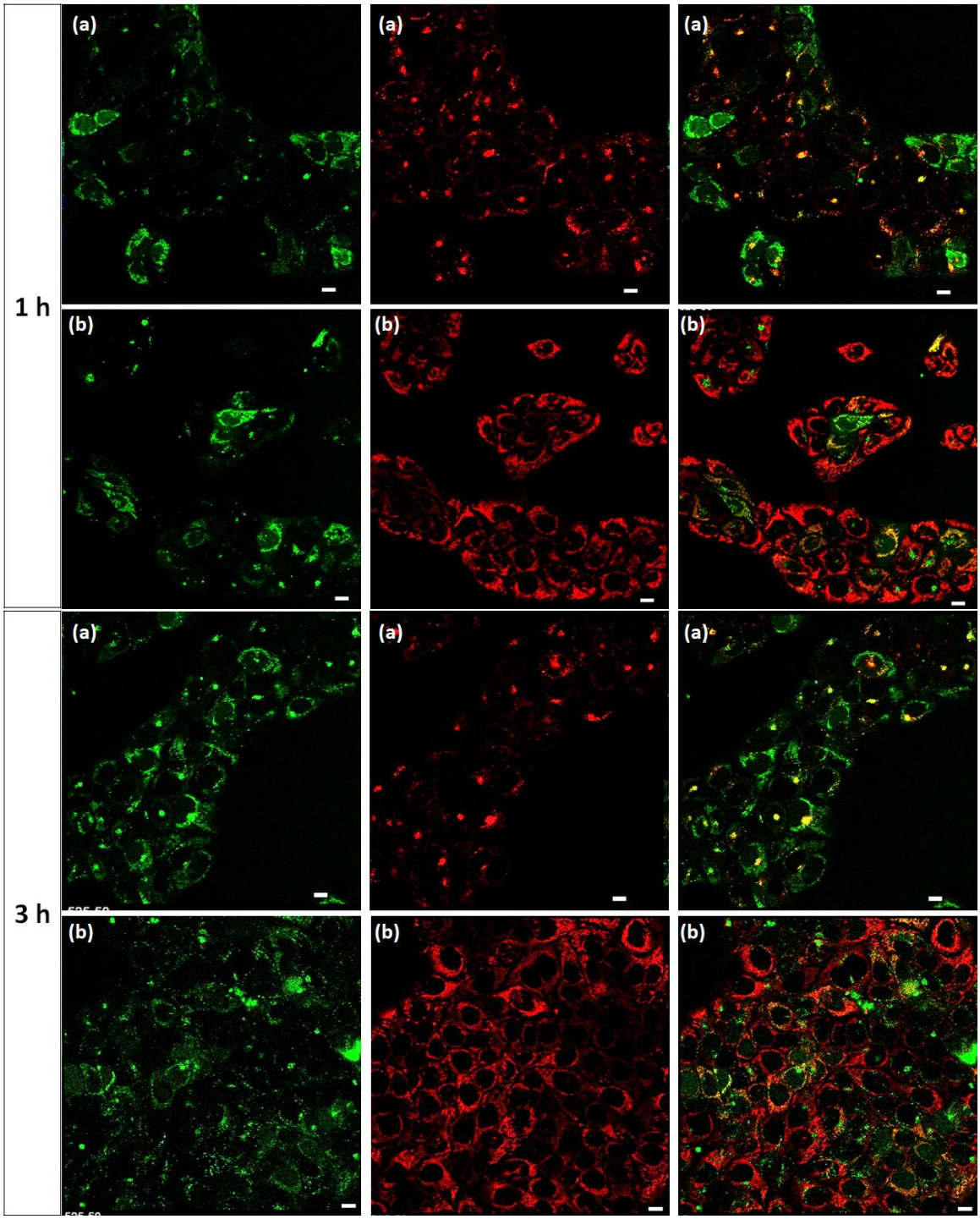

Figure 3.8 Confocal microscopy images showing the subcellular location of Fl-P14LRR at 5 µM in HaCat cells after 1 h and 3 h incubation.. Cell location was studied with (a) Lysotracker (red) and (b) Mitotracker. Scale bars = 10 µM, a yellow/orange color indicates co-localization. Three channels of each image are depicted: first column = peptide only (green), second column = tracking dye only (red) and third column = overlay of both channels.

3.4.3 Toxicity studies

Having established that **Fl-P14GAP** modified CAPHs are associated with cells to a significant extent, we next sought to determine whether any cytotoxicity concerns would arise when we incubated **Fl-P14GAP** with J774A.1 cells using the MTT assay (Figure 3.9A).[188] This study revealed that **Fl-P14GAP** shows good cell viability up to 5 µM, then it viability drops to about 50% at 10 µM. HaCat cell viability was also tested in the presence of **Fl-P14GAP** (Figure 3.9B). Under the same conditions, we found that HaCat cell viability was about 75% at 10 µM of **Fl-P14GAP**, but dropped at higher concentrations.

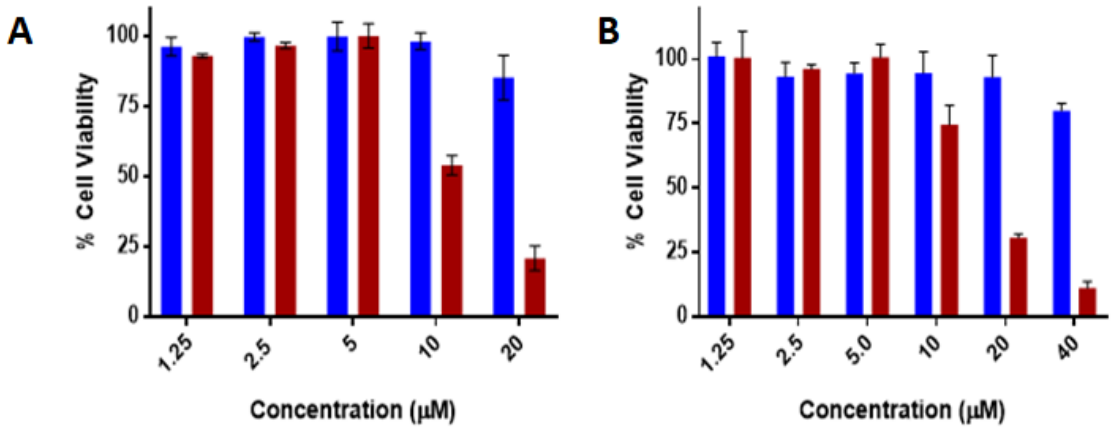

Figure 3.9 MTT assay showing cell viability of (A) J774A.1 and (B) HaCat cells after incubation with Fl-P14LRR (blue) and **Fl-P14GAP** (red) for 9 h at concentrations ranging from 1.25 to 20 µM.

To further investigate potential toxicity concerns, we employed a hemolysis assay to determine if **Fl-P14GAP** is harmful to human red blood cells (hRBCs). We monitored if **Fl-P14GAP** exhibited lytic behavior towards hRBCs at concentrations ranging from 0.625 to 80 µM (Figure 3.10). This study revealed that **Fl-P14GAP** does not exhibit RBC lysis at concentrations up to 10 µM. Beginning at 20 µM, however, we do begin to observe slight lytic activity, but not to the extent of hemolysis caused by known lytic CPP, melittin. The hRBC activity of **Fl-P14GAP** more closely resembles Fl-P14LRR, which has been previously established to have a non-lytic mode of action. Overall, **Fl-P14GAP** presents no toxicity concerns at 5 µM in either of the executed toxicity studies.

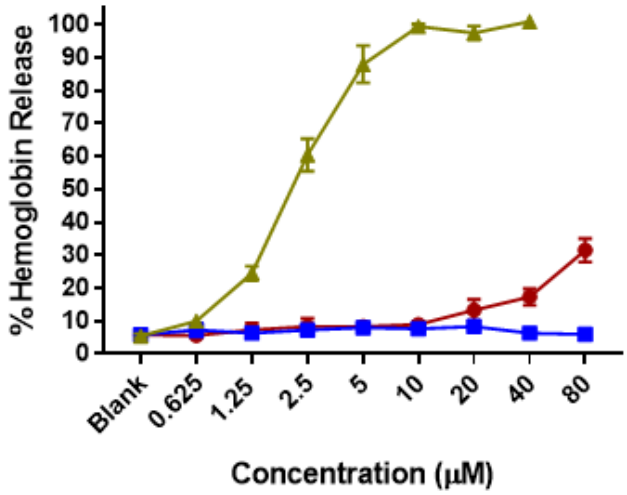

Figure 3.10 Hemolysis assay monitoring the release of hemoglobin from hRBCs in the presence of Fl-P14LRR (blue), **Fl-P14GAP** (red), and positive control Melittin (green) at 1 h incubation.

3.4.4 Analysis of cell surface binding

The results of our fluorescent confocal microscopy studies led us to question if the increase in cell uptake we previously observed was attributed to surface membrane binding rather than actual internalization of **Fl-P14GAP**. To probe this question, trypan blue was used to quench any membrane associated fluorescence.[195, 196] The amount of surface bound **Fl-P14GAP** versus internalized **Fl-P14GAP** was measured by comparing the arbitrary fluorescence (AF) of cellular fluorescence quenched with trypan blue to cells not quenched with trypan blue after 1 and 3 h incubations using flow cytometry (Figure 3.11). Both J774A.1 and HaCat cells were studied.

In the case of J774A.1 cells, a 1 h incubation with **Fl-P14GAP** followed by quenching membrane associated fluorescence resulted in a 22 and 33% decrease in cell fluorescence at 2.5 and 5 µM, respectively (Figure 3.11A). Additionally, the cellular fluorescence reduced by 30 and 17% at 2.5 and 5 µM for **Fl-P14GAP**, respectively, after a 3 h incubation (Figure 3.11B). Although this does demonstrate that some of the observed cell uptake was due to membrane binding, the level of membrane binding with **Fl-P14GAP** was no different than that of Fl-P14LRR under the same conditions. At 5 µM, Fl-P14LRR cellular fluorescence decreased by 26% in J774A.1 cells after 1 h and 28% after 3 h incubation. It is interesting to note that at 5 µM, after 3 h incubation a greater cellular fluorescence and a smaller percent decrease with trypan blue is observed with **Fl-P14GAP**,

meaning more peptide accumulated into the cells rather than the enhancement of cellular fluorescence being the result of increased membrane binding. Accordingly, under these conditions, more **Fl-P14GAP** is translocated into the cell with time. Interestingly, confocal microscopy images showed less cell internalization than these experiments would predict.

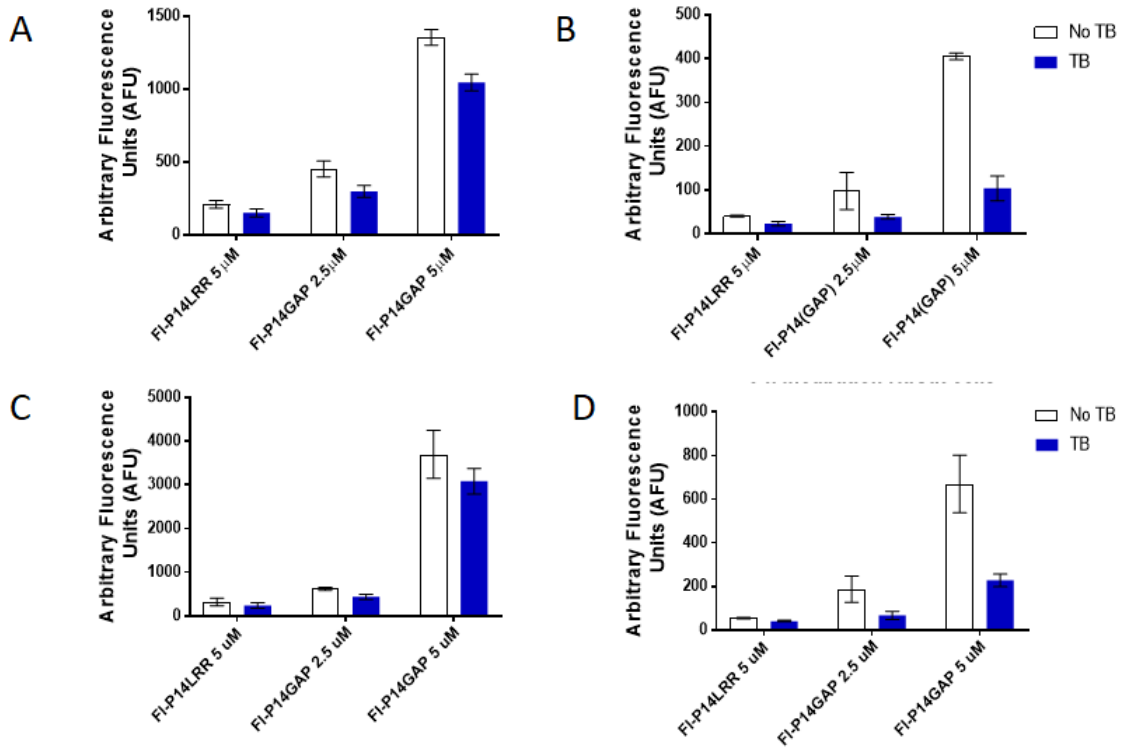

Figure 3.11 Cell uptake studies of **Fl-P14GAP** and Fl-P14LRR at (A) 1 h and (C)3 h in J774A.1 cells after (B) 1 h and (D) 3 h incubation in HaCat cells with trypan blue treatment (blue bar) and without trypan blue treatment (white bar).

On the contrary, HaCat cells demonstrated a completely different dependence on cell surface-associated cellular fluorescence. After 1 h incubation with **Fl-P14GAP** at 2.5 and 5 μM followed by quenching with trypan blue, the cellular fluorescence decreased by 60 and 75%, respectively. Additionally, cellular fluorescence decreased by 66% at 5 μM and 64% at 2.5 μM after 3 h incubation. Thus, the amount of membrane binding in HaCat cells does not decrease with longer incubation times in HaCat cells, unlike what was observed in J774A.1. In J774A.1 cells a longer incubation resulted in more **Fl-P14GAP** accumulating in the cell based on a smaller decrease in cellular fluorescence at 3 h versus 1 h at 5 μM (17 and 33%, respectively) in the presence of TB,

whereas, in HaCat cells the level of decrease in cellular fluorescence was similar between 1 h and 3 h (60 and 66%, respectively) after quenching surface binding with TB. Despite membrane binding accounting for some of the observed improvement in cell uptake, **Fl-P14GAP** still accumulates in J774A.1 and HaCat cells at about a 7-fold and 5-fold higher rate, respectively, than Fl-P14LRR. Thus, **Fl-P14GAP** remains a superior choice for penetrating J774A.1 and HaCat cells than Fl-P14LRR.

The cell membrane is a major obstacle that the peptide must overcome to achieve cell uptake. The results of the cell uptake studies and confocal microscopy studies that we reported herein show that the extent of uptake is dependent on both the concentration of the peptide and the properties of its guanidinium containing residues. The external layer of eukaryotic cells possesses a high level of negative charges due to the presence of anionic lipids, such as phospholipids and glycosaminoglycans, mediating the interaction between cationic peptides and the membrane through electrostatic affinity. Though this interaction helps cationic CPPs enter cells, it can also cause a substantial amount of peptide association with the plasma membranes even after extensive washing.[197] The binding of the anionic lipid head groups of cells is enhanced with the GAP amino acid, which has more organized and tightly packed guanidine groups that could efficiently interact with negatively charged components on the cell membrane. Additionally, the tight and rigid binding of the GAP monomer on the membrane surface could result in decreased membrane fluidity, causing the peptide to become trapped in the bilayer. Combined, these characteristics may explain the significant membrane association observed by **Fl-P14GAP** compared to the parent peptide Fl-P14LRR, which has a flexible guanidine group, P_R.

3.4.5 Minimum inhibitory concentration against bacterial isolates

With improved cell uptake confirmed, the next step was to determine if **Fl-P14GAP** also exhibited enhanced antimicrobial potency. The minimum inhibitory concentrations (MICs) of **Fl-P14GAP** against a number of enteric and ESKAPE bacterial strains was determined through a microbroth dilution assay (Table 3.1). The activity of **Fl-P14GAP** was directly compared to the activity of Fl-P14LRR. **Fl-P14GAP** was more potent than Fl-P14LRR across the board, displaying a 2 to 16-fold increase in antimicrobial activity against all tested strains. It is also important to note that all the MICs were well below 10 µM, the `concentration where we began to see *in cyto* toxicity. These

results indicate that incorporating the GAP amino acid into **Fl-P14GAP** did indeed result in superior antibacterial ability.

Table 3.1 Minimum inhibitory concentration (MIC) of **Fl-P14GAP** (highlighted yellow column) and Fl-P14LRR against pathogenic bacteria isolates using the microbroth dilution assay after 20 h of treatment. Controls vancomycin and gentamicin MIC in µg/mL. ND = not determined.

Minimum Inhibitory Concentrations (MIC)				
Strain ID	**Fl-P14LRR**	**Fl-P14GAP**	**Vancomycin**	**Gentamicin**
Activity against ESKAPE pathogens				
+ *E. faecium* 700221	2	1	> 32	> 32
+ *S. aureus* NRS 384	16	2	0.5	0.5
- *K. pneumoniae* 1706	> 32	8	> 32	2
- *A. baumannii* 1605	1	0.5	8	> 32
- *P. aeruginosa* 50573	16	2	> 32	0.25
- *E. cloacae* 1134	32	2	> 32	0.5
Activity against more *Staphylococcus* spp.				
***S. aureus* NRS 383**	32	2	4	> 32
***S. aureus* NRS 382**	32	2	1	0.5
***S. aureus* RN 4220**	32	2	0.5	0.5
***S. aureus* ATCC 6538**	16	1	0.5	0.125
***S. epidermidis* NRS 101**	2	1	2	32
VRSA 5	16	2	4	0.5
VRSA 10	8	2	> 32	0.5
Activity against more *Pseudomonas aeruginosa* strains				
***P. aeruginosa* 48982**	32	4	> 32	> 32
***P. aeruginosa* 31040**	32	2	> 32	16
***P. aeruginosa* 31041**	32	2	> 32	32
Activity against more *Acinetobacter baumannii* strains				
***A. baumannii* 1747**	1	0.5	> 32	0.25
***A baumannii* 19606**	2	1	32	16
Activity against enteric pathogens				
+ L. monocytogenes 191112	8	2	1	0.5
- S. *flexneri* 1a	4	1	> 32	0.5
- *S. enteritidis*	4	1	> 32	0.25
- *E.coli* 21922	4	1	> 32	2
- *S. typhimurium* LT2	16	1	> 32	0.5
Activity against *Streptococcus pyogenes* and *Mycobacterium tuberculosis* (µM)				

Table 3.1 continued

+ *S. pyogenes* MGSA 9254	8	0.125	0.125	4
+*S. pyogenes* MGSA 9882	> 16	0.25	0.5	4
***Mycobacterium Tuberculosis* NR 122**	8	4	ND	8

3.4.6 Bacterial lysis study using beta-galactosidase Assay

There are different mechanisms antimicrobial peptides use to achieve antimicrobial activity, including targeting vital bacterial proteins or through lysing the bacterial membrane[198 66]. To begin to elucidate the mechanism of antibacterial activity of **Fl-P14GAP**, we utilized a microbroth dilution assay to determine the MICs of **Fl-P14GAP**, Fl-P14LRR, and melittin against *E. coli* strain 25922 (Table 3.2).

Table 3.2 MIC values of **Fl-P14GAP**, Fl-P14LRR and Melittin against *E. coli*. ATCC 25922 after 6 h of treatment.

Minimum inhibitory concentration (MIC) against *E. coli* 25922		
Fl-P14LRR	**Fl-P14GAP**	Melittin
5	1.25	2.5

MIC values for **Fl-P14GAP**, Fl-P14LRR, and melittin against *E. coli* of 1.25, 5, and 2.5 µM, respectively, were obtained. Once the MICs were determined, we proceeded with a β-galactosidase (β-Gal) assay to determine if **Fl-P14GAP** demonstrated lytic behavior in *E. coli*. In this assay, *E. coli* lysis is indicated by the release of β-galactosidase causing the subsequent hydrolysis of o-nitrophenol galactoside. The concentration of o-nitrophenol release is proportional to the concentration of β-galactosidase release due to bacterial membrane lysis.

At their MIC values, **Fl-P14GAP** and Fl-P14LRR demonstrated no production of o-nitrophenol (Figure 3.12). Lytic behavior was, however, evident with the positive control, melittin, at its MIC. We did find, however, that at 2X its MIC, **Fl-P14GAP** showed signs of bacterial lysis, as o-nitrophenol production began to reach levels observed with melittin. By contrast, Fl-P14LRR, with established non-lytic behavior, demonstrated no membrane lysis at its MIC or at 2X its MIC.[87]

Overall, bacterial lysis does not seem to be the initial mode of action of **Fl-P14GAP** as it was non-lytic at its MIC. It is possible that **Fl-P14GAP** has an intracellular target within bacteria. However, at higher concentrations **Fl-P14GAP** causes bacterial membrane lysis. This could mean that **Fl-P14GAP** is capable of more than one mechanism of action. At higher concentrations, there would be enhanced surface concentration of **Fl-P14GAP**, which may lead to more effective membrane disruption.[66]

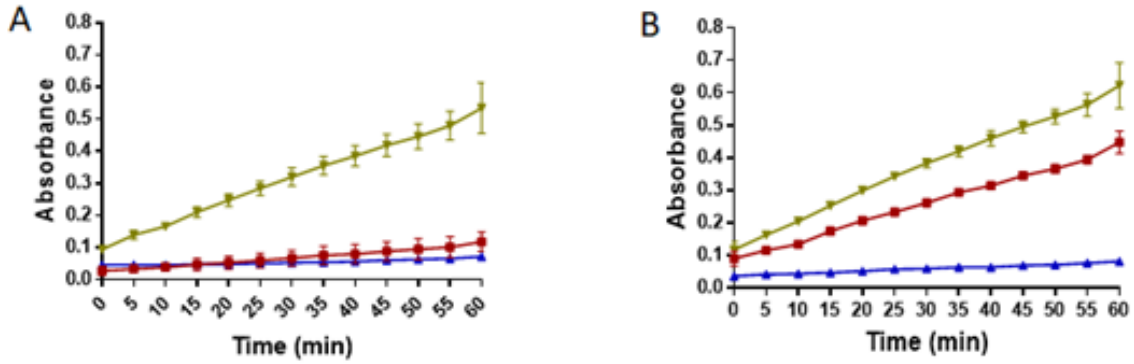

Figure 3.12 Monitoring the release of β- galactosidase over 1 h from *E. coli* ATCC 25922 after 1 h incubation with **Fl-P14GAP** (red) compared to Fl-P14LRR (blue), and positive control Melittin (green) at (A) 1X and (B) 2X MIC.

3.4.7 Antibiofilm activity

With evidence of its potent antimicrobial activity in hand, we were also curious to discover if **Fl-P14GAP** exhibited antibiofilm activity. This was determined by measuring biofilm viability with the XTT assay after 24 h exposure to **Fl-P14GAP**.[161] The ability of **Fl-P14GAP** to demonstrate antibiofilm activity was compared to the activity of Fl-P14LRR and the antibiotics, vancomycin and gentamicin. The antibiofilm activity was determined at concentrations of 16, 32, and 64 µM against preformed biofilms of *S. epidermidis* and *A. baumannii* (Figure 3.13). Predictably, increasing the concentrations of both CAPHs resulted in increased antibiofilm activity against preformed biofilm *S. epidermidis*. Notably, **Fl-P14GAP** exhibited significantly greater clearance of *S. epidermidis* biofilms at 32 and 64 µM (16 and 8%, respectively) than Fl-P14LRR (37 and 52%, respectively), while the level of clearance with vancomycin and gentamicin remained constant and negligible. This trend was not observed, however, with preformed *A. baumannii* biofilms. The viability of *A. baumanii* biofilms remained constant at about 50% viability in the

presence of **Fl-P14GAP** at all concentrations. In fact, at 64 µM concentration, both FL-P14LRR and gentamicin (37 and 41%, respectively) showed greater biofilm clearance than **Fl-P14GAP** (54%). Though **Fl-P14GAP** had high potency against platonic *A. baumannii* (MIC was 1 µM), curiously, it did not display the same potency against the preformed biofilm. The different response to antibiotics between the two biofilms may relate to the differences in the extracellular matrix that encompasses them. In other words, the difficulty in navigating through the biofilm matrix to target the bacteria that comprise it may play a key role in the ability of **Fl-P14GAP** to clear the biofilm.

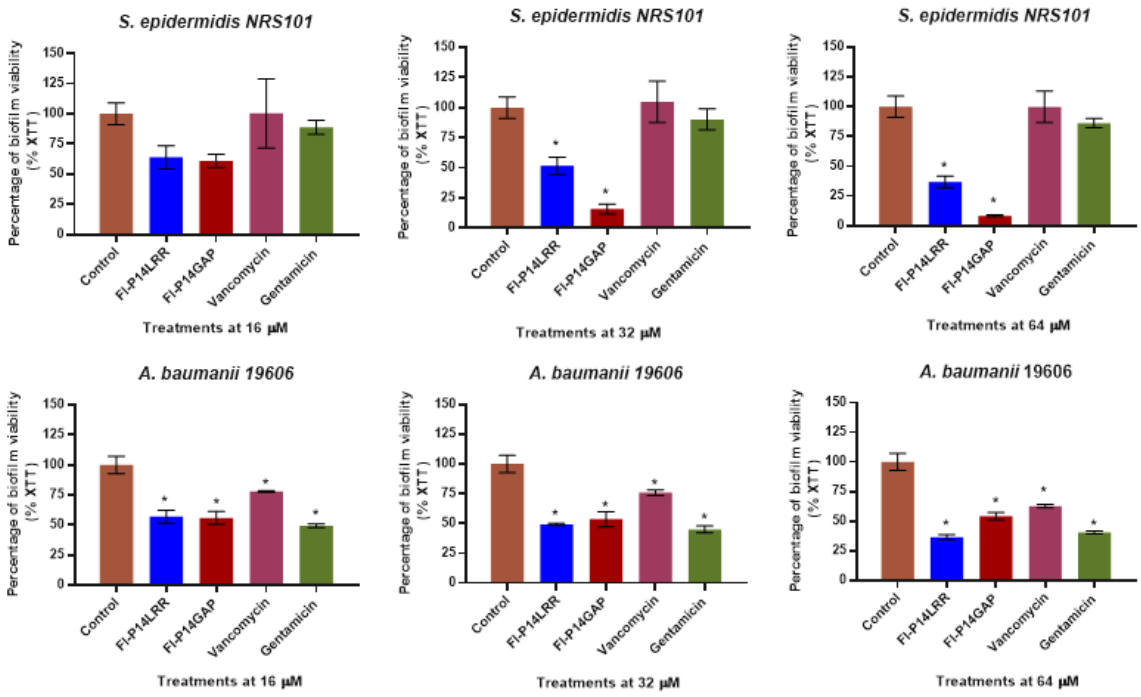

Figure 3.13 Antibiofilm activity of **Fl-P14GAP** (red) compared to Fl-P14LRR (blue), Vancomycin (pink), Gentamicin (green) against *S. epidermis* based on biofilm viability using the XTT assay after 24 h of treatment. Untreated biofilms (brown) served as the negative control.

3.4.8 *In cyto* antibacterial experiments

Finally, the ultimate goal to expand the ability of CAPHs to penetrate the cell membrane to efficiently eradicate intracellular bacteria was tested. This was achieved using an *in cyto* experiment where J774A.1 cells were infected with a variety of pathogenic bacteria (MRSA, *S. epidermidis, A. baumanii, Shigella or Listeria*) and subsequently treated with **Fl-P14GAP** at 5 µM concentration (Figure 3.14). The activity of **Fl-P14GAP** was compared to the activity of Fl-

P14LRR and known antibiotics ceftazidime and amoxicillin under the same conditions. We found that **Fl-P14GAP** completely eradicated *A. baumanii* and *Shigella* from the J774A.1 cells. It also was able to rescue J774A.1 cells infected with *S. epidermidis*, MRSA, and *Listeria* by reducing bacterial levels by 93, 85, and 68%, respectively. This is a drastic improvement over Fl-P14LRR, which did decrease intracellular bacterial levels of *S. epidermidis*, *A. baumannii*, MRSA, and *Listeria* and only decreased *Shigella* infection by 65%. **Fl-P14GAP** has demonstrated superior ability to target and eradicate intracellular bacteria, both when compared to Fl-P14LRR as well as some conventional therapeutics.

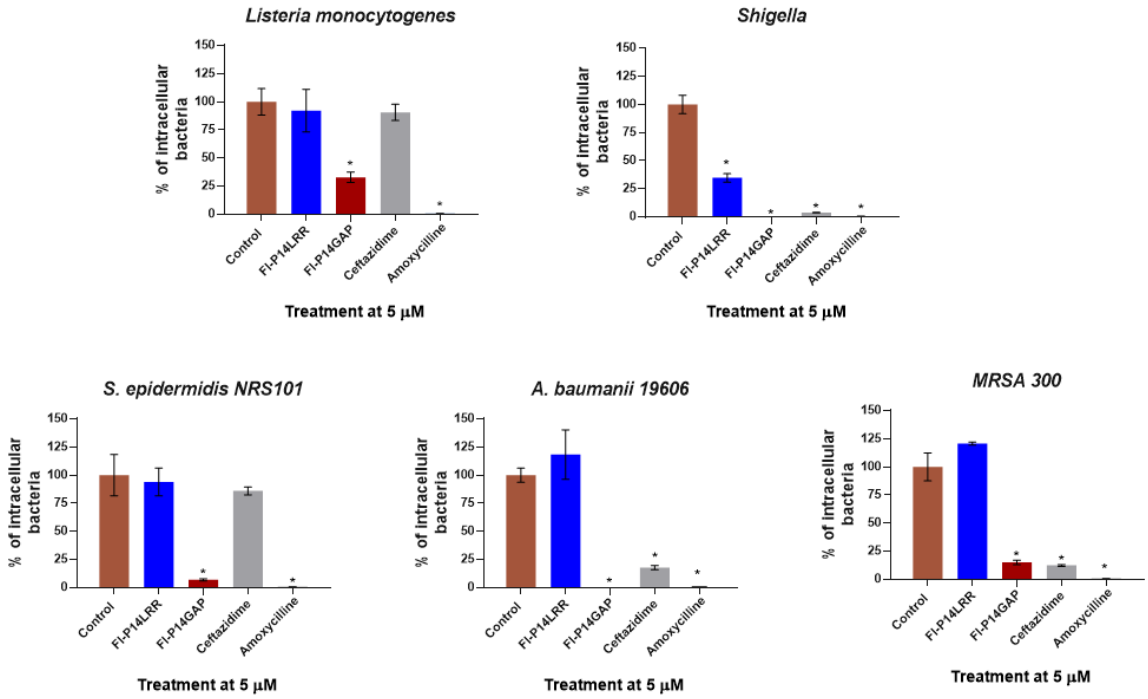

Figure 3.14 *In cyto* experiment results demonstrating the ability of **Fl-P14GAP** (green) at 5 µM to rescue infected J774A.1 cells from pathogenic bacteria based on percent intracellular bacteria remaining after 20 h treatment. This was in comparison to Fl-P14LRR (pink) and known antibiotics Ceftazidime (teal) and Amoxicillin (pink) at 5 µM.

3.4.9 **Fl-P14GAP/P_R** to circumvent membrane binding

Fl-P14GAP has shown exceptional activity, yet we were interested to see if additional structural modifications could be implemented to limit membrane binding and cytotoxicity. For each of these analogues, however, P_R was also integrated into each design to study if we could disrupt the

membrane binding behavior we observed with **Fl-P14GAP** while still maintaining the antimicrobial potency the use of GAP has enabled us to achieve.

3.4.9.1 Design and synthesis

The electrostatic interaction between Arg and the overall net negative charge of the plasma membrane is strengthened by bidentate hydrogen bonds that are formed between guanidine and anionic lipid head groups.[106, 109] Through the study of **Fl-P14GAP** we found this interaction to be robust due to the incorporation of rigid GAP, so we were interested to see if the incorporation of fewer GAP amino acids would weaken the overall interaction with membranes. Thus, four different peptide designs were developed in an attempt to rescue **Fl-P14GAP** from membrane binding (Figure 3.15). Each peptide has the same number of positively charged residues, but different variations of hydrophilic organization due to the incorporation of both GAP and P_R into each peptide sequences.

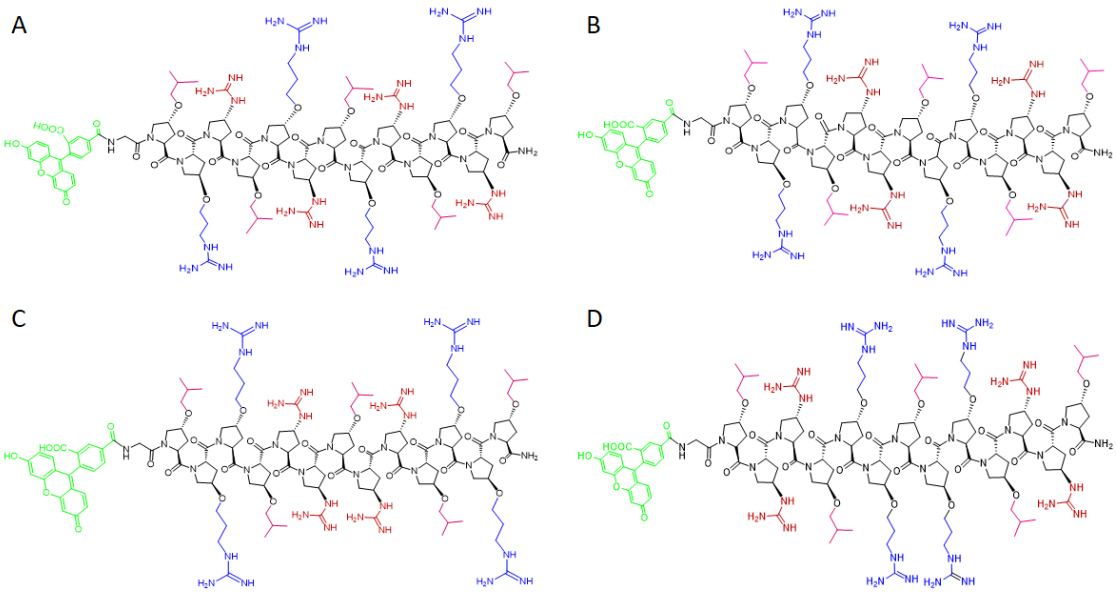

Figure 3.15 Structure of **Fl-P14GAP/P_R** peptides (A) P1, (B) P2, (C) P3, and (D) P4

The characteristic hydrophobic and hydrophilic face of CAPHs was maintained, but the hydrophilic face had a strategic combination of GAP or P_R monomer. Peptide 1 (P1) was composed of repeating units of P_L, GAP and P_R, which would provide this peptide with three different faces: a hydrophobic P_L face, a hydrophilic GAP face, and a hydrophilic P_R face (Figure 3.16A). Ideally,

depending on the mode in which CAPHs interact with the cell membrane, this would promote initial membrane contact with either the GAP face or P_R on the cell membrane. Peptide 2 (P2), which consists of alternating GAP and P_R residues along the two hydrophilic faces of the peptide, while maintaining the P_L hydrophobic face (Figure 3.16B). P2 was created with the idea that by having P_R and GAP next to each other on one face P_R may disrupt GAPs ability to tightly bind to the cell surface. The last two analogues were peptides 3 and 4 (P3 and P4) (Figure 3.16C and 3.16D). P3 and P4 were opposites in that the N and C termini either had P_R with GAP at the center of the peptide or GAP with P_R in the center or the peptide, respectively. With GAP having such a strong affinity for the cell membrane one would expect P3 and P4 to configure itself to promote GAPs membrane interaction. Hypothetically, this design would cause P3 and P4 to undergo conformational changes upon membrane interaction due to the placement of GAP promoting P3 to bend in a concave fashion to promote membrane association and P4 to bend in a convex fashion. With the initial step of CPP uptake relying on the hydrophilic face of the peptide interacting parallel to the membrane, we hoped that a lesser amount of the GAP amino acid would minimize surface binding while maintaining the same amount of cationic moieties. Monomers P_R, GAP and P_L and each peptide were synthesized using the same method as previously described.

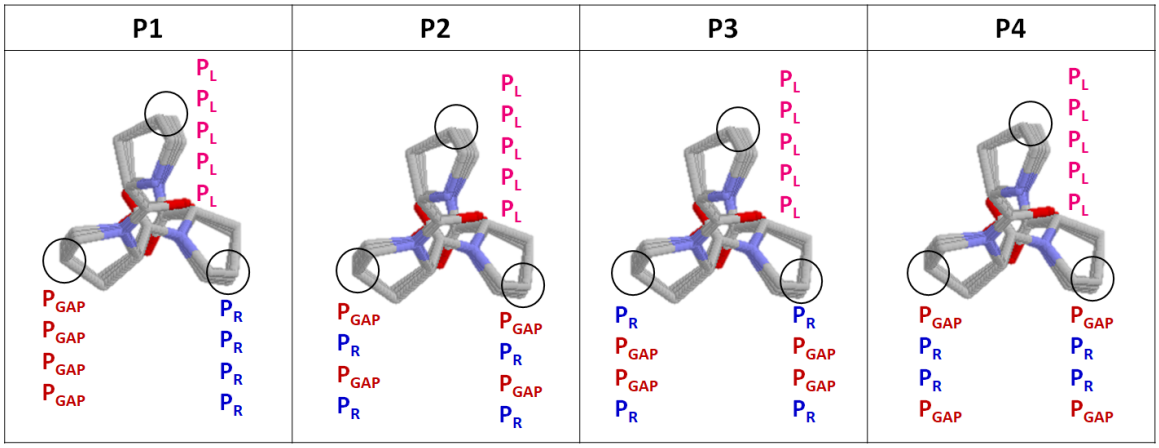

Figure 3.16 Top down view of a PPII scaffold representative of the **Fl-P14GAP/P$_R$** analogues. At the characteristic three faces on the helix. P_L, P_R, and GAP amino acids are listed in the way they are organized into each sequence.

3.4.9.2 Flow cytometry for cell uptake analysis

In order to study how these analogues differed in their cell uptake abilities compared to Fl-P14LRR and **Fl-P14GAP** we utilized flow cytometry (Figure 3.17). Through these experiments we determined that P1 behaved most similarly to **Fl-P14GAP** in cell uptake behavior at 2.5 and 5 µM. At 10 µM, however, P1, P2, and P3 associated with the cell more than **Fl-P14GAP**. P2 showed the lowest cell accumulation of the **Fl-P14GAP/P$_R$** peptides at all concentrations and P3 and P4 were about equal in their cell uptake abilities. The fact that P1 had the most similar uptake to **Fl-P14GAP** at 2.5 and 5 µM demonstrates that the GAP face is a contributing factor in cell uptake. It is also important to note that Fl-P14LRR had the lowest cell uptake of all the tested CAPHs, with 8.8, 8.9, and 4.4 fold lower cell uptake at 10, 5, and 2.5 µM than P1, the **Fl-P14GAP/P$_R$** CAPH with the greatest cell association activity. All together, these results support the GAP amino acid enables CAPHs to enter cells more effectively in comparison to the P$_R$ amino acid in Fl-P14LRR.

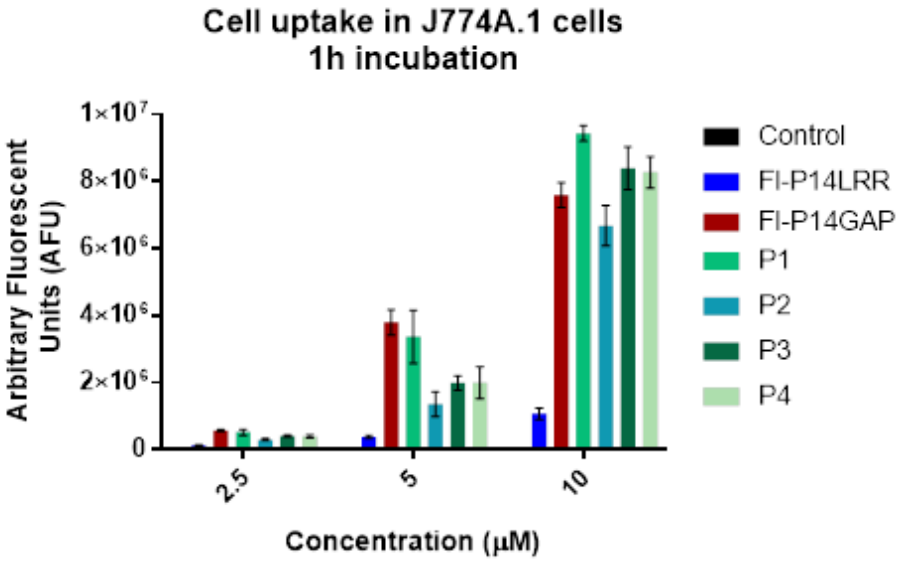

Figure 3.17 Flow cytometry results comparing arbitrary fluorescence in J774A.1 cells after 1 h treatment with GAP peptides P1, P2, P3 and P4 to the uptake of **Fl-P14GAP** and Fl-P14LRR.

3.4.9.3 Cytotoxicity study

Toxicity was a concern with **Fl-P14GAP**, more noticeably with J774A.1 cells, therefore we performed toxicity studies to determine if these CAPHs analogues were harmful to J774A.1 cells

(Figure 3.18). Previously, **Fl-P14GAP** began to show toxicity affects at 10 µM with cell viability dropping to about 50%. A similar drop in cell viability was observed at 10 µM for P1, P2, P3 and P4. P2 was the least toxic with about 70% viability at 10 µM and P3 and P4, which were about 60% viable at the same concentration. P1 was the most toxic causing 38% cell viability at 10 µM, the only **Fl-P14GAP/P$_R$** peptide to show greater toxicity than **Fl-P14GAP** at 10 µM. However, like **Fl-P14GAP**, all the peptides had above 90% viability at 5 µM.

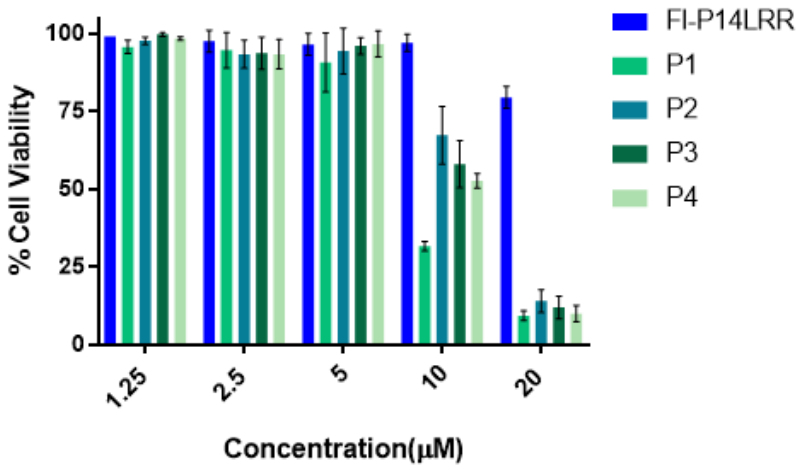

Figure 3.18 MTT assay showing cell viability of J774A.1 cells after incubation with Fl-P14LRR and GAP peptide analogues after 9 h at concentrations ranging from 1.25 to 20 µM.

3.4.9.4 Confocal microscopy studies

Having established that 5 µM is as a safe working concentration of the GAP/P$_R$ peptides, we next used fluorescent confocal microscopy to visualize if simultaneously incorporating GAP and P$_R$ into CAPHs allowed us to overcome the extensive membrane association we observed with **Fl-P14GAP**. We tested each peptide in J774A.1 cells at 5 µM with 1 h incubation. In these studies, we found that the **Fl-P14GAP/P$_R$** peptides showed unique accumulation in the interior of the cell described as follows.

P1) Some endosomal localization was present as seen previously with **Fl-P14GAP**, however, we also observed a significant level of localization with the mitochondria when imaging P1 (Figure 3.19). Membrane binding was still visible around the outline of the cells as well. Thus, peptide

organization with both a P_R and GAP face does not eliminate membrane binding, but does create a subcellular location that is a combination of the intracellular niches of Fl-P14LRR and **Fl-P14GAP**.

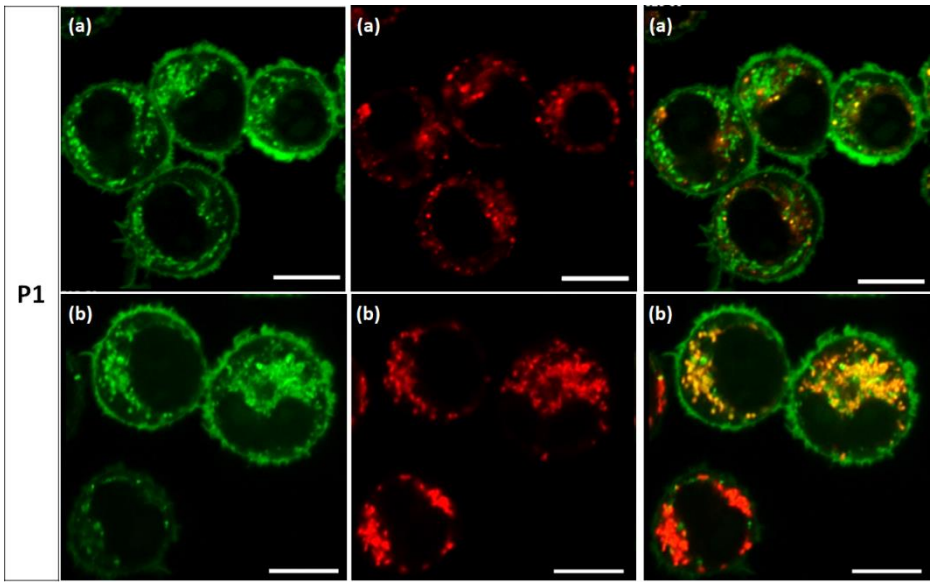

Figure 3.19 Confocal microscopy images showing the subcellular location of P1 at 5 µM in J774A.1 cells after 1 h incubation. Cell location was studied with (a) Lysotracker (red) and (b) Mitotracker. Scale bars = 10 µM, a yellow/orange color indicates co-localization. Three channels of each image are depicted: first column = peptide only (green), second column = tracking dye only (red) and third column = overlay of both channels.

P2) P2 had a similar cell location as P1 with both mitochondria and endosomal co-localization (Figure 3.20). It can also be seen that P2 was present around the outline of the cells as well. Although there are some cells that have distinct exterior outlining, these images show that alternating P_R and GAP on the hydrophilic face appears to direct more of the peptide to the cell interior.

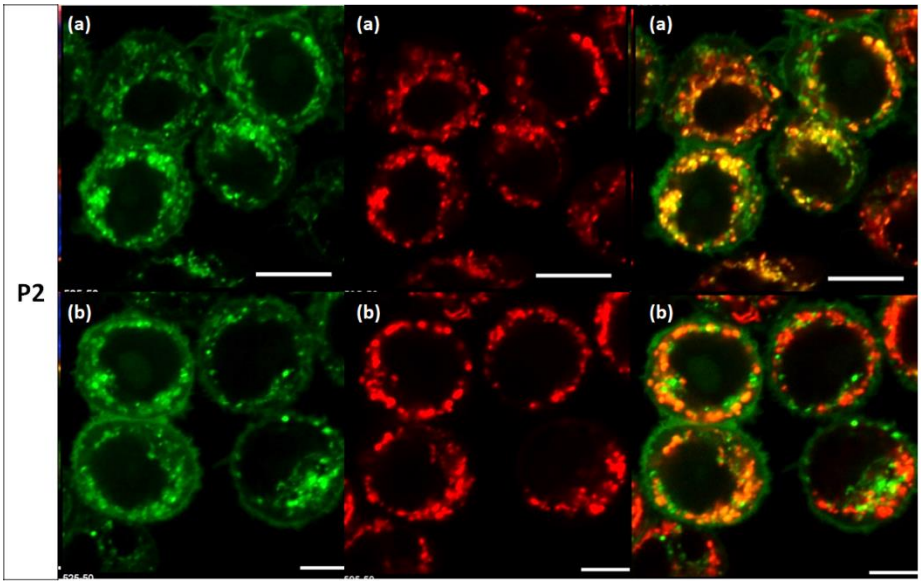

Figure 3.20 Confocal microscopy images showing the subcellular location of P2 at 5 µM in J774A.1 cells after 1 h incubation. Cell location was studied with (a) Lysotracker (red) and (b) Mitotracker. Scale bars = 10 µM, a yellow/orange color indicates co-localization. Three channels of each image are depicted: first column = peptide only (green), second column = tracking dye only (red) and third column = overlay of both channels.

P3) Endosomal, mitochondrial, and membrane localization was also apparent in P3 (Figure 3.21). The images of each of these CAPHs support that combing P_R and GAP into a peptide sequence encourages subcellular fate that is a combination of the intracellular localization of Fl-P14LRR and **Fl-P14GAP**. It is interesting to find that the placement of the amino acids does not seem to have a visible impact on the level of membrane binding observed in J774A.1. P1, P2, and P3 all have similar levels of membrane binding.

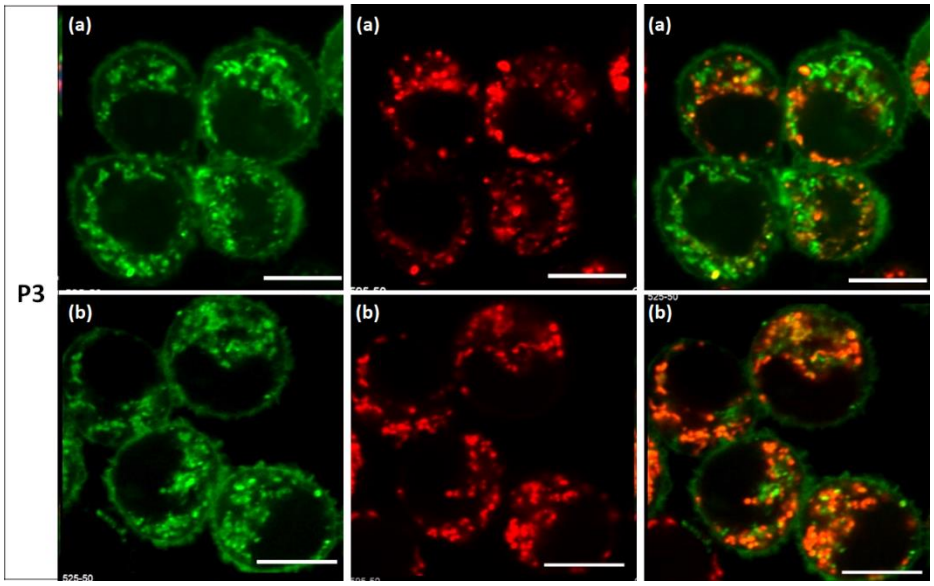

Figure 3.21 Confocal microscopy images showing the subcellular location of P4 at 5 µM in J774A.1 cells after 1 h incubation. Cell location was studied with (a) Lysotracker (red) and (b) Mitotracker. Scale bars = 10 µM, a yellow/orange color indicates co-localization. Three channels of each image are depicted: first column = peptide only (green), second column = tracking dye only (red) and third column = overlay of both channels.

P4) P4 also showed endosomal and mitochondrial localization. Membrane binding remained, however, less mitochondrial localization was visible (Figure 3.22). The subcellular location of P4 was similar to the other Fl-P14P_R/GAP peptides, with some lower membrane binding. However, there also appears to be some peptide in the cell cytoplasm.

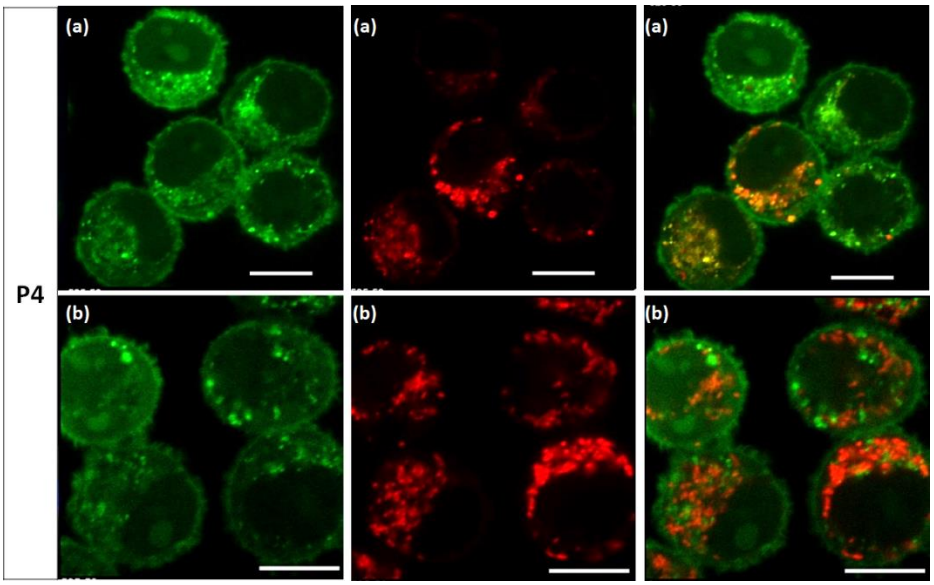

Figure 3.22 Confocal microscopy images showing the subcellular location of P3 at 5 μM in J774A.1 cells after 1 h incubation. Cell location was studied with (a) Lysotracker (red) and (b) Mitotracker. Scale bars = 10 μM, a yellow/orange color indicates co-localization. Three channels of each image are depicted: first column = peptide only (green), second column = tracking dye only (red) and third column = overlay of both channels.

Overall, simultaneously including GAP and P_R expanded the intracellular compartments that GAP containing peptides have access to in comparison to **Fl-P14GAP**. All **Fl-P14GAP/P_R** peptides demonstrated co-localization with mitochondria in addition to exhibiting endosomal and membrane association. Co-localization with mitochondria can be attributed to the presence of P_R, since Fl-P14LRR has been shown to associate with mitochondria under these conditions and **Fl-P14GAP** has not.[139] P4 was the only GAP/P_R analogue that showed lower membrane binding and appeared to have some cytoplasmic accumulation. The differences in the cell uptake as well as some differences in the subcellular niche between the **Fl-P14GAP/P_R** peptides demonstrates that the amino acid organization does impact how the peptides associate with J774A.1 cells.

The subcellular location of the GAP peptide analogues in J774A.1 cells prompted us to examine their cell uptake and subcellular fate in HaCat cells as well. We first used flow cytometry to test the cell accumulation of each peptide in HaCat cells at 5 μM after 1 h incubation (Figure 3.23). Overall, P1 had the highest cell uptake of the **Fl-P14GAP/P_R** peptides, consistent with what we observed in J774A.1 cells. P3 following close behind, but, unlike in J774A.1 cells where P4 had similar cell uptake as P3, in HaCat cells P4's cell accumulation was less than P3 and most similar

to P2. These results demonstrates that the position of the GAP and P_R monomers effects the cell uptake of CAPHs, as well as the cell type. The lower cell uptake with P2 and P4 is possibly result of decreased membrane association due to the distance between the GAP monomers. Both peptides have monomers in positions where GAP is not consecutively on the same helical face.

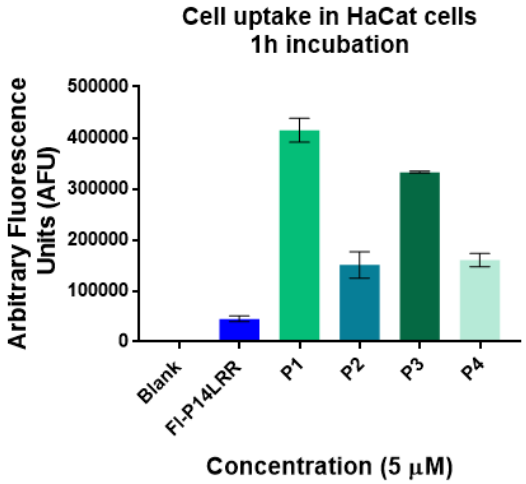

Figure 3.23 Cell uptake of **Fl-P14GAP/P_R** peptides in HaCat cells with 1 h incubation at 5 μM concentration.

Through confocal studies we also were able to visualize the subcellular fate of **Fl-P14GAP/P_R** CAPHs in HaCat cells. Each of the GAP analogues subcellular niche is described as follows:

P1) P1 showed predominantly endosomal co-localization in HaCat cells with some membrane binding (Figure 3.24). Interestingly, the peptide can be seen distributed throughout the intracellular space, unlike with **Fl-P14GAP**, which showed prominent membrane binding with some endosomal localization. P1 did not take on the same hybrid characteristics that it showed in J774A.1 cells, where both endosomal and mitochondrial localization were visualized. Instead, it had no mitochondrial association at all.

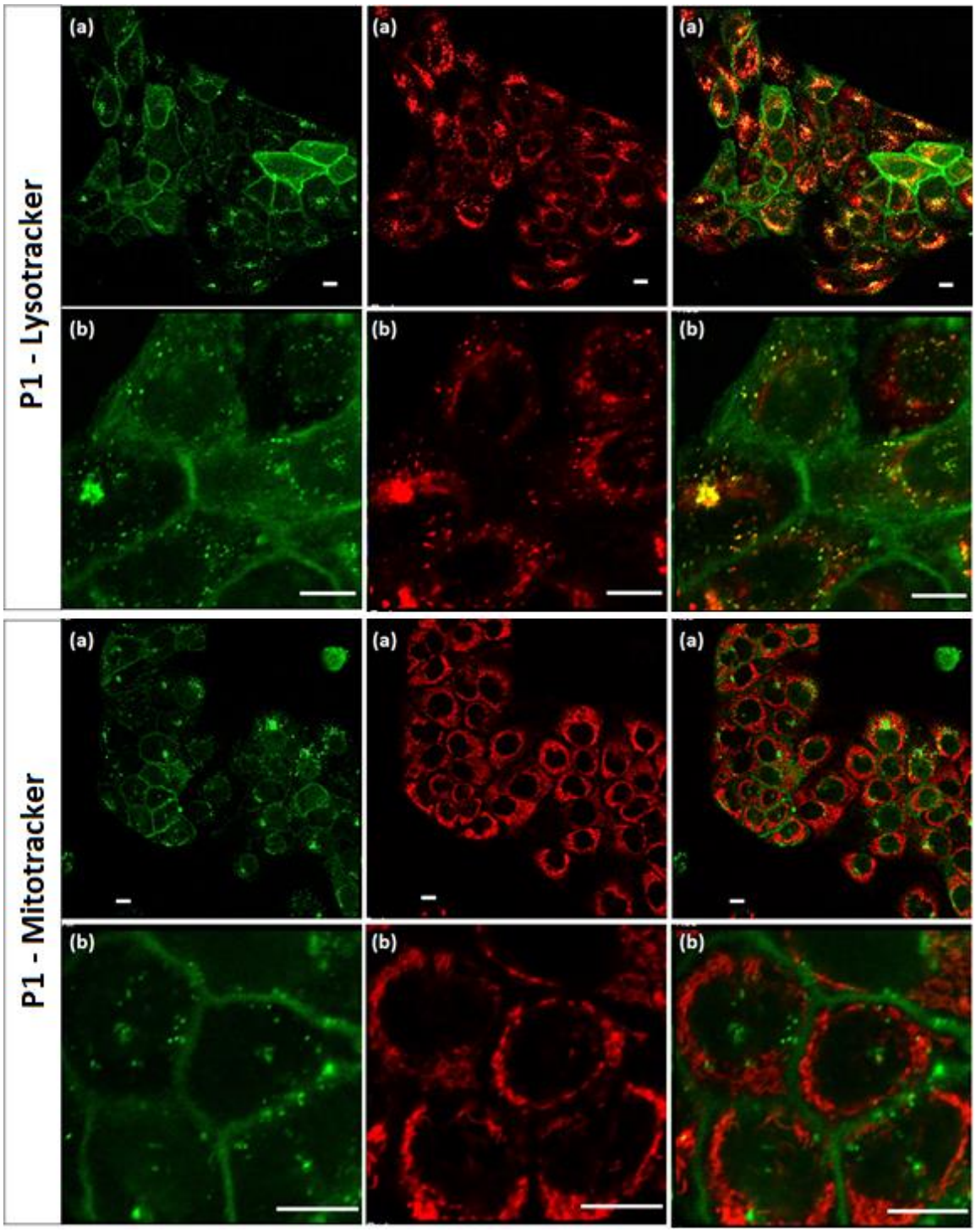

Figure 3.24 Confocal microscopy whole view (a) and zoomed (b) images of P1 (green) at 5 µM in HaCat cells after 1 h incubation. Cell location was studied with Lysotracker and Mitotracker (red) (Scale bars = 10 µM), a yellow-orange color, indicates co-localization.

P2) Similar to P1, P2 showed predominately endosomal location with no co-localization with mitochondria ((Figure 3.2). Addtionally, the membrane binding appears to be significnatly less prominent with P2 than it was with **Fl-P14GAP**. In contrast to P1, P2 appears noticeably more punctate and there is not the same level of cytoplasmic distribution in the cells as seen with P1.

P3) Endosomal localization was observed with P3 as well and no mitochondria co-localization was present at all (Figure 3.26). Additionally, there are a couple of cells that have more intense membrane binding than others, but overall the membrane binding appears to be significnatly less prominent with P3 than it was with **Fl-P14GAP**. P3 appears noticeably punctate and there appears to be a significant amount of cytoplasmic distribution in the cells as seen with P1.

P4) Lastly, P4, like P2, predominantly co-localizing with endosomes (Figure 3.27). This is in agreement with the cell uptake results where P2 and P4 had similar cell uptake ability in HaCat cells. P4 also demonstrates that, relative to **Fl-P14GAP**, some membrane binding may have subsided, however, peptide fluorescence on the periphery of the cell is still observed in some cases. P4 does not differ from the other **Fl-P14GAP/P_R** peptides in that it also shows no association with the mitochondria. Though P4 is mostly endosomal, there are a couple of cells that have peptide throughout the cytoplasm.

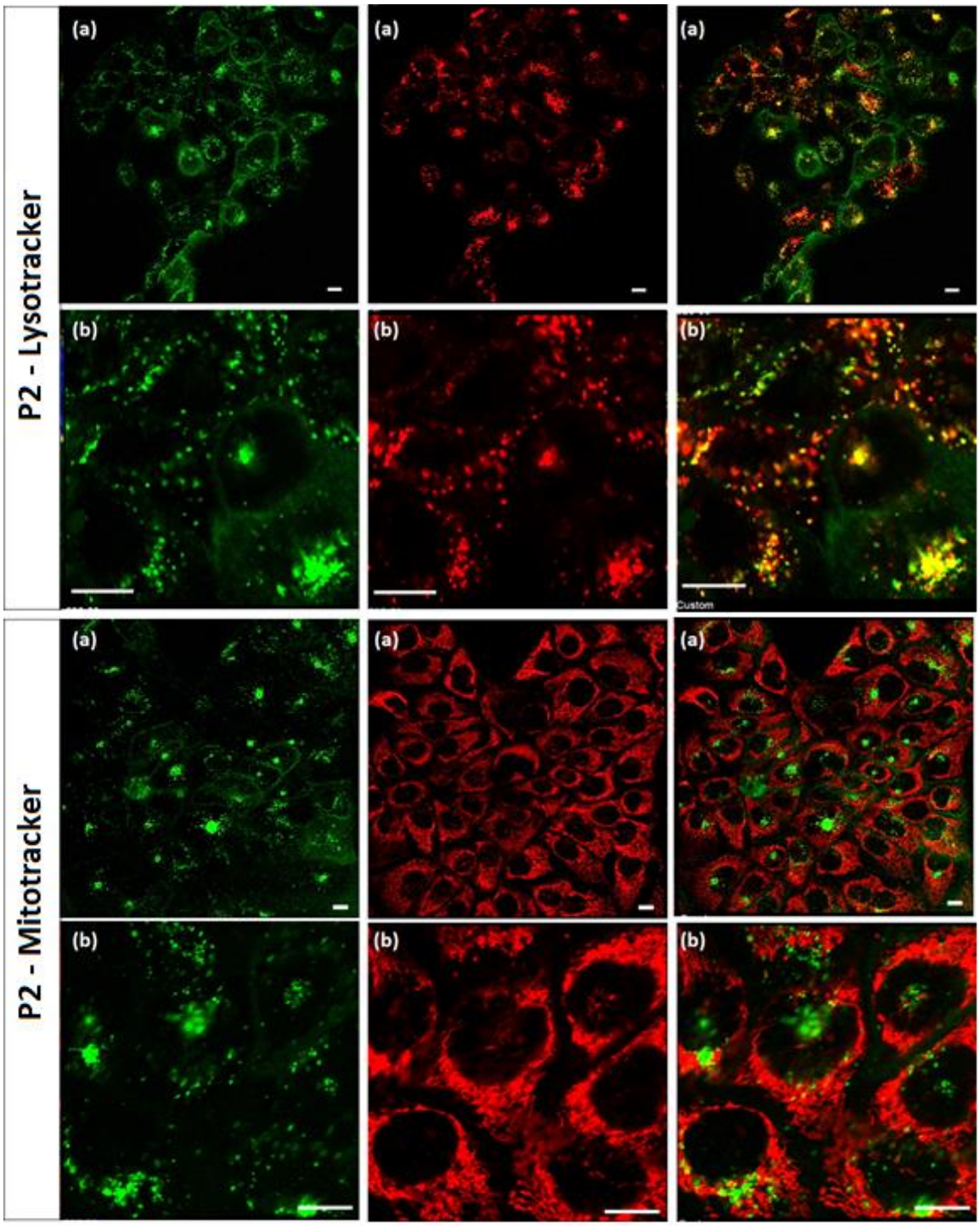

Figure 3.25 Confocal microscopy whole view (a) and zoomed (b) images of P2 (green) at 5 µM in HaCat cells after 1 h incubation. Cell location was studied with Lysotracker and Mitotracker (red) (Scale bars = 10 µM), a yellow-orange color, indicates co-localization..

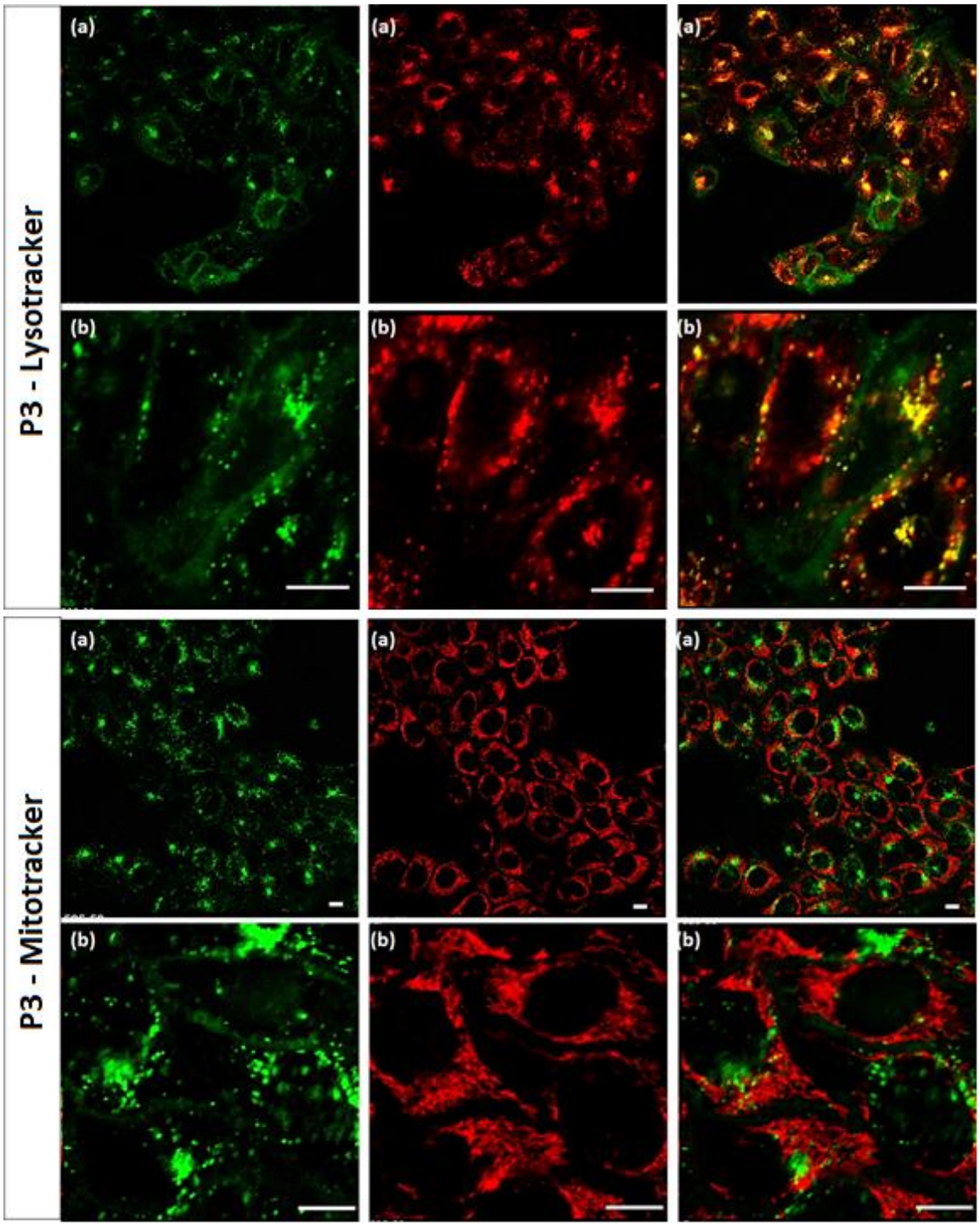

Figure 3.26 Confocal microscopy whole view (a) and zoomed (b) images of P3 (green) at 5 µM in HaCat cells after 1 h incubation. Cell location was studied with Lysotracker and Mitotracker (red) (Scale bars = 10 µM), a yellow-orange color, indicates co-localization.

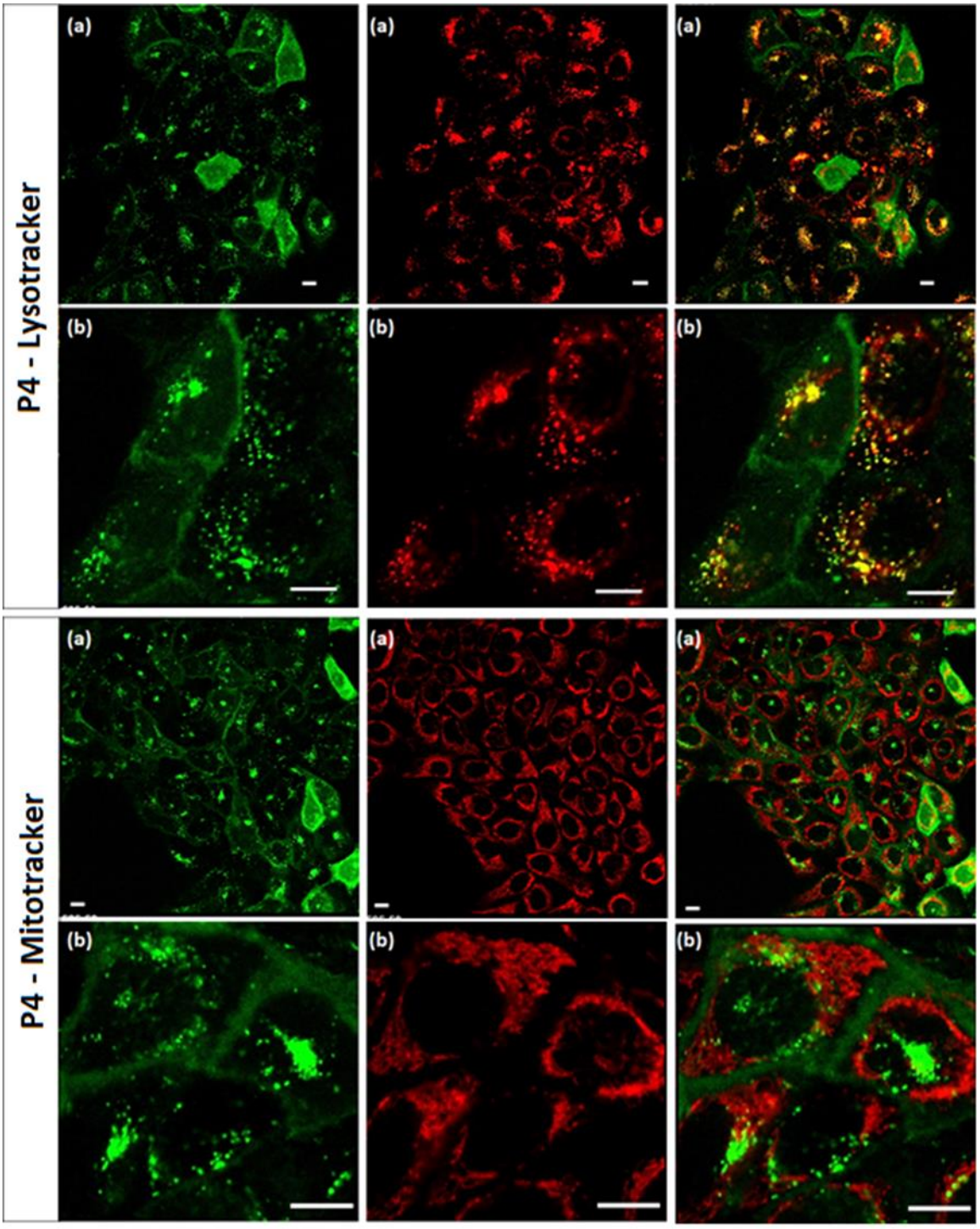

Figure 3.27 Confocal microscopy whole view (a) and zoomed (b) images of P4 (green) at 5 µM in HaCat cells after 1 h incubation. Cell location was studied with Lysotracker and Mitotracker (red) (Scale bars = 10 µM), a yellow-orange color, indicates co-localization..

Overall, it appears that we were able to expand the capacity of GAP containing peptides to simultaneously reach other cellular compartments by incorporating P_R. In this way, we were able to target mitochondria in J774A.1 cells and marginally reduce some of the membrane binding in HaCat cells. Of the **Fl-P14GAP/P_R** peptides, P1and P4 showed the ability to accumulate into the cell cytoplasm of HaCat cells, which was a shortcoming of **Fl-P14GAP** in HaCat cells where much of the peptide was membrane bound. Although all of the **Fl-P14GAP/P_R** peptides did not show the same level of cell uptake at the working concentration of 5 μM in J774A.1 and HaCat cells, it does appear that we are able to achieve better cell distribution intracellularly by mixing both GAP and P_R into CAPHs, which will potentially improve GAP containing CAPHs capacity to clear intracellular bacteria.

3.4.9.5 Cell uptake studies with trypan blue

With the subcellular fate of **Fl-P14GAP/P_R** CAPHs visually represented by confocal microscopy we next wanted to quantifiably measure if membrane binding was reduced by mixing both GAP and P_R into the peptide sequence and if the cationic residue organization helped decrease membrane binding. Since **Fl-P14GAP** previously showed significant levels of membrane binding in HaCat cells, this cell line was focused on to evaluate the level of membrane binding exhibited by the **Fl-P14GAP/P_R** peptides. Flow cytometry was used to measure cellular fluorescence of **Fl-P14GAP/P_R** CAPHs in the presence of trypan blue (TB), which, as previously mentioned, quenches any membrane associated fluorescence to provide a more accurate measurement of how much peptide is internalized by the cells.[196]

Cellular fluorescence with the **Fl-P14GAP/P_R** peptides after TB treatment partially supported what was seen through confocal microscopy with HaCat cells (Figure 3.28). Though the HaCat cells appeared to have more internal fluorescence with the **Fl-P14GAP/P_R** peptides, the results of these TB cell uptake experiments show similar membrane binding across the peptides evaluated, with the exception of P14LRR.. P2 and P4 had the lowest level of decrease in cellular fluorescence in the series , with the percent of peptide associated fluorescence reducing by 57 and 61%, respectively, in the presence of TB. P1 and P3 cellular fluorescence values reduced by 74 and 69% in the presence of TB, respectively. For **Fl-P14GAP**, TB reduced cellular fluorescence by 64%, which is a 7 and 3% greater reduction than P2 and P4, respectively. Thus, for P2 and P4, the

placement of the GAP amino acid had some impact on alleviating membrane binding. In contrast, the amino acid placement of P1 and P3 resulted in slightly increased membrane binding, in which their cellular fluorescence attributed to membrane binding was 10% and 5% greater than **Fl-P14GAP**. In the case of Fl-P14LRR TB minimized its cell association by 34%, which was significantly less than what was observed with the GAP containing CAPHs.

Membrane binding is an aspect of many CPPs, but the impact TB had on the fluorescence value of the **Fl-P14GAP/P$_R$** peptides demonstrates that they exhibit significant membrane binding properties. This is more apparent in the peptides that had an exclusively GAP face (P1) and consecutive GAP amino acids on two faces (P3) of the PPII helical structure. Thus, further confirming the influence of the GAP amino acid for CAPHs to tightly bind membrane surfaces. Still, regardless of the reduced cell accumulation uncovered by TB, P1, P2, P3, and P4 had 3, 2, 3, and 2 fold better cell uptake than Fl-P14LRR, respectively, which supports that the GAP amino acid enhances the cell uptake of CAPHs.

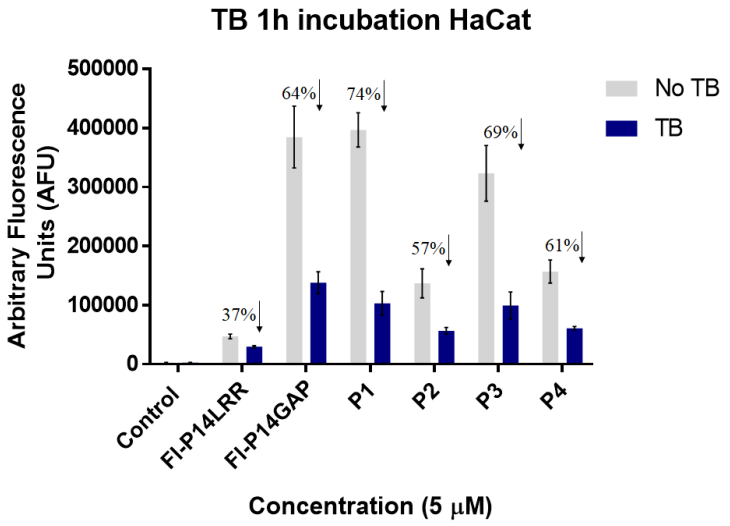

Figure 3.28 Cell uptake studies of P1, P2, P3,P4 and Fl-P14LRR at 1 h in J774A.1 cells with trypan blue treatment (blue bar) and without trypan blue treatment (grey bar).

Other CPP studies with guanidininum expressing peptides with fixed charges show enhanced cell uptake, which was attributed to greater binding of cell surface glycan, heparan sulfate, in the initial step of membrane permeation.[193] Thus, it is likely organized cationic charges that are displayed by

GAP heightened association with negatively charged surface motifs on the cell membrane.[193, 199, 200] Additionally, the differences in the cell association between the **Fl-P14GAP/P$_R$** peptides suggest that spacing between GAP residues influences peptide activity. Moreover, consecutive packing of the GAP amino acids within the helical faces of the peptide structure promotes higher CAPHs cell uptake than peptides with nonconsecutive GAP residues on their helical faces. P1 and P3 had 45 and 42% greater cell uptake than P2, respectively, and 34% and 38% better cell uptake than P4, respectively, in HaCat cells.

3.5 Conclusion

We have demonstrated that incorporating the GAP amino acid into CAPHs promotes enhanced cell uptake and superior antimicrobial activity. Discounting cell surface binding though a surface fluorescence quenching assay confirmed that **Fl-P14GAP** had better cell accumulation than Fl-P14LRR by up to 7-fold. This enhanced activity may be attributed to improved membrane association, which led to subsequent superior internalization of **Fl-P14GAP**. This cell uptake activity equipped **Fl-P14GAP** to effectively target intracellular bacteria.

The images from the confocal experiments showed the potential of **Fl-P14GAP** to become increasingly cytoplasmic with time, which would support its ability to reach subcellular targets. Taking on characteristics of arginine rich peptides capable of endosomal escape post endocytic cell entry, **Fl-P14GAP** may use a similar method to access the cytoplasm post cell internalization, since localization in endosomes was observed.[201] With the capacity to reach the cell cytoplasm, *in cyto* experiments revealed that **Fl-P14GAP** was able to completely eradicate two major pathogenic bacteria, *A. baumannii* and *Shigella*, from macrophage cells, as well as drastically decreased the amount of *Listeria, MRSA, and S. epidermidis*. Although the mode of antibacterial action of **Fl-P14GAP** is not yet understood, our results from the β-galactosidase assay supports that **Fl-P14GAP** operates primarily using a non-lytic mechanism since at its MIC against *E. coli* no bacterial lysis was observed. However, lysis was evident at 2X its MIC, which may indicate the use of more than one method for bactericidal activity. Overall, the combined results of this investigation support the therapeutic potential of **Fl-P14GAP**.

Confocal microscopy and flow cytometry experiments show that **Fl-P14GAP** exhibited significant membrane binding in both HaCat and J774A.1 cells. This characteristic remained despite our efforts to eliminate surface binding through the synthesis of the **Fl-P14GAP/P_R** peptides. The differences in cell uptake activity amongst Fl-P14LRR, **Fl-P14GAP**, and the **Fl-P14GAP/P_R** peptides indicate amino acid organization and peptide flexibility assist in the mechanism of cell uptake for CAPHs. Glycosaminoglycans and polysaccharides, such as heparan sulfate, coat the cell surface and are known to attract the binding of proteins to the cell membrane. Moreover, the metabolic cycle of glycosaminoglycans requires their internalization from the cell surface by vesicles through endocytic pathways, which could allow for the passive uptake of bound macromolecules.[202] Thus, this may be one method that GAP containing CAPHs utilize for cell internalization. Furthermore, incorporation of organized cationic charges with the GAP repeats may have allowed CAPHs to acquire more efficient binding to anionic surface molecules for enhanced cell uptake, which may not be as accessible with the level of cationic fluidity that is present with the flexible P_R residue. It was also interesting to find that, although cell surface binding was apparent with both J774A.1 cells and HaCat cells for **Fl-P14GAP**, the degree of membrane binding was greater in HaCat cells than J744A.1 cells according to the trypan blue studies. Thus, membrane composition likely plays a role in the observed cell association of **Fl-P14GAP**.

3.6 Future

Fl-P14GAP has far exceeded the capabilities of Fl-P14LRR in clearing intracellular pathogens and has great potential as a dual cell penetrating, antimicrobial agent. We are currently interested in developing different variations of the GAP monomer in order to eliminate the membrane binding, which may be holding GAP containing CAPHs back from reaching their full potential. It is also important to understand the mechanism of action involved in the insertion of the GAP peptides into the membrane. Since confocal microscopy and flow cytometry studies using trypan blue indicated that the GAP peptides were membrane bound it would be of interest to characterize the depth of lipid bilayer association. Moreover, it is important to determine whether the difference in cell association is occurring at the membrane surface or while transversing through the lipid bilayer. Through the elucidation of the mechanisms involved in the activity of the GAP peptides, we can better implement strategies to attain optimal CAPHs activity.

3.7 Materials and Methods

3.7.1 Materials

H-Rink Amide ChemMatrix resin for peptide synthesis was purchased from Pcas Biomatrix Inc. (Quebec, Canada). Sterile complete media (DMEM, L-glutamine, Penicillin-Streptomycin, supplemented with 10% fetal bovine serum (FBS) and buffers (PBS) used in cell culture were purchased from VWR (VWR Direct, IL). All cell lines for cell culture were purchased form ATCC (Manassas, VA). Starting material for Fmoc-P_L, Z-hydroxyproline, was purchased from Chem Impex (Wood Dale, IL) and other starting materials were purchased from Ark Pharm, Inc. (Arlington Heights, IL) All other chemicals and reagents were purchased commercially and were used without further purification unless mentioned from Sigma Aldrich (St. Louis, MO), Alfa Aesar (Haverhill, MA) or Thermo Fischer (Waltham, MA).

Each of the CAPH peptides was purified using Waters Delta Prep 4000 HPLC equipped with a Phenomenexr C18 semi-preparative column. CAPHs characterization was performed using Matrix Associated Laser Desorption Ionization time of flight (MALDI-TOF) mass spectrometry using an Applied Biosystem Voyager-DE TM BioSpectrometry workstation and analytical HPLC using Waters Delta Prep 4000 HPLC equipped with a C18 reverse phase analytical column (5 µm, 4.6 mm x 250 mm; Phenomenex Luna). CAPHs cellular uptake was measured using Becton Dickton Bioscines FACS Calibur Flow Cytometry, data was analyzed using Cell Quest (v.3.5) software. Cell uptake was also measured using BD sciences Acurri flow cytometer. Absorbance readings were obtained using microplate reader TECAN SpectraFluor Plus. or TECAN Infinite F PLEX. Confocal images were obtained using Nikon A1R inverted confocal fluorescence microscope equipped with 60x oil objective. NIS Elements software was used to process images.

3.7.2 Fmoc-GAP$(Boc)_2$ synthesis:

To Fmoc-L-Pro(4-NHBoc)-OH(2S,4R) (200 mg, 0.44 mmol) in a 25 mL round bottom flask with a stir bar was added a triflouroacetic acid (TFA) and dichloromethane (DCM) solution (1:1, 2 mL). The reaction was stirred for 3 h at room temperature. The TFA/DCM solution was removed *in vacuo* and dried under high vacuum for 12 h. The residue was solubilized in DCM (2 mL) with sonication and N,N'-di-tert-butoxycarbonyl-1H-pyrazole-1 (150.9 mg, 0.49 mmol) was added to the reaction flask followed by triethylamine (TEA) (249 µL, 1.77 mmol). The resulting solution

was stirred for 12 h at room temperature. The organic solvent was removed *in vacuo* and the crude material was purified by flash chromatography on silica gel with an eluent composed of 93% DCM and 7% methanol (MeOH). The desired fractions were collected and the solvent was removed *in vacuo* to yield a white solid, Fmoc-GAP(Boc)$_2$ in 50% yield.

Fmoc-GAP(Boc)$_2$ MW: 594, ESI$^+$MS: 595 m/z (M+ H$^+$)

^{1}H NMR (300 MHz, DMSO-*d*): δ 11.46 (s, 1H), 8.28 (t, J = 6 Hz, 1H), 7.87 (d, J = 7.5 Hz, 2H), 7.62 (t, J = 6 Hz, 2H), 7.40 (t, J = 7.5 Hz, 2H), 7.31 (d, J = 6.0 Hz, 2H), 4.55 (q, J = 6.8 Hz, 1H), 4.43 (m, 1H), 4.17 (m, 4H), 3.73 (m, 1H), 3.34 (m, 2H), 2.49 (s, 1H), 2.25 (m, 2H), 1.42 (s, 18H), 1.20 (s, 1H).

3.7.3 Compound 5

A flame-dried round bottom flask (RBF) equipped with a stir bar was purged with N_2 and loaded with dry tetrahydrofuran (THF) (50 mL). Z-Hydroxyproline (18.8 mmol, 5 g) was added to the flask, allowed to dissolve then brought to -40°C in dry ice and acetonitrile both. Potassium bis(trimethylsilyl)amide (KHMDS) (37.6 mmol, 43.95 mL) was added to the flask under nitrogen (N_2) using a dry glass syringe. The solution was allowed to stir for 30 min, followed by the addition of 3-bromo-2-methylpropene (75.2 mmol., 7.66 mL), then left to stir for another 30 min. Then, the reaction was removed from the ice bath and stirred at room temperature (RT) for 2.5 h. The reaction was cooled to 0°C. Then, 10% HCl was added dropwise to the flask to bring the pH to 1. Once at pH 1 the solution was extracted 3X with DCM (100 mL). The organic layers were combined and dried using magnesium sulfate. Finally, the crude solution was concentrated *in vacuo* and dried overnight under vacuum. Crude compound 1 was purified using silica gel flash chromatography with eluent composed of 95% DCM, 4% methanol and 1% acetic acid (AcOH). The desired fractions containing pure 5 were combined and the solvent was removed *in vacuo*. AcOH removal was achieved using toluene. Compound 5 was obtained at 67% yield as an oil.

MW: 319.35, ESI+MS: 320 m/z (M + H+).

^{1}H NMR (300 MHz, CDCl3): δ 7.31 (m, 5H), 5.15 (dd, J=8 and J=4 Hz, 2H), 4.93 (d, J=15 Hz, 2H), 4.50 (m, 1H), 4.12 (m, 1H), 3.86 (m, 2H), 3.61 (m, 2H), 2.36 (m, 1H), 2.22 (m, 1H), 1.71 (s, 3H).

3.7.4 Fmoc-P_L synthesis:

A stir bar was added to the flask containing compound 5(12.6 mmol, 4.033 g), which was purged with N_2 and dissolved in dry 15 mL MeOH. Palladium on carbon (Pd/C) (10 wt. %, 0.5 g) was added to the flask and the flask was purged with hydrogen gas (H_2) by adding two h hydrogen balloons. This reaction was allowed to go overnight at RT. Following this step the Pd/C was filtered by gravity filtration and the solution was concentrated i*n vacuo* and further dried under vacuum. The unpurified compound was dissolve in 20mL of deionized water followed by the addition of sodium bicarbonate ($NaHCO_3$) (75.6 mmol, 6.35 g), which was allowed to dissolve completely before bringing the solution to 0°C. Once the desired temperature was a solution of Fmoc N-hydroxysuccinimide ester (Fmoc OSu) (13.86 mmol, 4.675 g) dissolved in 20 mL acetone was added slowly, dropwise to the flask. Then, the reaction was left to stir overnight at RT. The pH of the solution was brought 4 using 10% citric acid. The resulting solution was extracted 3X with 50 mL of ethyl acetate. The extracted organic layers were combined, dried with $MgSO_4$, and concentrated i*n vacuo* and dried further under vacuum. Crude Fmoc-P_L was purified by silica gel flash column chromatography using 97% DCM, 2% MeOH and 1% AcOH. Pure fractions were combined, concentrated *in vacuo* with AcOH removal achieved using toluene. Fmoc P_L was obtained in 44% yield as a white, fluffy solid.

MW: 409.19, ESI+MS: 410 m/z (M + H+)

^{1}H NMR (300 MHz, CDCl3): 7.75 (t, J = 6.9 Hz, 2H), 7.57 (t, J = 6.9 Hz, 2H), 7.31 (m, 4H), 4.43 (m, 4H), 4.11, 3.61 (m, 2H), 3.16 (m, 2H), 2.32 (m, 3H), 1.80 (m, 1H), 0.78 (d, J = 6.7 Hz, 6H).

3.7.5 **Fl-P14GAP** peptide synthesis:

To a 10 mL peptide synthesis flask was added 50 mg of Rink-Amide ChemMatrix resin (0.24 mmol/g loading). The resin was washed with dimethylformamide (DMF) (2X, about 4 mL each). In a 13 X 100 mm culture tube amino acid, Fmoc-$P_{L,}$ (24.6 mg, 0.06 mmol) was activated with hexafluorophosphate azabenzotriazole tetramethyl uronium (HATU) (22.8 mg, 0.06 mmol) and diisopropylethylamine (DIEA) (20.9 µL, 0.12 mmol) in DMF (4 mL) with sonication for 10 min. The resulting solution was added to the peptide synthesis flask, and the flask was agitated for 4 h. The solution was drained from the synthesis flask and the resin was washed sequentially with DMF, DCM, MeOH, DCM and DMF (2X, about 4 mL each). Piperidine in DMF (20%, 4 mL) was added

to the reaction flask, and the flask was agitated for 30 min. The piperidine was drained and the resin was washed sequentially with DMF, DCM, MeOH, DCM and DMF (2X, about 4 mL each). Next, Fmoc-GAP(Boc)$_2$ (35.7 mg, 0.06 mmol) was activated with HATU (22.8 mg, 0.06 mmol) and DIEA (20.9 µL, 0.12 mmol) in DMF (4 mL) in a 13 X 100 mm culture tube with sonication for 10 min. The resulting solution was added to the peptide synthesis flask, and the flask was agitated for 4 h. The solution was drained from the synthesis flask and the resin was washed sequentially with DMF, DCM, MeOH, DCM and DMF (2X, about 4 mL each). Piperidine in DMF (20%, 4 mL) was added to the reaction flask, and the flask was agitated for 30 min. The piperidine was drained and the resin was washed sequentially with DMF, DCM, MeOH, DCM and DMF (2X, about 4 mL each). This procedure was repeated to until the desired peptide sequence was synthesized ending with P_L. Commercially available Fmoc-glycine (21.39 mg, 0.072 mmol) was activated with HATU (27.4 mg, 0.072 mmol) and DIEA (25 µL, 0.144 mmol) in DMF (4 mL) in a 13 X 100 mm culture tube with sonication for 10 min. The resulting solution was added to the peptide synthesis flask, and the flask was agitated for 3 h. The solution was drained from the synthesis flask and the resin was washed sequentially with DMF, DCM, MeOH, DCM and DMF (2X, about 4 mL each). Piperidine in DMF (20%, 4 mL) was added to the reaction flask, and the flask was agitated for 30 min. The piperidine was drained and the resin was washed sequentially with DMF, DCM, MeOH, DCM and DMF (2X, about 4 mL each). Completion of deprotection and coupling reactions were confirmed for primary and secondary amines using the Kaiser and Chloranil test, respectively.[186, 187] Finally, commercially available NHS-fluorescein (12.49 mg, 0.026 mmol) dissolved in DMF (4 mL) with added DIEA (8.3 µL, 0.048 mmol) was added to the reaction flask which was protected from light with foil. The flask was agitated for 24 h. The solvent was drained from the reaction flask and the resin was washed sequentially with DMF, DCM, MeOH, DCM (2X, about 4 mL each) followed by drying under high vacuum for 2 h.

3.7.6 Cleavage and Purification of P14-GAP Peptide:

About 5 mL of a TFA cocktail composed of 95% TFA, 2.5% triisopropylsilane (TIPS), and 2.5% water was added to the peptide synthesis flask. The flask was agitated for 2 h. The solution was drained into a 50 mL centrifuge tube, the resin was rinsed with 5 mL of TFA cocktail followed by 5 mL of DCM. The washes were drained into centrifuge tube containing the cleaved peptide. The solvent was removed *in vacuo*, the crude peptide was precipitated using cold diethyl ether (25 mL)

and the tube was placed in a -80°C freezer overnight. The precipitate was collected by centrifugation at 3500 rpm and the supernatant was decanted. The resulting precipitate was dissolved in deionized water (10 mg/ mL) and purified using reverse phase high performance liquid chromatography (RP-HPLC) using a C18 semi preparative column. The eluent was composed of solvent A (acetonitrile with 0.1% TFA) and solvent B (water with 0.1% TFA) at a gradient of 15% – 65% eluent A, flow rate of 12 mL/ min, and UV detection at 214 nm and 254 nm. Fractions of the desired peptide were combined, the solvent was removed *in vacuo*, and lyophilized to obtain **Fl-P14GAP** as a yellow solid. Analysis of the purity of the peptide was achieved by analytical RP-HPLC using a C18 analytical column, a flow rate of 1.2 mL/ min, and UV detection at 214nm and 254 nm; a purity of >95% was obtained with a retention time of 21.6 min. The peptide product was characterized using matrix assisted laser desorption ionization – time of flight (MALDI-TOF) mass spectrometry.

Mass expected: 2510 g/mol, MALDI-ToF Obtained Mass: 2510 m/z

View Appendix A.4: HPLC Analytical Trace and MALDI-ToF mass spectrum

Note: **Fl-P14GAP/P_R** peptides were synthesized using the exact same protocol as for the synthesis of **Fl-P14GAP**, but P_R (39.2 mg, 0.06 mmol) replaced GAP monomer during the coupling steps of the peptide syntheses as specified in their designs. Analysis of the purity of the peptides were achieved by analytical RP-HPLC using a C18 analytical column, a flow rate of 1.2 mL/ min, and UV detection at 214nm and 254 nm; a purity of >95% was obtained with a retention time of 20.8 min (P1), 20.4 min (P2) 20.8min (P3), 20.4 min (P4)

Expected Mass: 2743, MALDI-ToF Obtained Mass: 2743 m/z (P1), 2744 m/z (P2), 2743 m/z (P3), 2743 m/z (P4).

View Appendix A.5 – A.9: HPLC Analytical Trace and MALDI-ToF spectrum of **Fl-P14GAP/P_R** peptides.

3.7.7 Determination of peptide concentration using UV-Vis

In order to determine the concentration of **Fl-P14GAP** UV-Vis was utilized. 5 µL of the peptide solution was added to 1 mL of tris(hydroxymethyl)aminomethane (TRIS) buffer, pH 8. The absorbance value was obtained at 494 nm, the absorbance maximum of fluorescein, and the concentration was calculated using the extinction coefficient 70,000 M^{-1} cm^{-1}.

3.7.8 Cell uptake studies using flow cytometry

For all in vitro cell experiments HaCat cells and J774A.1 cells were cultured in Dulbecco Modified Eagle Medium (DMEM) media supplemented with 10% fetal bovine serum (FBS) at 37°C under 5% CO_2.

3.7.8.1 J774A.1 cells

J774A.1 cells were plated in 300 µL of complete DMEM media at 125,000 cells/well in round bottom tubes (BD Biosciences) and incubated for 18-24 h at 37°C under 5% CO_2. The cells were centrifuged at 1200 rpm and the spent media was aspirated using a Pasteur pipet and vacuum filter. The cells were then treated with 300 µL of peptide at concentrations ranging from 2.5 – 10 µM prepared in 10% FBS supplemented DMEM media and were allowed to incubate for the desired incubation time period at 37°C. Cells with no treatment (complete DMEM media only) served as the negative control for the experiment. Upon completion of the incubation period, the cells were centrifuged and the spent media was aspirated. The cells were then suspended in 300 µL of cold PBS in the round bottom tubes and the fluorescence of the cells was measured using a FACS Calibur flow cytometer (BD Biosciences). All samples were run in duplicate, and each experiment was repeated at least twice. The mean arbitrary florescence values of gated cells were measured and recorded upon excitation of the fluorophore, fluorescein, using the Fl-1 laser at 488 nm. For each experiment, a negative control of cells that were not incubated with fluorescent compound was also analyzed. Results were processed using the BD software.

3.7.8.2 HaCat cells

HaCat cells were plated in a 24 well plate at a volume of 400 µL with 100,000 cells per well in complete DMEM .The seeded cells were put in the incubator for 18-24 h at 5% CO_2 atmosphere at 37°C. The spent media was aspirated from the cells and the cells were washed with 300 µL of PBS. The cells were treated with 300 µL of peptide at desired concentrations prepared in 10% FBS supplemented DMEM media and were allowed to incubate for the desired incubation time at 37°C. Cells with no peptide (DMEM media only) served as the negative control for the experiment. Upon completion of the incubation period, the cells were washed with 300 µL of PBS and treated with 150 µL of trypsin for 6 min at 37°C. The trypsin was quenched with 400 µL of cold PBS and the cells were transferred to round bottom tubes. The fluorescence of the cells was measured using a

FACS calibur flow Cytometer (BD Biosciences). Data were obtained in duplicates from at least two independent experiments and were processed using the BD software. The mean arbitrary florescence values of gated cells were measured and recorded upon excitation of the fluorophore, fluorescein, using the Fl-1 laser at 488 nm.

3.7.8.3 Trypan blue studies in J774A.1 and HaCat cells

Cells were plated as previously described above and treated with peptide at concentrations 2.5 and 5 µM. After cells were incubated with peptide treatment for the desired incubation time the peptide treatment was removed from each cell type as previously described above. After treatment removal, J774A.1 cells were suspended in 300 µL of cold PBS or 300 µL of trypan blue (1mg/ mL in PBS). HaCat cells were washed with 300 µL of PBS and detached from the plate by treatment with 150 µL of trypsin for 6 min at 37°C. The trypsin was quenched with 400 µL of cold PBS or 400 µL of cold trypan blue (1mg/ mL) in PBS. The cells were transferred to round bottom tubes. The fluorescence of the cells was measured using a FACS calibur flow cytometer (BD Biosciences). Data were obtained in duplicates from at least two independent experiments and were processed using the BD software. The mean arbitrary florescence values of gated cells were measured and recorded upon excitation of the fluorophore, fluorescein, using the Fl-1 laser at 488 nm. For each experiment, a negative control of cells that were not incubated with fluorescent compound was also analyzed.

3.7.9 Cell viability assay

Cellular toxicity of the peptides was tested using the 3-(4,5-dimethylthiazol-2-yl)-2,5-diphenyltetrazolium bromide (MTT) cell viability assay.[188] J774A.1 cells and HaCat cells were tested for cytotoxicity after 9 h incubation with peptide treatment. J774A.1 cells and HaCat cells were seeded into a 96 well plates at 100 µL at a density of 20,000 cells/well and 10,000 cells/well, respectively, in complete DMEM media. After plating the cells, they were put in the incubator under 5% CO_2 atmosphere at 37°C for 18 to 24 h. The spent media was aspirated and the cells were washed with 100 µL PBS (phosphate buffered saline). Then, 50 µL of peptide treatment made in DMEM growth media was added to the cells at a concentrations ranging from 1.25 – 40 µM. The cells were put in the incubator under 5% CO_2 atmosphere at 37°C for 9 hr. Following incubation period the treatment media was aspirated and the cells were washed with 100 µL of

PBS. Then, 100 µL of fresh complete DMEM media was added followed by the addition of 10 µL of MTT solution (5 mg /mL MTT in PBS) to each well. The cells were incubated for an additional 2.5 hr. The MTT solution was aspirated and 100 µL of DMSO was added to each well to dissolve the formazan crystals that formed. For each experiment, a negative control of cells not incubated with peptide were analyzed. The samples were run in duplicates and each experiment was repeated at least twice. The mean absorbance for each sample was measured and recorded at 590 nm. Percent viability was determined by taking ratio of treated cells to untreated cells and multiplying by 100%.

3.7.10 Hemolysis assay

5 mL of human red blood cells (hRBCs) (Innovative Research, cat # IWB3CPDA) were collected by centrifugation at 2000 rpm for 5 min followed by washing three times with 5 mL PBS, pH 7.4. The supernatant of the final wash was aspirated and 100 µL of the cell pellet was added to 4.9 mL of PBS to make a 2% suspension (v/v), with a total volume of 5 mL. To a 96 well plate, 50 µL of the hRBC solution was added followed by 50 µL of peptide treatment prepared in PBS to achieve a 2-fold dilution of peptide and a final suspension of 1% (v/v) of hRBCs. The plate was incubated at 37 °C under 5% CO_2 for 1 h. The plate was subsequently centrifuged at 1000 rpm for 5 min at 4 °C. Next 75 µL aliquots of the supernatants in each well were carefully transferred to a new 96-well plate. The release of hemoglobin was monitored by measuring the absorbance at OD_{405} with a micro-plate reader. As controls, hRBCs were treated with PBS as anegative control, 0.1% Triton X-100 as a positive control, and melittin (Sigma M2272) as a positive control. The percent of hemolysis was calculated based on the 100% release with 0.1% Triton X-100. Data were obtained in duplicates from two independent experiments.

3.7.11 Laser scanning confocal microscopy of live cells

High resolution imaging of the subcellular localization of the peptides was performed in J774A.1 and HaCat cells using an inverted confocal florescent microscope (Nikon A1R) with a 60x oil objective. J774A.1 and HaCat cells were seeded into 4-well LabTek culture chamber at a density of 125,000 cells/well and 100,000 cells/well, respectively, in 500 mL of complete DMEM media. The cells were grown 12-24 hr in a humidified 5% CO2 atmosphere at 37°C. After pre-incubation, the cells were washed with 500 µL PBS. Then, 400 µL of peptide treatment prepared in growth

media was added to the wells at concentrations ranging from 1.25 to 5 µM. The cells were incubated for 1 h in the presence of the peptide treatment. Following incubation the cells were washed with 500 µL of PBS. Then, 400 µL of 100 nM Mitotracker solution prepared in growth media or 300 nM Lysotracker prepared in growth media were added to the wells and the cells were incubated for 30 minutes. After incubation the cells were washed with 500 µL of PBS. Next, 500 µL of growth media was added to each well prior to imaging. Live cells were then imaged using an 60 X oil objective using sequential laser scanning at 488 nm (green channel) and 572 nm (red channel).

3.7.12 MIC of CAPHs against pathogenic bacterial isolates:

The minimum inhibitory concentration (MIC) of peptides (in uM/ml) and control antibiotics (vancomycin and gentamicin) in µg/ml, were determined using the broth microdilution method against different bacterial strains. The antimicrobial activity of the tested peptides and control antibiotics against the tested isolates was performed following the Clinical and Laboratory Standards Institute guidelines[189]. Briefly, bacterial cells were cultured overnight on tryptic soya agar plates (Becton Dickinson). Colonies were picked and suspended in NaCl 0.9% to a density of 0.5 McFarland. The bacterial suspensions were further diluted 1:60 in cation adjusted Mueller-Hinton Broth (CA-MHB) (Becton Dickinson), and 100 µl portions of the bacterial suspension were added to 96-well plates (Corning Incorporated) containing the tested peptides and control antibiotics prepared in filtered deionized water at a concentrations ranging from 0.125 to 32 µM. The 96-well plates were incubated for 16–20 h at 37 °C before recording the MIC values. The MICs reported represent the lowest concentration of each peptide or standard antibiotic necessary to inhibit bacterial growth from at least two separate experiments done in duplicate.

3.7.13 Minimum inhibitory concentrations (MIC) of **Fl-P14GAP** against *E. coli* ATCC 25922

The peptide solutions were prepared in deionized water to have a final concentrations of 6.25 to 100 µM and a final volume of 30 µL. For all experiments Melittin was used as a positive control and deionized water was used as a negative control. Bacterial cells were cultured overnight on tryptic soya agar plates. Five colonies were picked with an inoculation loop and inoculated in an Erlenmeyer flask in 50 mL of tryptic soy broth (TSB) media until an optical density (OD) at 590 nm between 0.3 and 0.6 (log phase) was reached. Once the desired OD was obtained, 5 mL of the

bacteria solution was transferred to a 15 mL centrifuge tube. The media was replaced with Mueller Hinton Broth (MHB) media by pelleting the bacteria by centrifugation at 3500 rpm for 5 min 4°C and washing the pellet 3X with 5 mL MHB. Once the washes were complete the bacteria pellet was resuspended in 5 mL of MHB, which was diluted with MHB in a 50 mL centrifuge tube to make 20 mL of bacteria solution at an OD of 0.001. Once this desired OD was reached, 90 µL of the bacteria solution was added to each well in a 96 well plate. Following the addition of the bacteria, 10 µL of the peptide solution was added to the designated wells. The bacteria was incubated with the peptide treatment for 6 h. Once the incubation time was complete the OD_{590} was determined using a microplate reader (Tecan Infinite F PLEX, Cisbio). The MIC was determined based on the minimum concentration in which bacterial growth was inhibited based on the measured OD. The samples were run in duplicates and each experiment was repeated at least three times.

3.7.14 β-galactosidase assay using *E. coli* ATCC 25922

Peptide solutions were prepared in deionized water (DIW) to have make concentrations at 1X and 2X the determined MIC values for **Fl-P14GAP** against *E. coli* at a final volume of 30 µL. For all experiments Melittin was used as a positive control, DIW was used as a negative control, and Fl-P14LRR was included as a reference. *E. coli* was cultured overnight on tryptic soya agar plates and five colonies were picked with an inoculation loop and inoculated in an Erlenmeyer flask in 50 mL of Mueller Hinton Broth (MHB) media for about 2 h to the OD_{590} reached 0.1 and 5 mL of isopropyl-β-D thiogalactopyranoside (IPTG) (24 mg in 10 mL PBS) was added to bacteria solution for final concentration of 1 mM. The bacteria was further inoculated to an OD_{590} between 0.3 and 0.5. Once the desired OD was reached, a 10 mL aliquot of the bacteria in the IPTG/MHB media was removed and media was removed by centrifugation at 4000 rpm for 5 min and decanting the spent media. The pelleted bacteria was then washed twice with 10 mL of fresh MHB. Once the washes were complete the bacteria was suspended a 10 mL of MHB and the OD was noted. The bacteria were plated in a 96 well plate at 90 µL per well followed by the addition of 10 µL of the peptide solution. The bacteria was incubated with the peptide treatment for 1 h. The 96 well plate was centrifuged for 5 min at 4000 rpm and 80 µL of the supernatant was transferred to a new 96 well plate. Then, 20 µL of an freshly prepared 2-nitrophenyl-β-D-galactopyranoside (ONPG) (40 mg/ 10 mL of PBS) solution was added to each well for a final concentration of 0.8 mg/mL. The OD_{405} values were

read every 5 min over the course of 1 h using a microplate reader to monitor the levels of o-nitrophenol. The percent of β-galactosidase release from *E. coli* was calculated based on the absorbance value obtained for treated samples divided by the absorbance value obtained in non-treated samples. Data was obtained in duplicates from at least two independent experiments.

3.7.15 *In cyto* experiments

The activity of **Fl-P14GAP** against intracellular *Shigella flexneri*, *Listeria monocytogenes*, *S. epidermidis* NRS 101, MRSA US300, and *A. baumannii* 19606 were tested according to the following protocol. Briefly, J774A.1 murine macrophage-like cells were seeded at a density of 10000 cells per well in 96-well plates (Corning Incorporated) for 24 hours before being infected with bacteria. The cells were grown in DMEM supplemented with 10% heat-inactivated fetal bovine serum. Following incubation, the cells were washed once with DMEM. Then cells were infected with the respective bacteria (multiplicity of infection 1:10), for 45 min. At the end of the infection, cells were washed three times with DMEM medium containing 100 µg/ mL gentamicin (Sigma) and were further incubated for 3 hours with gentamicin (100 µg/ mL) to kill and non-phagocytized bacteria. Then DMEM medium supplemented with 10% fetal bovine serum containing the tested compounds at 5 µM (sub toxic concentration based on the toxicity study) were added to the cells. Control cells received sterile phosphate buffered saline (PBS). The plate was then returned to the incubator and the intracellular clearance activity of **Fl-P14GAP** and the tested antibiotic controls (ceftazidime and amoxicillin) were assessed after 12 hours. At the end of the incubation time, the infected cells were washed three times with PBS and lysed with 100 µL of 0.01% triton-x to collect the intracellular bacteria. The colony forming units (CFUs) of the bacteria in the lysates were determined by plating a series of 10-fold serial dilutions onto tryptic soy agar (TSA) and incubating the plates at 37°C for 24 hours. Statistical significance was assessed with one-way ANOVA, with post hoc Dunnet's multiple comparisons test ($P < 0.05$), utilizing GraphPad Prism 6.0 (GraphPad Software, La Jolla, CA).

3.7.16 Antibiofilm activity

The anti-biofilm activity of **Fl-P14GAP** peptide was assessed using XTT assay.[161, 190, 191] Briefly, overnight bacterial cultures of *A. baumannii* 19606, *P. aeruginosa*, 31040, MRSA US300, and *S. epidermidis* NRS 101, were diluted (1:100) in TSB medium and the plates were incubated at 37°C

for 24 h to allow the formation of bacterial biofilms. The plates were washed twice with PBS. **Fl-P14GAP** and the control antibiotics (gentamicin and vancomycin) were tested at three different concentrations (16, 32 and 64 uM). The tested compounds were serially diluted in TSB medium. 100 µl volumes of each treatment were added to the corresponding wells containing the tested biofilm and were then incubated for another 24 h at 37ºC. Wells containing the formed biofilm, but no drugs, served as negative control for each of the tested strains. Following incubation, biofilms were washed three times with sterile PBS and metabolic activity was determined using the XTT reduction assay. 100 µl volumes of XTT/ menadione solution were added to each well and the plates were incubated at 37°C in the dark for 1 h. Before reading, 80 µL of reaction mixture was transferred to a clean flat-bottomed microtiter plate and read in a microplate reader at 490 nm. Data were presented as the percentage of biofilm viability relative to the control.

REFERENCES

1. Center of Disease Control, Achievements in Public Health, 1900-1999: Control of Infectious Diseases. Centers for Disease Control and Prevention: Atlanta, GA, 2019; Vol. 48, pp 621-629.

2. Alexander Fleming Discovery and Development of Penicillin - Landmark - American Chemical Society. https://www.acs.org/content/acs/en/education/whatischemistry/landmarks/flemingpenicillin.html (accessed July 12).

3. Ferretti, J.; Köhler, W., History of Streptococcal Research. In *Streptococcus pyogenes : Basic Biology to Clinical Manifestations* [Online] Ferretti, J.; Stevens, D.; Fischetti, V., Eds. University of Oklahoma Health Sciences Center: Oklahoma City, OK, 2016. https://www.ncbi.nlm.nih.gov/pubmed/ (accessed 2016/02/10).

4. Reardon, S., WHO warns against 'post-antibiotic' era. *Nature News* **2019**.

5. Antibiotic/Antimicrobial Resistance. Center for Disease Control and Prevention: 2016.

6. Center of Disease Control. *Enteric Diseases Epidemiology Branch | DFWED | NCEZID | CDC*; 2018-12-17T04:45:38Z/, 2018.

7. Center of Disease Control, Salmonella. 2019; p https://www.cdc.gov/salmonella/index.html.(accessed June 8)

8. Center of Disease Control, Biggest, Threats and Data. In *Antibiotic/Antimicrobial Resistance*, Center for Disease Control and Prevention: 2018; Vol. 2019, p https://www.cdc.gov/drugresistance/biggest_threats.html (accessed July16).

9. FDA, U. Get the Facts about Listeria! https://www.fda.gov/animal-veterinary/animal-health-literacy/get-facts-about-listeria (accessed July 15).

10. Mulani, M. S.; Kamble, E. E.; Kumkar, S. N.; Tawre, M. S.; Pardesi, K. R., Emerging Strategies to Combat ESKAPE Pathogens in the Era of Antimicrobial Resistance: A Review. *Front Microbiol* **2019,** *10*, 539.

11. Center of Disease Control, Biggest Threats and Data. https://www.cdc.gov/drugresistance/biggest_threats.html (accessed July 12).

12. Asif, M.; Alvi, I. A.; Rehman, S. U., Insight into Acinetobacter baumannii: pathogenesis, global resistance, mechanisms of resistance, treatment options, and alternative modalities. *Infect Drug Resist* **2018,** *11*, 1249-60.

13. World Health Organization, WHO publishes list of bacteria for which new antibiotics are urgently needed. https://www.who.int/news-room/detail/27-02-2017-who-publishes-list-of-bacteria-for-which-new-antibiotics-are-urgently-needed (accessed July 20).

14. Demirdal, T.; Sari, U. S.; Nemli, S. A., Is inhaled colistin beneficial in ventilator associated pneumonia or nosocomial pneumonia caused by Acinetobacter baumannii? *Ann Clin Microbiol Antimicrob* **2016,** *15*, 11.

15. Hale, T. L.; Keusch, G. T., Shigella. In *Medical Microbiology*, 4th ed.; Baron, S., Ed. University of Texas Medical Branch at Galveston: Galveston, TX, 1996.

16. Farber, J. M.; Peterkin, P. I., Listeria monocytogenes, a food-borne pathogen. *Microbiol Rev* **1991,** *55* (3), 476-511.

17. Giannella, R. A., Salmonella. In *Medical Microbiology*, 4th ed.; Baron, S., Ed. University of Texas Medical Branch at Galveston: Galveston, TX, 1996.

18. Doyle J. Evans, J.; Evans, D. G., Escherichia Coli in Diarrheal Disease. In *Medical Microbiology*, 4th ed.; Baron, S., Ed. University of Texas Medical Branch at Galveston: Galveston, TX, 1996.

19. Auer, G. K.; Weibel, D. B., Bacterial Cell Mechanics. *Biochemistry* **2017,** *56* (29), 3710-3724.

20. Santajit, S.; Indrawattana, N., Mechanisms of Antimicrobial Resistance in ESKAPE Pathogens. *Biomed Res Int* **2016,** *2016*, 2475067. http://dx.doi.org/10.1155/2016/2475067

21. Miller, S. I., Antibiotic Resistance and Regulation of the Gram-Negative Bacterial Outer Membrane Barrier by Host Innate Immune Molecules. *mBio* **2016,** *7* (5), e01541-16.

22. Differences between Gram positive and Gram negative bacteria - Online Science Notes. https://onlinesciencenotes.com/differences-between-gram-positive-and-gram-negative-bacteria/ (accessed July 15).

23. Coates, A. R.; Halls, G.; Hu, Y., Novel classes of antibiotics or more of the same? *Br J Pharmacol* **2011,** *163* (1), 184-94.

24. Livermore, D. M., Linezolid in vitro: mechanism and antibacterial spectrum. *J Antimicrob Chemother* **2003,** *51*, (suppl_2), *ii9–ii16*.

25. Watanakunakorn, C., Mode of action and in-vitro activity of vancomycin. *J Antimicrob Chemother* **1984,** *14*, (suppl_D), 7-18.

26. Hancock, R. E. W.; Chapple, D. S., Peptide Antibiotics. *Antimicrob Agents Chemother* **1999,** *43* (6), 1317-23.

27. Jiang, L.; Lin, J.; Taggart, C. C.; Bengoechea, J. A.; Scott, C. J., Nanodelivery strategies for the treatment of multidrug-resistant bacterial infections. *Journal of interdisciplinary nanomedicine* **2018,** *3* (3), 111-121.

28. Brezden, A.; Mohamed, M. F.; Nepal, M.; Harwood, J. S.; Kuriakose, J.; Seleem, M. N.; Chmielewski, J., Dual Targeting of Intracellular Pathogenic Bacteria with a Cleavable Conjugate of Kanamycin and an Antibacterial Cell-Penetrating Peptide. *J Am Chem Soc* **2016,** *138* (34), 10945-9.

29. Lehar, S. M.; Pillow, T.; Xu, M.; Staben, L.; Kajihara, K. K.; Vandlen, R.; DePalatis, L.; Raab, H.; Hazenbos, W. L.; Hiroshi Morisaki, J.; Kim, J.; Park, S.; Darwish, M.; Lee, B.-C.; Hernandez, H.; Loyet, K. M.; Lupardus, P.; Fong, R.; Yan, D.; Chalouni, C.; Luis, E.; Khalfin, Y.; Plise, E.; Cheong, J.; Lyssikatos, J. P.; Strandh, M.; Koefoed, K.; Andersen, P. S.; Flygare, J. A.; Wah Tan, M.; Brown, E. J.; Mariathasan, S., Novel antibody–antibiotic conjugate eliminates intracellular S. aureus. *Nature* **2015,** *527*, 323-328.

30. Wang, L.; Hu, C.; Shao, L., The antimicrobial activity of nanoparticles: present situation and prospects for the future. *International journal of nanomedicine* **2017,** *12*, 1227-1249.

31. Chames, P.; Van Regenmortel, M.; Weiss, E.; Baty, D., Therapeutic antibodies: successes, limitations and hopes for the future. *Br J Pharmacol* **2009,** *157* (2), 220-33.

32. Guilhelmelli, F.; Vilela, N.; Albuquerque, P.; Derengowski Lda, S.; Silva-Pereira, I.; Kyaw, C. M., Antibiotic development challenges: the various mechanisms of action of antimicrobial peptides and of bacterial resistance. *Front Microbiol* **2013,** *4*, (353), 1-21.

33. Zhao, X.; Wu, H.; Lu, H.; Li, G.; Huang, Q., LAMP: A Database Linking Antimicrobial Peptides. *PloS one* **2013,** *8* (6), e66557-e66557.

34. Fleming, A.; Wright Almroth, E., On a remarkable bacteriolytic element found in tissues and secretions. *Proceedings of the Royal Society of London. Series B, Containing Papers of a Biological Character* **1922,** *93* (653), 306-317.

35. Hancock, R. E. W.; Sahl, H.-G., Antimicrobial and host-defense peptides as new anti-infective therapeutic strategies. *Nature Biotechnology* **2006,** *24* (12), 1551-1557.

36. Koo, H. B.; Seo, J., Antimicrobial peptides under clinical investigation. *Peptide Science* **2019,** *0* (0), e24122.

37. Mahlapuu, M.; Hakansson, J.; Ringstad, L.; Bjorn, C., Antimicrobial Peptides: An Emerging Category of Therapeutic Agents. *Front Cell Infect Microbiol* **2016,** *6*, 194.

38. Fox, J. L., Antimicrobial peptides stage a comeback. *Nature Biotechnology* **2013,** *31* (5), 379-382.

39. Turner, J.; Cho, Y.; Dinh, N. N.; Waring, A. J.; Lehrer, R. I., Activities of LL-37, a cathelin-associated antimicrobial peptide of human neutrophils. *Antimicrob Agents Chemother* **1998,** *42* (9), 2206-14.

40. Lohner, K.; Prenner, E. J., Differential scanning calorimetry and X-ray diffraction studies of the specificity of the interaction of antimicrobial peptides with membrane-mimetic systems. *Biochim Biophys Acta* **1999,** *1462* (1-2), 141-56.

41. Findlay, B.; Zhanel, G. G.; Schweizer, F., Cationic amphiphiles, a new generation of antimicrobials inspired by the natural antimicrobial peptide scaffold. *Antimicrob Agents Chemother* **2010,** *54* (10), 4049-58.

42. Javadpour, M. M.; Juban, M. M.; Lo, W.-C. J.; Bishop, S. M.; Alberty, J. B.; Cowell, S. M.; Becker, C. L.; McLaughlin, M. L., De Novo Antimicrobial Peptides with Low Mammalian Cell Toxicity. *Journal of Medicinal Chemistry* **1996,** *39* (16), 3107-3113.

43. Kobayashi, S.; Takeshima, K.; Park, C. B.; Kim, S. C.; Matsuzaki, K., Interactions of the novel antimicrobial peptide buforin 2 with lipid bilayers: proline as a translocation promoting factor. *Biochemistry* **2000,** *39* (29), 8648-54.

44. Brogden, K. A., Antimicrobial peptides: pore formers or metabolic inhibitors in bacteria? *Nat Rev Microbiol* **2005,** *3* (3), 238-50.

45. Park, C. B.; Kim, H. S.; Kim, S. C., Mechanism of action of the antimicrobial peptide buforin II: buforin II kills microorganisms by penetrating the cell membrane and inhibiting cellular functions. *Biochem Biophys Res Commun* **1998,** *244* (1), 253-7.

46. Yang, S. C.; Lin, C. H.; Sung, C. T.; Fang, J. Y., Antibacterial activities of bacteriocins: application in foods and pharmaceuticals. *Front Microbiol* **2014,** *5* (241), 1-25.

47. Collin, F.; Thompson, R. E.; Jolliffe, K. A.; Payne, R. J.; Maxwell, A., Fragments of the bacterial toxin microcin B17 as gyrase poisons. *PloS one* **2013,** *8* (4), e61459-e61459.

48. Lehrer, R. I.; Barton, A.; Daher, K. A.; Harwig, S. S.; Ganz, T.; Selsted, M. E., Interaction of human defensins with Escherichia coli. Mechanism of bactericidal activity. *The Journal of clinical investigation* **1989,** *84* (2), 553-561.

49. Kohn, E. M.; Shirley, D. J.; Arotsky, L.; Picciano, A. M.; Ridgway, Z.; Urban, M. W.; Carone, B. R.; Caputo, G. A., Role of Cationic Side Chains in the Antimicrobial Activity of C18G. *Molecules (Basel, Switzerland)* **2018,** *23* (2), 329.

50. Cutrona, K. J.; Kaufman, B. A.; Figueroa, D. M.; Elmore, D. E., Role of arginine and lysine in the antimicrobial mechanism of histone-derived antimicrobial peptides. *FEBS letters* **2015,** *589* (24 Pt B), 3915-3920.

51. Jiang, Z.; Vasil, A. I.; Hale, J. D.; Hancock, R. E. W.; Vasil, M. L.; Hodges, R. S., Effects of net charge and the number of positively charged residues on the biological activity of amphipathic alpha-helical cationic antimicrobial peptides. *Biopolymers* **2008,** *90* (3), 369-383.

52. Chen, Y.; Guarnieri, M. T.; Vasil, A. I.; Vasil, M. L.; Mant, C. T.; Hodges, R. S., Role of peptide hydrophobicity in the mechanism of action of alpha-helical antimicrobial peptides. *Antimicrob Agents Chemother* **2007,** *51* (4), 1398-406.

53. Chen, Y.; Mant, C. T.; Farmer, S. W.; Hancock, R. E.; Vasil, M. L.; Hodges, R. S., Rational design of alpha-helical antimicrobial peptides with enhanced activities and specificity/therapeutic index. *J Biol Chem* **2005,** *280* (13), 12316-29.

54. Kondejewski, L. H.; Lee, D. L.; Jelokhani-Niaraki, M.; Farmer, S. W.; Hancock, R. E.; Hodges, R. S., Optimization of microbial specificity in cyclic peptides by modulation of hydrophobicity within a defined structural framework. *J Biol Chem* **2002,** *277* (1), 67-74.

55. Li, W.; Tailhades, J.; O'Brien-Simpson, N. M.; Separovic, F.; Otvos, L., Jr.; Hossain, M. A.; Wade, J. D., Proline-rich antimicrobial peptides: potential therapeutics against antibiotic-resistant bacteria. *Amino Acids* **2014,** *46* (10), 2287-94.

56. Mishra, A. K.; Choi, J.; Moon, E.; Baek, K. H., Tryptophan-Rich and Proline-Rich Antimicrobial Peptides. *Molecules* **2018,** *23* (4), 815-861.

57. Bochicchio, B.; Tamburro, A. M., Polyproline II structure in proteins: identification by chiroptical spectroscopies, stability, and functions. *Chirality* **2002,** *14* (10), 782-92.

58. Scocchi, M.; Tossi, A.; Gennaro, R., Proline-rich antimicrobial peptides: converging to a non-lytic mechanism of action. *Cellular and Molecular Life Sciences* **2011,** *68* (13), 2317-2330.

59. Szabo, D.; Ostorhazi, E.; Binas, A.; Rozgonyi, F.; Kocsis, B.; Cassone, M.; Wade, J. D.; Nolte, O.; Otvos, L., Jr., The designer proline-rich antibacterial peptide A3-APO is effective against systemic Escherichia coli infections in different mouse models. *Int J Antimicrob Agents* **2010,** *35* (4), 357-61.

60. Pukala, T. L.; Brinkworth, C. S.; Carver, J. A.; Bowie, J. H., Investigating the Importance of the Flexible Hinge in Caerin 1.1: Solution Structures and Activity of Two Synthetically Modified Caerin Peptides. *Biochemistry* **2004,** *43* (4), 937-944.

61. Lee, K.; Shin, S. Y.; Kim, K.; Lim, S. S.; Hahm, K. S.; Kim, Y., Antibiotic activity and structural analysis of the scorpion-derived antimicrobial peptide IsCT and its analogs. *Biochem Biophys Res Commun* **2004,** *323* (2), 712-9.

62. Shin, S. Y.; Park, E. J.; Yang, S. T.; Jung, H. J.; Eom, S. H.; Song, W. K.; Kim, Y.; Hahm, K. S.; Kim, J. I., Structure-activity analysis of SMAP-29, a sheep leukocytes-derived antimicrobial peptide. *Biochem Biophys Res Commun* **2001,** *285* (4), 1046-51.

63. Park, C. B.; Yi, K. S.; Matsuzaki, K.; Kim, M. S.; Kim, S. C., Structure-activity analysis of buforin II, a histone H2A-derived antimicrobial peptide: the proline hinge is responsible for the cell-penetrating ability of buforin II. *Proc Natl Acad Sci U S A* **2000,** *97* (15), 8245-50.

64. Bahar, A. A.; Ren, D., Antimicrobial peptides. *Pharmaceuticals (Basel)* **2013,** *6* (12), 1543-75.

65. Zhu, W. L.; Lan, H.; Park, I. S.; Kim, J. I.; Jin, H. Z.; Hahm, K. S.; Shin, S. Y., Design and mechanism of action of a novel bacteria-selective antimicrobial peptide from the cell-penetrating peptide Pep-1. *Biochem Biophys Res Commun* **2006,** *349* (2), 769-74.

66. Li, J.; Koh, J. J.; Liu, S.; Lakshminarayanan, R.; Verma, C. S.; Beuerman, R. W., Membrane Active Antimicrobial Peptides: Translating Mechanistic Insights to Design. *Front Neurosci* **2017,** *11*, (73), 1-56.

67. Matsuzaki, K., Control of cell selectivity of antimicrobial peptides. *Biochim Biophys Acta* **2009,** *1788* (8), 1687-92.

68. Olsen, C. A., Peptoid-Peptide hybrid backbone architectures. *Chembiochem* **2010,** *11* (2), 152-60.

69. Lim, S. S.; Kim, Y.; Park, Y.; Kim, J. I.; Park, I. S.; Hahm, K. S.; Shin, S. Y., The role of the central L- or D-Pro residue on structure and mode of action of a cell-selective alpha-helical IsCT-derived antimicrobial peptide. *Biochem Biophys Res Commun* **2005,** *334* (4), 1329-35.

70. Carmona, G.; Rodriguez, A.; Juarez, D.; Corzo, G.; Villegas, E., Improved Protease Stability of the Antimicrobial Peptide Pin2 Substituted with d-Amino Acids. *The Protein Journal* **2013,** *32* (6), 456-466.

71. Di Grazia, A.; Cappiello, F.; Cohen, H.; Casciaro, B.; Luca, V.; Pini, A.; Di, Y. P.; Shai, Y.; Mangoni, M. L., d-Amino acids incorporation in the frog skin-derived peptide esculentin-1a(1-21)NH2 is beneficial for its multiple functions. *Amino Acids* **2015,** *47* (12), 2505-2519.

72. Chen, C.; Mangoni, M. L.; Di, Y. P., In vivo therapeutic efficacy of frog skin-derived peptides against Pseudomonas aeruginosa-induced pulmonary infection. *Scientific Reports* **2017,** *7* (1), 8548.

73. Shai, Y.; Oren, Z., Diastereoisomers of cytolysins, a novel class of potent antibacterial peptides. *J Biol Chem* **1996,** *271* (13), 7305-8.

74. Gao, Y.; Wu, D.; Xi, X.; Wu, Y.; Ma, C.; Zhou, M.; Wang, L.; Yang, M.; Chen, T.; Shaw, C., Identification and Characterisation of the Antimicrobial Peptide, Phylloseptin-PT, from the Skin Secretion of Phyllomedusa tarsius, and Comparison of Activity with Designed, Cationicity-Enhanced Analogues and Diastereomers. *Molecules (Basel, Switzerland)* **2016,** *21* (12), 1667.

75. Wade, D.; Boman, A.; Wåhlin, B.; Drain, C. M.; Andreu, D.; Boman, H. G.; Merrifield, R. B., All-D amino acid-containing channel-forming antibiotic peptides. *Proceedings of the National Academy of Sciences* **1990,** *87* (12), 4761.

76. Porter, E. A.; Wang, X.; Lee, H.-S.; Weisblum, B.; Gellman, S. H., Non-haemolytic β-amino-acid oligomers. *Nature* **2000,** *404* (6778), 565-565.

77. Hamuro, Y.; Schneider, J. P.; DeGrado, W. F., De Novo Design of Antibacterial β-Peptides. *Journal of the American Chemical Society* **1999,** *121* (51), 12200-12201.

78. Patch, J. A.; Barron, A. E., Helical Peptoid Mimics of Magainin-2 Amide. *Journal of the American Chemical Society* **2003,** *125* (40), 12092-12093.

79. Oliva, R.; Chino, M.; Pane, K.; Pistorio, V.; De Santis, A.; Pizzo, E.; D'Errico, G.; Pavone, V.; Lombardi, A.; Del Vecchio, P.; Notomista, E.; Nastri, F.; Petraccone, L., Exploring the role of unnatural amino acids in antimicrobial peptides. *Scientific Reports* **2018,** *8* (1), 8888.

80. Mowery, B. P.; Lee, S. E.; Kissounko, D. A.; Epand, R. F.; Epand, R. M.; Weisblum, B.; Stahl, S. S.; Gellman, S. H., Mimicry of Antimicrobial Host-Defense Peptides by Random Copolymers. *J. Am. Chem. Soc.* **2007,** *129* (50), 15474-15476.

81. Radzishevsky, I. S.; Rotem, S.; Bourdetsky, D.; Navon-Venezia, S.; Carmeli, Y.; Mor, A., Improved antimicrobial peptides based on acyl-lysine oligomers. *Nature Biotechnology* **2007,** *25*, 657-659.

82. Scott, R. W.; DeGrado, W. F.; Tew, G. N., De novo designed synthetic mimics of antimicrobial peptides. *Curr Opin Biotechnol* **2008,** *19* (6), 620-7.

83. Liu, D.; Choi, S.; Chen, B.; Doerksen, R. J.; Clements, D. J.; Winkler, J. D.; Klein, M. L.; DeGrado, W. F., Nontoxic Membrane-Active Antimicrobial Arylamide Oligomers. *Angewandte Chemie International Edition* **2004,** *43* (9), 1158-1162.

84. Choi, S.; Isaacs, A.; Clements, D.; Liu, D.; Kim, H.; Scott, R. W.; Winkler, J. D.; DeGrado, W. F., De novo design and in vivo activity of conformationally restrained antimicrobial arylamide foldamers. *Proceedings of the National Academy of Sciences of the United States of America* **2009,** *106* (17), 6968-6973.

85. Tew, G. N.; Scott, R. W.; Klein, M. L.; Degrado, W. F., De novo design of antimicrobial polymers, foldamers, and small molecules: from discovery to practical applications. *Acc Chem Res* **2010,** *43* (1), 30-9.

86. Kuriakose, J.; Hernandez-Gordillo, V.; Nepal, M.; Brezden, A.; Pozzi, V.; Seleem, M. N.; Chmielewski, J., Targeting intracellular pathogenic bacteria with unnatural proline-rich peptides: coupling antibacterial activity with macrophage penetration. *Angew Chem Int Ed Engl* **2013,** *52* (37), 9664-7.

87. Nepal, M.; Thangamani, S.; Seleem, M. N.; Chmielewski, J., Targeting intracellular bacteria with an extended cationic amphiphilic polyproline helix. *Org Biomol Chem* **2015,** *13* (21), 5930-6.

88. Hernandez-Gordillo, V.; Geisier, I.; Chmielewski, J., Dimeric Unnaturalpolyproline-rich peptides with enhanced antibacterial activity. *Bioorganic & Medicinal Chemistry Letter* **2014**, 556-559.

89. Mohamed, M. F.; Brezden, A.; Mohammad, H.; Chmielewski, J.; Seleem, M. N., Targeting biofilms and persisters of ESKAPE pathogens with P14KanS, a kanamycin peptide conjugate. *BBA - General Subjects* **2017,** *1861* (4), 848-859.

90. Nepal, M.; Mohamed, M. F.; Blade, R.; Eldesouky, H. E.; T, N. A.; Seleem, M. N.; Chmielewski, J., A Library Approach to Cationic Amphiphilic Polyproline Helices that Target Intracellular Pathogenic Bacteria. *ACS Infect Dis* **2018,** *4* (9), 1300-1305.

91. Geisler, I.; Chmielewski, J., Cationic amphiphilic polyproline helices: side-chain variations and cell-specific internalization. *Chem Biol Drug Des* **2009,** *73* (1), 39-45.

92. Li Li, I. G., Jean Chmielewski, Ji-Xin Cheng, Cationic amphiphilic polyproline helix P11LRR targets intracellular mitochondria. *Journl of Controlled Release* **2010,** *142* (2), 259-266.

93. Brezden, A. M.; University, P. The Design, Synthesis, and Investigation of Functional Cationic Amphiphilic Polyproline Helices (CAPHs). Purdue University, Purdue Univeristy, 2016.

94. Kristensen, M.; Birch, D.; Mørck Nielsen, H., Applications and Challenges for Use of Cell-Penetrating Peptides as Delivery Vectors for Peptide and Protein Cargos. *Int J Mol Sci* **2016,** *17* (2):185, 1-31.

95. Johnson, R. M.; Harrison, S. D.; Maclean, D., Therapeutic applications of cell-penetrating peptides. *Methods Mol Biol* **2011,** *683*, 535-51.

96. Bechara, C.; Sagan, S., Cell-penetrating peptides: 20 years later, where do we stand? *FEBS Lett* **2013,** *587* (12), 1693-702.

97. Pooga, M.; Langel, U., Classes of Cell-Penetrating Peptides. *Methods Mol Biol* **2015,** *1324*, 3-28.

98. Madani, F.; Lindberg, S.; Langel, Ü.; Futaki, S.; Gräslund, A., Mechanisms of Cellular Uptake of Cell-Penetrating Peptides. *Journal of Biophysics* **2011**, 1-10.

99. Gagat, M.; Zielinska, W.; Grzanka, A., Cell-penetrating peptides and their utility in genome function modifications (Review). *Int J Mol Med* **2017,** *40* (6), 1615-1623.

100. Trabulo, S.; Cardoso, A. L.; Mano, M.; Pedroso de Lima, M. C., Cell Penetratin Peptide-Mechanims of Cellular Uptake and Generation of Delivery. *Pharmaceuticals* **2010**, 961-993.

101. Vives, E.; Brodin, P.; Lebleu, B., A truncated HIV-1 Tat protein basic domain rapidly translocates through the plasma membrane and accumulates in the cell nucleus. *J Biol Chem* **1997,** *272* (25), 16010-7.

102. Kosuge, M.; Takeuchi, T.; Nakase, I.; Jones, A. T.; Futaki, S., Cellular internalization and distribution of arginine-rich peptides as a function of extracellular peptide concentration, serum, and plasma membrane associated proteoglycans. *Bioconjug Chem* **2008,** *19* (3), 656-64.

103. Milletti, F., Cell-penetrating peptides: classes, origin, and current landscape. *Drug Discov Today* **2012,** *17* (15-16), 850-60.

104. Margus Pooga, M. H., Matjal Zorko, and Uuml; Langel, l., Cell penetration by transportan. *The FASEB Journal* **1998,** *12* (1), 67-77.

105. Dupont E., P. A., Joliot A., Penetratin Story: An Overview. *Methods in Molecular Biology* **2010,** *683*, 21-29`.

106. Mitchell, D. J.; Kim, D. T.; Steinman, L.; Fathman, C. G.; Rothbard, J. B., Polyarginine enters cells more efficiently than other polycationic homopolymers. *J Pept Res* **2000,** *56* (5), 318-25.

107. Amand, H. L.; Fant, K.; Norden, B.; Esbjorner, E. K., Stimulated endocytosis in penetratin uptake: effect of arginine and lysine. *Biochem Biophys Res Commun* **2008,** *371* (4), 621-5.

108. Rothbard, J. B.; Jessop, T. C.; Lewis, R. S.; Murray, B. A.; Wender, P. A., Role of membrane potential and hydrogen bonding in the mechanism of translocation of guanidinium-rich peptides into cells. *J Am Chem Soc* **2004,** *126* (31), 9506-7.

109. Li, L.; Vorobyov, I.; Allen, T. W., The different interactions of lysine and arginine side chains with lipid membranes. *J Phys Chem B* **2013,** *117* (40), 11906-20.

110. Elmquist, A.; Hansen, M.; Langel, U., Structure-activity relationship study of the cell-penetrating peptide pVEC. *Biochim Biophys Acta* **2006,** *1758* (6), 721-9.

111. Walrant, A.; Vogel, A.; Correia, I.; Lequin, O.; Olausson, B. E.; Desbat, B.; Sagan, S.; Alves, I. D., Membrane interactions of two arginine-rich peptides with different cell internalization capacities. *Biochim Biophys Acta* **2012,** *1818* (7), 1755-63.

112. Walrant, A.; Correia, I.; Jiao, C. Y.; Lequin, O.; Bent, E. H.; Goasdoue, N.; Lacombe, C.; Chassaing, G.; Sagan, S.; Alves, I. D., Different membrane behaviour and cellular uptake of three basic arginine-rich peptides. *Biochim Biophys Acta* **2011,** *1808* (1), 382-93.

113. Klocek, G.; Seelig, J., Melittin Interaction with Sulfated Cell Surface Sugars†. *Biochemistry* **2008,** *47* (9), 2841-2849.

114. Deshayes, S.; Plenat, T.; Aldrian-Herrada, G.; Divita, G.; Le Grimellec, C.; Heitz, F., Primary amphipathic cell-penetrating peptides: structural requirements and interactions with model membranes. *Biochemistry* **2004,** *43* (24), 7698-706.

115. Magzoub, M.; Eriksson, L. E.; Graslund, A., Conformational states of the cell-penetrating peptide penetratin when interacting with phospholipid vesicles: effects of surface charge and peptide concentration. *Biochim Biophys Acta* **2002,** *1563* (1-2), 53-63.

116. Horton, K. L.; Stewart, K. M.; Fonseca, S. B.; Guo, Q.; Kelley, S. O., Mitochondria-penetrating peptides. *Chem Biol* **2008,** *15* (4), 375-82.

117. Patel, S. G.; Sayers, E. J.; He, L.; Narayan, R.; Williams, T. L.; Mills, E. M.; Allemann, R. K.; Luk, L. Y. P.; Jones, A. T.; Tsai, Y.-H., Cell-penetrating peptide sequence and modification dependent uptake and subcellular distribution of green florescent protein in different cell lines. *Scientific Reports* **2019,** *9* (1), 6298.

118. Durzynska, J.; Przysiecka, L.; Nawrot, R.; Barylski, J.; Nowicki, G.; Warowicka, A.; Musidlak, O.; Gozdzicka-Jozefiak, A., Viral and other cell-penetrating peptides as vectors of therapeutic agents in medicine. *J Pharmacol Exp Ther* **2015,** *354* (1), 32-42.

119. Fittipaldi, A.; Ferrari, A.; Zoppe, M.; Arcangeli, C.; Pellegrini, V.; Beltram, F.; Giacca, M., Cell membrane lipid rafts mediate caveolar endocytosis of HIV-1 Tat fusion proteins. *J Biol Chem* **2003,** *278* (36), 34141-9.

120. Kaplan, I. M.; Wadia, J. S.; Dowdy, S. F., Cationic TAT peptide transduction domain enters cells by macropinocytosis. *J Control Release* **2005,** *102* (1), 247-53.

121. Richard, J. P.; Melikov, K.; Brooks, H.; Prevot, P.; Lebleu, B.; Chernomordik, L. V., Cellular uptake of unconjugated TAT peptide involves clathrin-dependent endocytosis and heparan sulfate receptors. *J Biol Chem* **2005,** *280* (15), 15300-6.

122. Duchardt, F.; Fotin-Mleczek, M.; Schwarz, H.; Fischer, R.; Brock, R., A comprehensive model for the cellular uptake of cationic cell-penetrating peptides. *Traffic* **2007,** *8* (7), 848-66.

123. Caron, N. J.; Quenneville, S. P.; Tremblay, J. P., Endosome disruption enhances the functional nuclear delivery of Tat-fusion proteins. *Biochem Biophys Res Commun* **2004,** *319* (1), 12-20.

124. Jean, S. R.; Ahmed, M.; Lei, E. K.; Wisnovsky, S. P.; Kelley, S. O., Peptide-Mediated Delivery of Chemical Probes and Therapeutics to Mitochondria. *Acc Chem Res* **2016,** *49* (9), 1893-902.

125. Lei, E. K.; Pereira, M. P.; Kelley, S. O., Tuning the Intracellular Bacterial Targeting of Peptidic Vectors. *Angewandte Chemie International Edition* **2013,** *52* (37), 9660-9663.

126. Kamaruzzaman, N. F.; Kendall, S.; Good, L., Targeting the hard to reach: challenges and novel strategies in the treatment of intracellular bacterial infections. *British journal of pharmacology* **2017,** *174* (14), 2225-2236.

127. Kintarak, S.; Whawell, S. A.; Speight, P. M.; Packer, S.; Nair, S. P., Internalization of Staphylococcus aureus by human keratinocytes. *Infection and immunity* **2004,** *72* (10), 5668-5675.

128. Rollin, G.; Tan, X.; Tros, F.; Dupuis, M.; Nassif, X.; Charbit, A.; Coureuil, M., Intracellular Survival of Staphylococcus aureus in Endothelial Cells: A Matter of Growth or Persistence. *Frontiers in microbiology* **2017,** *8*, 1354-1354.

129. Ernst, R. K.; Guina, T.; Miller, S. I., How Intracellular Bacteria Survive: Surface Modifications That Promote Resistance to Host Innate Immune Responses. *The Journal of Infectious Diseases* **1999,** *179*, Suppl 2:S326-30.

130. Alonso, A.; García-del Portillo, F., *Hijacking of eukaryotic functions by intracellular bacterial pathogens*. 2004; Vol. 7, p 181-91.

131. Bravo-Santano, N.; Ellis, J.; Mateos, L.; Calle, Y.; Keun, H.; Behrends, V.; Letek, M., *Intracellular Staphylococcus aureus Modulates Host Central Carbon Metabolism To Activate Autophagy*. 2018; Vol. 3, p e00374-18.

132. Organization, W. H. Tuberculosis (TB). https://www.who.int/gho/tb/en/ (accessed July 16).

133. Smith, I., Mycobacterium tuberculosis Pathogenesis and Molecular Determinants of Virulence. *Clin Microbiol Rev* **2003,** *16* (3), 463-96.

134. Gideon, H. P.; Flynn, J. L., Latent tuberculosis: what the host "sees"? *Immunologic research* **2011,** *50* (2-3), 202-212.

135. Diacovich, L.; Lorenzi, L.; Tomassetti, M.; Méresse, S.; Gramajo, H., The infectious intracellular lifestyle of Salmonella enterica relies on the adaptation to nutritional conditions within the Salmonella-containing vacuole. *Virulence* **2017,** *8* (6), 975-992.

136. Portnoy, D. A.; Auerbuch, V.; Glomski, I. J., The cell biology of Listeria monocytogenes infection: the intersection of bacterial pathogenesis and cell-mediated immunity. *J Cell Biol* **2002,** *158* (3), 409-14.

137. Dabiri, G. A.; Sanger, J. M.; Portnoy, D. A.; Southwick, F. S., Listeria monocytogenes moves rapidly through the host-cell cytoplasm by inducing directional actin assembly. *Proc Natl Acad Sci U S A* **1990,** *87* (16), 6068-72.

138. Mellouk, N.; Enninga, J., Cytosolic Access of Intracellular Bacterial Pathogens: The Shigella Paradigm. *Front Cell Infect Microbiol* **2016,** *6*, 35, 1-26.

139. Kuriakose, J.; Hernandez-Gordillo, V.; Nepal, Manish; Brezdan, A.; Pozzi, V.; Seleem, M.; Chmielewski, J., Targeting Intracellular Pathogenic Bacteria Unnatural Proline Rich Peptides: Coupling Antibacterial Activity with Macrophage Penetration. *Angewandte Communications* **2013**, 9664-9667.

140. Kalafut, D.; Anderson, T. N.; Chmielewski, J., Mitochondrial targeting of a cationic amphiphilic polyproline helix. *Bioorganic and Medicnal Chemsitry Letters* **2012**, 561-563.

141. Manish Nepal, S. T., Mohamed N. Seleem, and Jean Chmielewski, Targeting Intraccellular Bacteria with an extended cationic amphiphilic polyproline helix. *The Royal Society of Chemistry* **2015,** *13*, 5930-5936.

142. Charles A Janeway, J.; Travers, P.; Walport, M.; Shlomchik, M. J., The front line of host defense. In *Immunobiology: The Immune System in Health and Disease. 5th edition.*, 5 ed.; Science, G., Ed. Garland Science: New York, 2001.

143. Bourke, C. D.; Prendergast, C. T.; Sanin, D. E.; Oulton, T. E.; Hall, R. J.; Mountford, A. P., Epidermal keratinocytes initiate wound healing and pro-inflammatory immune responses following percutaneous schistosome infection. *International journal for parasitology* **2015,** *45* (4), 215-224.

144. Mempel, M.; Schnopp, C.; Hojka, M.; Fesq, H.; Weidinger, S.; Schaller, M.; Korting, H. C.; Ring, J.; Abeck, D., Invasion of human keratinocytes by Staphylococcus aureus and intracellular bacterial persistence represent haemolysin-independent virulence mechanisms that are followed by features of necrotic and apoptotic keratinocyte cell death. *Br J Dermatol* **2002,** *146* (6), 943-51.

145. Edwards, A. M.; Potter, U.; Meenan, N. A. G.; Potts, J. R.; Massey, R. C., Staphylococcus aureus keratinocyte invasion is dependent upon multiple high-affinity fibronectin-binding repeats within FnBPA. *PloS one* **2011,** *6* (4), e18899-e18899.

146. Boukamp, P.; Petrussevska, R. T.; Breitkreutz, D.; Hornung, J.; Markham, A.; Fusenig, N. E., Normal keratinization in a spontaneously immortalized aneuploid human keratinocyte cell line. *The Journal of Cell Biology* **1988,** *106* (3), 761-771.

147. Choi, C. H.; Lee, E. Y.; Lee, Y. C.; Park, T. I.; Kim, H. J.; Hyun, S. H.; Kim, S. A.; Lee, S. K.; Lee, J. C., Outer membrane protein 38 of Acinetobacter baumannii localizes to the mitochondria and induces apoptosis of epithelial cells. *Cell Microbiol* **2005,** *7* (8), 1127-38.

148. Jabado, N.; Cuellar-Mata, P.; Grinstein, S.; Gros, P., Iron chelators modulate the fusogenic properties of Salmonella-containing phagosomes. *Proc Natl Acad Sci U S A* **2003,** *100* (10), 6127-32.

149. Lundin, P.; Johansson, H.; Guterstam, P.; Holm, T.; Hansen, M.; Langel, Ü.; Andaloussi, S. E., Distinct Uptake Routes of Cell-Penetrating Peptide Conjugates. **2008,** *19* (12), 2535-2542.

150. LeCher, J. C.; Nowak, S. J.; McMurry, J. L., Breaking in and busting out: Cell-penetrating peptides and the endosomal escape problem. *Biomol Concepts* **2017,** *8* (3-4), 131-41.

151. LIBERMAN, E. A.; TOPALY, V. P.; TSOFINA, L. M.; JASAITIS, A. A.; SKULACHEV, V. P., Mechanism of Coupling of Oxidative Phosphorylation and the Membrane Potential of Mitochondria. *Nature* **1996,** *222* (5198), 1076-1078.

152. Center of Disease control, Enteric Diseases Epidemiology Branch. CDC. https://www.cdc.gov/ncezid/dfwed/edeb/index.html.

153. Who Health Organization, WHO publishes list of bacteria for which new antibiotics are urgently needed. https://www.who.int/news-room/detail/27-02-2017-who-publishes-list-of-bacteria-for-which-new-antibiotics-are-urgently-needed (accessed June 19, 2019).

154. Choi, C. H.; Lee, J. S.; Lee, Y. C.; Park, T. I.; Lee, J. C., Acinetobacter baumannii invades epithelial cells and outer membrane protein A mediates interactions with epithelial cells. *BMC Microbiology* **2008,** *8* (216), 1-11.

155. Chen, M.; Wei, J.; Xie, S.; Tao, X.; Zhang, Z.; Ran, P.; Li, X., Bacterial biofilm destruction by size/surface charge-adaptive micelles. *Nanoscale* **2018,** *11* (3), 1410-1422.

156. Khatoon, Z.; McTiernan, C. D.; Suuronen, E. J.; Mah, T. F.; Alarcon, E. I., Bacterial biofilm formation on implantable devices and approaches to its treatment and prevention. *Heliyon* **2018,** *4* (12): e01067, 1-41.

157. Percival, S. L.; McCarty, S. M.; Lipsky, B., Biofilms and Wounds: An Overview of the Evidence. *Adv Wound Care (New Rochelle)* **2015,** *4* (7), 373-81.

158. Hoiby, N.; Ciofu, O.; Bjarnsholt, T., Pseudomonas aeruginosa biofilms in cystic fibrosis. *Future Microbiol* **2010,** *5* (11), 1663-74.

159. Mulcahy, L. R.; Isabella, V. M.; Lewis, K., Pseudomonas aeruginosa biofilms in disease. *Microb Ecol* **2014,** *68* (1), 1-12.

160. Kostakioti, M.; Hadjifrangiskou, M.; Hultgren, S. J., Bacterial biofilms: development, dispersal, and therapeutic strategies in the dawn of the postantibiotic era. *Cold Spring Harb Perspect Med* **2013,** *3* (4): a010306), 1-50.

161. Koban, I.; Matthes, R.; Hubner, N. O.; Welk, A.; Sietmann, R.; Lademann, J.; Kramer, A.; Kocher, T., XTT assay of ex vivo saliva biofilms to test antimicrobial influences. *GMS Krankenhaushygiene interdisziplinar* **2012,** *7* (1):Doc06, 1-19.

162. Beloin, C.; Renard, S.; Ghigo, J. M.; Lebeaux, D., Novel approaches to combat bacterial biofilms. *Curr Opin Pharmacol* **2014,** *18*, 61-8.

163. Terrone, D.; Sang, S. L. W.; Roudaia, L.; Silvius, J. R., Penetratin and Related Cell-Penetrating Cationic Peptides Can Translocate Across Lipid Bilayers in the Presence of a Transbilayer Potential. *Biochemistry* **2003,** *42* (47), 13787-13799.

164. Wallbrecher, R.; Ackels, T.; Olea, R. A.; Klein, M. J.; Caillon, L.; Schiller, J.; Bovee-Geurts, P. H.; van Kuppevelt, T. H.; Ulrich, A. S.; Spehr, M.; Adjobo-Hermans, M. J. W.; Brock, R., Membrane permeation of arginine-rich cell-penetrating peptides independent of transmembrane potential as a function of lipid composition and membrane fluidity. *J Control Release* **2017,** *256*, 68-78.

165. Geisler, I. M.; Chmielewski, J., Dimeric cationic amphiphilic polyproline helices for mitochondrial targeting. *Pharm Res* **2011,** *28* (11), 2797-807.

166. Burkhart, B. M.; Gassman, R. M.; Langs, D. A.; Pangborn, W. A.; Duax, W. L.; Pletnev, V., Gramicidin D conformation, dynamics and membrane ion transport. *Biopolymers* **1999,** *51* (2), 129-44.

167. Di Virgilio, F.; Lew, P.; Andersson, T.; Pozzan, T., Plasma membrane potential modulates chemotactic peptide-stimulated cytosolic free Ca2+ changes in human neutrophils. - PubMed - NCBI. *J Biol Chem.* **1987,** *262* (10), 4574-9.

168. David, J. M.; Owens, T. A.; Barwe, S. P.; Rajasekaran, A. K., Gramicidin A induces metabolic dysfunction and energy depletion leading to cell death in renal cell carcinoma cells. *Mol Cancer Ther* **2013,** *12* (11), 2296-307.

169. Sampath, P.; Pollard, T. D., Effects of cytochalasin, phalloidin and pH on the elongation of actin filaments. *Biochemistry* **1991,** *30* (7), 1973-1980.

170. Mager, I.; Eiriksdottir, E.; Langel, K.; El Andaloussi, S.; Langel, U., Assessing the uptake kinetics and internalization mechanisms of cell-penetrating peptides using a quenched fluorescence assay. *Biochim Biophys Acta* **2010,** *1798* (3), 338-43.

171. Heuser, J. E.; Anderson, R. G., Hypertonic media inhibit receptor-mediated endocytosis by blocking clathrin-coated pit formation. *J Cell Biol* **1989,** *108* (2), 389-400.

172. Zhang, X.; Jin, Y.; Plummer, M. R.; Pooyan, S.; Gunaseelan, S.; Sinko, P. J., Endocytosis and membrane potential are required for HeLa cell uptake of R.I.-CKTat9, a retro inverso Tat cell penetrating peptide. *Mol Pharm* **2009,** *6* (3), 836-48.

173. Yamashita, H.; Kato, T.; Oba, M.; Misawa, T.; Hattori, T.; Ohoka, N.; Tanaka, M.; Naito, M.; Kurihara, M.; Demizu, Y., Development of a Cell-penetrating Peptide that Exhibits Responsive Changes in its Secondary Structure in the Cellular Environment. *Scientific Reports* **2016,** *6*, 33003.

174. Abes, S.; Williams, D.; Prevot, P.; Thierry, A.; Gait, M. J.; Lebleu, B., Endosome trapping limits the efficiency of splicing correction by PNA-oligolysine conjugates. *J Control Release* **2006,** *110* (3), 595-604.

175. Kato, T.; Okada, S.; Yutaka, T.; Yabuuchi, H., The effects of sucrose loading on lysosomal hydrolases. *Mol Cell Biochem* **1984,** *60* (1), 83-98.

176. Gibson, A. E.; Noel, R. J.; Herlihy, J. T.; Ward, W. F., Phenylarsine oxide inhibition of endocytosis: effects on asialofetuin internalization. *Am J Physiol* **1989,** *257* (2 Pt 1), C182-4.

177. Radis-Baptista, G.; de la Torre, B. G.; Andreu, D., Insights into the uptake mechanism of NrTP, a cell-penetrating peptide preferentially targeting the nucleolus of tumour cells. *Chem Biol Drug Des* **2012,** *79* (6), 907-15.

178. Takano, M.; Koyama, Y.; Nishikawa, H.; Murakami, T.; Yumoto, R., Segment-selective absorption of lysozyme in the intestine. *Eur J Pharmacol* **2004,** *502* (1-2), 149-55.

179. Pooga M, H. M., Zorko M, Langel U., Cell penetration by transportan. *The FASEB Journal* **1998,** *12* (1), 67-77.

180. Frost, S. C.; Lane, M. D.; Gibbs, E. M., Effect of phenylarsine oxide on fluid phase endocytosis: further evidence for activation of the glucose transporter. *J Cell Physiol* **1989,** *141* (3), 467-74.

181. Khalil, I. A.; Kogure, K.; Futaki, S.; Harashima, H., High density of octaarginine stimulates macropinocytosis leading to efficient intracellular trafficking for gene expression. *J Biol Chem* **2006,** *281* (6), 3544-51.

182. Al Soraj, M.; He, L.; Peynshaert, K.; Cousaert, J.; Vercauteren, D.; Braeckmans, K.; De Smedt, S. C.; Jones, A. T., siRNA and pharmacological inhibition of endocytic pathways to characterize the differential role of macropinocytosis and the actin cytoskeleton on cellular uptake of dextran and cationic cell penetrating peptides octaarginine (R8) and HIV-Tat. *J Control Release* **2012,** *161* (1), 132-41.

183. He, L.; Sayers, E. J.; Watson, P.; Jones, A. T., Contrasting roles for actin in the cellular uptake of cell penetrating peptide conjugates. *Scientific Reports* **2018,** *8* (1), 7318.

184. Cervia, L. D.; Chang, C. C.; Wang, L.; Yuan, F., Distinct effects of endosomal escape and inhibition of endosomal trafficking on gene delivery via electrotransfection. *PLoS One* **2017,** *12* (2):e0171699, 1-26.

185. Dutta, D.; Donaldson, J. G., Search for inhibitors of endocytosis: Intended specificity and unintended consequences. *Cell Logist* **2012,** *2* (4), 203-8.

186. Kaiser, E.; Colescott, R. L.; Bossinger, C. D.; Cook, P. I., Color test for detection of free terminal amino groups in the solid-phase synthesis of peptides. *Anal Biochem* **1970,** *34* (2), 595-8.

187. Vazquez, J.; Qushair, G.; Albericio, F., Qualitative colorimetric tests for solid phase synthesis. *Methods Enzymol* **2003,** *369*, 21-35.

188. Mosmann, T., Rapid colorimetric assay for cellular growth and survival: application to proliferation and cytotoxicity assays. *J Immunol Methods* **1983,** *65* (1-2), 55-63.

189. Institute, C. a. L. S., Methods for Dilution Antimicrobial Susceptibility Tests for Bacteria That Grow Aerobically. In *Methods for Dilution Antimicrobial Susceptibility Tests for Bacteria That Grow Aerobically*, 11 ed.; CLSI: Clinical and Laboratory Standards Institute, 2012; Vol. 2019, p 112.

190. Melo, A. S.; Bizerra, F. C.; Freymuller, E.; Arthington-Skaggs, B. A.; Colombo, A. L., Biofilm production and evaluation of antifungal susceptibility amongst clinical Candida spp. isolates, including strains of the Candida parapsilosis complex. *Medical mycology* **2011,** *49* (3), 253-62.

191. Perez, L. M.; Alvarez, B. L.; Codony, F.; Fittipaldi, M.; Adrados, B.; Penuela, G.; Morato, J., A new microtitre plate screening method for evaluating the viability of aerobic respiring bacteria in high surface biofilms. *Letters in applied microbiology* **2010,** *51* (3), 331-7.

192. Yannick A. Fillon, J. P. A., and Jean Chmielewski, Cell Penetrating Agents Based on a Polyproline Helix Scaffold. *Journal of the Amercan Chemical Scoiety* **2005,** *127* (33), 11798–11803.

193. Nagel, Y. A.; Raschle, P. S.; Wennemers, H., Effect of Preorganized Charge-Display on the Cell-Penetrating Properties of Cationic Peptides. *Angew Chem Int Ed Engl* **2017,** *56* (1), 122-126.

194. Wender, P. A.; Mitchell, D. J.; Pattabiraman, K.; Pelkey, E. T.; Steinman, L.; Rothbard, J. B., The design, synthesis, and evaluation of molecules that enable or enhance cellular uptake: peptoid molecular transporters. *Proc Natl Acad Sci U S A* **2000,** *97* (24), 13003-8.

195. Nuutila, J.; Lilius, E. M., Flow cytometric quantitative determination of ingestion by phagocytes needs the distinguishing of overlapping populations of binding and ingesting cells. *Cytometry A* **2005,** *65* (2), 93-102.

196. Srivastava, G. K.; Reinoso, R.; Singh, A. K.; Fernandez-Bueno, I.; Hileeto, D.; Martino, M.; Garcia-Gutierrez, M. T.; Merino, J. M.; Alonso, N. F.; Corell, A.; Pastor, J. C., Trypan Blue staining method for quenching the autofluorescence of RPE cells for improving protein expression analysis. *Exp Eye Res* **2011,** *93* (6), 956-62.

197. Richard, J. P.; Melikov, K.; Vives, E.; Ramos, C.; Verbeure, B.; Gait, M. J.; Chernomordik, L. V.; Lebleu, B., Cell-penetrating peptides. A reevaluation of the mechanism of cellular uptake. *J Biol Chem* **2003,** *278* (1), 585-90.

198. Le, C. F.; Fang, C. M.; Sekaran, S. D., Intracellular Targeting Mechanisms by Antimicrobial Peptides. *Antimicrob Agents Chemother* **2017,** *61* (4), e02340-16.

199. Tyagi, M.; Rusnati, M.; Presta, M.; Giacca, M., Internalization of HIV-1 tat requires cell surface heparan sulfate proteoglycans. *J Biol Chem* **2001,** *276* (5), 3254-61.

200. Fuchs, S. M.; Raines, R. T., Pathway for Polyarginine Entry into Mammalian Cells. *Biochemistry* **2004,** *43* (9), 2438-2444.

201. Appelbaum, J. S.; LaRochelle, J. R.; Smith, B. A.; Balkin, D. M.; Holub, J. M.; Schepartz, A., Arginine topology controls escape of minimally cationic proteins from early endosomes to the cytoplasm. *Chem Biol* **2012,** *19* (7), 819-30.

202. Kasevayuth, K.; Yanagishita, M., Catabolism of heparan sulfate proteoglycans in Drosophila cell lines. *Biochem Biophys Res Commun* **2004,** *324* (1), 205-11.

APPENDIX

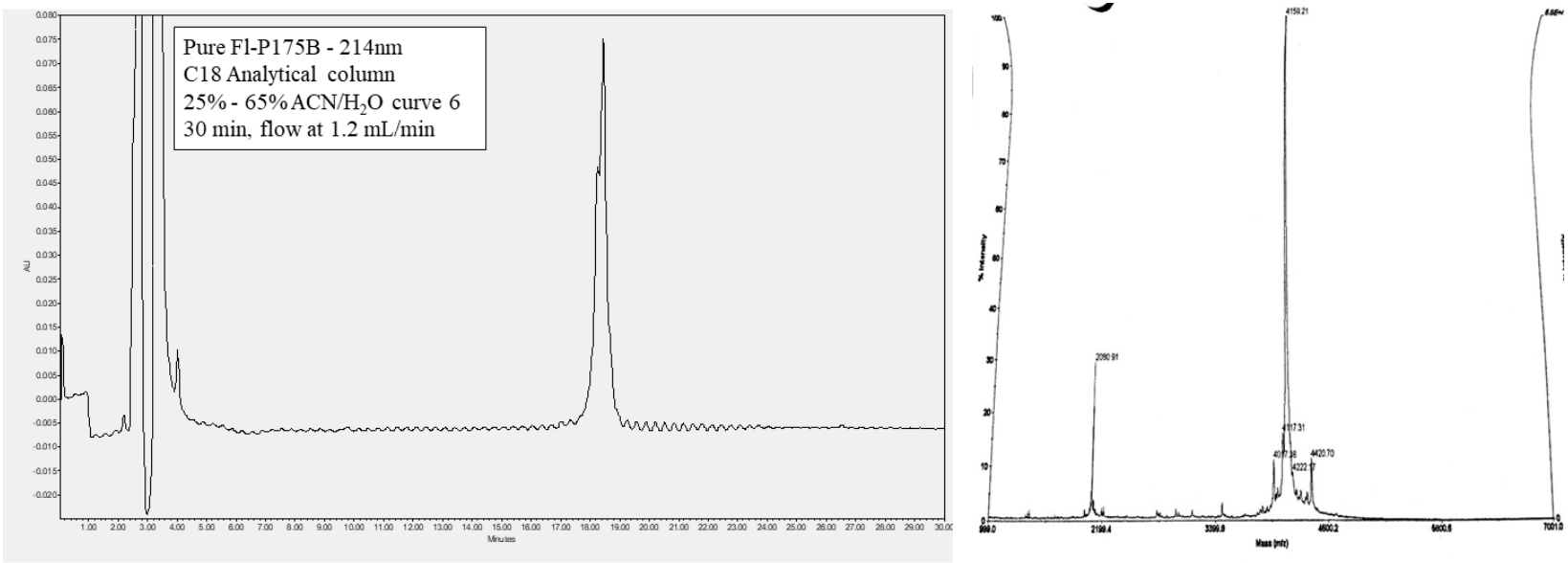

A 1 Pure Analytical Trace of **Fl-P17-5B** and image of MALDI-ToF spectrum

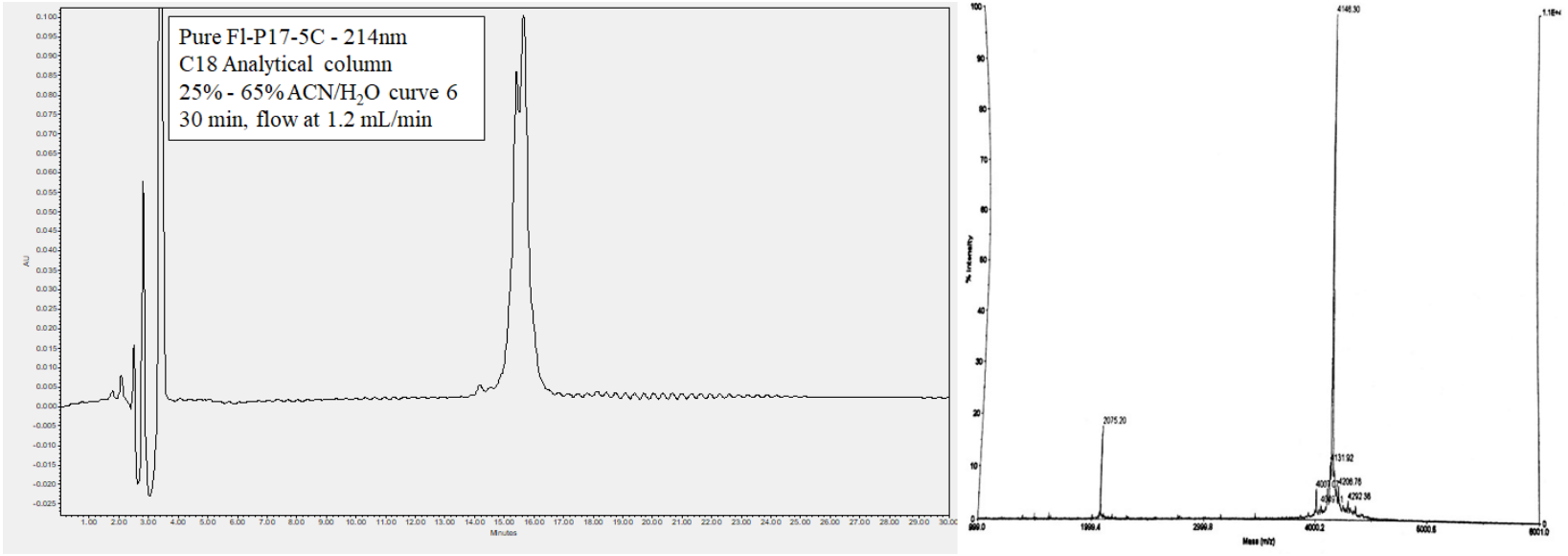

A 2 Pure analytical of **Fl-P17-5C** and image of MALDI-ToF spectrum

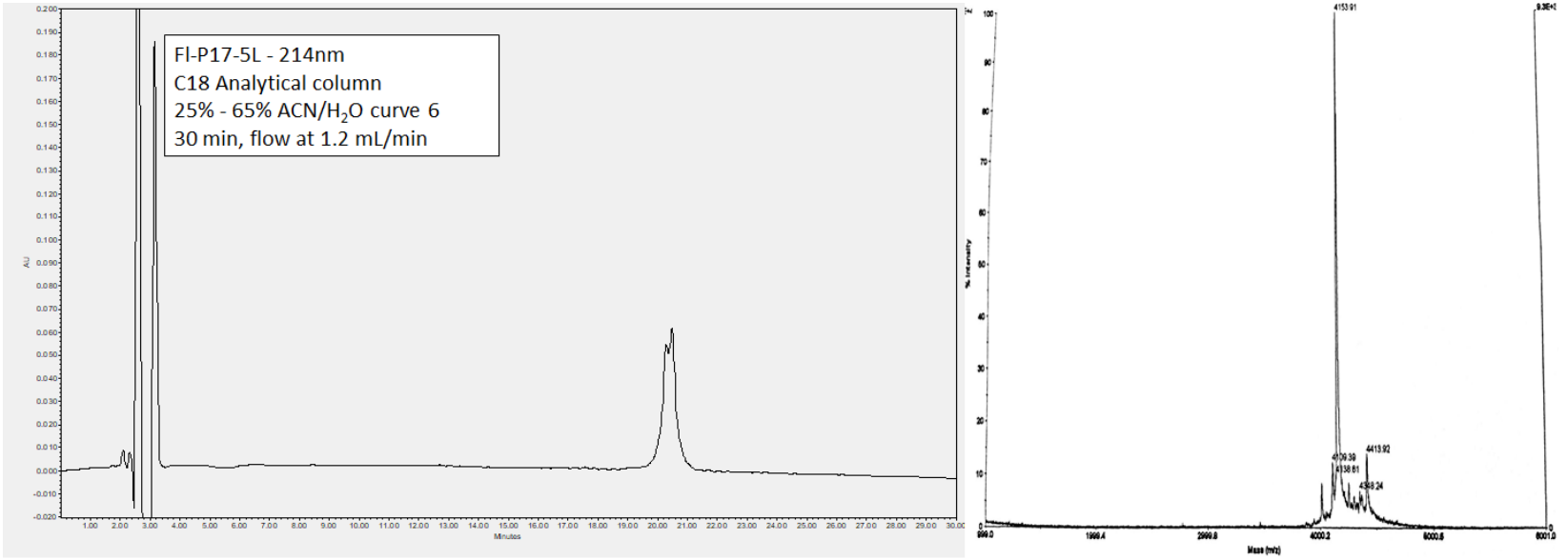

A 3 Pure analytical trace of **Fl-P17-5L** and image of MALDI-ToF spectrum

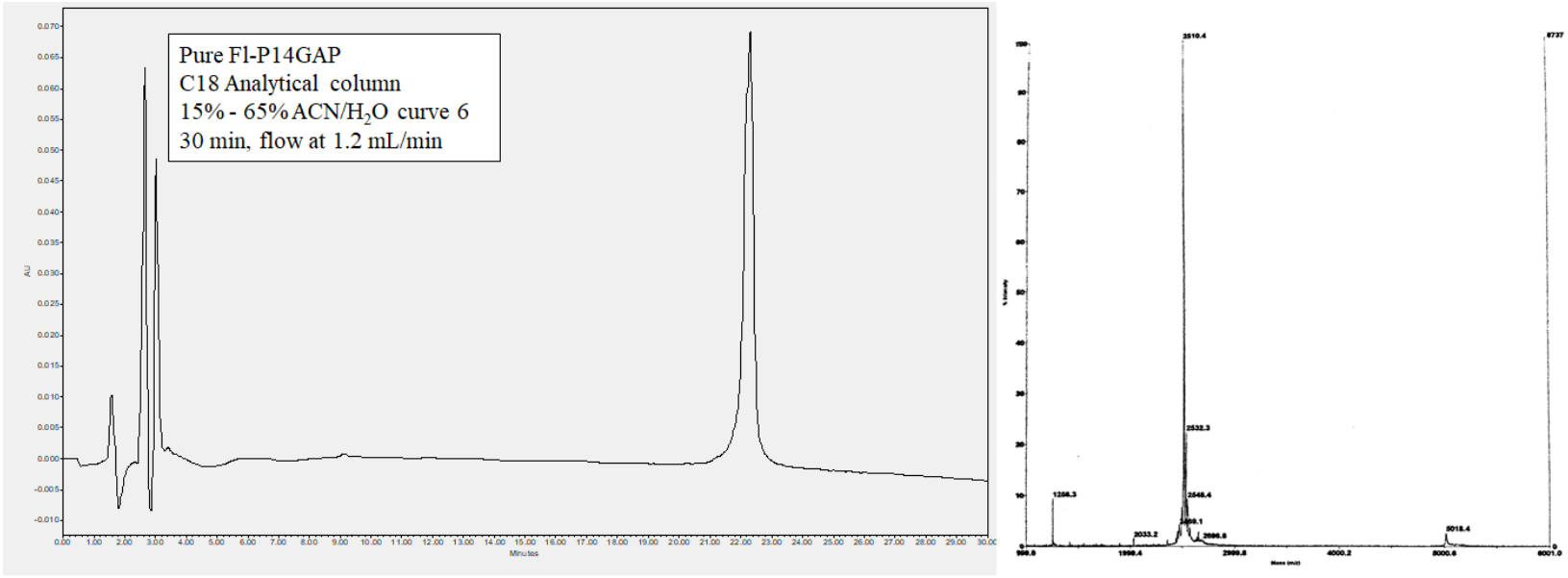

A 4 Pure analytical trace of **Fl-P14GAP** and image of MALDI-ToF spectrum

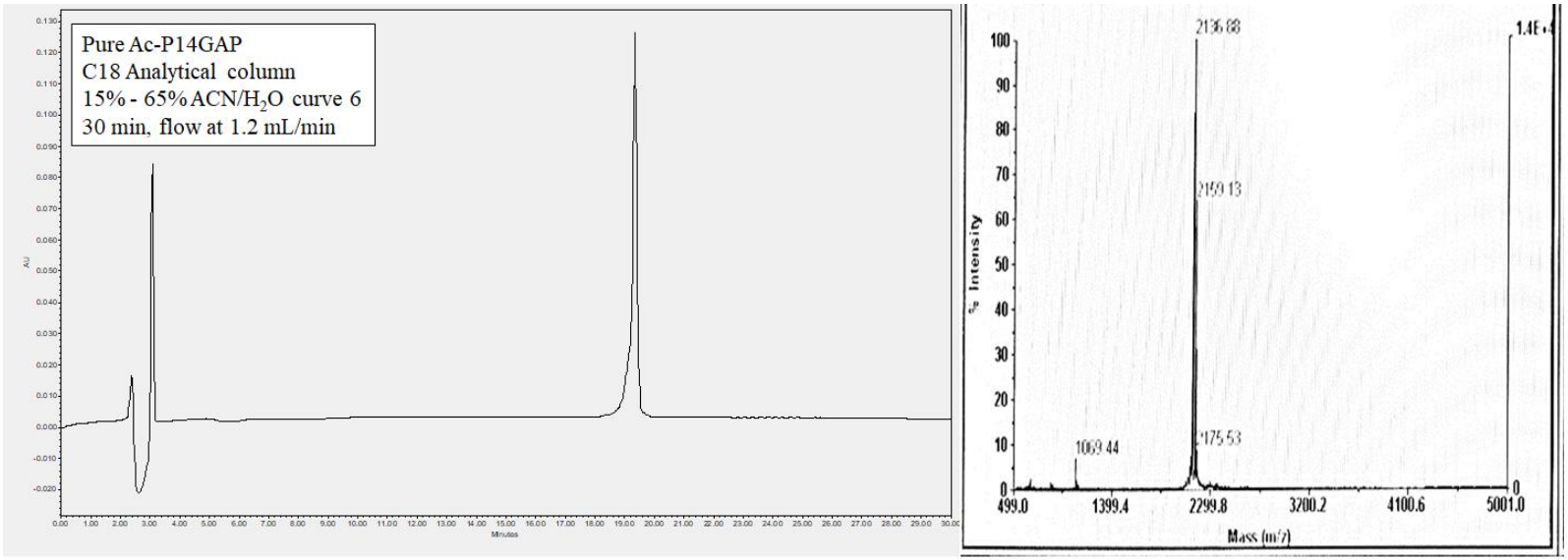

A 5 Pure analytical trace of Ac-P14GAP and image of MALDI-ToF spectrum

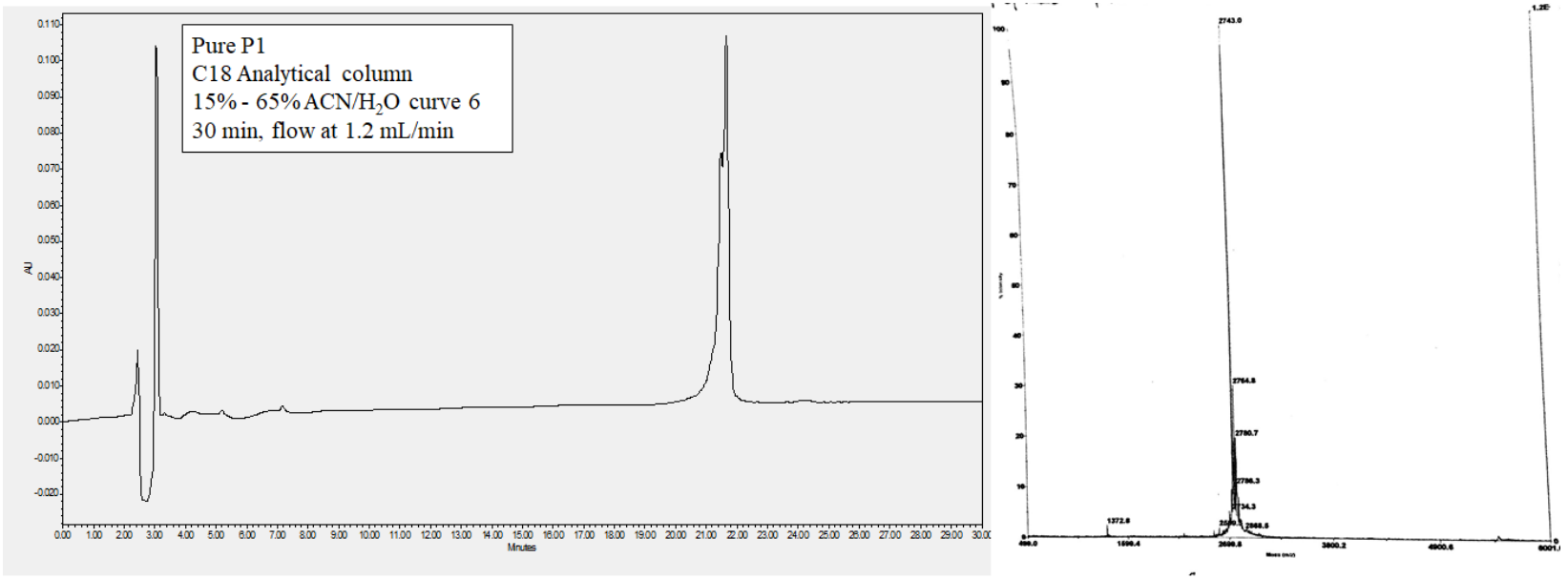

A 6 Pure analytical trace of **Fl-P14GAP/P$_R$**: P1 and image of MALDI-ToF spectrum

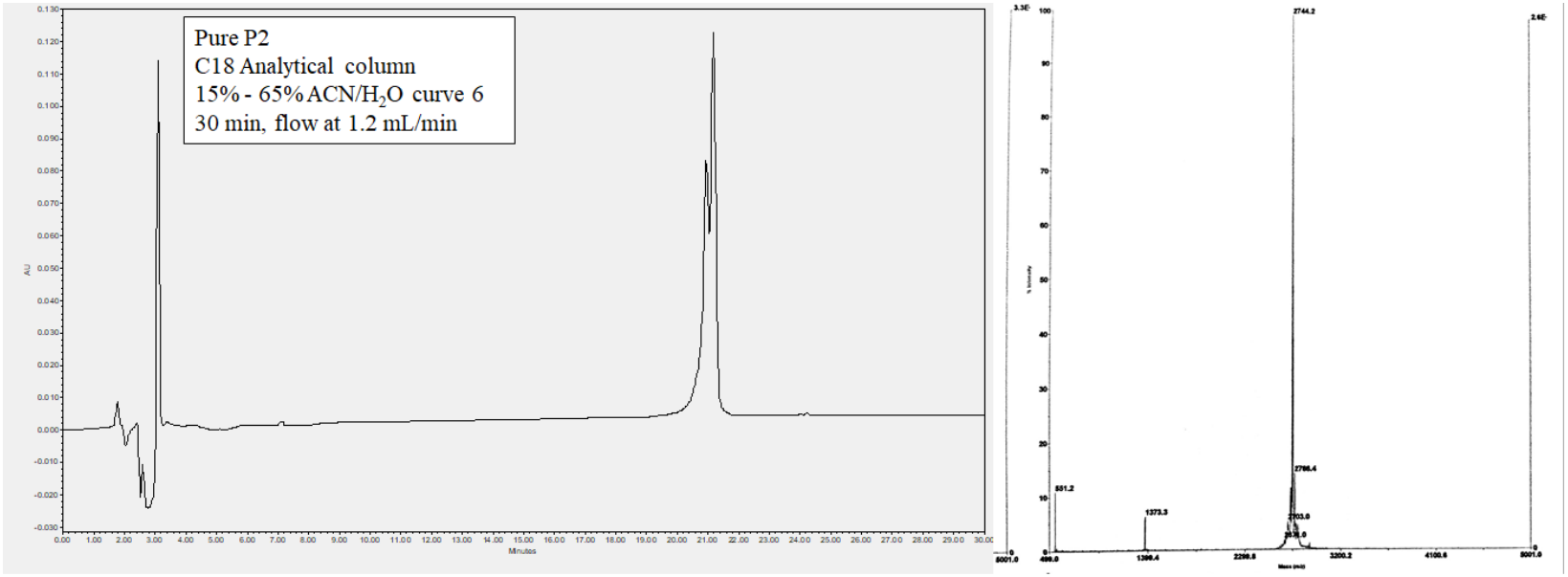

A 7 Pure analytical trace of **Fl-P14GAP/P$_R$**: P2 and image of MALDI-ToF spectrum

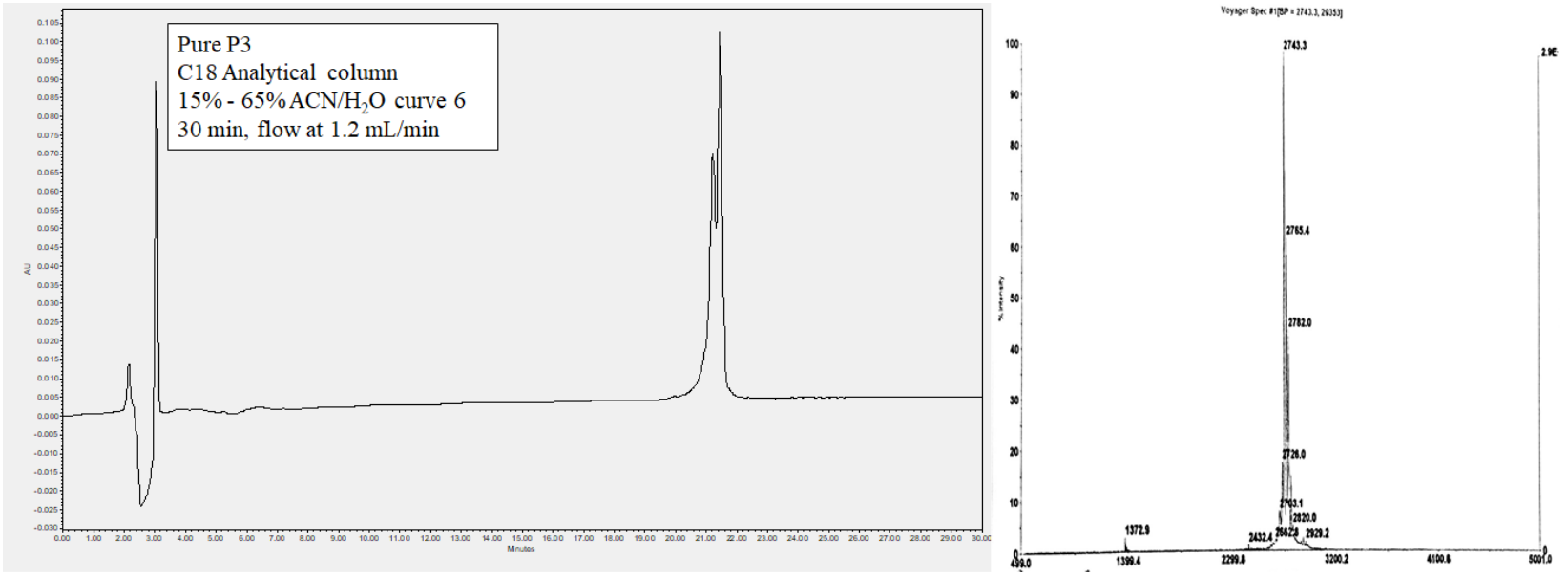

A 8 Pure analytical trace of **Fl-P14GAP/P$_R$**: P3 and image of MALDI-ToF spectrum

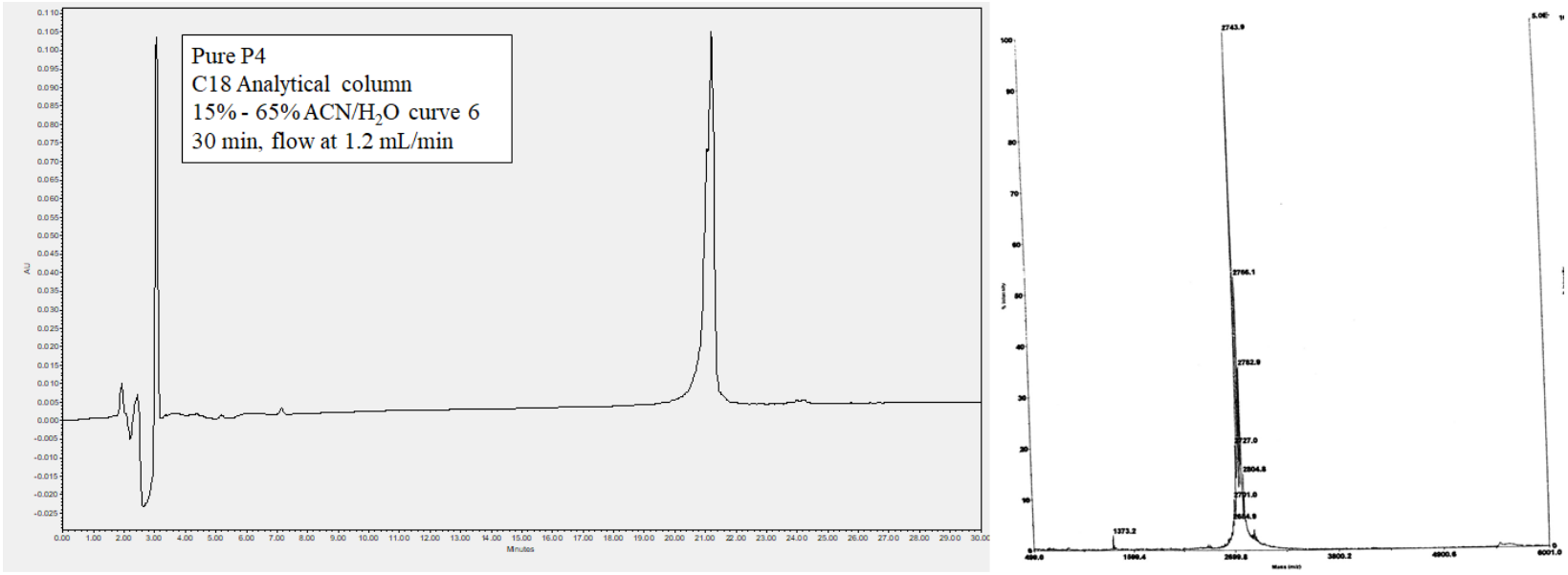

A 9 Pure analytical trace of **Fl-P14GAP/P$_R$**: P4 and image of MALDI-ToF spectrum

VITA

Reena Blade was born and raised in San Jose, CA. When she graduated from Evergreen Valley High School in 2009 she decided to move across the country to Hampton, VA to attend the historically black university, Hampton University, where she obtained her B.S. in chemistry. During her time at Hampton, Reena spent her time working under the guidance of the former department chair, Dr, Isai Urasa, in the environmental analytical lab and also participated in a number of summer research opportunities. Reena joined the chemistry department at Purdue University in September 2014 directly after completing her undergraduate studies. She will complete her studies in the area of chemical biology under the direction of Jean Chmielewski and will receive her PhD in chemistry in August 2019. Post graduation, Reena will begin her career at BASF as a PhD chemist in the Leadership Development Program.

PUBLICATION

ACS Infectious Diseases

Letter

Cite This: ACS Infect. Dis. 2018, 4, 1300−1305

A Library Approach to Cationic Amphiphilic Polyproline Helices that Target Intracellular Pathogenic Bacteria

Manish Nepal,[†] Mohamed F. Mohamed,[¶] Reena Blade,[†] Hassan E. Eldesouky,[¶] Tiffany N. Anderson,[†] Mohamed N. Seleem,[¶] and Jean Chmielewski*[,†]

[†]Department of Chemistry, Purdue University, 560 Oval Drive, West Lafayette, Indiana 47907-2027, United States

[¶]Department of Comparative Pathobiology, Purdue University, 625 Harrison Street, West Lafayette, Indiana 47907-2027, United States

Supporting Information

ABSTRACT: A number of pathogenic bacteria reproduce inside mammalian cells and are thus inaccessible to many antimicrobial drugs. Herein, we present a facile method to a focused library of antibacterial agents known as cationic amphiphilic polyproline helices (CAPHs). We identified three CAPHs from the library with superior cell penetration within macrophages and excellent antibacterial action against both Gram-positive and Gram-negative bacteria. These cell-penetrating antibacterial CAPHs have specific subcellular localizations that allow for targeting of pathogenic bacteria at their intracellular niches, a unique feature that promotes the successful clearance of intracellular pathogens (*Salmonella*, *Shigella*, and *Listeria*) residing within macrophages. Furthermore, the selected CAPHs also significantly reduced bacterial infections in an *in vivo* model of *Caenorhabditis elegans*, with minimal *in vivo* toxicity.

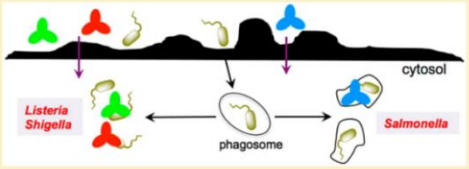

KEYWORDS: *intracellular pathogenic bacteria, antibiotic, cell penetration*

A significant challenge for effective treatment of infectious diseases arises from intracellular pathogens that have evolved to reside inside mammalian cells, including phagocytic macrophages, and establish replication niches. Bacterial pathogens such as *Mycobacterium*, *Salmonella*, *Brucella*, *Shigella*, and *Listeria* thrive within mammalian cells and hence evade the humoral defense system.[1−4] Once sheltered inside host cells, many potent antibiotics fail to effectively clear these pathogens because of either reduced cell penetration or their susceptibility to drug efflux transporters.[5−8] As a result, some intracellular pathogens cause persistent and chronic infections that lead to significant human mortality and morbidity.[9−11]

The difficulties in targeting intracellular pathogens have spurred development of nanomedicine strategies.[12−15] More recently, elegant studies have conjugated antibiotics with peptides or proteins to target intracellular pathogens,[16,17] including an antibiotic and anti-*Staphylococcus aureus* (*S. aureus*) monoclonal antibody conjugate,[18] a methotrexate and cell penetrating peptide construct,[16,19] and peptide nucleic acids conjugated to cell penetrating peptides.[17] Our efforts to target intracellular bacteria led to the development of a class of cell-penetrating, antibacterial peptides based on a cationic amphiphilic polyproline helix (CAPH) scaffold.[20,21] CAPHs such as **P14LRR** (Figure 1) exhibited broad spectrum antibacterial activity and demonstrated modest reduction in *Brucella* and *Salmonella* levels within macrophages.[20] In an effort to improve the intracellular potency of CAPHs, we prepared a cleavable conjugate of the amino glycoside antibiotic kanamycin and CAPHs, resulting in significantly improved performance against intracellular pathogenic bacteria.[22] We wished to investigate the critical question, however, of whether the structural features of CAPH peptides could be more effectively engineered for enhanced clearance of pathogens from mammalian cells.

Once intracellular pathogenic bacteria undergo phagocytosis, they reside in different subcellular locations, such as vacuoles (*Salmonella* and *Mycobacterium*) and the cytosol (*Listeria*, *Shigella*, *Rickettsia*).[3] Peptide sequences have been reported with a range of subcellular localizations, but these peptides do not possess intrinsic antimicrobial activity.[23−25] A novel antibacterial agent targeting intracellular pathogens should, therefore, penetrate mammalian cells and localize to a desired subcellular site with bacteria. Herein, we present our efforts to engineer the hydrophobic face of CAPHs through a focused library approach to develop antibacterial agents that exhibit superior cell penetration with specific subcellular localization, excellent antibacterial activities, and targeting of intracellular pathogens, both *in cyto* and *in vivo*.

In an effort to prepare highly potent CAPHs against intracellular bacteria, we developed a library approach to more easily access new agents (Scheme 1). CAPHs contain a polyproline scaffold that forms a type II polyproline helix with hydrophobic groups along one face of the helical structure. The guanidinium groups of the cationic face are an essential feature of CAPHs, but the nature of the hydrophobic group

Received: May 18, 2018
Published: July 6, 2018

DOI: 10.1021/acsinfecdis.8b00124
ACS Infect. Dis. 2018, 4, 1300−1305

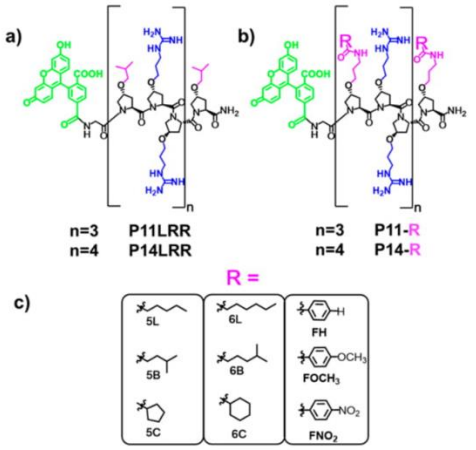

Figure 1. Cationic amphiphilic polyproline helices (CAPHs). (a) Structure of the CAPHs **P11LRR** and **P14LRR** with the hydrophobic groups in pink, the cationic moiety in blue, and fluorescein in green, (b) structure of the modified proline residues within CAPHs for the designed library with the proline modification in pink, and (c) hydrophobic moieties (R) used to create the library.

Scheme 1. (a) Synthesis of Unnatural Amino Acids for the Construction of CAPH Peptides; (b) On-Resin Installation of Hydrophobic Groups onto the CAPH Scaffold

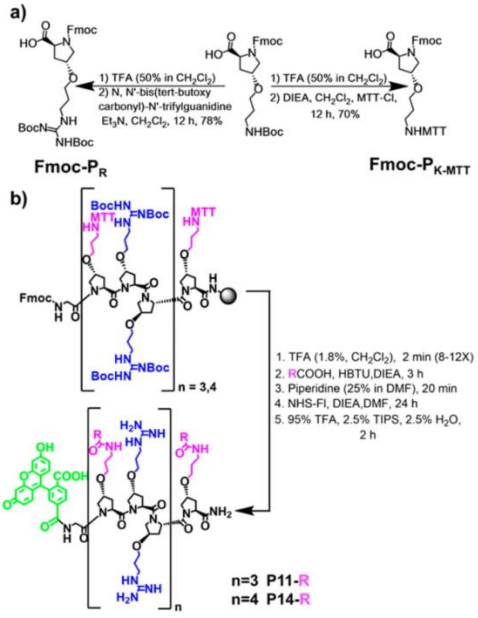

has not been explored. In preparing CAPHs such as **P14LRR**, the hydrophobic groups were attached to the proline residues through a direct ether linkage (Figure 1a). However, the ether-based approach limited the ability to prepare a diverse library of CAPHs quickly, as a new amino acid was needed for the synthesis of each peptide. Therefore, to allow for the facile preparation of focused libraries of CAPHs, we developed the use of an amide linkage between the hydrophobic group and an amino-modified proline residue, **Fmoc-P$_{K\text{-}MTT}$**, that was derived from a common intermediate, **Fmoc-P$_{K\text{-}Boc}$**, used to construct **Fmoc-P$_R$** (Scheme 1a, Figures S8 and S9). Two general classes of hydrophobic modifications were prepared: (1) aliphatic groups with 5- to 6-carbons and (2) phenyl moieties (Figure 1c). Straight, branched, and cyclic aliphatic groups were designed, whereas electron rich and poor aromatic groups were investigated. Further, the effect of different lengths of the CAPHs was probed with **P11-R** and **P14-R** (Figure 1b, Scheme 1b). Overall, a library of CAPHs with two chain lengths and a range of hydrophobic modifications was prepared on resin. The peptides were cleaved from the resin with a trifluoroacetic acid (TFA) cocktail, purified to homogeneity by HPLC, and characterized by matrix-assisted laser desorption ionization (MALDI) mass spectrometry (Figure S7 and Tables S1−S3).

One of the major obstacles in treating intracellular pathogens is the inability of therapeutics to accumulate in sufficient concentrations inside of cells. Therefore, we assessed the cell accumulation of the CAPH library in J774A.1 macrophage cells using flow cytometry. Cells were treated with the individual library components, and the cellular fluorescence was measured (Figures 2a and S1). Ideally, we were interested in CAPHs that were about equipotent with **P14LRR** (Figure 2a blue bar) or better for cell uptake. We identified about ten compounds that fell into this category, most of which were based on the P14 scaffold with hydrophobic alkyl groups, with **P14-6C** and **P14-5L** demonstrating about 3-fold higher cellular accumulation as compared to **P14LRR**.

In order to develop effective therapies targeting intracellular pathogens, acceptable mammalian cell viability is desired. Hence, we screened the CAPHs library for cell viability against J774A.1 cells using the 3-(4,5-dimethylthiazol-2-yl)-2,5-diphenyltetrazolium bromide (MTT) assay under conditions that would be used for pathogen-infected cell experiments (Figures 2b and S2). The **P11** and **P14** series of CAPHs modified with 5-carbon alkyl chains exhibited minimal or no toxicity to the macrophages. However, lengthening the hydrophobic groups attached to the CAPHS to 6-carbons significantly decreased the cell viability except for **P11-6C**, but this compound had poor cell accumulation. Similarly, when the CAPHs were modified with aryl groups, only modest cell viability was observed (30−64%). The substantial drop in cell viability observed with these subtle 5- to 6-carbon side chain modifications reveals the significance of hydrophobic chain length on the biocompatibility of CAPHs. On the basis of our screening of the CAPHs library, we concluded that the peptides modified with 5-carbon alkyl chains possessed the most favorable characteristics overall to move forward, with acceptable cell viability and cellular uptake that was comparable or better than **P14LRR**, specifically for the longer P14 variants. Therefore, we selected three CAPHs, **P14-5L**, **P14-5B**, and **P14-5C** (Figure 2 red bars), and the 15 μM concentration to limit cytotoxicity for our continuing studies.

As discussed above, intracellular pathogens reside at a number of subcellular locations. Therefore, to understand which intracellular pathogens would make suitable targets for these peptides, the subcellular localization of **P14-5L**, **P14-5B**, and **P14-5C** was determined via confocal microscopy. J774A.1 cells were

DOI: 10.1021/acsinfecdis.8b00124
ACS Infect. Dis. 2018, 4, 1300−1305

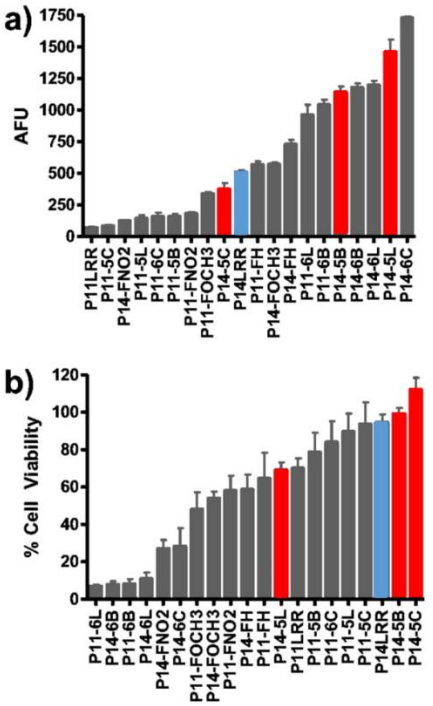

Figure 2. Screening of the CAPHs library for cell accumulation and cytotoxicity in J774A.1 cells. (a) Cellular fluorescence after addition of peptides (15 μM) for 1 h was measured with flow cytometry. (b) Cell viability was monitored by treating J774A.1 cells with the CAPHs library (15 μM) for 9 h using the MTT assay. **P14LRR** data are shown in blue, and data for library members chosen for further studies are shown in red.

treated with the CAPHs (15 μM), and the cells were further treated with Lysotracker or Mitotracker to label endosomes or mitochondria, respectively. As early as 15 min, **P14-5L** and **P14-5B** were found localized in the cytosol of the macrophages, with some endosomal, mitochondrial, and nuclear localization also observed, and this was maintained through 3 to 9 h (Figure S3). At 15 min and 1 h time points, **P14-5C**, however, mostly showed endosomal localization. Some release into the cytosol was only observed after 3 and 9 h. These data demonstrate that varied subcellular localization of CAPHs can be achieved through modification of the hydrophobic groups. This feature may provide a means to target specific intracellular pathogens at a subcellular level. For instance, **P14-5L** and **P14-5B** may be useful in clearing cytosolic pathogens, such as *Listeria* and *Shigella*, whereas **P14-5C** may be used for bacteria that reside in phagosomes, such as *Salmonella*.

With these data in hand, we first tested the *in vitro* antibacterial activity of the three CAPHs against *Salmonella enteritidis*, *Listeria monocytogens*, and *Shigella flexneri* using an *in vitro* broth dilution assay as compared to **P14LRR** (Table 1). The modified CAPHs displayed antibacterial activity that was 2-fold more potent than **P14LRR** against *Salmonella*, equipotent against *Shigella*, and 2- to 4-fold less active than **P14LRR** against

Table 1. *In Vitro* Antibacterial Activity of CAPHs against Pathogenic Intracellular Bacteria

	minimum inhibitory concentration (MIC), μM		
compounds	*Salmonella*	*Shigella*	*Listeria*
P14LRR	32	8	8
P14-5L	16	8	16
P14-5B	16	16	32
P14-5C	16	8	32

Listeria in vitro. We also evaluated the activity of the peptides lacking the fluorophore and found that these peptides were either equipotent or somewhat more potent (2- to 4-fold) depending on the bacteria and the compound (Table S4). Investigation of the mode of action of these peptides against bacteria using a hemolysis assay and a β-galactosidase release assay, used commonly to monitor membrane integrity in bacteria,[26] demonstrated that the antibacterial activity was not due to membrane lysis (Figures S4 and S5) as has been shown for **P14LRR**.[20]

The establishment of **P14-5L**, **P14-5B**, and **P14-5C** as dual cell penetrating and antibiotic peptides inspired us to combine these properties to target intracellular pathogens hiding within mammalian macrophages. Cellular clearance of *Shigella*, *Listeria*, and *Salmonella* was studied *in cyto* with J774A.1 macrophages (Figure 3). All three of the CAPHs derived from the

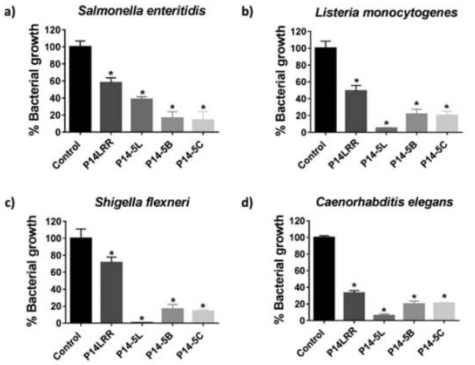

Figure 3. Reduction of pathogenic bacteria from within J774A.1 macrophages with CAPHs (15 μM) after 9 h. Cells were infected with (a) *Salmonella*, (b) *Listeria*, and (c) *Shigella* and washed with gentamycin to remove extracellular bacteria, and the levels of bacteria remaining were quantified. (d) Bacteria levels within *Listeria*-infected *C. elegans* treated with CAPHs (64 μM) for 12 h. *P values of $\leq$0.05 are considered significant.

library outperformed the starting peptide, **P14LRR**, in reducing levels of the three intracellular bacteria. **P14-5B** and **P14-5C** both demonstrated fairly similar clearance across the three intracellular pathogens, with about 80−85% reductions observed. After 9 h, the subcellular localization of **P14-5B** and **P14-5C** is fairly similar (Figure S3), so it is reasonable that the intracellular clearance would be complementary. **P14-5L** demonstrated the most striking results with 95% and 99% clearance of *Listeria* and *Shigella*, respectively, from the macrophages but only about 60% reduction of *Salmonella*. These intracellular results are due to a combination of variables, including CAPH mammalian cell penetration, antibacterial activity, and subcellular

DOI: 10.1021/acsinfecdis.8b00124
ACS Infect. Dis. 2018, 4, 1300−1305

localization within the macrophages. For instance, the CAPHs **P14-5L** and **P14-5C** are equipotent *in vitro* against *Shigella* and *Salmonella* (Table 1), but **P14-5L** enters macrophages more effectively than **P14-5C**. **P14-5C** mostly localizes within endosomes, with endosomal escape observed after 9 h, whereas **P14-5L** is found mostly within the cytosol and the nucleus even after 9 h (Figure S3). Taking these data into account, if subcellular localization was not an issue, **P14-5L** should have been more potent than **P14-5C** against intracellular *Salmonella*, but the reverse is observed. The more effective subcellular localization of **P14-5C** within endosomes may allow this CAPH to colocalize with endosome-residing *Salmonella* (*vida infra*), thus resulting in an improved intracellular clearance of the pathogen. **P14-5L** accumulates in the cytosol of macrophages, and this CAPH was able to significantly lower the population of the cytosol-dwelling *Listeria* and *Shigella* from J774A.1 cells. These findings provide support for the importance of delivering therapeutics at the subcellular level for enhanced clearance of intracellular pathogens.

The above data suggests that colocalization of bacteria and CAPHs translates to more effective pathogenic bacteria clearance from macrophages. To more specifically address this issue, we used confocal microscopy to monitor the intracellular location of green fluorescent protein (GFP)-labeled *Shigella flexneri* within J774A.1 macrophages with the addition of rhodamine-labeled **P14-5L** and GFP-labeled *Salmonella* within J774A.1 macrophages with the addition of rhodamine-labeled **P14-5C**. After 1 h, minimal interaction was observed between the **P14-5L** (red) and *Shigella* (green) (Figure 4a), but after 3 h, definite

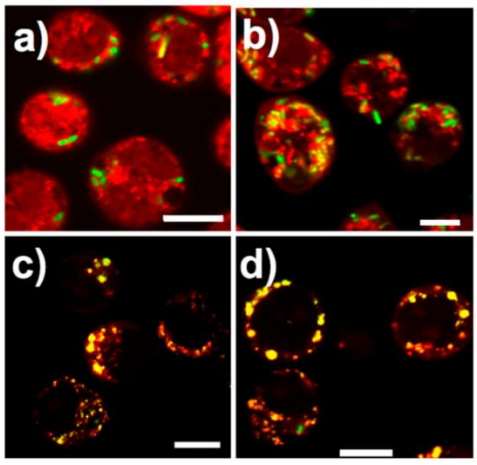

Figure 4. Cellular colocalization of rhodamine labeled CAPHs with bacteria: (a and b) *Shigella* (green) infected J774A.1 cells were treated with **P14-5L** (15 μM, red) for either 1 h (a) or 3 h (b) and (c and d) *Salmonella* (green) infected J774A.1 cells were treated with **P14-5C** (15 μM, red) for either 1 h (c) or 3 h (d). Samples were visualized with confocal microscopy, and yellow regions in the merged panels represent colocalization (scale bar 10 μm).

interactions between the peptide and *Shigella* were seen, with colocalization observed in the merged image (Figure 4b). With **P14-5C** and *Salmonella*, colocalization was observed at both 1 and 3 h time points (Figure 4c,d). This study clearly demonstrates that CAPHs possess the potential to interact with these bacteria within cells and may have the potential for greater potency when colocalized with bacteria within cells.

After the encouraging cell-based results with **P14-5L**, **P14-5B**, and **P14-5C**, we evaluated these agents for *in vivo* antibacterial activity within *Caenorhabditis elegans* (*C. elegans*). First, the viability of *C. elegans* in the presence of the CAPHs was evaluated. Worms were treated with **P14-5L**, **P14-5B**, and **P14-5C** (64 μM), and their survival rate was monitored over 48 h (Figure S6). After 24 h, very limited toxicity was observed with the three peptides; after 48 h of treatment, very close to 100% *C. elegans* survival was found with **P14-5B** and **P14-5C**, and 90% survival was observed with **P14-5L**. Since the peptides showed minimal toxicity to *C. elegans*, we investigated bacterial clearance from infected worms. *C. elegans* were infected with *Listeria* and then treated with **P14-5L**, **P14-5B**, and **P14-5C** for 12 h at 64 μM. All three CAPHs demonstrated reductions in bacteria levels within *C. elegans* and were more effective than **P14LRR** (Figure 3d). As observed with the *in cyto* studies, **P14-5L** was the most effective peptide in reducing the population of *Listeria* within *C. elegans* with a 95% reduction in bacteria levels (Figure 3d). Overall, the selected CAPHs were able to substantially reduce the bacterial infection in an *in vivo C. elegans* model with minimal toxicity to the worms.

In conclusion, intracellular pathogens represent a particularly difficult challenge in the development of anti-infective therapies. In our studies, we designed a focused library of CAPHs and identified three promising agents that exhibited potent cell penetrating and antibacterial activities that were harnessed to reduce levels of *Salmonella*, *Listeria*, and *Shigella* within macrophages. Interestingly, the CAPH **P14-5L** that localized in the cytoplasm was found to clear cytosolic *Listeria* and *Shigella* more effectively but was much less effective in reducing phagosome-residing *Salmonella* than the endosome-localizing **P14-5C**. Issues of cell penetration, antibacterial potency, and subcellular localization all play a role in the overall activity of CAPHs against intracellular pathogenic bacteria. CAPHs also demonstrated a notable reduction in *Listeria* levels in an *in vivo* model with infected *C. elegans* with minimal toxicity. On the basis of their potent activity against intracellular bacteria, the CAPHs described herein provide an excellent platform to develop therapies to treat intracellular pathogenic bacterial infection.

METHODS

Cell Uptake. J774A.1 cells were cultured in Dulbecco's Modified Eagle Medium (DMEM) supplemented with 10% fetal bovine serum (FBS) and at 37 °C under 5% CO_2. Briefly, J774A.1 cells (125 000) were harvested and transferred to round-bottom tubes (BD Biosciences). These cells were treated with CAPHs (15 μM) in 10% FBS supplemented DMEM (300 μL) and were allowed to incubate for 1 h at 37 °C. Cells with no treatment (DMEM only) served as the control for the experiment. Upon completion of the incubation period, the cells were centrifuged and the spent media was aspirated. The cells were resuspended in phosphate buffered saline (PBS; 400 μL), and the fluorescence of the cells was measured using a FACS Calibur Flow Cytometer (BD Biosciences). Data were obtained in duplicates from two independent experiments and were processed using the BD software.

Subcellular Localization. J774A.1 cells were seeded at a density of 200 000 cells per well in 4-well Lab-Tek chambered slides (Thermo Fisher Scientific 155383) and allowed to grow for 18 h at 37 °C under 5% CO_2. The media was aspirated, and

DOI: 10.1021/acsinfecdis.8b00124
ACS Infect. Dis. 2018, 4, 1300−1305

the cells were washed with 400 μL of PBS (1×). Next, CAPHs (15 μM, **P14-5L**, **P14-5B**, and **P14-5C**) were added to each well in 400 μL of DMEM supplemented with 10% FBS. The cells were allowed to incubate with the peptides for desired time (15 min, 1 h, 3 h, 9 h) at 37 °C under 5% CO_2. Excess media was aspirated, and the cells were washed with 400 μL of PBS (1×). The cells were further treated with Hoechst 33342 (1000 nM) and either Mitotracker (100 nM) (Invitrogen 7512) or Lysotracker (300 nM) (Invitrogen L7528) for 30 min at 37 °C. The excess dye was aspirated; the cells were washed with PBS, and fresh DMEM was added to each well. Imaging was performed using a Nikon A1R multiphoton inverted confocal microscope under 60× oil objective. Fluorescein, Hoechst 33342, and Mitotracker/Lysotracker were excited using 488, 350, and 561 nm lasers, respectively.

Intracellular Clearance. J774A.1 cells were seeded at a density of 1×10^5 cells per well in 96-well plates (Corning Incorporated) for 22 h before being infected with the bacteria. Following incubation, the cells were washed once with DMEM. Then, the cells were infected with *S. enteritidis*, *S. flexneri*, or *L. monocytogenes* (at a multiplicity of infection of 1:10 for *S. enteritidis* and 1:100 for *S. flexneri* or *L. monocytogenes*) in DMEM supplemented with 10% FBS for 45 min. At the end of the infection, the cells were washed three times with DMEM containing 50 μg/mL gentamicin (Sigma) and were further incubated for 30 min to kill and wash off nonphagocytized bacteria. Then, DMEM supplemented with 10% fetal bovine serum with 15 μM CAPHs was added. The plates were returned to the incubator for 9 h. Finally, the infected cells were washed three times with DMEM and lysed with 100 μL of 0.01% triton X in PBS to collect the intracellular bacteria. The colony forming units (CFUs) of the bacteria in the lysates were determined by plating a series of 10-fold serial dilutions onto tryptic soy agar (TSA) and incubating the plates at 37 °C for 20 h. Experiments were performed in triplicate in two independent experiments. Statistical significance was assessed with Graph Pad Prism 6.0 (Graph Pad Software, La Jolla, CA). *P* values were calculated by the two-tailed unpaired Student *t* test. *P* values ≤0.05 were considered as significant.

Bacteria-CAPHs Colocalization Study. Rhodamine-functionalized **P14-5L** and **P14-5C** peptides were prepared for this experiment. J774A.1 cells were seeded at a density of 1.5×10^5 cells/well in 4-well Lab-Tek chambered slides in DMEM supplemented with 10% fetal bovine serum (FBS) and incubated at 37 °C in a 5% CO_2 atmosphere for 20 h. The media was aspirated, and the cells were washed 1× with 400 μL of PBS. The cells were infected with GFP-*Shigella* ATCC 12022GFP or GFP-*Salmonella* ATCC 14028GFP (at multiplicity of infection, 100 bacteria: 1 macrophage cell) in DMEM with 10% FBS for 1 h. After infection, the wells were washed three times with 200 μL of DMEM with gentamicin (final concentration of 50 μg/mL) to kill extracellular bacteria. Next, 15 μM rhodamine-labeled **P14-5L** or **P14-5C** was added to the cells and allowed to incubate for 1 and 3 h at 37 °C under 5% CO_2. The cells were washed 3× with PBS and visualized under a 60× oil objective of a Nikon A1R multiphoton inverted confocal microscope. GFP-*Shigella*/GFP-*Salmonella* and rhodamine-labeled peptides were excited using 488 and 561 nm, respectively.

***In Vivo* Efficacy in a Worm Infection Model.** The infection and treatment of *Caenorhabditis elegans* were performed as reported previously.[17,27] A pathogen-sensitive strain of *C. elegans* {glp-4(bn2) I; sek-1(km4)} was used in this study. Approximately 40 worms infected with *Listeria monocytogenes* (100 μL of PBS) were transferred to 1.5 mL microcentrifuge tubes. The CAPHs (64 μM) were added to tubes in triplicate, with negative control tubes containing only PBS. After 12 h, the tubes were centrifuged, and the supernatant was removed. The worms were washed twice with 1 mL of PBS, and 200 μg of autoclaved silica carbide was added to each tube. The worms were vortexed for 1 min, and an aliquot (100 μM) from each tube was diluted 10-fold serially in PBS. The aliquots were plated and incubated for 16 h at 37 °C, and *Listeria* colonies were counted. Statistical analysis was performed using the two-tailed student *t* test ($P \leq 0.05$ was considered significant).

■ ASSOCIATED CONTENT

Supporting Information

The Supporting Information is available free of charge on the ACS Publications website at DOI: 10.1021/acsinfecdis.8b00124.

Synthetic procedures and compound characterization; cell localization, hemolysis, and β-galactosidase data (PDF)

■ AUTHOR INFORMATION

Corresponding Author

*E-mail: chml@purdue.edu.

ORCID

Mohamed N. Seleem: 0000-0003-0939-0458

Jean Chmielewski: 0000-0003-4958-7175

Notes

The authors declare no competing financial interest.

■ ACKNOWLEDGMENTS

The National Science Foundation (1012316-CHE) and the Purdue Research Foundation are acknowledged for financial support.

■ ABBREVIATIONS

C. elegans, *Caenorhabditis elegans*; CAPHs, cationic amphiphilic polyproline helices; MTT, 3-(4,5-dimethylthiazol-2-yl)-2,5-diphenyltetrazolium bromide; DMEM, Dulbecco's Modified Eagle Medium; GFP, green fluorescent protein; h, hour; MALDI, matrix-assisted laser desorption ionization; PBS, phosphate buffered saline; TFA, trifluoroacetic acid

■ REFERENCES

(1) Ray, K., Marteyn, B., Sansonetti, P. J., and Tang, C. M. (2009) Life on the inside: the intracellular lifestyle of cytosolic bacteria. *Nat. Rev. Microbiol.* 7 (5), 333−340.

(2) Flannagan, R. S., Cosio, G., and Grinstein, S. (2009) Antimicrobial mechanisms of phagocytes and bacterial evasion strategies. *Nat. Rev. Microbiol.* 7 (5), 355−366.

(3) Diacovich, L., and Gorvel, J. P. (2010) Bacterial manipulation of innate immunity to promote infection. *Nat. Rev. Microbiol.* 8 (2), 117−128.

(4) LaRock, D. L., Chaudhary, A., and Miller, S. I. (2015) Salmonellae interactions with host processes. *Nat. Rev. Microbiol.* 13 (4), 191−205.

(5) Carryn, S., Chanteux, H., Seral, C., Mingeot-Leclercq, M. P., Van Bambeke, F., and Tulkens, P. M. (2003) Intracellular pharmacodynamics of antibiotics. *Infect. Dis. Clin. North Am.* 17 (3), 615−634.

(6) Monack, D. M., Mueller, A., and Falkow, S. (2004) Persistent bacterial infections: the interface of the pathogen and the host immune system. *Nat. Rev. Microbiol.* 2 (9), 747−765.

(7) Barcia-Macay, M., Seral, C., Mingeot-Leclercq, M. P., Tulkens, P. M., and Van Bambeke, F. (2006) Pharmacodynamic evaluation of the

DOI: 10.1021/acsinfecdis.8b00124
ACS Infect. Dis. 2018, 4, 1300−1305

intracellular activities of antibiotics against Staphylococcus aureus in a model of THP-1 macrophages. *Antimicrob. Agents Chemother. 50* (3), 841−851.
(8) Garzoni, C., and Kelley, W. L. (2009) Staphylococcus aureus: new evidence for intracellular persistence. *Trends Microbiol. 17* (2), 59−65.
(9) Crump, J. A., Luby, S. P., and Mintz, E. D. (2004) The global burden of typhoid fever. *Bull. W. H. O. 82* (5), 346−353.
(10) Majowicz, S. E., Musto, J., Scallan, E., Angulo, F. J., Kirk, M., O'Brien, S. J., Jones, T. F., Fazil, A., and Hoekstra, R. M. (2010) The global burden of nontyphoidal Salmonella gastroenteritis. *Clin. Infect. Dis. 50* (6), 882−889.
(11) Maertens de Noordhout, M., Devleesschauwer, B., Angulo, F. J., Verbeke, G., Haagsma, J., Kirk, M., Havelaar, A., and Speybroeck, N. (2014) The global burden of listeriosis: a systematic review and meta-analysis. *Lancet Infect. Dis. 14* (11), 1073−1082.
(12) Briones, E., Colino, C. I., and Lanao, J. M. (2008) Delivery systems to increase the selectivity of antibiotics in phagocytic cells. *J. Controlled Release 125* (3), 210−227.
(13) Armstead, A. L., and Li, B. (2011) Nanomedicine as an emerging approach against intracellular pathogens. *Int. J. Nanomed. 6*, 3281−3293.
(14) Seleem, M. N., Munusamy, P., Ranjan, A., Alqublan, H., Pickrell, G., and Sriranganathan, N. (2009) Silica-antibiotic hybrid nanoparticles for targeting intracellular pathogens. *Antimicrob. Agents Chemother. 53* (10), 4270−4274.
(15) Kohane, D. S., Tse, J. Y., Yeo, Y., Padera, R., Shubina, M., and Langer, R. (2006) Biodegradable polymeric microspheres and nanospheres for drug delivery in the peritoneum. *J. Biomed. Mater. Res., Part A 77A* (2), 351−361.
(16) Lei, E. K., Pereira, M. P., and Kelley, S. O. (2013) Tuning the intracellular bacterial targeting of peptidic vectors. *Angew. Chem., Int. Ed. 52* (37), 9660−9663.
(17) Abushahba, M. F. N., Mohammad, H., Thangamani, S., Hussein, A. A. A., and Seleem, M. N. (2016) Impact of different cell penetrating peptides on the efficacy of antisense therapeutics for targeting intracellular pathogens. *Sci. Rep. 6*, 1−12.
(18) Lehar, S. M., Pillow, T., Xu, M., Staben, L., Kajihara, K. K., Vandlen, R., Mariathasan, S., et al. (2015) Novel antibody-antibiotic conjugate eliminates intracellular S. aureus. *Nature 527* (7578), 323−328.
(19) Pereira, M. P., Shi, J., and Kelley, S. O. (2015) Peptide targeting of an antibiotic prodrug toward phagosome-entrapped Mycobacteria. *ACS Infect. Dis. 1* (12), 586−592.
(20) Kuriakose, J., Hernandez-Gordillo, V., Nepal, M., Brezden, A., Pozzi, V., Seleem, M. N., and Chmielewski, J. (2013) Targeting intracellular pathogenic bacteria with unnatural proline-rich peptides: coupling antibacterial activity with macrophage penetration. *Angew. Chem., Int. Ed. 52* (37), 9664−9667.
(21) Nepal, M., Thangamani, S., Seleem, M. N., and Chmielewski, J. (2015) Targeting intracellular bacteria with an extended cationic amphiphilic polyproline helix. *Org. Biomol. Chem. 13* (21), 5930−5936.
(22) Brezden, A., Mohamed, M. F., Nepal, M., Harwood, J. S., Kuriakose, J., Seleem, M. N., and Chmielewski, J. (2016) Dual targeting of intracellular pathogenic bacteria with a cleavable conjugate of kanamycin and an antibacterial cell-penetrating peptide. *J. Am. Chem. Soc. 138* (34), 10945−10949.
(23) Cerrato, C. P., Kunnapuu, K., and Langel, U. (2017) Cell-penetrating peptides with intracellular organelle targeting. *Expert Opin. Drug Delivery 14* (2), 245−255.
(24) Jean, S. R., Ahmed, M., Lei, E. K., Wisnovsky, S. P., and Kelley, S. O. (2016) Peptide-mediated delivery of chemical probes and therapeutics to mitochondria. *Acc. Chem. Res. 49* (9), 1893−1902.
(25) Field, L. D., Delehanty, J. B., Chen, Y., and Medintz, I. L. (2015) Peptides for specifically targeting nanoparticles to cellular organelles: quo vadis? *Acc. Chem. Res. 48* (5), 1380−1390.
(26) Turner, J., Cho, Y., Dinh, N. N., Waring, A. J., and Lehrer, R. I. (1998) Activities of LL-37, a cathelin-associated antimicrobial peptide of human neutrophils. *Antimicrob. Agents Chemother. 42* (9), 2206−2214.
(27) Alajlouni, R. A., and Seleem, M. N. (2013) Targeting Listeria monocytogenes rpoA and rpoD genes using peptide nucleic acids. *Nucleic Acid Ther. 23* (5), 363−367.

DOI: 10.1021/acsinfecdis.8b00124
ACS Infect. Dis. 2018, 4, 1300−1305